A NEW APPROACH FOR NON-INVASIVE CONTINUOUS ARTERIAL BLOOD PRESSURE MEASUREMENT IN HUMAN

Thesis submitted for the degree of

Doctor of Philosophy

at the University of Leicester

by

Kong Yien Chin

Department of Cardiovascular Sciences

Medical Physics Group

University of Leicester

December 2010

Kong Yien Chin

A New Approach for Non-Invasive Continuous Arterial Blood Pressure Measurement in Human

Abstract

The need for continuous noninvasive arterial blood pressure (ABP) monitoring from an artery closer to the heart (i.e. the ascending aorta) has led to the research and development work presented in this thesis. Clinical applications of continuous ABP waveform include assessments of cardiac function, cerebral autoregulation, autonomic function, arterial elasticity, physiological measurements in aerospace research, and also monitoring in anaesthesia and critical care.

The superficial temporal artery (STA) was chosen as the measurement site and the measurement technique was the arterial volume clamping with photoplethysmography (PPG). The optoelectronic circuitry to measure PPG is contained in a specially designed probe placed over the STA and kept in place with a lightweight aluminium head frame. The complete prototype device (*STAbp*) also includes original designs for the pneumatic, electronic, signal processing, control and display sub-systems. A self-calibration feature that regularly updates the PPG reference level (*Setpt*) was also included to ensure accurate continuous ABP recording.

The performance of the *STAbp* was compared against the *Finapres*®. Five parameters were evaluated: resting ABP (agreement, signal bandwidth, frequency response and magnitude squared coherence, and assessment of drift) and ABP dynamic change during isometric handgrip exercise. The agreement of resting ABP gave bias (SD) of -23.1 (15.05), -10.8 (13.83) and -12.4 (12.93) mmHg for systolic, mean (MAP) and diastolic pressures respectively.

Further investigations were carried out to understand factors that can affect the accuracy of ABP measurements, notably the sensitivity of ABP to perturbation of the *Setpt*. Also, differences between the external compressing pressure at the PPG peak pulsation amplitude and the MAP were found to be normally distributed with mean (SD) of -4.7 (5.63) mmHg.

In conclusion, it is demonstrated that the new *STAbp* device has great potential as a new tool for a wide range of clinical and research applications which require continuous ABP waveforms.

Acknowledgements

My deepest gratitude:

To the Department of Medical Physics led by Professor David Evans for giving me the opportunity to pursue a PhD in this project.

To my supervisor Professor Ronney B. Panerai for his continuous patience, guidance and support throughout the duration of my PhD studentship.

To Dr. Kevin Martin for his invaluable advice and support at the early stage of my PhD studentship before his retirement.

To Mr. Graham Aucott, Mr. Glen Bush and Mr. Michael Squires from the electronic and mechanical workshops for their ideas and support in providing the necessary test equipments, and advice in the development of the prototype device.

To all volunteer subjects who have been supportive and endured the measurements for this project.

To my line manager Dr. Christopher Degg for his ongoing encouragement and allowed extra time off from my full time job while I was completing this thesis.

Finally, to so many more family members, friends and other colleagues who have been kind and patient for me to progress with this project and to complete the thesis.

CONTENTS

LIST OF FIGURES

LIST OF TABLES

LIST OF ABBREVIATIONS

		First used in Chapter
ABP	Arterial blood pressure	1
ANOVA	Analysis of variance	4
BRS	Baroreceptor reflex sensitivity	1
CBF	Cerebral blood flow	1
CLP	Closed Loop Procedure	3
CoNIBP	Continuous noninvasive ABP	1
DBP	Diastolic blood pressure	4
DFT	Discrete Fourier transform	4
FFT	Fast Fourier transform	4
Finap1	*Finapres* #1 (reference device)	4
Finap2	*Finapres* #2 (test device)	4
IHG	Isometric handgrip	4
IRED	Infrared emitting diode	3
MAP	Mean arterial pressure	4
MRI	Magnetic resonance imaging	2
n	Sample size	4
OLP	Open Loop Procedure	3
PD	Photodetector	3
PPG	Photoplethysmogram	2
RMSE	Root mean squared error	4
SBP	Systolic blood pressure	4
SD	Standard deviation	2
Setpt	PPG reference value used in *STAbp*	3
STA	Superficial temporal artery	2
STAbp	Prototype device to monitor ABP in the STA	1

CHAPTER 1 INTRODUCTION

Overview

The history of arterial blood pressure (ABP) measurement was documented as early as 1628 by William Harvey when he described the existence of blood circulation in his book *De Motu Cordis*. Today, ABP measurement plays an essential role in healthcare establishments such as clinics, operation theatres, hospital wards, and accident and emergency departments. Its relevance expands from providing an initial clinical assessment for hypertension or hypotension, continuous ABP monitoring in operation theatres and critical care, to contributing as an important parameter in a wide range of physiological research.

Chapter Outline

This chapter will set the scene regarding ABP measurements that became the driving force for the research work presented in this thesis. In the following section 1.1, the physiology of ABP generation is first described. Section 1.2 will then describe the rationale of the research in more detail regarding the importance of continuous and noninvasive as opposed to single, intermittent, or invasive ABP measurement modalities. The importance of monitoring ABP from an artery close to the heart will also be emphasized. Section 1.3 describes the applications, whether clinical or in research, that require continuous ABP waveforms. The aim and objectives of this thesis will then be established in section 1.4. Finally, the outline of subsequent chapters will be presented, the contents of which will demonstrate its contributions towards the advancement in the field of continuous noninvasive ABP (CoNIBP) measurements.

1.1 Physiology of ABP Generation

The human cardiovascular system is a closed network of blood vessels. ABP generation starts with left ventricular contraction and it propagates from the ascending aorta to other arteries, arterioles and capillaries. The changes in ABP during cyclical pumping of the heart generate a pressure wave that reaches a maximum and then a minimum in each cardiac cycle, known as the systolic and diastolic pressures respectively. Figure 1.1 shows an example where a continuous ABP waveform is recorded.

A complex regulatory system of inter-related mechanisms is involved to ensure sufficient blood flow reaches the tissues and vital organs. They are broadly categorised as short-, intermediate- and long- term ABP regulatory mechanisms (Guyton and Hall, 1997). The short-term ABP change is mainly regulated by the baroreceptor feedback, central nervous system response to ischaemia and chemoreceptor mechanisms. These also include local myogenic and metabolic mechanisms, and central sympathetic control of peripheral resistance to ensure adequate blood flow supply through the vascular network (Levy and Pappano, 2007). These mechanisms react within seconds to return the ABP level back to normal. During this process, there may be changes in vasomotor tone (i.e. vasoconstriction or vasodilation), heart rate, heart contractility and cardiac output.

The intermediate-term pressure regulatory mechanisms are activated a few minutes after an acute ABP change. These involve the renin-angiotensin vasoconstrictor mechanism, stress-relaxation of the vasculature and fluid shift through capillary walls. When the ABP decreases, angiotensin activates vasoconstriction in the arterioles which raises the

blood pressure. It also causes water and salt retention in the blood through the kidneys. Lastly, the long-term blood flow is further regulated by the kidneys through the renal-blood volume pressure control mechanism. It usually takes at least a few hours to show significant response. Angiotensin causes the secretion of aldosterone in the adrenal glands which increases water and salt re-absorption by the kidney tubules. The interaction of the renin-angiotensin mechanism with aldosterone regulates the water and salt retention in the body fluid until the ABP is returned to normal.

Along the vessel pathway, the pressure wave is changed. This is due to a combination of the expansion-recoil effect of the elastic vessel wall, vasomotor tone and peripheral resistance (Thibodeau and Patton, 2002). These lead to different intensity and timing of pulse wave propagation (forward flow) and wave reflection (backward flow) along the pathway (Avolio, 1992; Belardinelli and Cavalcanti, 1992; O'Rourke et al., 2003; O'Rourke and Yaginuma, 1984; Westerhof et al., 2006). The propagating wave from the ascending aorta overlaps with the reflected wave from the periphery. The central ABP waveform is hence the summation of the cyclical pressure, the propagated and the reflected pressure waves. This phenomenon also applies to the ABP along the rest of the arterial tree and results in different ABP waveshapes in different arteries.

In comparison with ascending aortic pressure, peripheral ABP waveforms in young individuals with more elastic vessel walls tend to produce delayed and increased systolic peak, steeper ejection gradient to systolic peak and a slightly lower diastolic value with more distinct trough. In addition to this, there is a small drop in mean pressure due to a pressure gradient in smaller arteries (Avolio, 1992; Karamanoglu et al., 1993; O'Rourke, 1992; O'Rourke et al., 2003; O'Rourke and Yaginuma, 1984;

Westerhof et al., 2006). As the arterial wall stiffens with age, vessel resistance is increased. This usually leads to a raised mean ABP in the elderly. The pulse wave travels faster due to the stiffer vessel walls, with reflected wave returning quicker towards the aorta. This further raises the systolic pressure close to the heart (i.e. ascending aorta) (Levy and Pappano, 2007). In all age groups, local regulation of blood flow at the periphery with strong sympathetic innervation may further distort the ABP waveforms (Wesseling et al., 1995). Figure 1.2 shows an illustration of ABP waveforms measured from the ascending aorta to the femoral artery in three adult humans (O'Rourke and Nichols, 2005). Consequently, the site of ABP measurement needs to be selected appropriately with reference to the pathology and clinical queries.

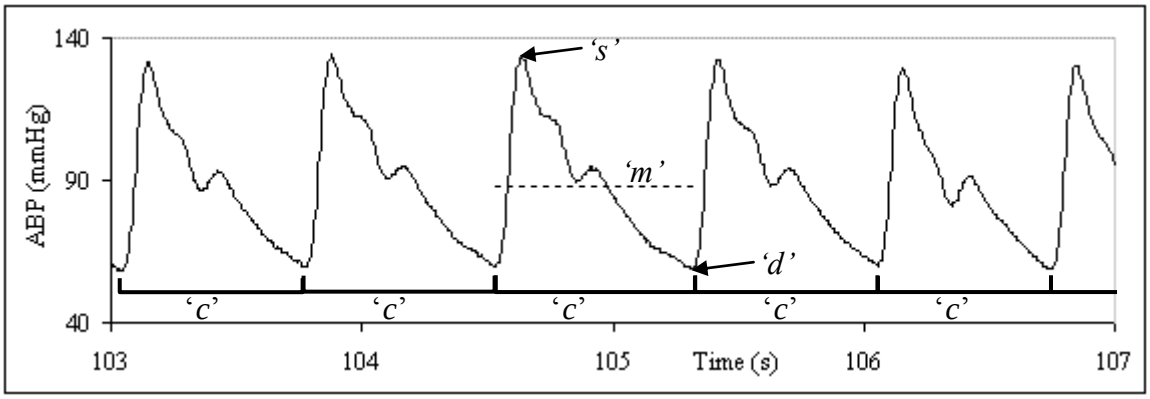

Figure 1.1 A recording of a continuous ABP waveform.
The instantaneous change of the ABP is recorded. In each cardiac cycle (indicated as 'c'), the systolic ('s'), mean ('m') and diastolic ('d') pressures can be computed.

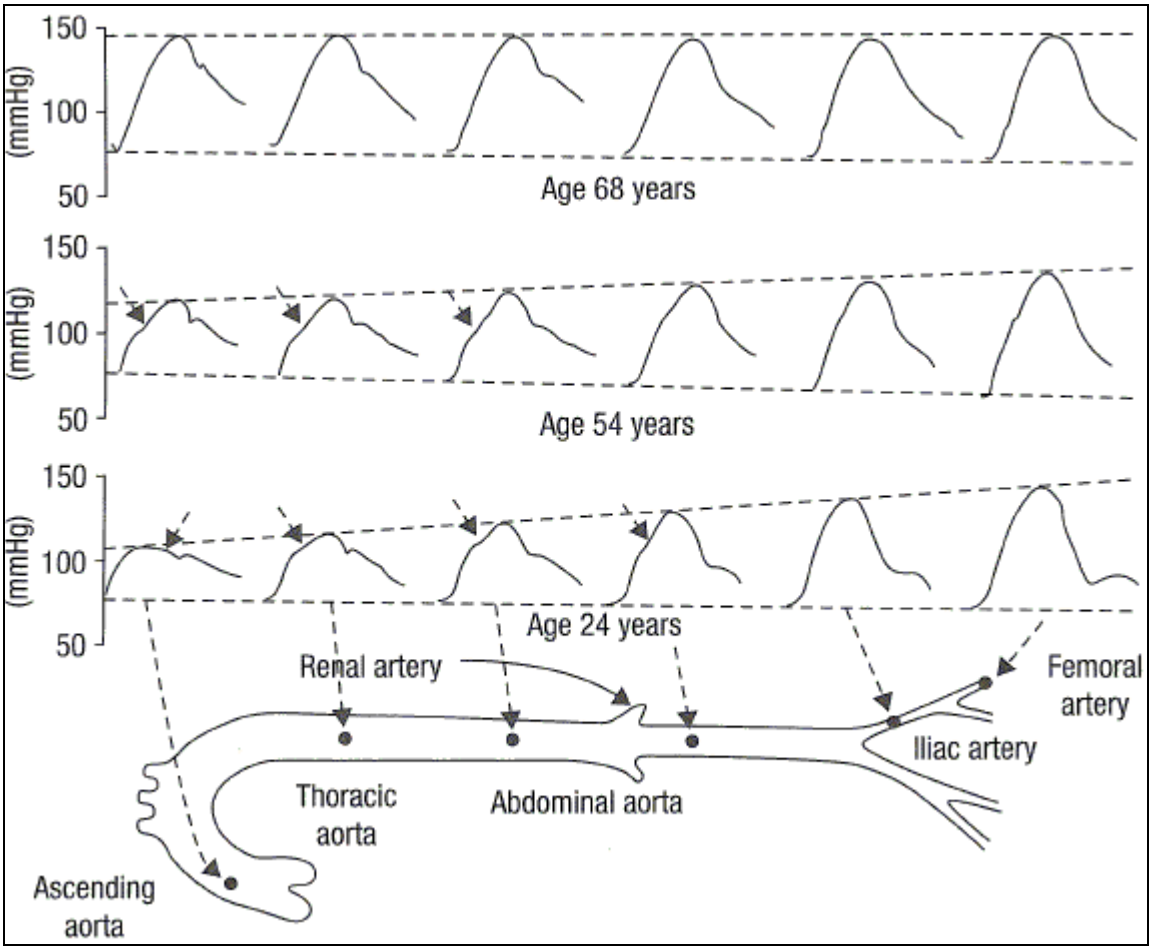

Figure 1.2 Variation of ABP waveforms in different arteries.
ABP waveforms measured along the arterial pathway from the ascending aorta to the femoral artery in three adult humans aged 24, 54 and 68 years. In the oldest subject, there is little amplification in the pressure wave; whereas, in the youngest subject, the amplitude of the pressure pulse wave is increased towards the periphery (image adapted from O'Rourke and Nichols (2005)).

1.2 Rationale

In clinical and research practice, there is still a lack of suitable CoNIBP monitoring devices that can suit different needs. Ideally, such devices should monitor the ABP from an artery close to the heart, i.e. the ascending aorta. The availability of such devices will not only encourage its use in clinical areas, it will also increase research endeavours that particularly require continuous recording of the ABP waveform. This will potentially further generate new knowledge in the field of physiological measurements. Three main characteristics of ABP measurement devices should be considered and they are described in the subsections below.

1.2.1 Continuous vs. Intermittent Measurements

ABP measurement is often performed using single or intermittent measurements of systolic, mean, and diastolic pressures to detect hypertension or hypotension. The frequency of the measurements will depend on clinical needs or specific research protocol. In single or intermittent measurements, beat-to-beat changes of ABP are not available.

In continuous measurements, on the other hand, an instantaneous ABP change is recorded. Close observation of continuous ABP measurements is essential in many clinical or research applications where additional information can be extracted from the ABP waveform or where values of systolic, mean and diastolic pressures are required for all heart beats during a given period of time.

1.2.2 Noninvasive vs. Invasive Measurements

Historically, before the advent of CoNIBP measurement techniques, the clinical assessments of ABP were based on invasive measurements. Although the invasive measurement method is used as the 'gold standard', it carries a high risk of infection and other clinical complications (Carroll, 1988; Murray, 1981; Prian, 1977; Toll, 1984; West et al., 1991). These include haemorrhage (Pierson and Hudson, 1983), arrhythmia and ischaemia (Murray, 1981; Puri et al., 1980), local skin discolouration, bruising and haematoma, neurological damage (Bull et al., 1980; Luce et al., 1976), embolism and thrombosis (Bedford, 1978; Downs et al., 1974; Evans and Kerr, 1975; Jones et al., 1981; Prian et al., 1978), and arterial vasospasm (Kurki et al., 1987; Smith et al., 1985).

Two main types of intravascular catheters will be described later in section 2.4.1. They are the fluid-filled type and the catheter-tip type catheters. They are designed for single use only. The catheter-tip type catheter is much more expensive, often in excess of £400 each. In addition to that, the procedure is a specialised skill and hence it can only be carried out by a trained person.

A noninvasive device does not normally require disposable parts and the measurement process is easily repeatable. It is usually a much less expensive alternative in the long run. The risk of infection and other complications that are common in invasive measurement techniques are negligible. Patients can leave the clinic or continue with their daily lives immediately after a noninvasive ABP measurement procedure is completed. These same benefits also apply to research studies. More studies can hence be carried out with less ethical issues involved.

1.2.3 Central vs. Peripheral Blood Pressure

As described in section 1.1, the ABP waveform varies dependent on the measurement site (Figure 1.2). The ABP waveforms in different arteries are influenced by the pulse wave propagation and reflection (Avolio, 1992; O'Rourke, 1992; O'Rourke et al., 2003; O'Rourke and Yaginuma, 1984). Local regulation of blood flow further affects the agreement between the central (i.e. ascending aorta) and peripheral ABP. Assessments based on peripheral ABP waveforms, for instance, measured with the *Finapres*, may hence lead to misdiagnosis and/or inadequate treatment (Williams et al., 2006).

1.2.4 State-of-the-Art CoNIBP Devices

The three previous sections provide brief justification for the need of devices that can perform continuous noninvasive measurements of ABP close to the heart. Not surprisingly, there are already several CoNIBP measurement devices currently in the market. These devices include the *Finapres*® (superseded by *Portapres*® and *Finometer*®), *SphygmoCor*®, *Colin*®, and *Millar*® *Mikrotip*®. *Finapres* measures the ABP from the digital (finger) artery (Imholz et al., 1998; Maestri et al., 2005; Schmidt et al., 1992); *SphygmoCor* tonometer measures the pulse waveform from the radial and carotid arteries; *Colin* tonometer from the radial artery (Birch and Morris, 2003; Zion et al., 2003), and *Millar* micromanometer-tipped tonometric probe from the radial and carotid arteries (Chen et al., 1995; Kelly et al., 1989).

The availability of such devices gave considerable impetus to many laboratory based applications, but for several reasons they do not cover all the clinical and research needs for CoNIBP measurement. For instance, carotid ABP should not be measured

continuously as this may interrupt its blood supply to the head, especially the brain. Similarly, the finger ABP cannot be reliably monitored in some patient groups, namely, premature neonates due to small and vulnerable digits, patients with lower arm diseases, e.g. Raynaud's disease and arthritis (Nelesen and Dimsdale, 2002; Panerai et al., 2006), and patients with lower arm burns or amputees. Other devices like *SphygmoCor*, *Colin* and *Millar* are not self-calibrating and can lead to significant errors in long term recordings. The self-calibration feature will be explained in more detail in section 2.5.

In summary, despite the availability of different types of CoNIBP devices that meet some of the needs for continuous ABP monitoring, there are still limitations and unmet needs which justify the search for alternative approaches. Within this broad remit, the following sections review the wide field of ABP applications, which will provide the basis for a detailed proposal in section 1.4.

1.3 Applications of Continuous ABP Waveforms

The applications of continuous ABP waveform encompass the areas of anaesthesia and critical care, cardiac function, arterial elasticity, autonomic function, cerebral autoregulation and space research. As mentioned in previous sections, the use of a noninvasive measurement device would always be preferred although currently this option is not always available.

1.3.1 Anaesthesia and Critical Care

ABP monitoring is mandatory during anaesthesia, but the need for continuous measurement is usually restricted to cardiac surgery and other critical conditions where there is a risk of rapid cardiovascular deterioration (Hutton and Prys-Roberts, 1994; Kemmotsu et al., 1991b).

Continuous ABP monitoring in very ill patients ensures that the patient's blood pressure is stable during recovery or following administration of medications (Andriessen et al., 2004; Rolfe et al., 1987). This applies especially to patients in critical care such as the coronary and neonatal intensive care units. Continuous ABP monitoring in coronary care is particularly relevant to assess patients' cardiac function before, during or after heart surgery (Hirai et al., 2005; Pinna et al., 2000; West et al., 1991). Any abnormal or sudden blood pressure change can be rapidly detected and hence immediate action can be taken (Hughes et al., 1994; Hutton, 1994).

1.3.2 Assessment of Cardiac Function

Combined with other clinical measurements, continuous ABP waveform recording provides additional information in the evaluation of cardiac and coronary haemodynamics to identify abnormal conditions such as congenital heart disease, dysrhythmias, pulsus alternans (Euler, 1999), stenosis (Nichols and O'Rourke, 2005) and valve dysfunction (Levin, 1972; Murgo et al., 1980). The evaluation is also useful to minimise risks such as atrial fibrillation, left ventricular hypertrophy, cardiac failure or sudden death (O'Rourke and Brunner, 1992).

Several parameters can be derived from the continuous ABP waveform in the assessment of cardiac function. These include aortic input impedance (Murgo et al., 1980), cardiac output (Jansen et al., 2001), systolic time intervals (Weissler et al., 1968), myocardial contractility (Brown and MacGregor, 1982) and left ventricular ejection time (Gerhardt et al., 2000). In comparison with healthy subjects, these parameters were altered in patients with cardiac pathology (Ferro et al., 1995; Martin et al., 1974; Nichols and O'Rourke, 2005; Takazawa et al., 1998; Weissler et al., 1968).

1.3.3 Assessment of Arterial Elasticity

With advancing age or pathology, progressive changes in the collagen and elastic content of the arterial wall (Levy and Pappano, 2007) can lead to reductions in arterial elasticity. Different terminologies have been used in this field, i.e. compliance, distensibility and stiffness (O'Rourke and Nichols, 2005). With reduced arterial elasticity, changes in ABP waveshape can be detected and used to quantify the extent of

arterial wall damage (Lehmann et al., 1992; Lopez-Beltran et al., 1998; Sollers, III et al., 2006).

Reduced arterial elasticity is considered a risk factor for cardiac failure, myocardial infarction and stroke (O'Rourke and Nichols, 2005). The arterial elasticity is quantified by a range of indices. These include the augmentation index, pulse wave velocity, arterial distensibility, arterial compliance, pulse pressure, diastolic decay and characteristic impedance (O'Rourke and Brunner, 1992; O'Rourke and Nichols, 2005; Stergiopulos et al., 1999; Tanaka et al., 2002). The computation of these indices requires the use of continuous ABP waveform, although only a small number of cardiac cycles is usually sufficient.

As examples, increases in augmentation index and pulse wave velocity have shown associations with cardiovascular disease (e.g. atherosclerosis, ischaemic heart disease, left ventricular hypertrophy and coronary disease) (Avolio et al., 1985; Cockcroft and Wilkinson, 2002; Millasseau et al., 2002; Nurnberger et al., 2002; Roman et al., 1995; Saba et al., 1993; Sollers, III et al., 2006; Vaitkevicius et al., 1993), diabetes, hypertension (Davies and Struthers, 2003; Meaume et al., 2001; Stergiopulos et al., 1999), end stage renal disease (London et al., 2001), and an increase in mortality and morbidity from coronary heart disease in the elderly (Lind et al., 2004; Sugawara et al., 2007).

1.3.4 Assessment of Autonomic Function

Within its many functions, the autonomic nervous system plays a major role in the short term control and regulation of ABP. The ABP is constantly monitored by baroreceptors located primarily in the carotid sinus and aortic arch, but to a lesser extent in the walls of arteries, veins and right atrium (Marieb, 2004). A change in ABP triggers impulses firing from the baroreceptors, which are transmitted to the cardioregulatory centre of the central nervous system in the medulla oblongata. From the cardioregulatory centre, efferent impulses are conducted by the vagus and sympathetic nerves to regulate the blood pressure back to the normal level by changes in heart rate, left ventricular contractility and peripheral resistance (Guyton and Hall, 1997).

The effectiveness of the short term ABP regulation can be assessed by the parameter known as the baroreceptor reflex sensitivity (BRS) (Dawson et al., 1997; Lucini et al., 1994; Persson et al., 2001; Smyth et al., 1969). BRS is expressed by the change in cardiac cycle duration for a given change in systolic ABP (units of ms/mmHg). BRS can be computed in the time or frequency domain (Dawson et al., 1997; Frattola et al., 1997; Persson et al., 2001; Smith et al., 2008). Analysis in either domain requires the use of a continuous ABP waveform (Pinna et al., 2000).

While studies showed that there is generally a progressive decline of BRS with advancing age in healthy subjects (Dawson et al., 1999b; James et al., 1996; O'Brien et al., 1986), a decline of the BRS is also reported in pathological conditions such as heart failure, myocardial infarction (Persson et al., 2001), ischaemic stroke (Atkins et al., 2010; Eveson et al., 2005), cerebrovascular disease or injuries (Baguley et al., 2008; Johnson et al., 2006), diabetes (Ewing et al., 1985; Weston et al., 1996b), renal failure,

traumatic quadriplegia (Omboni et al., 1996), abnormal left ventricular function, pre-eclampsia during pregnancy (Rang et al., 2002), hypertension (Sleight, 1991), alcoholism (Kollensperger et al., 2007), Parkinson's disease (Goldstein et al., 2002; Parati et al., 1995), syncope (Krediet et al., 2005; van Lieshout et al., 2003), orthostatic intolerance (Imholz et al., 1990; Swenne et al., 1995; ten Harkel et al., 1992) and pure autonomic failure (Goldstein et al., 2002; Omboni et al., 1996; Rang et al., 2002).

1.3.5 Assessment of Cerebral Autoregulation

Cerebral blood flow (CBF) autoregulation is a homeostatic mechanism that maintains the mean CBF (or CBF velocity) relatively constant despite changes in cerebral perfusion pressure (Panerai, 1998). Impaired cerebral autoregulation was found in several conditions, e.g. hypercapnia (Birch et al., 1995; Dineen et al., 2010), carotid artery disease (Hu et al., 1999; Panerai, 2008; Reinhard et al., 2004), middle cerebral artery stenosis (Dawson et al., 1999a; Haubrich et al., 2003), severe head injury and subarachnoid haemorrhage (Panerai, 2008), prematurity of the newborn (Panerai et al., 1998) and stroke (Atkins et al., 2010; Dawson et al., 2003).

Continuous ABP waveform is needed in the assessment of dynamic cerebral autoregulation (Dineen et al., 2010; Panerai et al., 1999; Sammons et al., 2007). The transient change in the CBF (or CBF velocity) following a rapid change in the ABP can be analysed (Aaslid et al., 1989). CBF is usually monitored using the transcranial Doppler ultrasound technique. The ABP waveform (as input) is analysed in the frequency domain by computing a transfer function in relation to the CBF (as output).

For example, a reduced phase response indicates an impairment of the cerebral autoregulation (Panerai, 2008).

1.3.6 Physiological Measurements in Aerospace Research

With the expansion of space exploration, the assessment of cardiovascular physiology in space travel continues to play a crucial role to monitor the cardiovascular health of astronauts (Karemaker, 1995; Krol and Simons, 1995). Astronauts have been found to experience short term orthostatic intolerance, impaired exercise performance and other changes in their cardiovascular health after returning to earth from a long stay in space with zero gravity. To study these alterations, continuous recording of ABP waveform has been seen as essential (Hughson, 2009; Sigaudo-Roussel et al., 2002).

1.4 Aims and Objectives

Aims

The previous sections highlighted the increasing importance of CoNIBP monitoring for specialised clinical applications and research work. Although considerable progress has been achieved with existing devices, further work in this area is needed to explore the possibility of performing measurement at alternative sites, for example closer to the heart as compared to the finger. Also of considerable importance is to develop in-house expertise to allow future developments that could benefit industry in the United Kingdom.

Objectives

To achieve the aims above, specific objectives would be:

i. To identify suitable site of measurement with appropriate measurement technique;
ii. To design and develop a prototype device;
iii. To perform preliminary evaluation of the prototype device.

Thesis Outline

The following chapters will first begin with an overview of the evolution of ABP measurements, measurement techniques and site of measurement (chapter 2). This will be followed by the detailed description of a new CoNIBP monitoring prototype device known as the *STAbp* (chapter 3). Chapter 4 will evaluate the *STAbp* device against the *Finapres*, a commercial CoNIBP monitoring device. Further investigations relevant to the *STAbp* device are presented in chapters 5 and 6. These chapters address possible refinements for future improvements of the prototype device. Finally, chapter 7 will present the conclusions and suggestions for further work.

CHAPTER 2 BLOOD PRESSURE MEASUREMENT

2.1 Introduction

Chapter 1 presented the rationale of the thesis, which is the need for a CoNIBP monitoring device measured from an artery closer to the heart. The applications of continuous ABP waveform in a wide range of physiological assessments and research encourage the use of a noninvasive technique rather than invasive measurements that carry a significant risk of infection and other clinical complications, and also has cost implications. The outcome of these applications shows the potential to provide clinicians with additional information to treat and manage illnesses more effectively.

The objectives of this chapter are:

i. To give an overview of the evolution of ABP measurement (section 2.2);
ii. To present the selection process for an alternative ABP measurement site closer to the heart, followed by the anatomy and physiology of the selected site (section 2.3);
iii. To give an overview of the classical ABP measurement techniques and the techniques for CoNIBP measurement (sections 2.4 and 2.5);
iv. To identify potential causes of error in noninvasive ABP measurement techniques (section 2.6);
v. To present the selection process and decide on a suitable technique for CoNIBP monitoring (section 2.7).

2.2 The Evolution of ABP Measurement

The history of blood pressure measurement can be traced back to William Harvey when he described the existence of blood circulation in his book *De Motu Cordis* in 1628 (Hutton and Clutton-Brock, 1994; Paskalev et al., 2005; Wesseling, 1995). About a century later, Reverend Stephen Hales (1733) first measured blood pressure directly from the femoral and carotid arteries of non-anaesthetised horses by inserting a long glass tube upright into an incision on a horse's artery. Blood pressure was estimated by monitoring the change in height of the blood level in the tube as the heart pumped cyclically.

In 1826, Jean Poiseuille constructed a more convenient mercury column manometer, and the millimetre of mercury (mmHg) was used as the unit of measurement. Approximately two decades later, Carl Ludwig successfully recorded invasive continuous blood pressure in animals graphically inscribed on a slowly rotating sooted drum, called the kymograph. Jean Faivre later (1856) demonstrated the direct intra-arterial pressure measurement in man and used the mercury column to establish the mean blood pressure. His measurements focused on the humeral and femoral arteries.

In 1858, Étienne-Jules Marey measured the blood pressure in the forearm with a sealed water-filled chamber. As the pressure in the chamber was raised, its pressure was monitored with a mercury column manometer. The blood pressure pulsation was simultaneously recorded graphically on a polygraph. Marey observed that the blood pressure showed a change of oscillation amplitude as the water pressure was increased, forming an approximately bell-shape amplitude curve. It was later considered by

Angelo Mosso in 1895 that at maximum oscillation, the internal and external pressures were equal (Hutton and Clutton-Brock, 1994).

The concept of systolic and diastolic pressures began to unfold when Samuel von Basch recorded the first noninvasive measurement of systolic blood pressure in 1880 from the radial artery of a patient (Paskalev et al., 2005). Towards the end of the 19th century, Scipione Riva-Rocci invented an inflatable upper arm rubber cuff to obstruct the blood flow of the brachial artery. A mercury column was used to measure the pressure required to inflate the arm cuff until the pulse distal to the cuff became impalpable. During cuff deflation, when the pulse distal to the cuff reappears, it was identified as the systolic pressure (Paskalev et al., 2005; Riva-Rocci, 1896). However, determining the diastolic pressure remained an unresolved issue at the time. Furthermore, although revolutionary, his cuff was too narrow, resulting in inaccurate measurements. Heinrich von Recklinghausen (1901) later recognised this error and widened the cuff from 5 to 13 cm. At about the same time, Nikolai Korotkoff (1905) described the auscultatory sounds heard with a stethoscope placed over the brachial artery below an encircling upper arm cuff during gradual deflation. The five phases of Korotkoff sounds were later described by Edward Goodman and Alexander Howell in 1911 to determine the systolic and diastolic pressures (Hutton and Clutton-Brock, 1994). The measurement protocol which has now become standard was recommended by Joseph Erlanger (1916a).

By 1933, Bertel von Bonsdorff had developed a monitoring system that compared the finger blood pressure with the intra-arterial pressure near the elbow. He emphasised the importance of appropriate frequency response in measurement devices to reproduce the blood pressure pulsations faithfully.

The need for measuring the ABP more frequently throughout the day was gradually recognised due to changes in blood pressure. The phenomenon of white coat hypertension further encouraged intermittent measurements of ABP throughout the day to assess its variation. White coat hypertension is a temporarily raised ABP in patients due to anxiety in a clinical environment (Celis and Fagard, 2004; Pickering et al., 1988).

With the need for intermittent measurements, automated noninvasive ABP measurement devices began to emerge. Numerous models became available both for home and clinical use. Such devices gained popularity due to their ease of use and negligible risk of infection, in addition to their low cost and high reusability. This development facilitated ambulatory ABP monitoring which provides a profile of the patient's blood pressure in conditions that are more representative of the patient's lifestyle.

Continuous recording of ABP waveform continues to play an important role clinically. The risk of infection and other clinical complications, and cost implications have motivated the development of noninvasive approaches for recording instantaneous variation of ABP. The development of CoNIBP monitoring using the volume clamping technique was pioneered by Jan Penaz in 1967 (Penaz, 1973), and the importance and potential of his contribution was increasingly recognised by researchers and clinicians in the 1980s. Taking full advantage of microprocessors, software programming, pneumatics, optoelectronics and feedback control mechanisms, a measurement device using this technique automatically monitors the finger ABP continuously. Penaz's invention was later developed commercially and marketed as *Finapres*® by the Ohmeda Company (Imholz et al., 1993; Langewouters et al., 1998; Wesseling, 1995). At about

the same time, a similar research led by Ken-ichi Yamakoshi from Japan had also developed a finger ABP monitoring device based on Penaz's technique and several notable papers were published (Kawarada et al., 1991; Nakagawara and Yamakoshi, 2000; Tanaka and Yamakoshi, 1996; Yamakoshi et al., 1983; 1988; 1980). *Finapres* was later superseded by the *Portapres*® and *Finometer*® which also monitor the finger ABP. With regards to the Japanese group, their many contributions were not followed by further communications, evaluative studies or industrial developments, which included the ABP measurements from the finger and superficial temporal arteries.

The development of CoNIBP monitoring devices opened up new research interests for a wide range of clinical applications due to the additional information that can be extracted from continuous ABP waveforms (section 1.3). On the other hand, the need for measurement of ABP at a more central site is still a challenge.

2.3 ABP Measurement Site

The second objective set out in section 2.1 is to select an alternative ABP measurement site closer to the heart suitable for CoNIBP monitoring. The following subsection describes the selection process, from which a decision for the measurement site is made. This is then followed by a more detailed description of its anatomy and physiology.

2.3.1 Selection of Alternative ABP Measurement Site

To begin from a general perspective, an alternative ABP measurement site should meet the following desirable criteria:

i. Proximity to the heart;
ii. Prolonged compression without causing irreversible physiological damage, such as ischaemia, necrosis or bleeding;
iii. Ease and convenience of locating the arterial pulsation through palpation;
iv. Possibility of compressing the artery by external means;
v. Variation of the arterial pulse can be measured with current sensor technology;
vi. Low sensitivity to temperature change in the surrounding.

Figure 2.1 shows the possible measurement sites for CoNIBP monitoring (Hall, 2001; Marieb, 2004). Criteria (i) and (ii) are the dominant factors. Any measurement site that fails to meet these two criteria was excluded before the other criteria were considered.

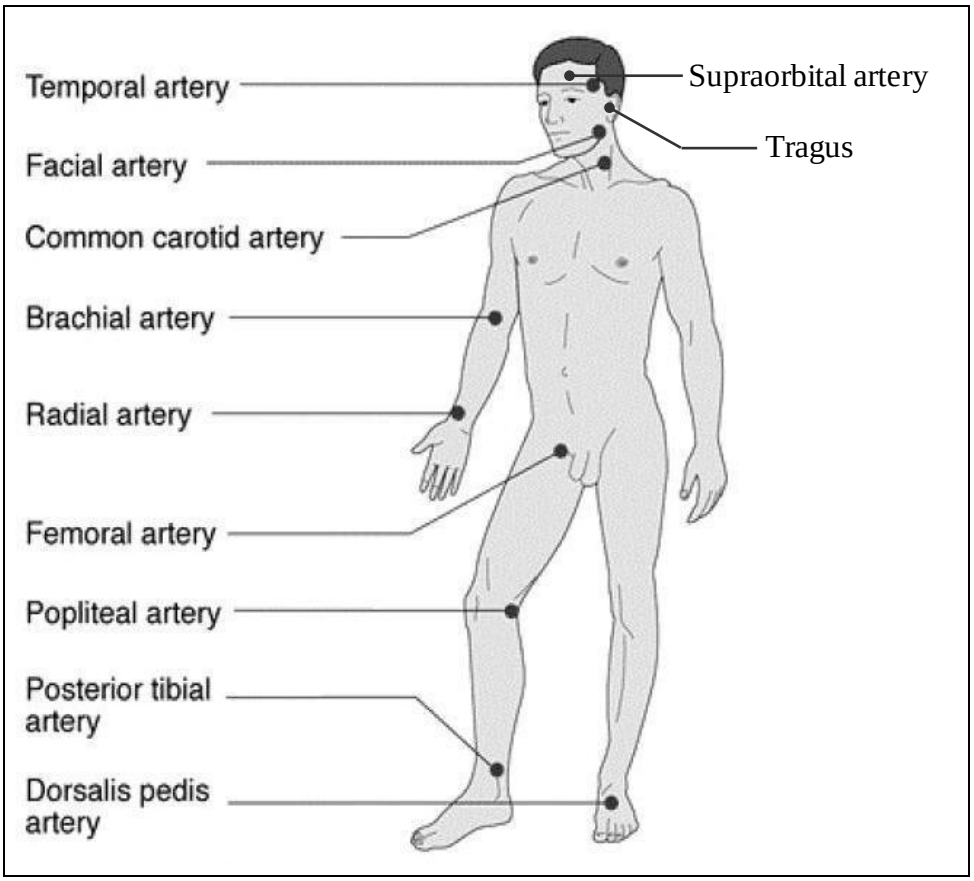

Figure 2.1 Potential locations for CoNIBP measurement.
(Image adapted from Hall (2001)).

Starting with criterion (i), arteries shown in Figure 2.1 further away from the heart than the radial artery were first excluded. Therefore, the remaining arteries are the tragus of the ear, the brachial, common carotid, facial, supraorbital, superficial temporal and femoral arteries. Next, three of these remaining arteries were considered not suitable to meet criterion (ii). They are the common carotid, brachial and femoral arteries. The common carotid artery supplies blood to the head intra- and extra- cranially, any prolonged compression could cause severe cerebral damage. For the brachial artery, prolonged compression could lead to venous congestion or ischaemia in the forearm, wrist and the hand (Boehmer, 1987; Dorlas et al., 1985; Gravenstein et al., 1985; van Egmond et al., 1985; Wesseling et al., 1985). For the femoral artery, due to its location near the groin, privacy is a concern and prolonged compression would impair blood circulation in the lower limb.

From this exclusion process, there are only four measurement sites to be considered further, i.e. the tragus of the ear, facial, supraorbital and superficial temporal arteries. These arteries are superficially located in the skin tissue. This means that criteria (iv) and (v) can be met. To locate these four arteries through palpation (criterion (iii)), it is very much trial and error for the artery in the tragus of the ear, supraorbital artery on the forehead and the facial artery (Koizumi et al., 2009; Lee et al., 1995). Hence, criterion (iii) may not be met consistently between individuals. Also, the tragus was reported to be very sensitive to temperature change (Koizumi et al., 2009).

The only remaining measurement site is the superficial temporal artery (STA). Although the STA is not the closest to the heart when comparing with other possible

measurement sites, it is closer to the heart than the radial and finger arteries, which are currently the most common CoNIBP measurement sites.

Reviewing the list of desirable criteria, criteria (ii) to (v) are met by the STA. However, it is uncertain if criterion (vi) can be met consistently within subjects and in different individuals. To verify this, a separate experiment will be required for further evaluation. This is not covered within the scope of the thesis.

The selection process demonstrated that no one particular measurement site fulfils all desirable criteria. However, the overall selection process shows that the STA is the best candidate for the alternative measurement site. Hence, a more detailed description of its anatomy and physiology will be presented in the next section.

2.3.2 Anatomy and Physiology of the STA

The STA is found on each side of the head at the temporal region (Figure 2.2). The tissue structure at the temporal region consists of five main layers (Figure 2.3). The superficial layers are the skin and dense subcutaneous connective tissue (Bienfang, 1984; Clearkin and Watts, 1991; Czerwinski, 1992; Nakajima et al., 1995; Sheldon, 1982). The next layer is the temporoparietal fascia. The STA is embedded in this layer. The STA emerges within the parotid tissue as the smaller terminal branch of the external carotid artery just behind the neck of the mandible (Gray, 1918).

The temporoparietal fascia is a band of fibrous connective tissue between the dense subcutaneous tissue and the loose areolar tissue deeper beneath. The loose areolar layer

allows the superficial layers to move freely over the deeper and more fixed temporalis muscular fascia, temporalis muscle and pericranium. The pericranium is the deepest layer of the tissue and it adheres to the cranial bone.

The STA ascends in front of the auricle, it is normally easy to locate by palpation anterior to the ear. Ten variations of the STA anatomy were documented (Marano et al., 1985). A large majority of subjects has STA that gives rise to two terminal branches 3 to 5 cm above the zygomatic arch, i.e. the frontal and parietal branches (Figure 2.2) (Chen et al., 1999; Marano et al., 1985; Stock et al., 1980). It was also reported that there is no significant difference in the anatomy and dimension between male and female subjects. These studies showed the adult STA with a mean outside diameter (SD) of 2.1 (0.14) mm.

The frontal branch extends anteriorly to supply blood at the forehead (frontal region), whereas the parietal branch extends upward to supply blood at the top of the head (parietal region). Furthermore, the frontal branch anastomoses with other anterior arteries, e.g. the supraorbital and supratrochlear arteries, whereas the parietal branch anastomoses with the contralateral and the posterior arteries (Okada et al., 1998). Anastomosis is the interconnection of blood vessels. These form a complex vascular network which provides a reliable perfusion with stable and uniform collateral blood supply to the tissues extra-cranially (Bergersen, 1993). This reduces clinical concern regarding venous congestion or ischaemia if there is a prolonged compression on the STA.

The STA has a reasonably flat cranial bone surface underneath which would be suitable as a boundary for compression. The skull protects the intra-cranial tissue from external compression (Marieb, 2004).

Figure 2.4 shows an example of a 3-dimensional scan of an adult STA using the magnetic resonance imaging (MRI) technique. The head was scanned at a relaxed state with the temporal skin tissue uncompressed. The STA is located at approximately 7.0 mm below the skin surface. The artery diameter is measured at approximately 2.0 mm. The image shows that the artery is not a straight and cylindrically uniform blood vessel that extends anteriorly to the ear in the temporal region.

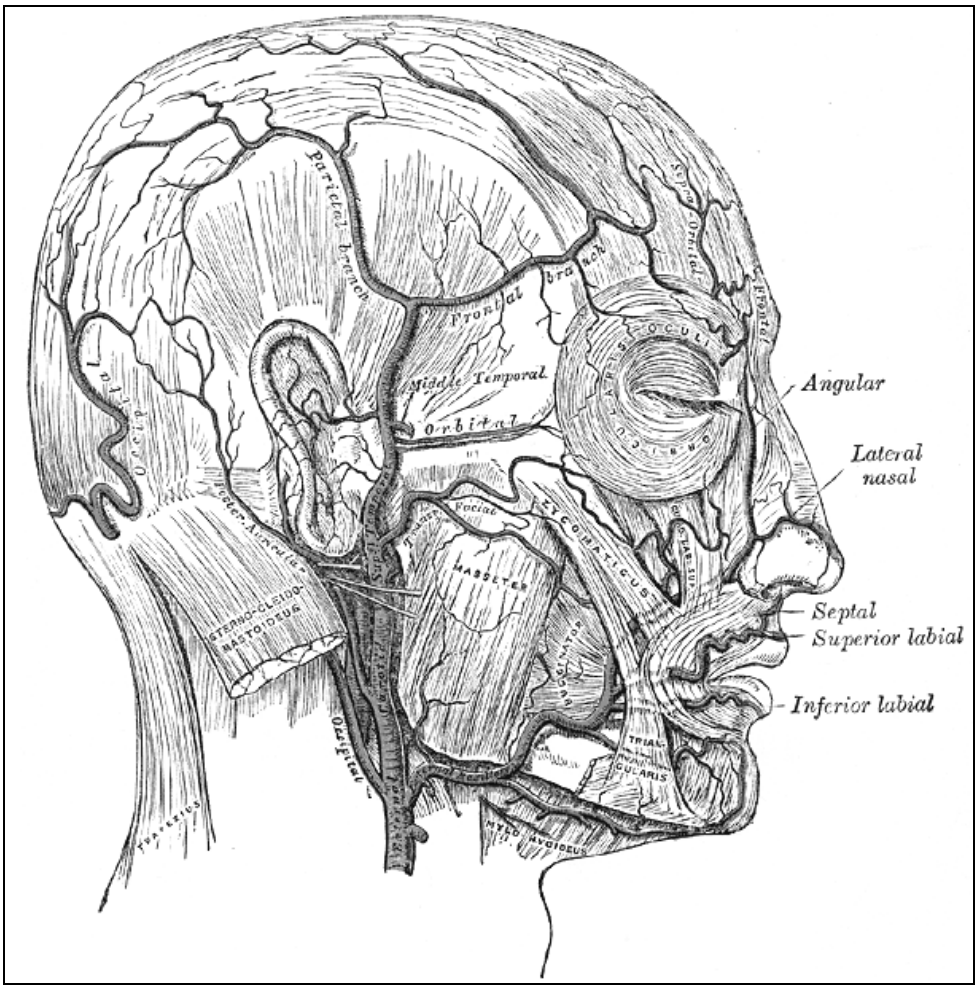

Figure 2.2 The arterial network of the face and scalp.
It shows the pathway of STA located anteriorly to the ear (image adapted from http://www.bartleby.com/107/illus508.html). See detailed description in section 2.3.2.

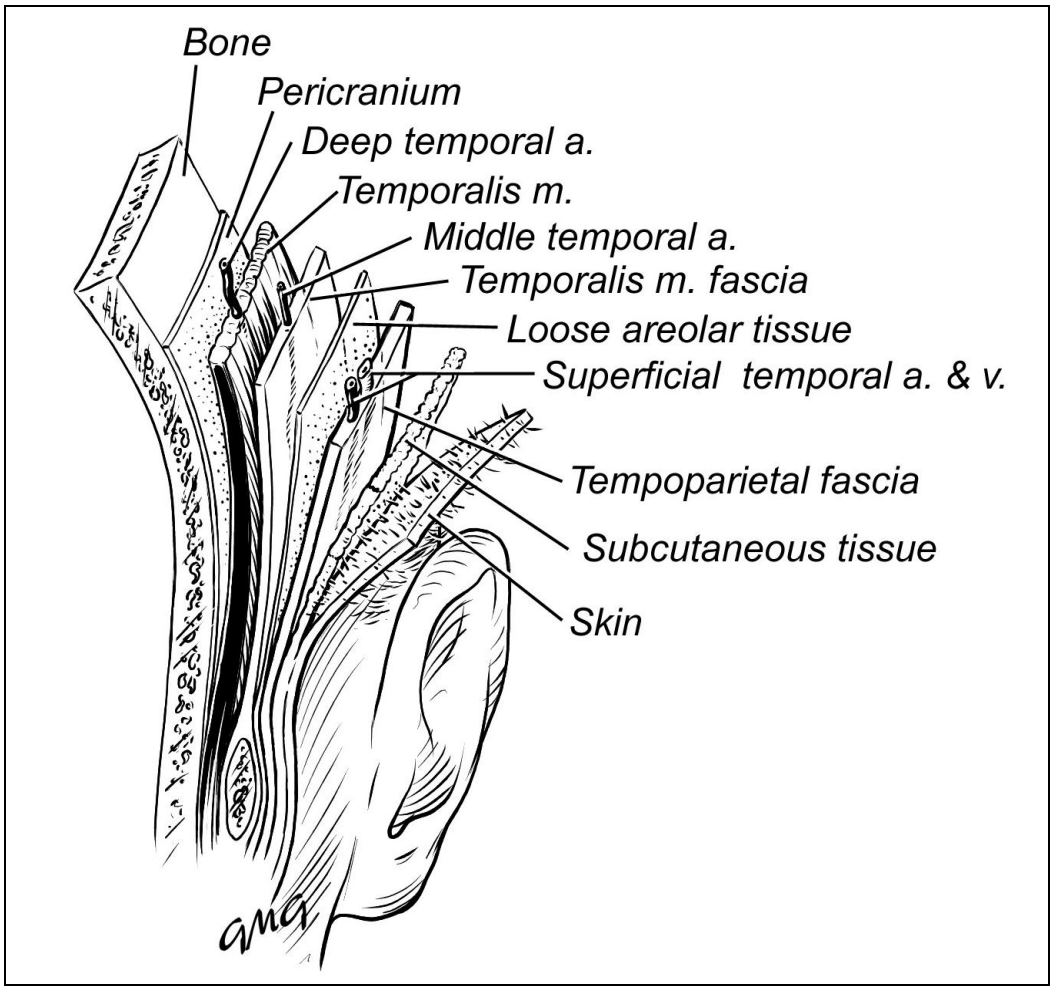

Figure 2.3 Tissue layers at the temporal region of the head.
The STA is embedded in the temporoparietal fascia (image adapted from http://www.emedicine.com/ent/topic735.htm). See detailed description in section 2.3.2.

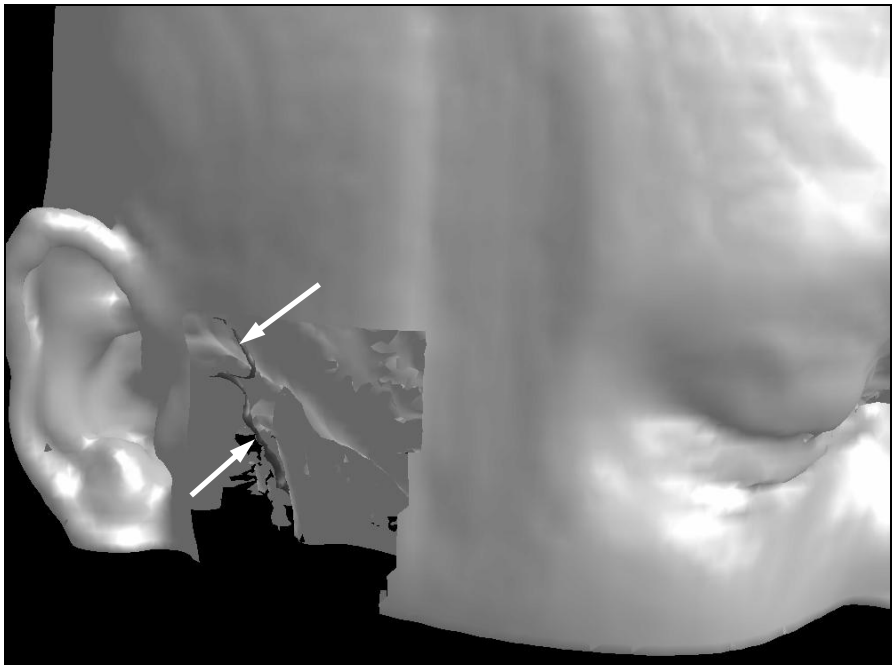

(a)

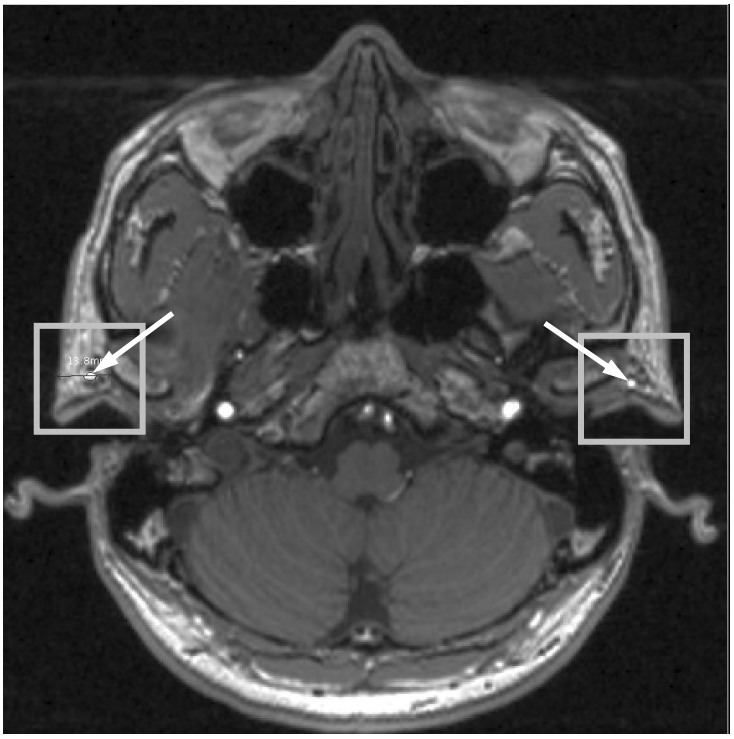

(b)

Figure 2.4 An adult STA imaged with MRI.
(a) Orientation of the STA anterior to the ear in the temporal region, as indicated by the arrows; (b) Transverse view of the right and left STA from the top of the head, as indicated by the arrows as two white spots. The diameter of the STA is approximately 2.0 mm (images courtesy of Dr. Mark Horsfield, University of Leicester).

2.4 Classical ABP Measurement Techniques

With the STA selected in section 2.3 as the alternative measurement site for CoNIBP monitoring, the next step is to select a suitable noninvasive measurement technique. In-depth evaluation of all measurement techniques is beyond the scope of the thesis. Nevertheless, an overview of the main measurement techniques will be described to provide sufficient background for selecting a suitable CoNIBP monitoring technique.

The classical ABP measurement techniques will first be described, beginning with the gold standard, i.e. the invasive intravascular measurement technique. This is followed by the auscultatory and oscillometric measurement techniques, which are conventionally the most common noninvasive alternatives to the intravascular measurement technique. These noninvasive techniques have so far been developed for single or intermittent measurement purposes. Section 2.5 will then describe the currently available CoNIBP measurement techniques, i.e. applanation tonometry and arterial volume clamping technique with photoplethysmography. Lastly, the potential causes of error in noninvasive ABP measurements are identified (section 2.6) before the selection process for a suitable ABP measurement technique for the STA is presented (section 2.7).

2.4.1 Intravascular Measurements

Intravascular catheterisation has been the gold standard for blood pressure measurement. The most common sites of measurement are the radial artery or ascending aorta. A catheter can also be inserted into smaller arteries although this may affect the

accuracy of the pressure measurement due to the interference of the catheter to blood flow.

The most accurate modality has the pressure sensor positioned within the artery at the tip of the catheter. The other modality has the pressure sensor located external to the artery outside the human body, where it is connected to the external end of a catheter. The following subsections describe two types of catheter in relation to the types of modality used, i.e. the catheter-tip type and the fluid-filled type. These catheters have been designed for single use only.

2.4.1.1 Catheter-tip type catheter

Two main types of pressure sensor have been used in this modality. One sensor technology consists of four piezo resistors, forming a Wheatstone bridge (Hutton, 1994). The wiring is connected within the sealed catheter until it reaches outside the body where it is connected to an electronic amplifier. The electronic signal output is calibrated in mmHg. The frequency response of this type of catheter is at least in the order of kHz, for instance, the Millar Mikro-Tip® catheter has its frequency response flat to at least 10kHz (Aubert et al., 1995; Colan, 1984).

The second type of sensor technology uses a length of light-emitting optical fibre. The light reflection is detected by a pair of optical fibres arranged in parallel to the light emitting fibre (Hackman et al., 1991; Wolthuis et al., 1993). The tip of the fibres is sealed with a diaphragm. When the blood pressure changes, the diaphragm is deflected. The deflection changes the detected light intensity. The detected light intensity is connected to an electronic amplifier, which is external to the body. The electrical output

is then calibrated into blood pressure values (Hansen, 1983; Neuman, 1988; Peura, 2009; Roos and Carroll Jr., 1985).

2.4.1.2 Fluid-filled type catheter

The fluid-filled type catheter is less expensive and hence more frequently used. However, the setup is more complicated to ensure accuracy of the ABP measurement. The catheter has a length of patent tubing with the tip of the catheter placed at the required measurement location in the artery. The other end of the catheter is terminated externally with a 3-way stopcock at the skin surface. This type of catheter requires an external pressure transducer. To obtain accurate zero values, one outlet of the stopcock can be opened to the atmosphere, while the other outlet is connected to the pressure sensor and a fast-flush valve. The pressure sensor typically consists of a diaphragm connected to a sealed strain gauge. The pulsating blood pressure distorts the diaphragm. The distortion of the diaphragm changes the potential difference of the strain gauge and generates a voltage output to be calibrated in mmHg.

With the measurement setup in place, zeroing of the pressure transducer is necessary before the ABP measurement begins. The pressure transducer is placed at the subject's heart level at the midaxillary line with the 3-way stopcock temporarily opened to the atmospheric pressure (Darovic and Zbilut, 2002; Gardner and Hollingsworth, 1986). The pressure transducer is zeroed and the stopcock then reconnects the catheter to the pressure transducer. This task is necessary to ensure no offset error between the blood pressure in the catheter and the pressure measured by the transducer.

In most applications, the fast-flush valve has one end connected to a bag of heparinised saline pressurised at approximately 300 mmHg. A small amount of saline is dripped at a

controlled flow rate into the catheter to maintain its patency and to minimise clot formation. The saline bag is pressurised to prevent backflow of blood into the catheter.

The fast-flush valve also plays an important role in fast-flush testing to assess the dynamic response of the measurement setup. During fast-flush testing, the fast flush valve is opened very briefly and closed again to generate a sudden high pressure saline flow from the pressurised bag that temporarily interrupts the blood pressure waveform. This resembles a square wave. The response to this short burst of high pressure flow is measured by the pressure transducer. The response waveform can then be used to calculate the natural frequency and the damping coefficient of the catheter setup. The natural frequency needs to be well above the frequency content of the blood pressure waveform and the damping coefficient should be appropriate (i.e. not under- or over-damped) to achieve adequate dynamic response (Darovic and Zbilut, 2002; Gardner, 1981; Peura, 2009; Runciman et al., 1981; Shinozaki et al., 1980).

Fast-flush testing can be performed from time to time to ensure that the dynamic response is still satisfactory. It is also essential to remove air bubbles trapped near the stopcock as they can degrade the accuracy of the measured blood pressure (Gabe, 1972; Gardner and Hollingsworth, 1986; Gibbs and Gardner, 1988; Soule and Powner, 1984).

2.4.2 Sphygmomanometry

Sphygmomanometry has a long-standing historical use in the clinical environment. It is based on the auscultatory technique which detects and interprets the sound generated as the blood pushes through the artery. It is a noninvasive blood pressure measurement

technique. It is also known as the Riva-Rocci or Korotkoff method (Korotkoff, 1905; Riva-Rocci, 1896).

Sphygmomanometry has traditionally been used to measure the brachial ABP in the upper arm. An encircling cuff is wrapped around the patient's upper arm. The patient is asked to relax and stay still throughout the ABP measurement process, either in a supine or seated upright position with the upper arm placed at the heart level (Netea et al., 1999; Sykes et al., 1981; Terent and Breig-Asberg, 1994).

The arm cuff is an inflatable bladder that can be pressurised to at least 300 mmHg. The bladder is usually covered by a cloth fabric with hook-and-loop fasteners (e.g. *Velcro*®) at both ends for quick and easy fastening and removal (Drzewiecki, 1995). To increase the cuff pressure, an elastic air-bulb connected to the cuff is compressed repeatedly while a mercury column manometer (or aneroid pressure gauge) monitors the cuff pressure. The air-bulb has a one-way valve built inside it to prevent air leakage when it is not compressed. The pneumatic setup is connected through low compliance rubber tubing.

A stethoscope is placed over the brachial artery at the distal end of the cuff at the cubital fossa (Shenoy et al., 1993). As the inflating cuff compresses the artery, the clinician listens to the blood flow sound. The cuff pressure is increased continuously until the blood flow sound has stopped. The cuff pressure may be increased further for approximately 20 mmHg to ensure that the sound has completely stopped, then the cuff pressure is gradually deflated at a rate of 2 to 3 mmHg/s while the clinician simultaneously listens for the return of the sound. The cuff pressure is released by gradually opening the air relief valve.

While the cuff pressure is reduced, the clinician continuously observes and reads the pressure scale based on the meniscus level in the mercury column manometer (or the gauge pointer of the aneroid pressure gauge) to determine the blood pressure. The clinician listens for the five phases of blood flow sound known as the Korotkoff sounds (Drzewiecki et al., 1989; Hutton and Clutton-Brock, 1994).

When a soft tapping sound is first heard, this is referred to as phase I and is identified as the systolic pressure. As the cuff pressure continues to drop, the tapping sound becomes louder (phases II and III) and gradually diminishes to a muffling sound (phase IV) until the flow sound has disappeared completely (phase V). The cuff pressure at phase V is usually chosen as the diastolic pressure. However, this is not always possible. In some subjects, the blood flow sound persists until the cuff pressure reaches zero mmHg, for example, subjects who were undergoing intensive exercise, in children and in pregnant women. In such cases, clinicians may choose phase IV as the diastolic pressure (Hutton and Clutton-Brock, 1994; Kirkendall et al., 1980; Perloff et al., 1993; Petrie et al., 1986; Short, 1976).

An automated version based on the auscultatory technique uses a micro air compressor instead of the elastic air-bulb and a microphone instead of the stethoscope (Crombie et al., 1988; Regueiro-Gomez and Pallas-Areny, 1998; Shenoy et al., 1993). It analyses the Korotkoff vibration sounds of the blood flow, either in the frequency or in the time domain. They are then matched to the five phases of Korotkoff sounds to determine the blood pressure (Blank et al., 1988; Cozby and Adhami, 1993; Drzewiecki et al., 1989; Golden, Jr. et al., 1974; Maurer and Noordergraaf, 1976; McCutcheon et al., 1969; Ng and Small, 1994; Segall, 1975; Ware and Anderson, 1966; Wolthuis et al., 1974).

2.4.3 Oscillometry

The setup in oscillometry is very similar to the auscultatory technique except that a cuff pressure transducer is used instead of a stethoscope or a microphone. An inflatable encircling cuff is wrapped around the artery of interest, e.g. brachial or radial artery (Davis and Kenny, 2003). Prior to the measurement, the patient is asked to sit upright or lie in a supine position with the measured artery at the heart level. The patient is asked to relax and stay still during measurement to prevent recording of motion artefacts that will distort the cuff pressure measurement (Netea et al., 1999; Sykes et al., 1981; Terent and Breig-Asberg, 1994).

The cuff is inflated using an electrically operated small air compressor normally built-in inside a portable unit. The pneumatic setup is connected with low compliance rubber tubing. As the cuff is inflated to compress the artery, the pressure oscillation in the cuff is monitored by a pressure transducer. The oscillation is due to the arterial pulsation superimposed on the gradually increasing cuff pressure measurable by the pressure transducer. The cuff pressure is further increased until the oscillation has completely stopped.

When the oscillation component has disappeared, the cuff pressure is then deflated at a rate of 2 to 3 mmHg/s using electronically controlled pressure relief valve (Hutton and Clutton-Brock, 1994). During cuff deflation, the oscillation component in the measured cuff pressure will reappear and gradually increase in amplitude. The pulsation amplitude increases to a maximum and then gradually decreases until it disappears again. This phenomenon is due to the non-linear elastic properties of arterial wall and its surrounding tissue (Drzewiecki, 1995). An oscillation profile is constructed from the

series of pulsation amplitudes with respect to the cuff pressure. The profile is analysed using proprietary algorithms by each manufacturer to determine the systolic, diastolic and mean blood pressure values, and the heart rate.

Due to commercial reasons, specific algorithms used in each device are usually kept confidential (Staessen, 2000; Staessen et al., 2001). Nevertheless, several methods have been highlighted in published articles. For example, at the largest pulsation amplitude of the oscillation profile, the cuff pressure is estimated as the mean arterial pressure (Shimazu et al., 1989).

The systolic and diastolic pressures may be obtained using a pre-determined amplitude ratio from the oscillation profile during the cuff deflation process. The reported ratios vary from 0.45 to 0.75 and 0.60 to 0.86 for systolic and diastolic pressures respectively (Drzewiecki et al., 1994; Geddes et al., 1982; Kalaitzakis et al., 1988; Ng and Small, 1994; Sapinski, 1992; Ursino and Cristalli, 1996). Another algorithm that may be used is to monitor the rate of change of the pulsation amplitude during cuff deflation. The systolic pressure is obtained when the positive rate of change is the largest. Likewise, the diastolic pressure is obtained when the negative rate of change is the largest (Erlanger, 1916b; Geddes et al., 1982; Ng and Small, 1993; Shimazu et al., 1989).

The oscillometric measurement device currently available in the market has only been designed for single or intermittent measurements. Hence, it does not produce a continuous ABP waveform (Brinton et al., 1997; Chia et al., 1990; Lee et al., 2002; Lee and Westenkow, 1998).

2.5 Techniques for CoNIBP Measurement

Section 1.3 described a wide range of applications that require continuous ABP waveform. In the following sections, two CoNIBP measurement techniques are described. They are applanation tonometry and the volume clamping technique with photoplethysmography.

2.5.1 Applanation Tonometry

Applanation tonometry is the registration of an intra-arterial blood pressure pulse noninvasively by applying a pressure sensor on the external surface of an artery. The pulse waveform is measured when the arterial wall under the sensor is flattened. The theory of tonometry is based on the Imbert-Fick's principle (also known as the Laplace equation). According to the principle, the transmural pressure is inversely proportional to the radius of the artery and proportional to the arterial wall tension (Drzewiecki et al., 1983; Kemmotsu et al., 1991b; Markiewitz, 1960). The transmural pressure is the difference of the intra-arterial pressure minus the external pressure. Hence, when the arterial wall under the sensor is flattened, the radius becomes infinite, the radial wall tension is eliminated and the transmural pressure approaches zero. The principle assumes that the arterial wall is infinitely thin and the pressure attenuation through the tissue is minimal (Drzewiecki et al., 1983; Matthys and Verdonck, 2002; O'Rourke and Nichols, 2005).

The currently available tonometer is a hand-held pen-sized probe, with a flat strain gauge pressure sensor at the tip. Whenever possible, the measurement site is first placed

at the heart level. The artery is palpated to determine its location, usually the radial or carotid artery (Chen et al., 1996; Kelly et al., 1989). The tip of the probe is then placed transversely on the artery at the most prominent palpation location. When a pressure is applied from the tip of the probe to the artery, the pulse waveform is recorded. The accuracy of the measurement relies on a skilled placement of the probe on the artery.

To determine if the applanation is achieved, the tissue is first compressed through a range of pressure values which usually encompasses the physiological range of systolic and diastolic pressures. The pulse waveform is monitored simultaneously. When the pulse waveform with the largest pulse amplitude is obtained, it is estimated that the compressing pressure is the same as the mean ABP, giving a transmural pressure of zero. The compressing pressure that produces this largest pulse amplitude should be kept constant at this level as long as possible. The pulse waveform is then monitored at this state.

The tonometer requires a separate ABP measurement device, usually an auscultatory or oscillometric measurement device on the arm to measure the blood pressure intermittently. The tonometric pulse waveform is then calibrated in a corresponding ABP waveform (Drzewiecki et al., 1983; Kelly et al., 1989; Kemmotsu et al., 1991a; 1991b; Matthys and Verdonck, 2002).

To improve the sensitivity of the pressure sensor positioning, some designs are equipped with a multi-array of piezo-resistive pressure sensors to locate the artery more accurately (Birch and Morris, 2003; Drzewiecki, 1995; Drzewiecki et al., 1983; Kemmotsu et al., 1991b). The currently available tonometers are more suited for

recording the pulse waveform to assess arterial elasticity (Cameron et al., 1998; Chen et al., 1996; Cockcroft and Wilkinson, 2002; Davies and Struthers, 2003; Kelly et al., 1989; Millasseau et al., 2002; O'Rourke and Gallagher, 1996; Sugawara et al., 2007).

2.5.2 Volume Clamping Technique

The volume clamping technique is also known as the vascular unloading technique (Langewouters et al., 1998; Penaz, 1973; Rüddel and Curio, 1991; Yamakoshi et al., 1983; Yamakoshi et al., 1980) and the volume compensation technique (Kawarada et al., 1991; Tanaka and Yamakoshi, 1996; Yamakoshi et al., 1988; Yamakoshi, 1995). Measurement devices using this technique was developed to monitor the ABP in the finger (Lal et al., 1993; Penaz, 1992; Wesseling, 1996), brachial (Laurent et al., 2005) and superficial temporal (Tanaka and Yamakoshi, 1996) arteries. However, nearly all recordings in clinical and research protocols have been obtained from the finger artery due to the availability of the *Finapres*, and its later models *Portapres* and *Finometer* (Imholz et al., 1998).

The volume clamping technique incorporates the use of photoplethysmography as the sensor to monitor arterial blood volume changes. Photoplethysmography uses an infrared emitting light source to illuminate the tissue with the underlying artery. Depending on the measurement site, a photodetector is placed in either reflectance or transmittance configuration to measure the light transmitted through, scattered and/or reflected by the pulsating arterial blood. The recording of this photo-signal produces the photoplethysmogram (PPG).

Whenever possible, the measurement site is first placed at the heart level. When a range of increasing external compressing pressures is applied on the tissue with the underlying artery, there is a gradual reduction of arterial blood and extra-cellular fluid shift in the surrounding tissue. When recording the PPG, an oscillation component due to the pulsating arterial blood can be observed (an example waveform is shown in Figure 3.9). The oscillation component is superimposed on a gradual increase in the PPG baseline. The amplitude of the oscillation component increases to a maximum as the compressing pressure approximates the mean ABP.

The change in the PPG pulsation amplitude could be explained from the perspective of arterial non-linear compliance and transmural pressure (P_{tr}) (Drzewiecki et al., 1997; Yamakoshi, 1995). Compliance is the derivative of the arterial volume in relation to the arterial pressure (i.e. $\Delta V/\Delta P$); whereas, P_{tr} is the ABP minus the external compressing pressure. At low external compressing pressure, i.e. at positive P_{tr}, the artery is already partially distended. Variation in ABP during each cardiac cycle has a smaller effect on the change in arterial volume, hence a small pulsation amplitude in the PPG.

However, as the $+P_{tr}$ is decreased, the artery is less distended and its compliance increases. This leads to a PPG pulsation amplitude that is increasingly larger. As the $+P_{tr}$ is approximately zero, the external compressing pressure equals to the mean ABP. At zero P_{tr}, the artery is considered to have reached its unloaded state, where the arterial wall is neither distended nor compressed (Wesseling et al., 1995; Yamakoshi et al., 1980). The arterial compliance is at the maximum and the largest pulsation amplitude can be observed in the PPG (Boehmer, 1987; Penaz, 1995). The mean of the PPG pulse at this compressing pressure is estimated as a reference value (Penaz, 1992; Yamakoshi

et al., 1980). Then, at negative P_{tr}, the artery is compressed beyond the systolic pressure until it fully collapses. Hence, the PPG pulsation amplitude gradually reduces until it is zero.

By incorporating a servo-feedback control mechanism, the ABP monitoring device is designed to partially compress (hence 'volume clamping') the artery with the real time PPG maintained at the reference value mentioned above. As the arterial blood volume changes with cyclical blood flow, the servo feedback continuously adjusts the external compressing pressure to clamp the arterial blood volume constant at this reference value. For example, when the blood volume reduces at a lower blood pressure, the PPG signal increases; the servo feedback instantaneously reduces the compressing pressure to allow more blood into the tissue. This decreases the PPG until it returns to the reference value. Conversely, when the blood volume increases at a higher blood pressure, the PPG signal reduces; the servo feedback instantaneously increases the compressing pressure to allow less blood into the tissue. This increases the PPG until it reaches the reference value. The compressing pressure is recorded continuously thus representing an estimate of the intra-arterial blood pressure.

The PPG reference value is reviewed from time to time due to the change in physiological conditions. During this review process, the continuous ABP monitoring is temporarily interrupted. The PPG reference value is then updated and the servo-feedback control operation is recommenced.

2.6 Potential Causes of Error in ABP Measurement

Sections 2.4 and 2.5 presented an overview of the main noninvasive measurement techniques. The description of each measurement technique is based on ideal conditions. However, there are various factors, whether technical, environmental or physiological that may potentially affect the accuracy of noninvasive measurements. Awareness of these potential causes of error is crucial when developing a new ABP measurement device. The potential causes of error for intravascular catheterisation are not included in order to focus on the noninvasive techniques.

Some of the potential causes of error are common to at least two of the noninvasive techniques, while others are specific to a given technique. The common causes of error are first presented, this is then followed by the specific causes of error for each technique.

Table 2.1 shows a list of the potential causes of error common to at least two of the noninvasive measurement techniques. The potential causes of error are grouped as the technical, environmental and physiological factors. The technical factor refers to the incorrect measurement setup or incompetent interpretation of measurements; the environmental factor refers to the disturbance from the surroundings; and the physiological factor refers to central, peripheral or local changes of physiological conditions. These factors are indicated as ‘t’, ‘e’ and ‘p’ respectively in brackets in Table 2.1. Other factors, such as the influence of drugs or medication are not considered. The following paragraphs describe the potential causes of error specific to each of the noninvasive ABP measurement techniques.

Table 2.1 Potential causes of error in noninvasive ABP measurement.
Each tick (✓) means that the specific potential cause of error can affect the accuracy of ABP measurement using the respective noninvasive measurement techniques.

	Potential causes	Noninvasive Measurement Technique			
		Auscultatory	Oscillometry	Applanation Tonometry	Volume clamping with photoplethysmography
1.	Encircling cuff fitting [(t)]	✓	✓		✓
2.	encircling cuff size [(t)]	✓	✓		✓
3.	cuff deflation rate [(t)]	✓	✓		✓
4.	Electronic noise [(t)]	✓ *	✓	✓	✓
5.	Area under external compression [(t)]	✓	✓	✓	✓
6.	Leakage or kinking in the pneumatic connections [(t)]	✓	✓		✓
7.	Placement and positioning of sensor relative to location of artery [(t)]	✓	✓	✓	✓
8.	Low ambient temperature [(e)]		✓	✓	✓
9.	Motion artefacts [(p)]	✓	✓	✓	✓
10.	Hydrostatic pressure difference [(p)]	✓	✓	✓	✓
11.	Skin burns, or injuries close to artery [(p)]	✓	✓	✓	✓
12.	Irregular heart rate or cardiac output [(p)]	✓	✓	✓	✓
13.	Hypotension / weak arterial pulse [(p)]	✓	✓	✓	✓
14.	Arterial sclerosis or stiffening [(p)]	✓	✓	✓	✓

Additional notes:
* applies to automated device only.
[(t)] technical factor
[(e)] environmental factor
[(p)] physiological factor

Auscultatory technique

The first two causes of error are common to both the manual and automated devices, whereas the rest are specific to either the manual or the automated device as indicated in brackets:

- choice of Korotkoff sound phase IV or V for diastolic pressure;
- estimation of the mean ABP as $\frac{\left(P_{systolic}+2P_{diastolic}\right)}{3}$ (Kobayashi et al., 1990; Rogers and Oosthuyse, 2000). Ideally, the mean pressure is the integrated average in each cardiac cycle. However, this can only be calculated from a continuous ABP waveform (Chemla et al., 2005);
- hearing acuity of clinician (*manual*) (Hessel, 1986; Neufeld and Johnson, 1986; Pereira et al., 1985);
- placement of stethoscope (*manual*);
- observer bias of the pressure scale on the mercury column manometer or the aneroid pressure gauge (*manual*) (Rithalia et al., 1999);
- calibration of mercury column manometer or aneroid gauge (*manual*) (Davis and Kenny, 2003);
- frequency response of microphone (*automated*);
- interference of ambient noise on microphone (*automated*).

Oscillometric technique

- It has been reported that many automated devices have not been validated according to approved protocols (Amoore et al., 2010; O'Brien and Atkins, 1994; Sims et al., 2005a; Sims et al., 2005b; van Egmond et al., 1993). Often, the algorithms used by these devices cannot be scrutinised due to commercial implications.

Applanation tonometry

- Inappropriate compressing pressure manually applied on the artery. This could lead to a recording of poor quality pulse wave;
- Calibration of the pulse waveform into blood pressure requires a separate ABP measurement device from a different artery. This can affect the accuracy of the ABP waveform mainly for recordings lasting several minutes (Drzewiecki et al., 1983);
- Poor mechanical stability of transducer positioning which limits duration of recordings to only a few cardiac cycles.

Volume clamping technique

- Bright ambient lighting interferes with the photocurrent generated in the photodetector;
- Dark skin colour attenuates more of the emitting light source. This may generate smaller PPG pulse amplitude and hence smaller signal-to-noise ratio (Magee and Tooley, 2005).

In summary, the evaluation for the potential causes of error shows that no single method is immune to measurement errors. Effort to prevent these errors is important to minimise their influence on the accuracy of noninvasive ABP measurements.

2.7 Selection of a Suitable ABP Measurement Technique

An overview of the operation principles of noninvasive ABP measurement techniques was presented in sections 2.4 and 2.5. Section 2.6 then presented the potential causes of error that can affect the accuracy of noninvasive ABP measurements. Through the selection process described in section 2.3, the STA was chosen as the alternative ABP measurement site.

The STA was measured using the auscultatory (Shenoy et al., 1993) and volume clamping (Tanaka and Yamakoshi, 1996) techniques. However, they were at the research and development stages, no further evaluations of these devices were published. Hence, it has not been possible to keep track of their development. No published articles were found for monitoring the STA using the applanation tonometry or the oscillometric technique. The oscillometric technique has never been validated for continuous ABP measurement and for this reason will not be considered further.

With the applanation tonometry, a separate ABP measurement device on a different artery is required to calibrate the tonometric pulse wave into an ABP waveform. This requirement imposes technical and practical limitations. Using a different artery for calibration, for example, based on systolic values is highly questionable. Moreover, the long term reliability of each calibration event is uncertain and frequent calibrations are not practical and can be disruptive in many monitoring or measurement protocols.

With the auscultatory measurement device, it was reported that the Korotkoff vibration sound in the STA did not exhibit the same distinctive phases as those of the brachial

artery. The vibration sound is also much smaller in amplitude than the brachial artery. Hence, it may be more susceptible to ambient noise interference (Shenoy et al., 1993).

With the volume clamping technique, one advantage is that self-calibration can be carried out during continuous ABP monitoring. Also, comparison with other CoNIBP measurement devices, for example, the *Finapres*, will be more straightforward as it uses the same measurement technique.

The considerations above suggest that arterial volume clamping is the best candidate noninvasive technique to measure ABP in the STA continuously. The outcome of this selection process shows the same measurement technique used by Tanaka and Yamakoshi on the STA (1996). Nevertheless, as mentioned in section 2.2, their contributions were not followed by further communications, evaluative studies or industrial developments. The limitations of their device were also noted. It was mainly regarding the long duration of fixing the PPG sensor fastened tightly around the head with a head belt, resulting in subjects feeling uncomfortable or slightly dizzy. This is possibly due to continuous compression of arteries and/or veins in the extracranial region.

Despite initial development by Tanaka and Yamakoshi, the design and development of a new device to measure ABP continuously in the STA still presents a considerable challenge given the lack of a blueprint or any technical details about such device. Furthermore, the evaluation of this new device and more in-depth analysis of its performance should also be regarded as original work worthy of a dedicated research project.

2.8 Conclusion

This chapter has taken a systematic approach to select an alternative ABP measurement site with a suitable measurement technique. The evaluation has also raised the awareness that none of the measurement techniques is immune to potential causes of error. This needs to be taken into consideration when a new measurement device is developed.

The STA has been chosen as the alternative measurement site and the ABP will be monitored using the volume clamping technique with photoplethysmography. Chapter 3 will describe the system architecture of this new device, known as the *STAbp*. The prototype will then be evaluated in chapter 4.

CHAPTER 3 SYSTEM ARCHITECTURE

3.1 Introduction

Chapter 2 described the systematic approach taken to select an alternative ABP measurement site with a suitable measurement technique. The STA was chosen and the volume clamping technique with photoplethysmography will be used to monitor the ABP continuously. The operation principle of the volume clamping technique was described in section 2.5.2. To implement this technique, a prototype device was designed and built. It will be referred to as the *STAbp*.

The objectives of this chapter are:

i. To set out the design criteria for the *STAbp* prototype device (section 3.2);

ii. To describe the instrumentation of the *STAbp* (section 3.3);

iii. To carry out initial assessments of the *STAbp* (sections 3.4);

iv. To present illustrative measurement results of the *STAbp* (section 3.5). This will be followed by discussion (section 3.6) and conclusion (section 3.7).

3.2 Design Criteria

The working principle of the volume clamping technique described in section 2.5.2 indicates that different components of hardware and software are required. These components are integrated as a continuous ABP monitoring device. To achieve this, the main design criteria were first set out as follows:

i. Wavelength of emitting light source

Different constituents in living tissue have varying absorption and scattering properties to emitting light sources of different wavelengths (Mobley and Vo-Dinh, 2003). The arterial blood in the STA will need to have a distinctive absorption rate to a specific wavelength in comparison with its surrounding constituents, especially water, melanin, skin and the skull. This means that light scattered or reflected from the tissue represents the blood volume change in the STA when the tissue is illuminated with a chosen wavelength.

ii. Photo-detection

To measure the scattered or reflected light from the tissue, a photodetector is required. The photodetector needs to have a peak wavelength sensitivity matched to the wavelength of the emitting light source. This is important to attenuate interference from ambient lighting. The light emitter and the photodetector will be collectively known as the optoelectronic components in the rest of the thesis.

iii. Frequency Response

The frequency response of the *STAbp* needs to exceed the frequency content of the ABP waveform. This is important to obtain an accurate recording of the waveform.

iv. Compression on the STA

The artery needs to be compressed by a range of external pressures which encompasses the systolic and diastolic pressures. This is necessary for the determination of appropriate PPG setpoint (*Setpt*), which will be defined in section 3.3.7. As will be described later, the *Setpt* has major implications for the accuracy of the *STAbp*.

v. Pressure sensing

A pressure sensing mechanism is required to monitor the external compressing pressure which is applied on the tissue with the underlying STA.

vi. Size

The means to externally compress the STA as well as to monitor the blood volume change with the optoelectronic components is constrained by the anatomy at the temporal region. Hence, appropriate size and dimensions of these components are important. Portability is not crucial for the prototype device.

vii. Weight

The optoelectronic components and the means of compressing the STA need to stay fixed throughout the ABP monitoring. To maintain the position of these components, some form of fastening and support is necessary. The issue of weight is more critical at the front end where these components are to be placed and fixed over the STA. The

weight distribution of the fastening and support mechanism needs to be balanced to minimise any potential turning moment or additional pressure applied on the STA.

viii. Comfort

For continuous ABP monitoring, the placement of the optoelectronic components, the pressure sensing mechanism, and the fastening and support mechanism are fixed for a relatively long duration. Hence, comfort for the subject needs to be taken into account. Physical movement, for instance, due to discomfort may generate motion artefacts that interfere with the ABP monitoring.

ix. Data Management

Relevant input signals, e.g. the ABP and PPG waveforms, need to be recorded, processed and displayed. The selected hardware needs to have sufficient memory space for data storage and a suitable display screen. The hardware also needs to incorporate suitable software to allow real time signal processing and continuous ABP monitoring.

x. Safety Considerations

Prior to use, the safety aspects of the design need to be considered. These aspects aim to comply with the British Standard BS EN 60601-1 for patient and operator safety. They are as follows:

a) Upper limit of compressing pressure: automatic protection needs to be included if the external compressing pressure reaches an upper threshold.
b) Leakage current: the prototype device is to be electrically safety tested; the leakage current flow through the subject must be within the safe limit.

c) Tissue heating: due to localised illumination by the emitting light source, it is necessary to ensure that generated heat does not cause excessive local heating on the tissue.

d) Risk of tissue ischaemia: ensure that normal blood flow in the head is not obstructed during ABP monitoring.

The fulfillment of these design criteria will be addressed where relevant in the following sections 3.3 to 3.5.

3.3 Instrumentation

Figure 3.1 shows a block diagram of the *STAbp* integrated prototype device based on the volume clamping technique. Labels with prefixes G, R and C are used in the figure. The definitions of these prefixes apply to the rest of the chapter. Prefix G refers to a block where an input is converted to an output; prefix R refers to the command output signals from the PC operating base; and prefix C refers to signal flow between specific blocks. Table 3.1 explains the meaning of each label.

The operation principle of the volume clamping technique was described in section 2.5.2. The following subsections will describe each block separately while establishing their connections as part of a complete system.

3.3.1 Probe

In Figure 3.1, the shaded box labelled as probe consists of two components, i.e. the blood volume sensor (G1) and the regulated compressing pressure (G3). The shaded box only encloses part of G1 and G3 because these two blocks include other subcomponents that are not fitted into the probe. G1 will be described in this section, whereas G3 will be described in section 3.3.3.

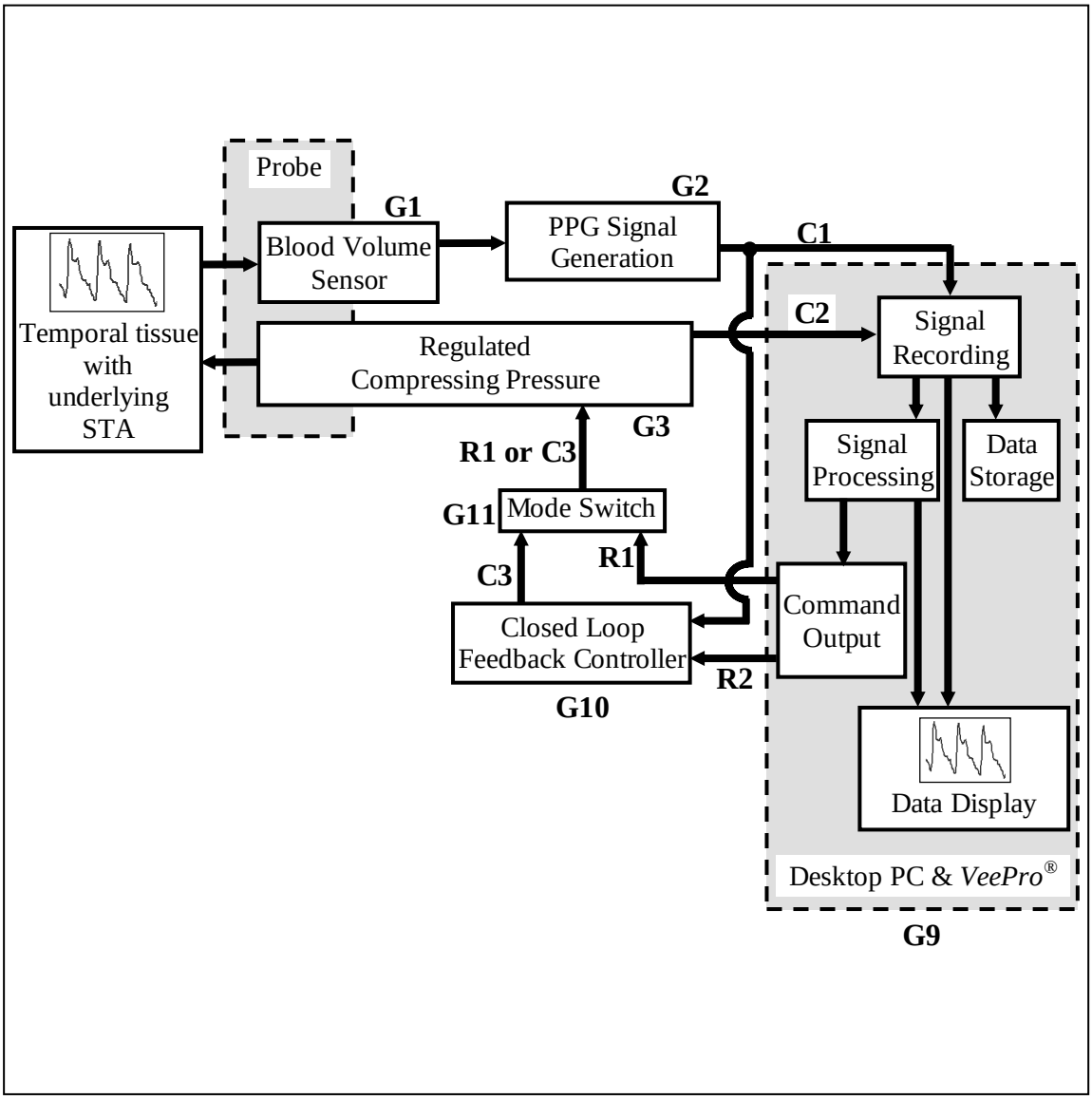

Figure 3.1 Block diagram of the STAbp integrated prototype device.
Individual blocks are labelled with prefix G. Each of them is described separately in section 3.3. The STAbp is required to monitor the arterial blood volume change in the STA to generate a PPG signal. The PPG waveform is then analysed to produce a reference value that can be used in the closed loop feedback operation to continuously measure the ABP in the STA. The real time ABP is recorded, stored and displayed. The labels with prefixes G, R and C are explained in Table 3.1.

Table 3.1 Explanation of labels in Figure 3.1.
G4 to G8 are not shown in Figure 3.1 but will be described in section 3.3.3. The 'Setpt' will be defined in section 3.3.7.

G1	blood volume sensor
G2	PPG signal generation
G3	regulated compressing pressure, consists of five sub-blocks:
	G4 regulated compressed air supply
	G5 controller
	G6 piezo valve
	G7 inflatable sealed air chamber
	G8 pressure transducer
G9	computer base and software
G10	closed loop feedback controller
G11	mode switch
R1	command output for *Open Loop Procedure* (= required compressing pressure)
R2	command output for *Closed Loop Procedure* (= *Setpt*)
C1	real time PPG signal
C2	transducer pressure output
C3	closed loop feedback controller output

G1 consists of an infrared emitting diode (IRED) and four photodetectors. The IRED illuminates the tissue with the underlying STA, while the photodetectors measure the scattered and reflected infrared light from the tissue. Multiple photodetectors are useful to identify the most probable location of the STA.

The circuit diagram for the optoelectronics is shown in the Appendix (Figure A.1). The IRED driver circuit uses a low current supply to switch on the IRED. Low current supply minimises the risk of local heating on the tissue in the temporal region. The peak emission wavelength of the IRED is 880 nm (SME2470, Honeywell). This is within the diagnostic window dedicated to physiological monitoring in the electromagnetic wave spectrum (Mobley and Vo-Dinh, 2003). The photodetectors (SMD2420, Honeywell) have matching peak wavelength sensitivity to the IRED. The dimensions for each of the optoelectronic components are small (height 2.1 mm x length 3.8 mm x width 2.5 mm).

Figure 3.2 shows the prototype design of the probe. A small circuit board is fitted inside the front end of the probe which has an internal diameter of 14 mm. The circuit board consists of an IRED at the centre surrounded by four photodetectors, all soldered equidistantly from the IRED at 4.5 mm. Their distances are above the minimum distance advised by the manufacturer to avoid cross talk.

The probe is made of lightweight brass. The advantages of brass are that it does not rust and it is a strong material. The front end surface of the probe is covered with a thin non-compliant layer of polyethylene, sealed with a white acetal ring to form an inflatable air chamber. When fully inflated, it forms the shape of a dome with a diameter of

approximately 18 mm. The inflatable sealed air chamber is also part of G3, which will be mentioned again in section 3.3.3.

The inflatable air chamber and optoelectronic components are connected close to a separate interface unit through a rigid and hollow shaft of the probe. The interface unit consists of the remaining components of G1 and G3.

The interface unit is connected close to the probe for two reasons. First, low compliance pneumatic tubing is used to allow air flow in and out of the sealed air chamber through the shaft as the compressing pressure is changed. The length of the pneumatic tubing between the probe and the interface unit is kept short to minimise the total air volume. This is important to improve the frequency response.

Second, the wiring for the optoelectronic components is aligned through the shaft to be connected to the interface unit where the remaining components of G1 are located. The wiring is kept as short as possible. They are electrically shielded individually to minimise signal cross talk. The probe itself is also electrically shielded to further attenuate external electromagnetic interference.

In addition to these two reasons, the shaft is required to be fastened onto a specially designed head frame so that the front end of the probe is fixed on the skin surface with the underlying STA. The length of the shaft is 7.5 cm. The head frame is described in the next section.

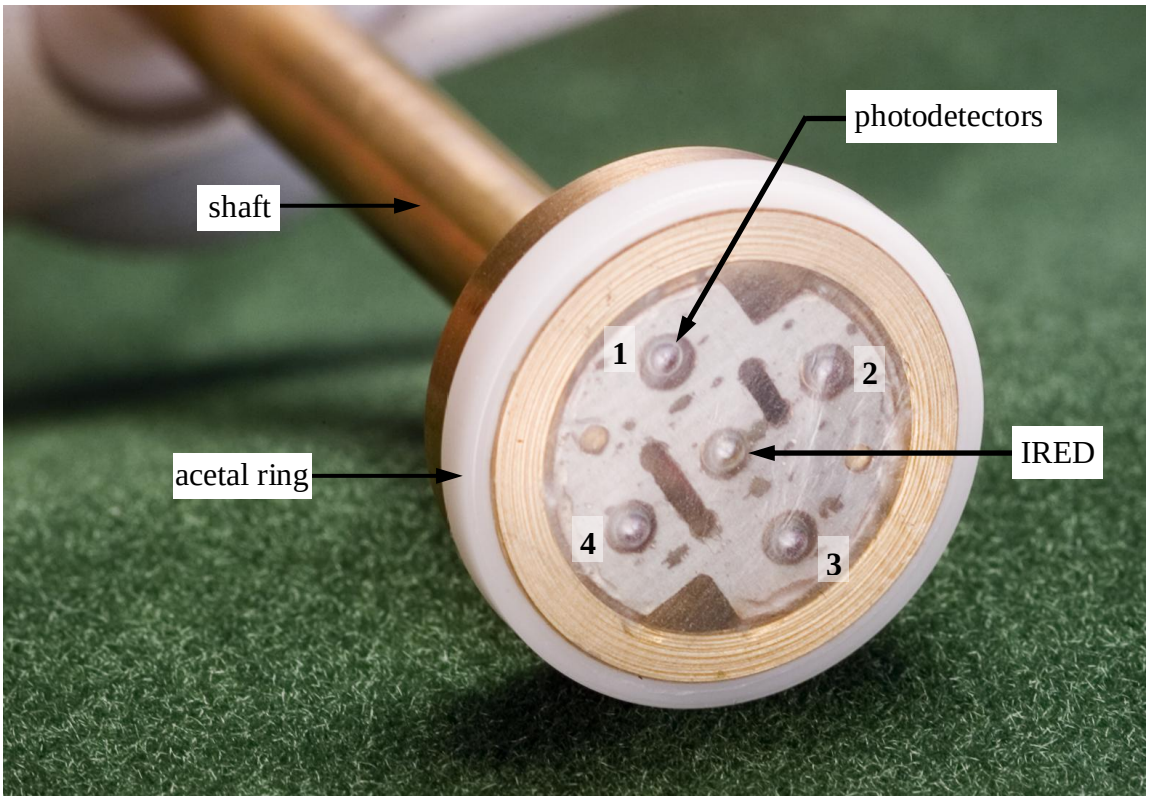

Figure 3.2 The prototype design of the probe for the STAbp.
The probe consists of a chamber built-in with four photodetectors numbered 1 to 4, arranged equidistantly from an infrared emitting diode (IRED) at the centre. The front-end surface of the probe is covered with a thin non-compliant layer of polyethylene, sealed with a white acetal ring to form an inflatable air chamber. The front end of the probe is extended to the back with a shaft. See text in section 3.3.1 for detailed description.

3.3.2 Head Frame

A custom designed head frame is required to maintain the distance between the front end of the probe and the STA. To determine the size of the head frame, measurements of head dimensions (i.e. length and width) at the level of the temporal region were taken from 31 adults (18 males, 13 females, age (mean ± SD) 35 ± 9 years). The length of the head is the horizontal distance between the anterior and posterior of the head at the said level, whereas the width is the horizontal distance between the right and left side of the head at the same level. These gave an average (SD) of 18.7 (1.30) cm and 15.4 (1.04) cm respectively. To include all subjects, a simple circular head frame was constructed, based on the largest length or width measurement, whichever greater, as the internal diameter. This was found to be 21 cm.

Figure 3.3 shows the prototype design of the head frame. It consists of four components:

i. a rigid circular frame: The internal diameter is 22 cm. It is slightly larger than the adult head dimensions described above. This is to provide sufficient spacing for all the necessary brackets to be fastened onto the frame with the probe positioned over the STA. The circular frame is made of lightweight aluminium.

ii. bracket for the probe: It is a specially designed bracket to fix the position and the orientation of the probe. Two such brackets are shown in Figure 3.3. Each holds a probe placed on both sides of the head (indicated by circles). Although the photograph shows the placements of two probes, the *STAbp* is designed to operate one probe at a time only. Each bracket has a slot along its length. It allows the probe to slide vertically and horizontally, and then fastened in an angle relative to

the bracket. The probe can be placed above or below the circular frame. This versatility is necessary to cater for different head dimensions and the location of the STA. The probe and the bracket are designed to monitor the right or left STA when fastened. When the position of the probe is decided, the bracket itself can be tightened onto the circular frame with a screw;

iii. four support brackets: Two of the four support brackets are shown in Figure 3.3 (indicated by arrows). They have been constructed to maintain the position of the circular frame relative to the head during continuous ABP monitoring. These support brackets were initially equipped with a small square head with soft padding (as shown in the figure). The soft padding is pressed against the scalp when the brackets are fastened. However, the square head was later replaced with a longer and slim metal plate covered with soft padding. The larger area of padding distributes the pressure more evenly on the scalp. This minimises discomfort and potential tissue ischaemia;

iv. an overhead support frame: This is to prevent the circular frame from sliding downward when loaded with the probe and all the necessary brackets. Hook-and-loop (*Velcro*®) straps were used as the overhead support frame. *Velcro* straps are flexible and lightweight. They are also easy to adjust. Furthermore, the straps were found more comfortable than other alternatives to support the weight of the frame.

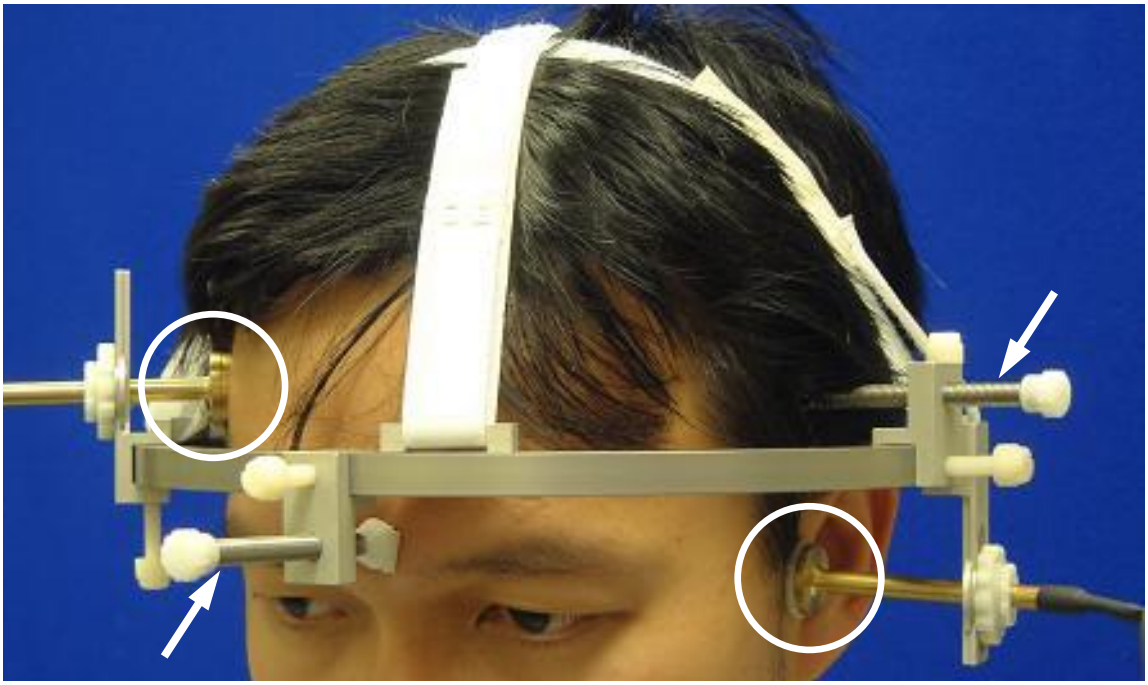

Figure 3.3 Prototype design of the head frame for the STAbp.
The head frame consists of four components. They are the rigid circular frame, the brackets for the probe, the additional support brackets, and the overhead support frame. This photograph shows the placement of two probes (indicated by white circles) to demonstrate the versatility of the brackets to cater for different head dimensions and location of the STA. Nevertheless, the STAbp is designed to operate one probe at a time only. Additional support brackets with screws (indicated by white arrows) and overhead Velcro straps are available to immobilise the probe and the circular frame against the head during continuous ABP monitoring. See text in section 3.3.2 for detailed description.

3.3.3 Regulated Compressing Pressure

Referring to Figure 3.1, a regulated compressing pressure (G3) is required to control the pressure applied on the tissue with the inflatable sealed air chamber in the probe. To achieve this, Figure 3.4 shows the contents of G3. It consists of five sub-blocks, i.e. the regulated compressed air supply (G4), controller (G5), piezo valve (G6), inflatable sealed air chamber (G7) and pressure transducer (G8).

G3 has one input and two outputs. Input R1 (or C3) is the required compressing pressure. Output C2 is the pressure measurement obtained with the pressure transducer (G8). The inflatable sealed air chamber (G7) applies compressing pressure on the STA.

G4

The arrangement of G4 is shown in the Appendix (Figure A.2). A micro air compressor (Medo AC0105), capable of supplying 2.6 l/min of air, is more than adequate to provide the necessary flow rate in the sealed air chamber (G7). The output of the compressed air is connected to a pressure regulator (Airtrol R-920-10) to produce a constant pressure at 5 psi (approximately 260 mmHg). The regulated pressure output is connected to the inlet of the piezo valve (G6). It is also connected to a pressure switch (Airtrol F-4200-15) and a pressure transducer (PrTx2). The pressure switch operates as a safety precaution to switch off the air compressor in the event of the regulated pressure exceeding 5 psi. This is important to prevent sudden exertion of high pressure onto the temporal tissue. The pressure transducer is included to monitor the stability of the regulated pressure output (note: PrTx2 and G8 are two separate pressure transducers).

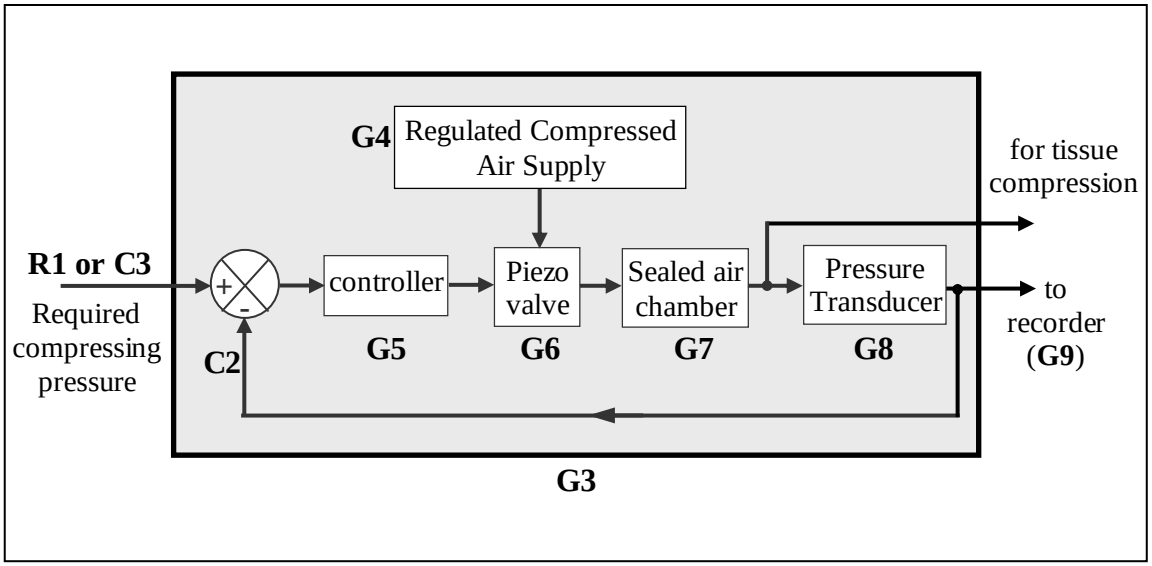

Figure 3.4 Block diagram of the regulated compressing pressure (G3).
G3 consists of five sub-blocks (G4 to G8) with one input and two outputs. Input R1 (or C3) is the required compressing pressure and output C2 is the pressure measured with the pressure transducer (G8). The inflatable sealed air chamber (G7) applies compressing pressure on the STA. C2 also provides a negative feedback signal to generate regulated compressing pressure in G3. See text in section 3.3.3 for detailed description.

G6

G6 is a 3/2 way piezo valve (Hoerbiger-Origa PS11010-31LR). The structure of G6 is shown in the Appendix (Figure A.2). It consists of a strip of element that bends in response to a change in potential difference applied on two points of the element (Hoerbiger, 2004). To inflate G7, the piezo element is bent to close its relief port temporarily. Conversely, to deflate G7, the piezo element is partially bent in the opposite direction to open the relief port to release air.

G5

The bending characteristic of G6 is not linearly related to the applied potential difference. This is overcome by incorporating a controller (G5) to linearise the compressing pressure in G7. Without this, hysteresis occurs when G6 is used on its own. The tuning process of G5 is explained in more detail in the literature (Astrom and Hagglund, 1995; Shinskey, 1999). The electronic circuitry of G5 is shown in the Appendix (Figure A.3).

G8

Output C2 from G8 serves two purposes. Firstly, it is part of the closed loop negative feedback to control the air flow in G6 and compressing pressure in G7 at the required pressure by input R1 (or C3).

Secondly, C2 is recorded to represent the ABP in the STA when the tissue is compressed by G7 to maintain the real time PPG signal at the *Setpt*. C2 is calibrated as 100 mmHg/V. *Setpt* will be defined later in section 3.3.7. G3 and C3 will be mentioned

again later in sections 3.3.5 and 3.3.6 to describe G10 and G11 respectively. The circuit diagram of G8 is shown in the Appendix (Figures A.4).

3.3.4 PPG Signal Generation

Following the photo-signal generated in the blood volume sensor G1 (Figure 3.1 and section 3.3.1), signal conditioning is required to obtain a PPG waveform with satisfactory signal-to-noise ratio. The PPG signal generation is labelled as G2. The circuit diagram of G2 is shown in the Appendix (Figures A.5).

The circuitry of G2 consists of a unity gain low pass filter with a cut-off frequency of 20 Hz to attenuate noise (Peura, 2009). The low pass filter is also beneficial for anti-aliasing when the signal is digitally sampled. An 8^{th} order Bessel Sallen-Key configuration is used (Karki, 2002b; 2002a). This filter design gives a flat response in its frequency band and a steep roll-off from its cut-off frequency. It also gives maximum phase flatness throughout the passband. The filtered signal is further amplified with sufficient gain (approximately 50 times) to optimise dynamic range.

3.3.5 Closed Loop Feedback Controller

Referring to Figure 3.1, the closed loop feedback controller is labelled as G10. The circuit diagram of G10 is shown in the Appendix (Figure A.6). G10 has two inputs and one output. R2 is the PPG *Setpt* output from G9 and C1 is the real time PPG from G2. R2 subtracts C1 to generate an error signal into the controller to generate a control output C3. *Setpt* will be defined in section 3.3.7.

The control output C3 is fed to G3 (Figures 3.1 and 3.4) to adjust the compressing pressure in the sealed air chamber (G7) to clamp the tissue in the temporal region at *Setpt* (=R2).

Figure 3.1 shows that G3 only receives one input at a time, i.e. either R1 or C3. For continuous ABP monitoring, the *STAbp* is designed to automatically switch between these two inputs without having to restart the ABP monitoring process. To achieve this, a mode switch is incorporated before G3 to select the input R1 or C3 during the operation of the *STAbp*. The mode switch is described in the next section.

3.3.6 Mode Switch

The regulated compressing pressure (G3) is controlled by two possible inputs, i.e. R1 or C3. R1 is used when a range of compressing pressures is applied to the tissue to obtain the PPG pulse amplitudes profile. C3 is used when the compressing pressure is continuously adjusted to maintain the artery at the *Setpt* (=R2).

A mode switch (G11) is incorporated before G3 to alternate R1 and C3 (Figure 3.1). The schematic diagram of G11 is shown in the Appendix (Figure A.7). G11 consists of a comparator, a flip-flop circuit and an analog switch (Philips Semiconductors, 1995; Philips Semiconductors, 2001). Input R1 is enabled in G11 during the *Open Loop Procedure* whereas input C3 from G10 is enabled during the *Closed Loop Procedure*. The output from G11 (i.e. R1 or C3) then controls the compressing pressure in G3. The *Open*- and *Closed- Loop Procedures* are described in the next section.

3.3.7 Operating Base and Software

The operation of the *STAbp* is coordinated by the operating base and software, labelled as G9 in Figure 3.1. The tasks of G9 include signal recording, signal processing, command output, data storage and data display. The operating base is the desktop computer incorporated with the Agilent *VEEPro*® *6.2* graphical programming software. Digitisation of the input signals is performed with an 8-channel analog-to-digital converter with 12-bit resolution (DT300, Data Translation®). The sampled input signals are stored continuously into a dedicated file in the hard disk during ABP monitoring. They are stored in an appropriate format convenient for offline data review. The real time ABP waveform can also be displayed on the screen.

G9 has two main inputs and two outputs. The inputs are labelled as C1 and C2, whereas the outputs are labelled as R1 and R2:

- C1 is the real time PPG waveform. The waveform is analysed and processed to generate a suitable *Setpt* as command output R2;
- C2 is the output from the pressure transducer (G8) that monitors the compressing pressure in the inflatable sealed air chamber (G7). C2 also indirectly records the intra-arterial pressure in the STA;
- R1 is the required compressing pressure input to G3;
- R2 is the PPG *Setpt*.

The *Setpt* is the PPG reference value which will be defined in the next subsection. It is required in the closed loop feedback control operation (G10) when the ABP in the STA is continuously monitored. The *Setpt* is updated from time to time due to physiological changes in the tissue. To achieve this, the software algorithm is developed into two

main functions, known as the *Open Loop Procedure* (*OLP*) and the *Closed Loop Procedure* (*CLP*). The *OLP* is activated at each start-up of the ABP monitoring process. When the *OLP* is complete, the *CLP* is activated and repeats in a loop for the rest of the continuous ABP monitoring until the operation of the *STAbp* is externally terminated. The following subsections first describe the *OLP*. The *CLP* is then described with its subfunction known as the *Setpt Self-Update*.

3.3.7.1 Open Loop Procedure

Figure 3.5 shows the flowchart of the *OLP*. The operation of the *STAbp* is first started (1). The compressing pressure in the sealed air chamber (G7) is increased (e.g. 70 mmHg) to slightly compress the artery (*2*). This is achieved by applying R1 to G3 (Figure 3.1 and section 3.3.3). The slight compression on the artery tends to generate better quality PPG waveforms. PPG from each of the four photodetectors is then recorded for several cardiac cycles (*3*). The PPG waveforms are then visually assessed. The photodetector with the best signal is selected for continuous ABP monitoring (*4*). With the selected photodetector, the compressing pressure is temporarily reduced below the diastolic pressure before it is increased again in steps of 5 mmHg (*5*) until it is above the systolic pressure. As the artery is gradually compressed by G7, the PPG and compressing pressure are simultaneously recorded by G9 (*6*). To determine the *Setpt*, the PPG pulse with the largest pulsation amplitude is first located (*7*). The corresponding compressing pressure when this PPG pulse occurs is retrieved as *refPr* (*8*). The mean of the PPG pulse with the largest pulsation amplitude is computed as the *Setpt* (*9*). The compressing pressure is then adjusted to *refPr* and output as R1 (*10*). Finally, the *OLP* is completed and the *CLP* is activated (*11*).

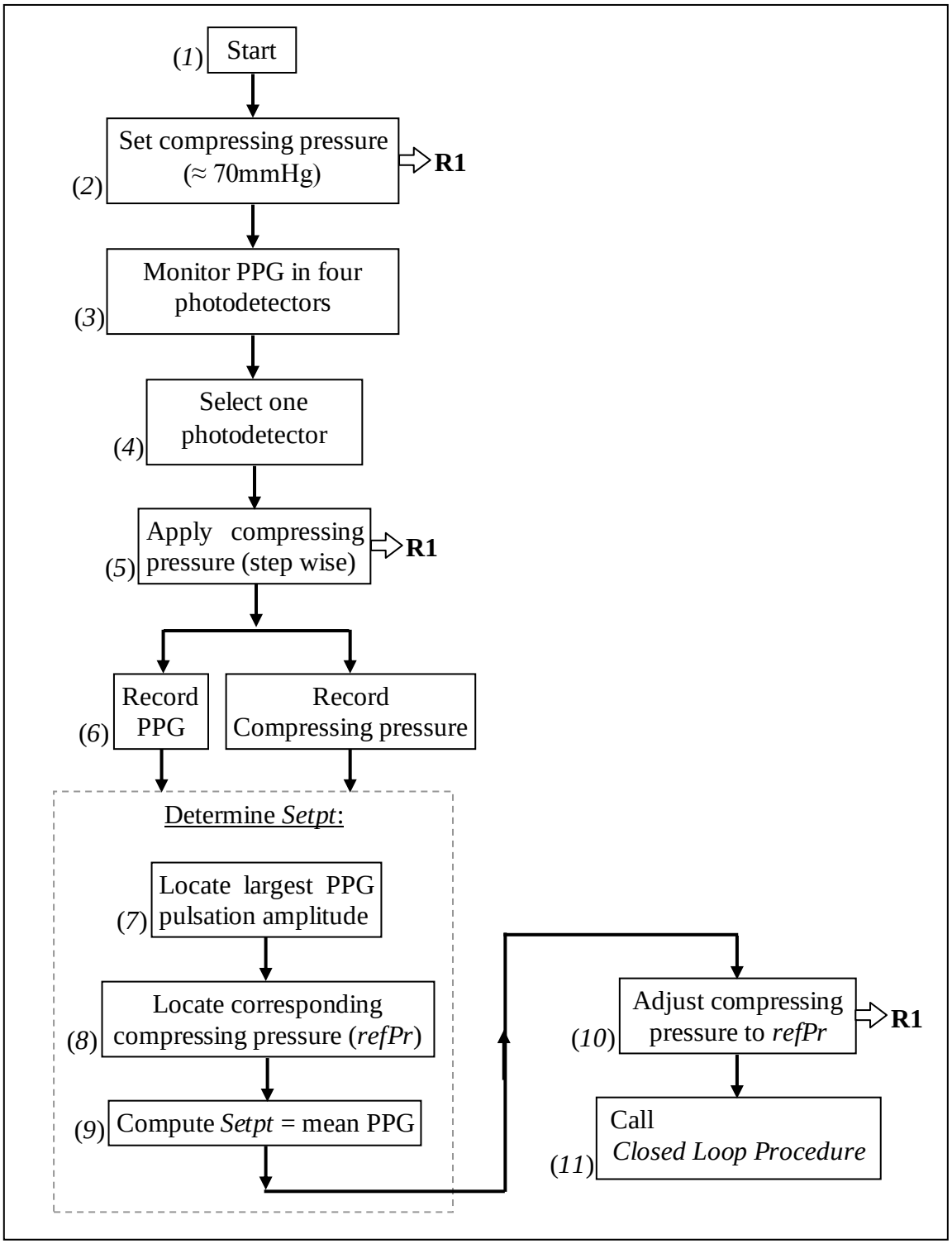

Figure 3.5 Flowchart of the Open Loop Procedure (OLP).
The activation of OLP kick starts the operation of the STAbp. The light arrows indicate that R1 is the output from G9 that represents the required compressing pressure on the STA (Figure 3.1 and section 3.3.3). During the OLP, the Setpt and refPr are determined before the CLP is activated. See text in section 3.3.7.1 for detailed description.

3.3.7.2 Closed Loop Procedure

CLP is activated immediately after the *OLP*. The continuous ABP monitoring is temporarily interrupted from time to time by the *CLP* subfunction, *Setpt Self-Update*, to obtain an updated *Setpt*. The time interval between consecutive *Setpt* re-evaluation is dependent on the absolute percentage change between consecutive *Setpt*. The default timer duration is 10s.

Figure 3.6 shows the flowchart of the *CLP*. The *Setpt* determined during the *OLP* is output as R2 from G9 to G10 (*1*). The ABP is monitored continuously (*3*) until the timer is up (4). When the timer is up, the absolute percentage difference between consecutive *Setpt* is compared (*5*). If the absolute percentage difference is within 10%, the timer duration is increased at 5s increment steps (*6*). Otherwise, it is reset to its default 10s (*7*). This new timer duration is only used after the operation of the subfunction is complete (*8*) and it returns to the beginning of the *CLP* (*2*). The *CLP* is repeated in a loop until it is externally terminated by the operator. When the *CLP* is terminated, it indicates the end of the continuous ABP monitoring with the *STAbp*.

Figure 3.7 shows the flow chart of the *Setpt Self-Update* subfunction. The subfunction temporarily interrupts the operation of the *CLP* to determine a new *Setpt*. The range of compressing pressures used to re-evaluate the *Setpt* is narrower than the range in *OLP*. The compressing pressure in the sealed air chamber (G7) is first reduced (*1*) by 10 mmHg below the latest recorded mean ABP or the *refPr*, whichever is lower. It is then increased in steps of 2 mmHg/s until it reaches 10 mmHg above the latest recorded mean ABP or the *refPr*, whichever is higher (*2*). During this process, the PPG and transducer pressure are recorded simultaneously (*3*). These waveforms are analysed

immediately after the required range of compressing pressure is applied to determine a new *Setpt*. The PPG pulse with the largest pulsation amplitude is first located (*4*). The corresponding compressing pressure is retrieved as *refPr* (*5*). The mean of the PPG pulse with the largest pulsation amplitude is computed as the *Setpt* (*6*). This is followed by adjusting the compressing pressure to *refPr* (*7*). The *CLP* is then resumed (*8*) to continue with the ABP monitoring.

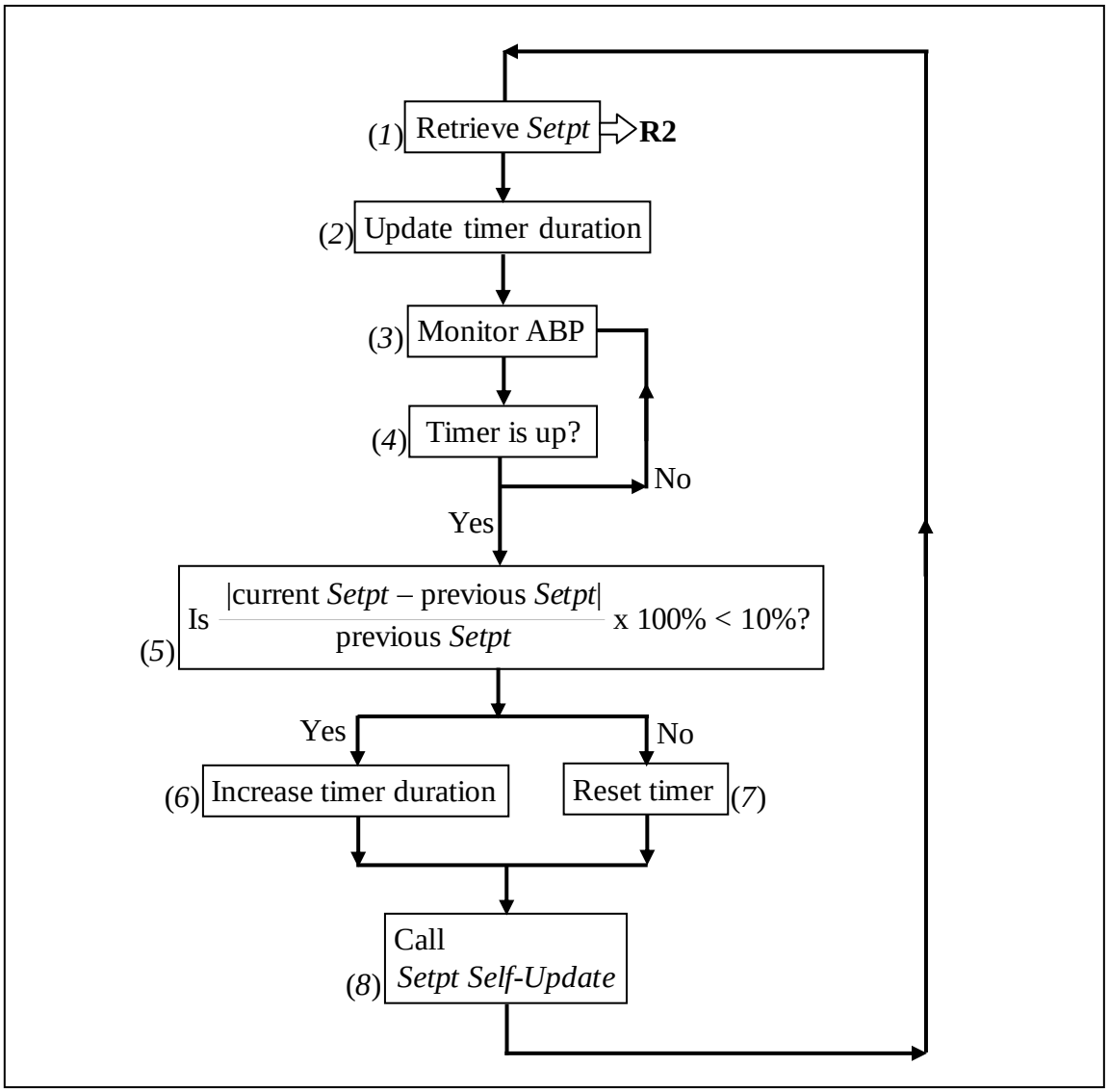

Figure 3.6 Flowchart of the Closed Loop Procedure (CLP).
The ABP is monitored continuously during CLP with the specified timer duration. The absolute percentage change of consecutive Setpt is calculated to check if it is within 10%. If it is, the timer duration is increased by 5s. This new timer duration is only used when the sequence returns to the beginning of the CLP (indicated as '2'). Otherwise, the timer is reset to its default duration, i.e. 10s. The Setpt Self-Update subfunction is then activated to update the Setpt value. The CLP repeats in a loop until it is externally terminated by the operator to indicate the end of the continuous ABP monitoring. The light arrow indicates output of R2 from G9. R2 is the Setpt. See text in section 3.3.7.2 for detailed description.

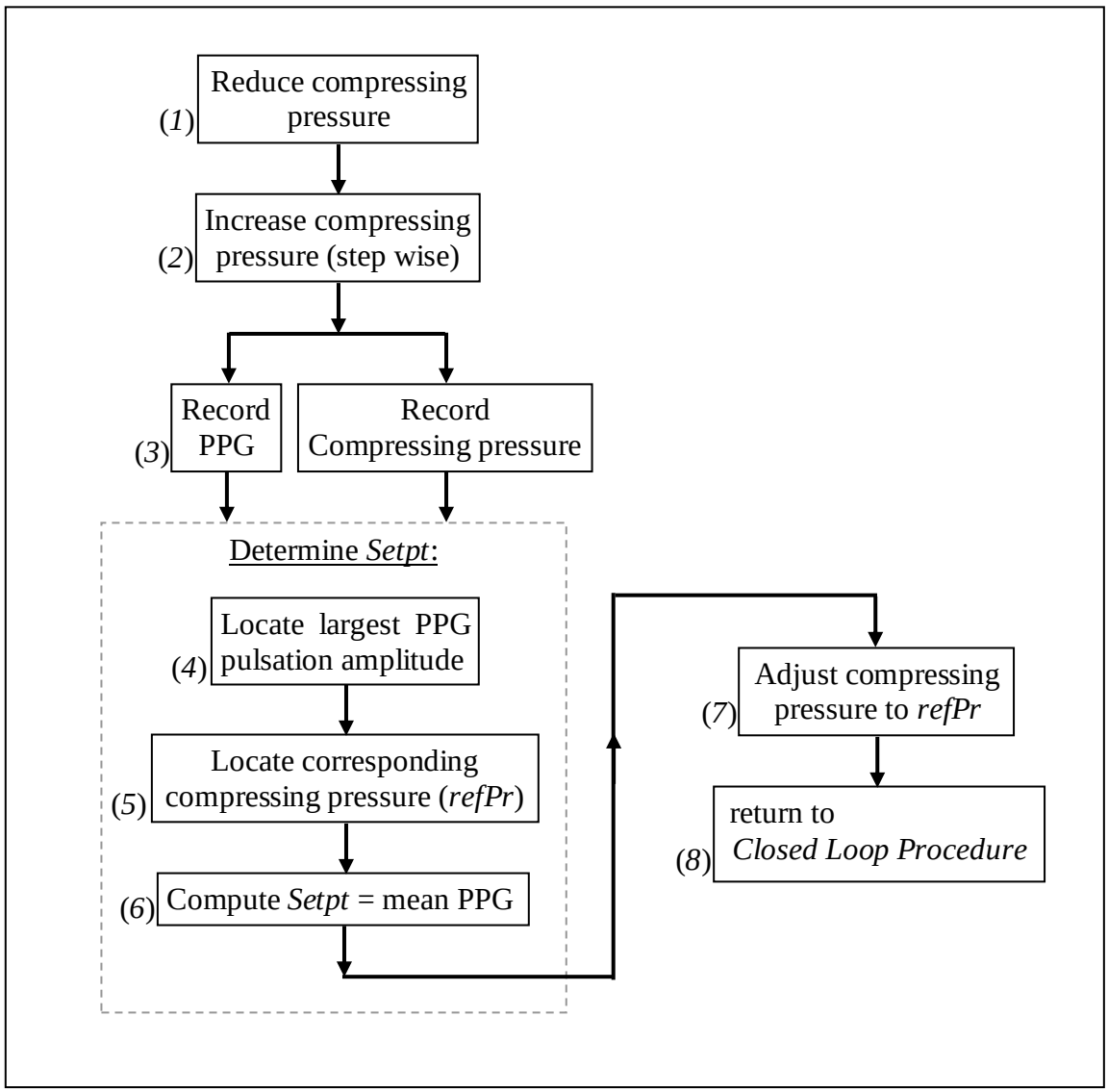

Figure 3.7 Flowchart of the Setpt Self-Update subfunction.
This subfunction is activated from time to time during the CLP. The Setpt and refPr are updated before the CLP is resumed. See text in section 3.3.7.2 for detailed description.

3.4 Initial Assessments

Section 3.3 described the instrumentation of the *STAbp* prototype. The design criteria highlighted in section 3.2 are incorporated into the prototype. The following subsections describe two assessments on the *STAbp*, i.e. the frequency response test and the prototype device safety evaluation.

3.4.1 Frequency Response Test

Referring to the description of G3 in section 3.3.3 (see also Figures 3.1 and 3.4), G3 consists of five sub-blocks (G4 to G8), which form a local feedback control loop to linearise the compressing pressure in the probe as required by input R1 (or C3). As explained in section 3.3.3, pressure hysteresis will occur if the piezo valve (G6) is used alone.

An experiment was set up to assess the frequency response of G3. The setup is illustrated in Figure 3.8. The front end surface of the probe is placed on the surface of a workbench with a gap of approximately 1.0 mm. The gap distance was arbitrarily chosen but it is aimed to simulate the distance between the surfaces of the probe and the skin when an external compressing pressure is applied on the tissue. The probe is fixed with a clamp and the clamp is fastened against a supporting stand. A mean compressing pressure of 75 mmHg with sine wave peak-to-peak amplitude of 60 mmHg was fed to the input of G3. The sine wave frequency began at 1 Hz and was gradually increased to 100 Hz. During this process, the gain and phase responses were recorded. The experiment was repeated with mean compressing pressures of 100 and 125 mmHg. The experimental results are presented in section 3.5.2.

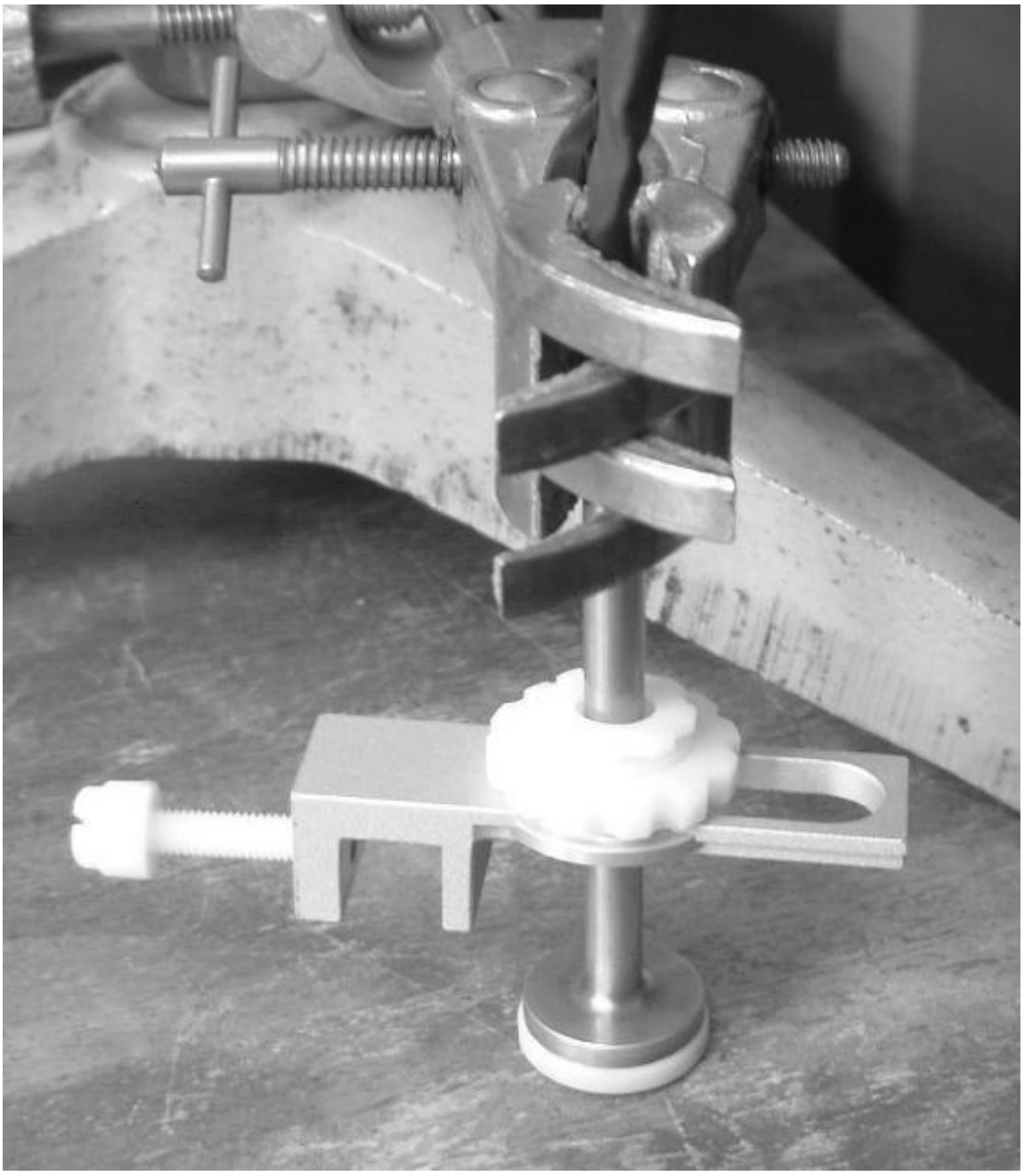

Figure 3.8 Experimental setup to evaluate frequency response of G3.
The setup adopted is to evaluate the frequency response of the regulated compressing pressure (G3) described in section 3.3.3. The front end surface of the probe is placed on the surface of a workbench. The probe is fixed with a clamp and the clamp is fastened against a supporting stand. See text in section 3.4.1 for detailed description.

3.4.2 Device Safety Evaluation

Safety considerations described in section 3.2 raised four device safety issues. The following describes steps taken to meet these considerations:

a) Upper limit of compressing pressure: the compressing pressure of the sealed air chamber (G7) is supplied up to 260 mmHg. G7 was tested to withstand air pressure of at least 350 mmHg. A pressure switch is connected to the mains supply for the micro air compressor (Figure A.2 in the Appendix). The mains supply to the air compressor is cut off if the pressure output from the regulated compressed air supply (G4) exceeds 260 mmHg.

b) Leakage current: the electrical connection at the probe is powered with an isolated voltage supply to prevent current leakage to flow through the subject. The isolation can withstand up to 1500Vrms (Burr-Brown, 1997).

c) Tissue heating: IRED with low current consumption is used to minimise local heating on the temporal tissue (section 3.3.1). Initial trial had no reported sensation of heating or redness on the skin. This will be reassessed in chapter 4 when the *STAbp* was tested in a group of healthy subjects (section 4.6.5).

d) Risk of tissue ischaemia: multiple large and soft paddings fastened around the head with the head frame provide evenly distributed pressure on the scalp tissue (section 3.3.2). Initial trial had not shown evidence of pain, dizziness or other discomfort. This will be reassessed in chapter 4 when the *STAbp* was tested in the group of subjects to obtain their feedback (section 4.6.5).

3.5 Results

Following the descriptions of the operations with the *Open*- and *Closed*- *Loop Procedures* in section 3.3.7, the results of the preliminary testing are presented in the following. The results of the frequency response test described in section 3.4.1 are presented in subsection 3.5.2.

3.5.1 Open Loop Operation

Figure 3.9 illustrates an example of recorded transducer pressure and PPG waveforms during the *OLP* to determine the *Setpt*. The compressing pressures encompass the physiological range of systolic and diastolic pressures. The PPG pulse with the largest pulsation amplitude is located. The *Setpt* is computed as the mean of this PPG pulse. The corresponding compressing pressure value is retrieved as *refPr*. Once the *Setpt* and *refPr* are obtained, the *OLP* is complete. It is immediately followed by the *CLP*.

3.5.2 Frequency Response

Figure 3.10 shows the frequency response of the regulated compressing pressure (G3). The gain did not drop below the conventional -3 dB point within the 0 to 100 Hz frequency range. It only began to drop below zero dB at frequencies above 40 Hz. Similarly, the phase shift started to lag from -10º only when the frequency had increased to at least 25 Hz. The graphs show three curves at mean compressing pressures of 75, 100 and 125 mmHg respectively. The frequency response is scarcely affected by the level of the mean compressing pressures.

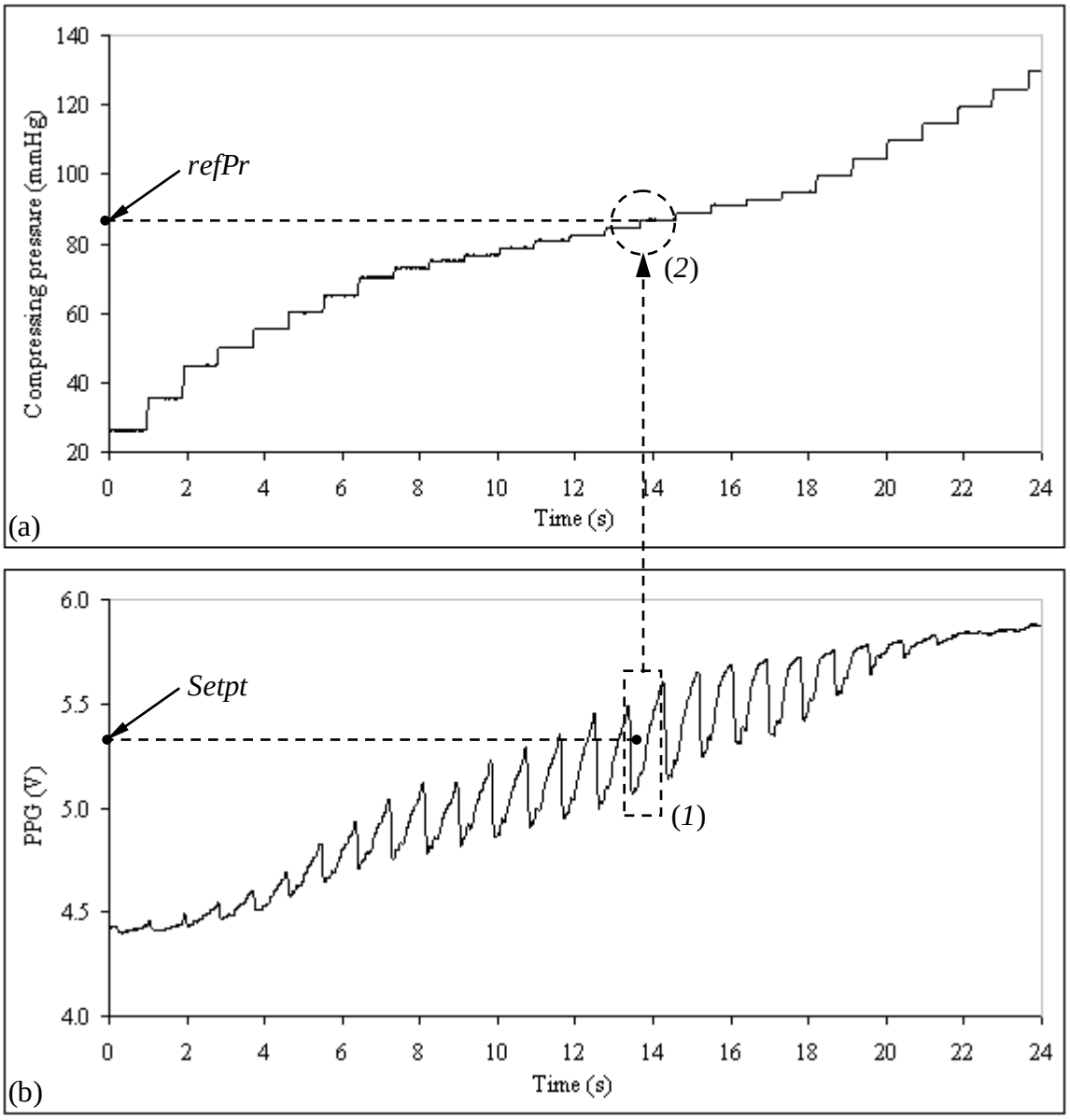

Figure 3.9 Recorded PPG waveform during Open Loop Procedure (OLP).
(a) Transducer pressure recording; (b) simultaneous recording of PPG waveform. The PPG pulse with the largest pulsation amplitude is first located (indicated as '1'). The Setpt is computed as the mean of this PPG pulse. The corresponding compressing pressure value is retrieved as refPr (indicated as '2').

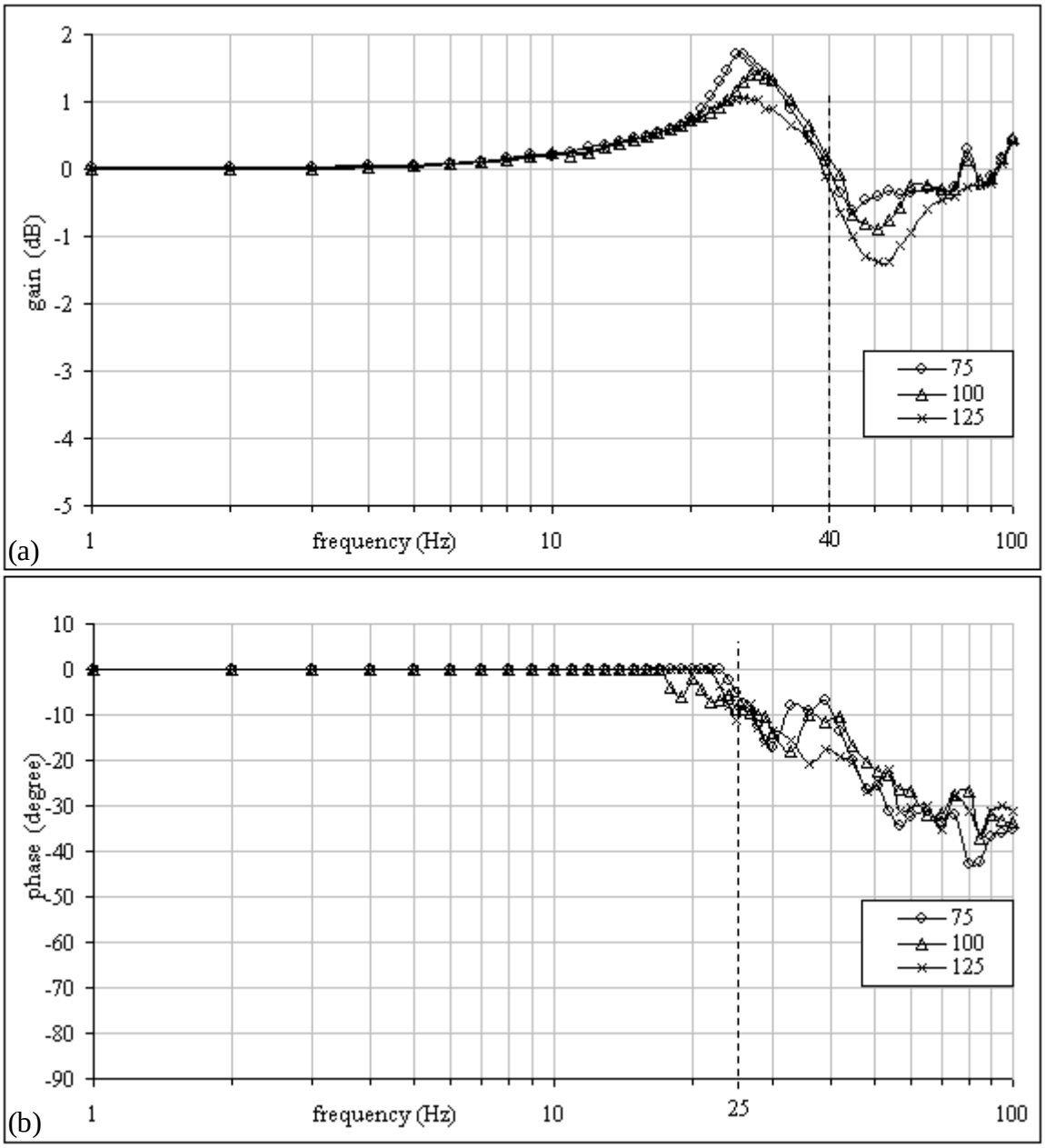

Figure 3.10 Frequency response curves of the regulated compressing pressure (G3). The gain (a) and phase (b) responses are shown. Three mean compressing pressures were applied: 75 (diamond), 100 (triangle) and 125 (cross) mmHg with peak-to-peak sinusoidal amplitude of 60 mmHg. The gain response shows that it only began to drop below zero dB at frequencies above 40 Hz. Correspondingly, the phase shift started to lag from -10º only at frequencies above 25 Hz.

3.5.3 Closed Loop Operation

Figure 3.11 shows a representative paired recording of the *STAbp* on the right STA and the *Finapres* on the right middle finger for 16 cardiac cycles. *Finapres* ABP was used for comparison. They were measured from a healthy adult while sitting in an upright position on a chair with back support. Hydrostatic pressure difference was taken into account when the waveforms were recorded.

Figure 3.12 shows a representative ABP trace of the *STAbp* and *Finapres* in response to the Valsalva manoeuvre (Looga, 2005; Nishimura and Tajik, 1986; Taylor, 1996). Simultaneous variation of the ABP can be observed. This shows that the *STAbp* is able to track the ABP changes during the manoeuvre.

These measurement results are only illustrative. A more formal assessment will be presented in chapter 4.

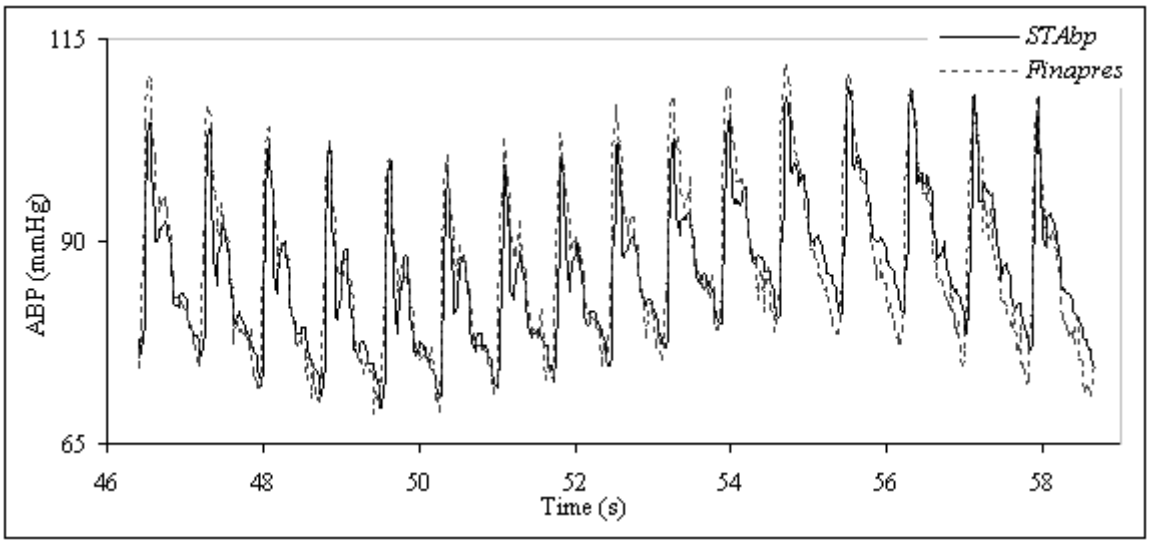

Figure 3.11 Resting ABP recording (STAbp vs. Finapres).
This example shows paired resting ABP waveforms recorded with the STAbp (continuous line) and Finapres (dashed line) for 16 cardiac cycles.

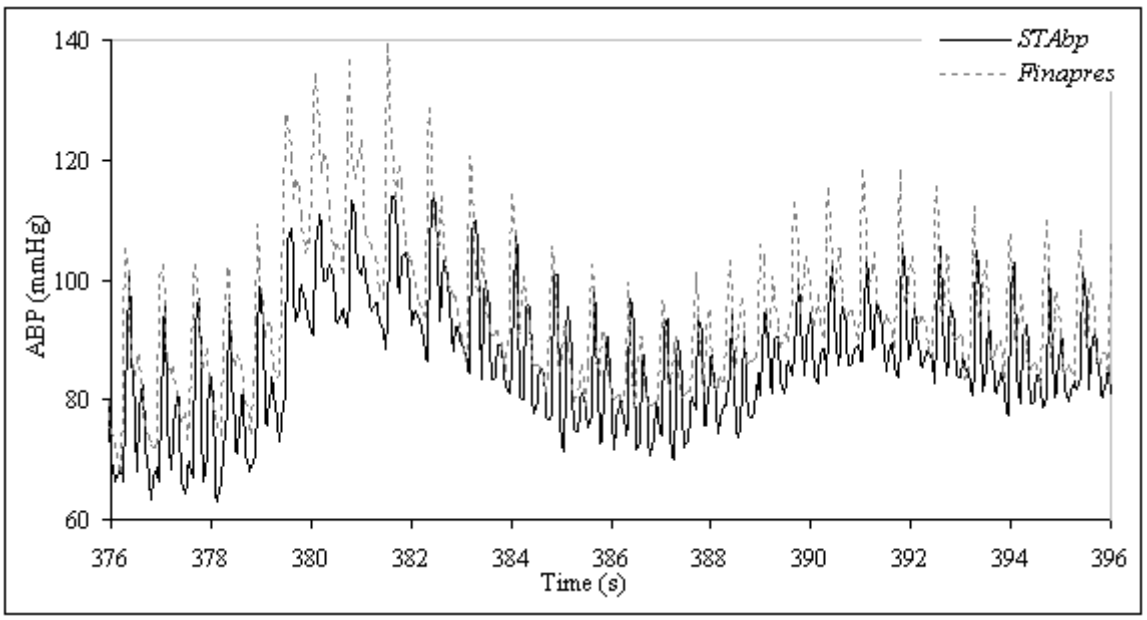

Figure 3.12 ABP recording during Valsalva Manoeuvre (STAbp vs. Finapres).
This example shows the simultaneous ABP variation of the STAbp (continuous line) and Finapres (dashed line).

3.6 Discussion

The instrumentation of the *STAbp* was described in section 3.3. Preliminary measurement results were shown in section 3.5. In the following paragraphs, four areas of the device development are discussed. These refer to the quality of the PPG waveform, the arrangement of optoelectronic components in the probe, area of compression on tissue, and the frequency response test of G3.

PPG waveform

The PPG signal is generated when the scattered or reflected light from the tissue illuminated by the IRED reaches the photodetector. Factors that can affect the quality of the PPG waveform include:

- the absorption and scattering properties of the arterial blood, surrounding tissue and the temporal bone beneath the tissue. It is assumed that these properties in the surrounding tissue and bone remain constant. Hence, the fluctuation observed in the PPG is only caused by the blood volume pulsation in the STA;
- the depth of artery from skin surface along the temporal region. It is assumed that the depth remains constant and the arterial dimension is uniform. Otherwise, it could affect the optical pathway of the light illumination;
- the distance between the artery and optoelectronic components. It is assumed that the distance remains the same throughout the continuous ABP monitoring;
- due to tissue elasticity, the artery may be pushed away from the optoelectronic components as the compressing pressure increases. This can change the initial distance and the optical pathway. It is assumed that this distance stays the same;

- interferences such as motion artefacts, electronic noise, change of temperature in the surroundings and change of ambient lighting. Strong ambient lighting with similar emitting wavelength as the IRED could potentially drive the current in the photodetector to saturation;
- pulse pressure. Decreased pulse pressure or weak pulse tends to give smaller PPG pulse amplitude, thus worsening the signal-to-noise ratio;
- physical characteristics of optoelectronic components, e.g. lens of the IRED which directs the illumination, intensity of emitted light and photosensitive active area in the photodetector;
- potential venous pulsation from blood vessels nearby, e.g. superficial temporal vein.

All the above factors could be seen as potential limitations and their validity should be the object of further scrutiny.

Optoelectronics in the probe

As described in section 3.3.1, four photodetectors are fitted inside the probe. It was then described in section 3.3.7.1 that only one photodetector is used during continuous ABP monitoring. This design offers the advantage to search the location of the STA with more confidence based on the quality of the PPG waveforms before continuous ABP monitoring begins.

However, it is not possible to identify the exact location and orientation of the STA. The possible placements of the IRED and the four photodetectors (PD) inside the probe relative to the STA are shown in Figure 3.13. In placement 1, the IRED, PD1 and PD3 are placed directly over the STA. In placement 2, the IRED and PD1 to PD3 are placed at approximately the same distance from the artery, but the optical pathway for PD2

may be different as compared for PD1 and PD3. In placement 3, PD2 is directly over the STA; however, the IRED is relatively further away from the artery. Lastly, in placement 4, the IRED is placed directly over the STA while the distances of all the four PD from the artery are relatively further away.

These possible placements generally illustrate that the optical pathway is different when the position of the optoelectronic components relative to the STA is changed. These could lead to a different PPG amplitude and waveshape recorded, and potentially a poorer quality of the ABP waveform is produced. Furthermore, section 3.3.1 described that a dome shape is produced when the sealed air chamber (G7) is fully inflated. The STA may not always be aligned on the tip of the dome. This may then pose as a limitation for the *STAbp* as the STA may not be evenly compressed. Placement 1 is probably the best in terms of optical pathway and uniformity of compression.

To understand better the optical pathway and the compression on the tissue with the underlying STA, further work will be required. For instance, mathematical modelling may be beneficial or to construct a specific experimental test rig to learn more about the properties of the optical pathway and effect of uneven compression on the PPG and ABP measurements. These further works are not presented in the subsequent chapters as they are beyond the scope of the thesis.

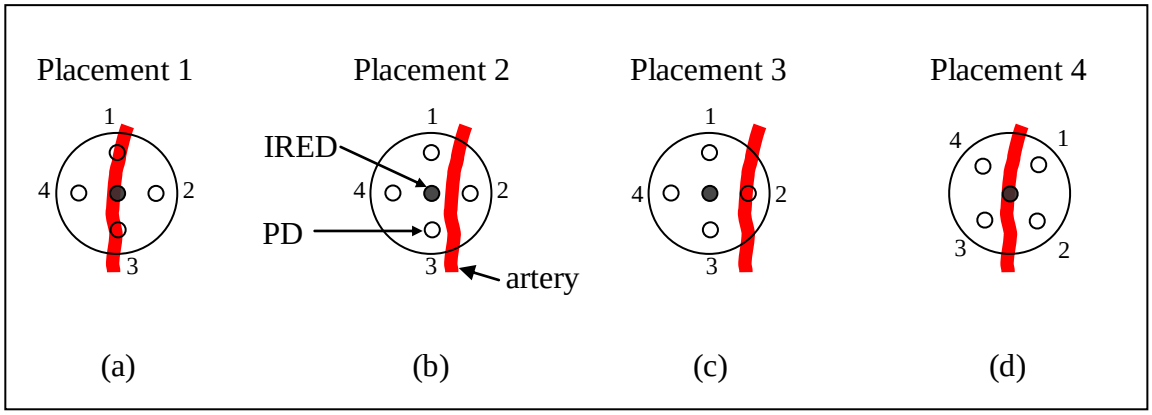

Figure 3.13 Possible placements of optoelectronic components relative to the STA. (a) The IRED, PD1 and PD3 are placed directly over the STA; (b) the IRED and PD1 to PD3 are placed at approximately the same distance from the artery, but the optical pathway for PD2 may be different as compared for PD1 and PD3; (c) PD2 is directly over the STA, however, the IRED is relatively further away from the artery; (d) the IRED is placed directly over the STA while the distances of all the four PD from the artery are relatively further away.

Area of compression on tissue

In addition to the dome shape of the inflated sealed air chamber, the area of compression on tissue may affect the effectiveness of pressure transmission through the tissue. In the *Finapres* and many arm-cuff oscillometric measurement devices, different cuff sizes are provided to cater for different dimensions of the measurement site, for instance, the circumference of the finger or the upper arm (Boehmer, 1987; Hirai et al., 1976; Imholz et al., 1998; Jones et al., 1993). It is well known that inappropriate cuff size leads to inaccurate ABP measurements (Geddes and Whistler, 1978; Manning et al., 1983; Ng and Small, 1993). The same physical principles may apply to the STA in the temporal region. The current area of compression of the probe in the *STAbp* has a diameter of 18 mm. Further work may be necessary to investigate the effect of different areas of compression on the accuracy of ABP measurement.

Frequency response of G3

Referring to Figure 3.1 and section 3.4.1, the limitation of the frequency response test is that only the frequency response of the regulated compressing pressure (G3) was tested instead of the complete integrated device. The frequency response test of the integrated device requires R2 (= *Setpt*) as the control input, C1 (= real time PPG) as the control loop feedback signal, and G10 as the feedback controller. Such arrangement requires living tissue as part of the closed loop. The frequency response may consequently be considered unreliable due to changes in physiological conditions and mechanical properties of the tissue within- and between individuals. This limitation will be addressed again when the frequency response and magnitude squared coherence analyses are described in chapter 4.

3.7 Conclusion

The design and instrumentation of the *STAbp* prototype demonstrates the integration of different hardware and software components to monitor the ABP continuously. Relevant design criteria were considered and they were incorporated into the device.

Initial assessments on the *STAbp* shows that appropriate steps have been taken to ensure safety of use in human subjects. Preliminary results show that the ABP waveforms measured with the *STAbp* are comparable against the *Finapres*. A more formal assessment of the *STAbp* on a group of subjects will be presented in the next chapter.

CHAPTER 4 PROTOTYPE DEVICE EVALUATION

4.1 Introduction

Chapter 3 described the system architecture of the *STAbp* prototype. Preliminary measurement results showed that it was satisfactory to carry out a more formal assessment with more human subjects.

A separate measurement device is required to evaluate the *STAbp*. The best option would be the gold standard, which is intravascular measurement. However, due to the high risk of infection, other clinical complications and costs implications (Bedford and Wollman, 1973; Carroll, 1988; Murray, 1981; Puri et al., 1980), it was deemed safer to first evaluate the *STAbp* against another noninvasive device. This approach also offers the opportunity to further understand the practical use of the new measurement device, to identify and make necessary improvements or modifications to the prototype before it is evaluated against an intravascular counterpart.

In this chapter, *Finapres* was chosen as the reference noninvasive measurement device for *STAbp*. An overview about the accuracy and reliability of the *Finapres* was given in several publications for a wide range of pathological and physiological conditions and in subjects of different age groups (Imholz et al., 1998; Wesseling, 1995; Wesseling et al., 1995). It is to note that the accuracy of the *Finapres* itself was evaluated against another measurement site, whether through invasive or noninvasive methods. Not surprisingly, discrepancies in ABP will occur due to different measurement locations.

Sections 1.1 and 1.2.3 mentioned that arterial pressure waveforms in different arteries are susceptible to the effect of pulse wave propagation and reflection. Also, there is usually a small drop in mean pressure in peripheral arteries. The ideal design would be to evaluate the *Finapres* against an intravascular measurement on a finger artery. However, such literature could not be found.

The *Finapres* is the next best option available after the intravascular measurement technique to evaluate the *STAbp*. Prior to this evaluation, two *Finapreses* of the same specifications and model number (Ohmeda 2300) were first compared to assess their inherent differences. The results were then used to define appropriate boundaries when interpreting the comparative study of the *STAbp* and *Finapres*.

The objectives of this chapter are:

i. To describe data analysis techniques common to both comparative studies (section 4.2). Analysis techniques specific to a comparative study will be described in respective sections 4.3 and 4.4;
ii. To describe the comparative study of two *Finapreses*, followed by analysis results (section 4.3). The *Finapreses* are referred to as *Finap1* and *Finap2*, with *Finap1* as the reference;
iii. To describe the comparative study of the *STAbp* and *Finapres*, followed by analysis results (section 4.4). The same *Finap1* was used as reference;
iv. To further compare the analysis results between both comparative studies (section 4.5), followed by discussion (section 4.6) and conclusion (section 4.7).

4.2 Data Analysis Techniques

The data analyses carried out for both comparative studies are very similar. This is to enable direct comparisons of results between both studies and to interpret the differences accordingly. This section describes analysis techniques common to both studies, whereas analysis techniques specific to a single comparative study will be described in that section.

In each comparative study, analyses were based on two types of physiological conditions, i.e. resting ABP and the ABP dynamic change due to activity. The ABP at both measurement sites were recorded simultaneously by two monitoring devices. The two devices will be initially denoted as reference device A and test device B in this section. They will be specified clearly later in each comparative study. The ABP waveforms were each digitally sampled at 200 Hz, operated with a desktop computer incorporating the Agilent VEEPro® 6.2 software.

Four parameters of the resting ABP will be evaluated. They are the agreement between simultaneously recorded ABP waveforms, frequency bandwidth of ABP pulses, frequency response and magnitude squared coherence analyses, and the assessment of ABP drift. Furthermore, the agreement between ABP waveforms during a dynamic change due to activity was also assessed. These five parameters will be described in the following subsections.

Comparison between the two devices were performed within the analysis of agreement framework proposed by Bland and Altman (1986). The statistical parameters to report included the mean of differences (bias), standard deviation of differences (SD), limits of

agreement and the root mean squared error (RMSE). A value of $p < 0.05$ was taken as the level of statistical significance. This criterion applies to all statistical analyses in this chapter.

4.2.1 Resting ABP: Agreement

Simultaneously recorded (or paired) resting ABP waveforms were recorded by devices A and B for several minutes in each subject. 16 cardiac pulses at the beginning of the recording were retrieved for analysis. This range was selected to avoid non-stationarity of the ABP waveforms.

Starting with device A recording, 16 systolic, mean and diastolic pressure values (SBP, MAP and DBP respectively) were calculated from the selected range of ABP waveform. The detections of these pressure values were produced automatically with a software programme developed in-house. An average was then computed for the SBP, MAP and DBP values respectively. The same process was repeated for device B recording. The differences between each pair of SBP, MAP and DBP averages were computed for each subject. Bias (SD) was then computed from all subjects' differences for the SBP, MAP and DBP respectively. The corresponding mean (SD) of all subjects' RMSE were also computed.

4.2.2 Resting ABP: Bandwidth

The frequency content of an ABP pulse waveform recorded at rest can be influenced by factors such as the physiological conditions of the measurement site, heart rate, cardiac

function and pulse wave propagation and reflection. It was suggested that a minimum of six harmonics is sufficient to reconstruct the original pressure wave with relatively close agreement (O'Rourke and Nichols, 2005).

In this section, the frequency content of a resting ABP pulse is quantified as the bandwidth containing either the 95% or the 99% of its total spectral power. To compute these bandwidth limits, the power spectrum is required. It is assumed that the pulse duration and waveshape of consecutive resting ABP pulses are approximately the same.

The discrete Fourier transform (DFT) of individual ABP pulses was first computed. The DFT is given by

$$X(f_k) = \sum_{n=0}^{N-1} x_n e^{-j2\pi nk/N} \tag{4.1}$$

where N is the sample size of an ABP pulse. x_n refers to the sampled ABP values for n = 0, 1, 2, …, N-1. k = 0, 1, 2, …, $\frac{N}{2}$ is the array for the frequency values (f_k) from zero to half the sampling frequency (f_s); this gives ($\frac{N}{2}$+1) number of f_k values which represents the positive half of the transformed values. The frequency interval is dependent on N and f_s, i.e. in the increment of $\frac{f_s}{N}$. Therefore, each frequency value plotted along the abscissa is $f_k = \frac{kf_s}{N}$ (Bendat and Piersol, 1986; Brigham, 1988). For simplicity, the subscript k in f_k will not be shown in the following text, i.e. $X(f_k) = X(f)$.

$X(f)$ is usually a complex number. For an ABP measured with the reference device A, let $G_{AA}(f)$ represents the discrete power spectrum given by

$$G_{AA}(f) = A^*(f) \cdot A(f) \equiv A(f)_{\mathrm{Re}}^2 + A(f)_{\mathrm{Im}}^2 \equiv |A(f)|^2 \quad (4.2)$$

where *A(f)* replaces *X(f)* in Equation 4.1. *A*(f)* is the complex conjugate of *A(f)*. A normalised cumulative power spectrum for the ABP pulse was then computed and the 95% and 99% bandwidth limits were identified. Linear interpolation was used for a bandwidth limit between frequency points.

The same computation process was repeated for test device B. Similar to Equation 4.2, the power spectrum for test device B is given by

$$G_{BB}(f) = B^*(f) \cdot B(f) \equiv B(f)_{\mathrm{Re}}^2 + B(f)_{\mathrm{Im}}^2 \equiv |B(f)|^2 \quad (4.3)$$

where *B*(f)* is the complex conjugate of *B(f)*.

The same 16 paired ABP pulses selected in section 4.2.1 were used to compute the 95% and 99% bandwidth limits. The following explains the step-by-step computation process:

1. compute the 95% bandwidth limit from each of the 16 ABP pulses recorded with reference device A (denoted as $K_{A,95}$);
2. compute an intra-subject average from step 1 ($\overline{K}_{A,95} = \frac{\sum_{m=1}^{16} K_{A,95,m}}{16}$);
3. compute the 95% bandwidth limit from each of the 16 ABP pulses recorded with test device B (denoted as $K_{B,95}$);
4. compute an intra-subject average from step 3 ($\overline{K}_{B,95} = \frac{\sum_{m=1}^{16} K_{B,95,m}}{16}$);
5. compute intra-subject difference for 95% bandwidth limit ($\Delta K_{95} = \overline{K}_{B,95} - \overline{K}_{A,95}$);
6. repeat steps 1 to 5 to obtain $\overline{K}_{A,95}$, $\overline{K}_{B,95}$ and ΔK_{95} for all subjects;
7. compute respective mean (SD) of $\overline{K}_{A,95}$ and $\overline{K}_{B,95}$;

8. repeat steps 1 to 7 for 99% bandwidths to obtain $\overline{K}_{A,99}$, $\overline{K}_{B,99}$ and ΔK_{99} for all subjects;
9. compute respective mean (SD) of $\overline{K}_{A,99}$ and $\overline{K}_{B,99}$.

4.2.3 Resting ABP: Frequency Response and Magnitude Squared Coherence

The frequency response test described in section 3.4.1 only applies to the block G3 in the *STAbp* system architecture (Figure 3.1 and section 3.3.3). G3 provides regulated compressing pressure in the probe to compress the STA. The probe was described in section 3.3.1.

The frequency response test was not carried out on the whole *STAbp* device as it needs to incorporate the living tissue component, which may vary within- and between-individuals. For this reason, the frequency response of the *STAbp* device was assessed by a frequency response analysis using the *Finapres* signal as input.

The frequency response analysis is useful to estimate the dynamic relationship between paired recordings of ABP waveforms in the frequency domain. The computation of the frequency response will give the gain and phase spectra. The magnitude squared coherence is complementary to the frequency response analysis to assess for consistent frequency coupling between the paired ABP waveforms. The spectral comparison between two *Finapreses* will give the frequency response that can be used as reference when interpreting the frequency response in the spectral comparison between the *STAbp* and *Finapres*.

To compute the frequency response ($H(f)$) and the magnitude squared coherence ($\gamma^2(f)$), the auto- and cross- spectra were first computed. The ABP waveforms from the reference device A and test device B were the input and output functions respectively.

The auto (power) spectra $G_{AA}(f)$ and $G_{BB}(f)$ have been given in Equations 4.2 and 4.3. The cross spectrum ($G_{AB}(f)$) is given as

$$G_{AB}(f) = A^*(f) \cdot B(f) \tag{4.4}$$

In theory, $H(f)$ and $\gamma^2(f)$ are defined as $H(f) = \frac{G_{AB}(f)}{G_{AA}(f)}$ and $\gamma^2(f) = \frac{|G_{AB}(f)|^2}{G_{AA}(f) \cdot G_{BB}(f)}$ respectively. However, due to the presence of noise component in real time signals, the auto- and cross- spectra were first computed from individual fast Fourier transform (FFT) of 16 windowed ABP waveform segments, and then averaged (Bendat and Piersol, 1993; Brigham, 1988). The number of windows was not increased to avoid potential non-stationarity of the waveform. Each window of ABP waveform consists of 512 sample points, corresponding to 2.56s. This approach allows the use of stable segments of the ABP waveform which always include at least one complete cardiac cycle and also to smoothen the spectral estimates.

Before the FFT was applied, the mean of the windowed waveform was first removed. Each windowed waveform was then multiplied with a 20% cosine-tapered Hanning window (Bloomfield, 2000; Harris, 1978). This overcomes the discontinuity of windowed waveform, hence spectral leakage is minimised. After multiplication by the Hanning window, the residual mean of the tapered waveform was further removed to obtain zero offset. This process was repeated for 16 windows with 50% Welch

overlapping from the continuous ABP waveform (Oppenheim and Schafer, 1975; Proakis and Manolakis, 1996). There are other advantages of using a windowed ABP waveform. One is to overcome the variation of pulse duration, and the other is to retain the phase difference between the paired waveforms.

To apply *H(f)* and $\gamma^2(f)$ in practice, if *m* is the number of windowed ABP waveform segments from each ABP recording, the estimates of *H(f)* and $\gamma^2(f)$ now become

$$\hat{H}(f) \equiv \frac{\sum_{i=1}^{m} G_{AB}(f)_i}{\sum_{i=1}^{m} G_{AA}(f)_i} \tag{4.5}$$

$$\hat{\gamma}^2(f) \equiv \frac{\left|\sum_{i=1}^{m} G_{AB}(f)_i\right|^2}{\sum_{i=1}^{m} G_{AA}(f)_i \cdot \sum_{i=1}^{m} G_{BB}(f)_i} \tag{4.6}$$

As $\hat{H}(f)$ is usually complex, the average gain ($|\hat{H}(f)|$) and phase ($\hat{\Phi}(f)$) spectra can be obtained from the real part $\hat{H}(f)_{\mathrm{Re}}$ and imaginary part $\hat{H}(f)_{\mathrm{Im}}$, as $\left|\hat{H}(f)\right| = \left[\left(\hat{H}(f)_{\mathrm{Re}}\right)^2 + \left(\hat{H}(f)_{\mathrm{Im}}\right)^2\right]^{1/2}$ and $\hat{\Phi}(f) = \tan^{-1}\left[\frac{\hat{H}(f)_{\mathrm{Im}}}{\hat{H}(f)_{\mathrm{Re}}}\right]$ respectively. The upper frequency bandwidth was identified at the gain of 0.707, which is equivalent to the conventional -3 dB cut-off frequency. The minimum level of acceptance for the magnitude squared coherence was chosen at 0.5 as a conservative criterion which is widely used in the literature (de Boer et al., 1985).

4.2.4 Resting ABP: Assessment of Drift

The assessment of drift in ABP measurement describes the agreement of paired ABP waveforms after the resting ABP is monitored for several minutes. To quantify drift, the difference between percentage changes in the paired ABP waveforms was calculated. The percentage change in ABP is denoted as Ψ (unit is %). The generic equation is derived as

$$\Psi_i \Big|_{SBP,MAP,DBP} = \left(\frac{\overline{P}_{i(end)} - \overline{P}_{i(begin)}}{\overline{P}_{i(begin)}} \right) \times 100\% \Big|_{SBP,MAP,DBP} \quad (4.7)$$

i refers to reference device A or test device B. $\overline{P_i}$ is an average calculated from 16 cardiac pulses. Ψ_i was computed for SBP, MAP and DBP.

The same 16 cardiac pulses selected in section 4.2.1 were used for $\overline{P}_{i(begin)}$. Another 16 cardiac pulses towards the end of the same recorded waveform were selected for $\overline{P}_{i(end)}$. The difference ($\Delta\Psi = \Psi_B - \Psi_A$) was calculated for each subject. The mean (SD) of Ψ_A, Ψ_B and $\Delta\Psi$ from all subjects were then computed for SBP, MAP and DBP.

4.2.5 ABP Dynamic Change during Activity

The above sections 4.2.1 to 4.2.4 described analysis techniques on resting ABP waveforms. This section describes the assessment on the agreement of paired ABP waveforms with dynamic change due to specific manoeuvres. The comparative studies described in sections 4.3 and 4.4 carried out two different activities to assess this type of agreement. In section 4.3, a Valsalva manoeuvre was conducted, whereas in section 4.4, an isometric handgrip (IHG) exercise was conducted. The choice of activity was

different because a Valsalva manoeuvre may interfere with the ABP measurement in the STA, for example, the motion artifacts due to upper body or jaw movement during the manoeuvre could have a larger interference on the *STAbp* device. Thus, it was replaced by the IHG exercise. For similar reason, IHG exercise was not carried out for the finger ABP measurements as both hands were needed for finger cuff fitting.

To quantify the agreement of ABP dynamic change, the difference between percentage changes in the paired ABP waveforms was calculated. The percentage change in ABP is denoted as Φ (unit is %). The generic equation is derived as

$$\Phi_{i,j}\Big|_{SBP,MAP,DBP} = \left(\frac{\overline{P}_{i,j(end)} - \overline{P}_{i,j(begin)}}{\overline{P}_{i,j(begin)}}\right) \times 100\% \Big|_{SBP,MAP,DBP} \quad (4.8)$$

i refers to reference device A or test device B; j refers to Valsalva manoeuvre (VM) or the IHG exercise (IHG). $\overline{P_{i,j}}$ is an average calculated from 10 cardiac pulses. $\Phi_{i,j}$ was computed for SBP, MAP and DBP. The difference ($\Delta\Phi_j = \Phi_{B,j} - \Phi_{A,j}$) was calculated for each subject. The mean (SD) of $\Phi_{A,j}$, $\Phi_{B,j}$ and $\Delta\Phi_j$ from all subjects were then computed for SBP, MAP and DBP.

Valsalva manoeuvre (for section 4.3 only)

$\overline{P}_{i,VM(begin)}$ refers to the average from 10 cardiac pulses prior to the strain of the manoeuvre. $\overline{P}_{i,VM(end)}$ refers to the average from 10 cardiac pulses at the peak of phase IV after the strain was released (Looga, 2005; Nishimura and Tajik, 1986; Taylor, 1996).

IHG exercise (for section 4.4 only)

$\overline{P}_{i,IHG(begin)}$ refers to the average from 10 cardiac pulses prior to the beginning of the handgrip. $\overline{P}_{i,IHG(end)}$ refers to the average from 10 cardiac pulses just before the handgrip was released.

4.3 Comparative Study of two *Finapreses*

Paired ABP measurements with two *Finapreses* of the same model will be described in this section. This is to characterise their inherent differences before the *STAbp* is evaluated. The two *Finapreses* are referred to as *Finap1* (device A) and *Finap2* (device B) with *Finap1* as reference.

4.3.1 Method

11 subjects were recruited for this study (6 males, 5 females, age (mean ± SD) 36 ± 12 years). The participants were all staff from the Medical Physics department. Consent was given by each participant prior to the arrangement for the ABP measurements. The study was approved by the Leicestershire ethics committee (reference number: 4680).

Each subject was requested to avoid stressful activities prior to the ABP measurement. The subjects had no history of conditions affecting their hands or its circulation. Each subject sat on a chair with back support. Both hands were resting comfortably on a bench at the same height as the heart level. The room temperature was maintained at approximately 22 ºC. Two fingers from a combination of middle and annulus fingers of both hands were selected. With two *Finapreses* and two fingers selected for ABP measurements, there are twelve possible combinations (Table 4.1). Only four out of the twelve possible combinations were tested in this study, indicated as Tests #1 to Test #4 in bold in the table. The sequence of the four tests was randomised with a lapse of at least 30 minutes apart between tests to allow the fingers to rest.

Table 4.1 Twelve possible combinations of two Finapreses and two fingers.
The abbreviations refer to the right hand (R), left hand (L), middle finger (3) and annulus finger (4). Only four out of the twelve combinations were tested with Finap1 and Finap2 (i.e. Tests #1 to #4), as shown in bold. Finap1 was used as reference.

Combination	*Finap1*	*Finap2*	Experiment
Ipsi-lateral fingers	**R3**	**R4**	**Test #1**
	R4	**R3**	**Test #2**
	L3	L4	- not tested -
	L4	L3	- not tested -
Contra-lateral fingers	**R3**	**L3**	**Test #3**
	L3	R3	- not tested -
	R3	L4	- not tested -
	L4	R3	- not tested -
	R4	L3	- not tested -
	L3	R4	- not tested -
	R4	**L4**	**Test #4**
	L4	R4	- not tested -

Each selected finger was fitted with a suitable *Finapres* cuff according to the guidelines provided by the manufacturer. The ABP in both fingers were monitored simultaneously with the *Finapreses*. The subject was asked to relax and breathe normally during ABP measurements. The ABP was monitored for several minutes until the ABP was stable. The *Finapres* has the capability to self-calibrate during continuous ABP monitoring, known as *Physiocal* (Wesseling et al., 1995). When stable ABP waveforms were obtained in both recorders, this feature in both devices was temporarily switched off before the recording began.

Each paired ABP recording lasted for 4 min. At the second minute, a Valsalva manoeuvre was performed and lasted for approximately 20s (Dawson et al., 1997; Dawson et al., 1999a; Weston et al., 1996a). 16 cardiac pulses at the beginning and 16 cardiac pulses towards the end of the 4 min recording were retrieved. The analysis techniques for these ranges of waveforms were described in sections 4.2.1 to 4.2.4. The recorded waveforms during the Valsalva manoeuvre were analysed with the approach described in section 4.2.5.

The following paragraph describes statistical computations specific to this comparative study in addition to the techniques described in section 4.2. For each parameter considered, the null hypothesis states that there is no statistical significance between mean values.

The two *Finapreses* and the combination of two fingers' ABP measurements (Tests #1 to #4) gave a '2 way 4 levels' design. A two-way within subjects (repeated measures) analysis of variance (ANOVA) was carried out to test the main hypothesis (Roberts and

Russo, 1999). The ANOVA factors were denoted as '*Finap*' (2 levels) and '*Test*' (4 levels). If the null hypothesis was rejected, post hoc *Scheffe* testing (Maxwell and Delaney, 2004; Roberts and Russo, 1999) was carried out and the four tests were assessed separately. Conversely, if the null hypothesis was accepted, the measurement results were pooled.

4.3.2 Results

Paired ABP recordings from 11 subjects (Tests #1 to #4) were all of good quality. The resting ABP were stable during the 4 min recording with a clear dynamic change in the second minute during the Valsalva manoeuvre. No waveforms were excluded from the analysis.

The presentation of results follows the sequence described in section 4.2 and adopts the same headings. Figure 4.1 shows an example of the paired resting ABP recordings with 16 cardiac pulses at the beginning and 16 cardiac pulses towards the end of the 4 min recording respectively. The former waveform segment was analysed according to the first three data analysis techniques described in sections 4.2.1 to 4.2.3. Both waveform segments were then analysed for the assessment of drift according to the technique described in section 4.2.4. Lastly, the analysis technique described in section 4.2.5 was used for the assessment of the ABP dynamic change during Valsalva manoeuvre. An example recording during the Valsalva manoeuvre is shown in Figure 4.2.

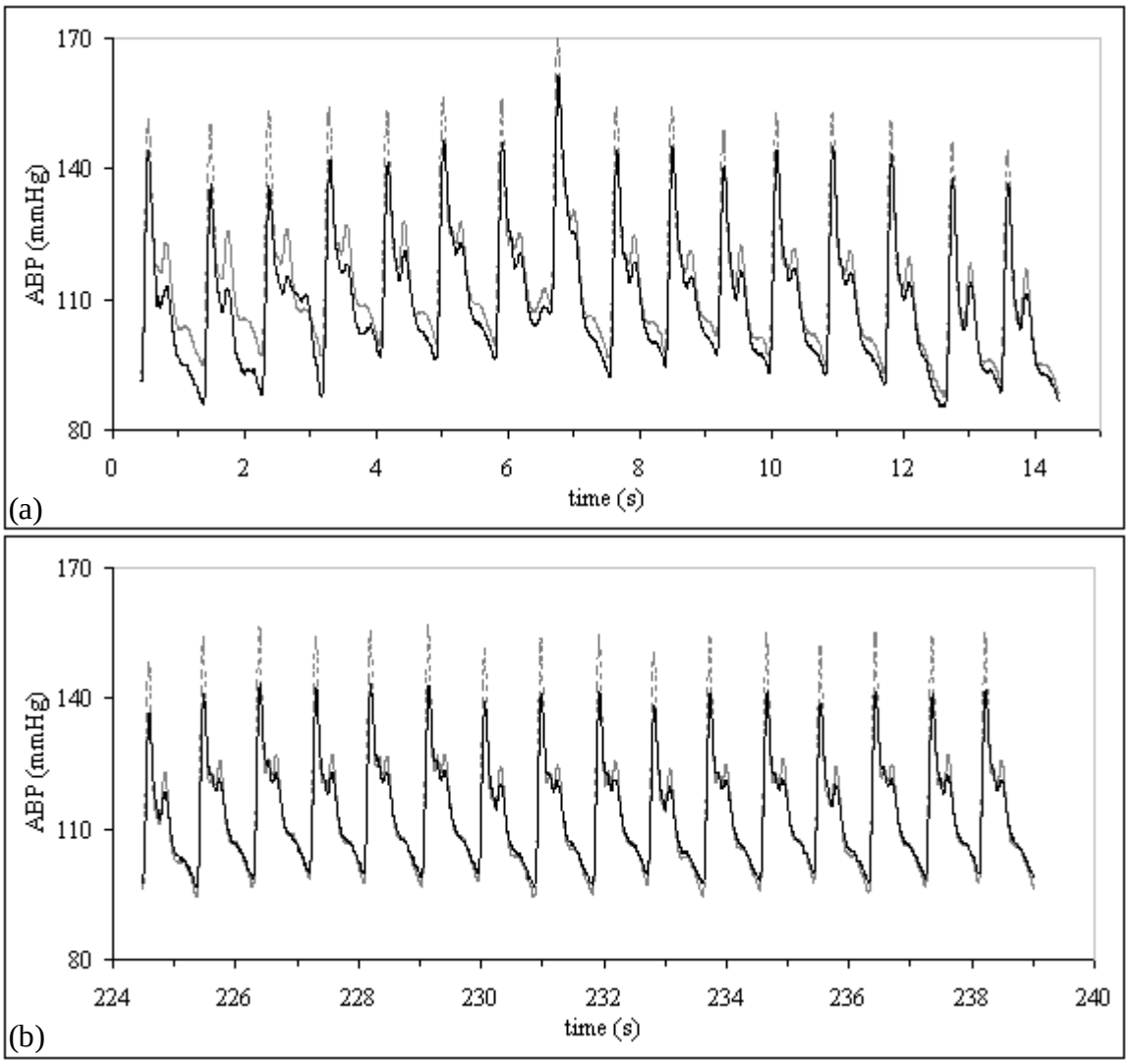

Figure 4.1 Resting ABP waveforms (Finap2 vs. Finap1).
Example of 16 cardiac pulses at the beginning (a) and 16 cardiac pulses towards the end (b) of a 4 min recording with Finap2 (black continuous line) and Finap1 (grey dashed line). Finap1 was used as reference.

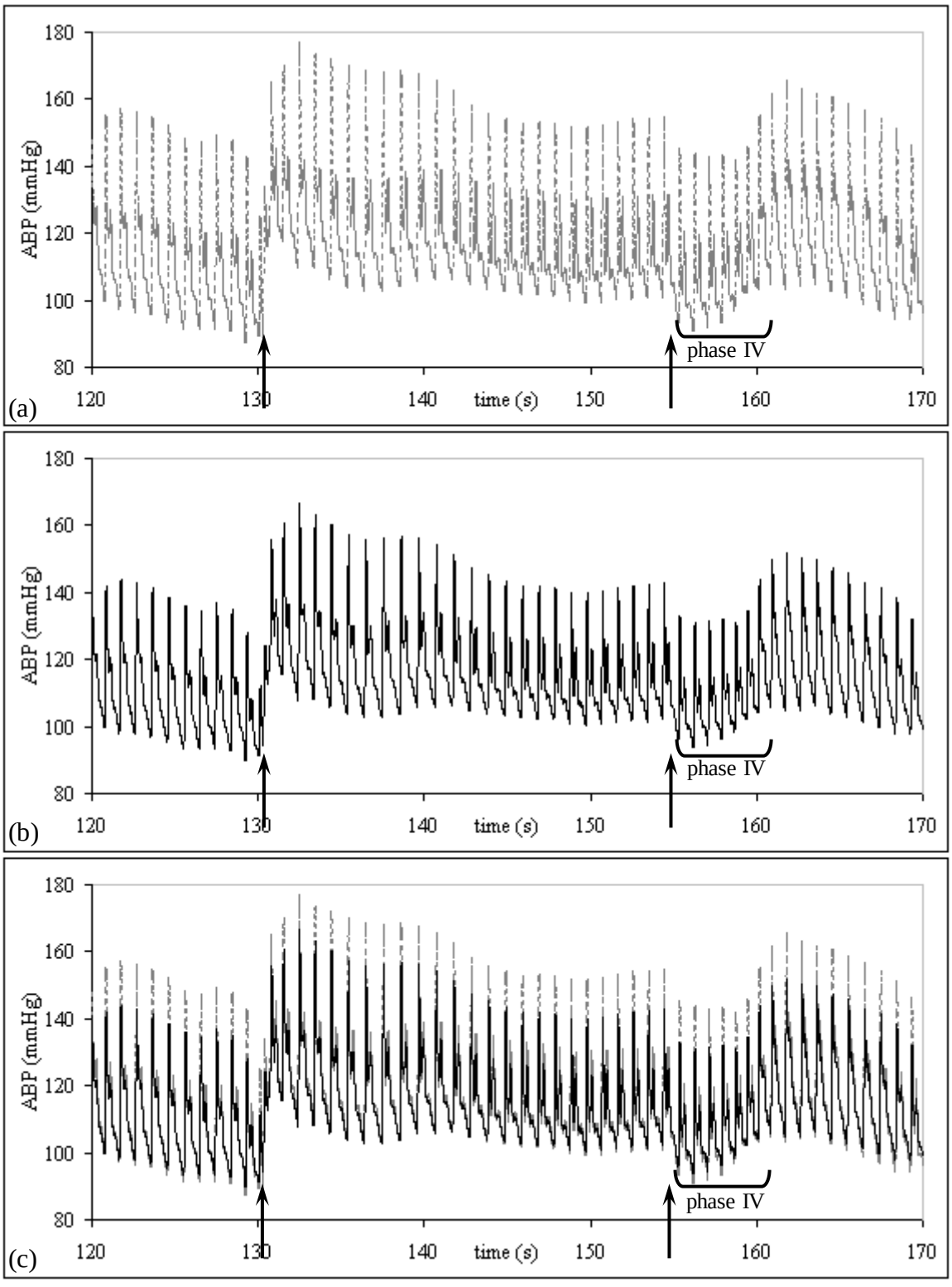

Figure 4.2 ABP waveforms during Valsalva manoeuvre (Finap2 vs. Finap1). Example of (a) Finap1 recording; (b) Finap2 recording; (c) Finap2 (black continuous line) and Finap1 (grey dashed line). Finap1 was used as reference. The arrows show the beginning and end of the Valsalva manoeuvre. Phase IV (as indicated in the graphs) is the classical ABP overshoot observed upon release of the expiratory strain.

4.3.2.1 Resting ABP: Agreement

The statistical analysis results for the agreement between paired resting ABP waveforms are presented as follows:

- Tables 4.2 to 4.4: ANOVA results with p-values (2 ways 4 levels design) for SBP, MAP and DBP. Significant values are printed in bold. Consequently, the null hypothesis was rejected and the tables have included results of post-hoc *Scheffe* testing.

  The ANOVA results show significant differences in the '*Finap*' main effect for SBP (p=0.010), MAP (p=0.008) and DBP (p=0.021). Significant differences were obtained in the '*Test*' main effect for SBP (p=0.030) and MAP (p=0.043), but not for DBP. No significant differences were obtained in the '*Finap* x *Test*' interaction for SBP, MAP and DBP (Tables 4.2(a), 4.3(a) and 4.4(a)).

  Post hoc *Scheffe* tests on the '*Test*' main effect show no significant differences in Tests #1 to #4 for SBP, MAP and DBP. However, post hoc *Scheffe* tests on the '*Finap* x *Test*' interaction show six significant values for SBP (Table 4.2(c)), three for MAP (Table 4.3(c)) and one for DBP (Table 4.4(c)). All the significant p-values are related to '*Finap2* Test #1' (labelled as $\{5\}$);

- Figure 4.3: plots of means of SBP, MAP and DBP for the '*Finap*' and '*Test*' main effects;
- Figure 4.4: plots of means of SBP, MAP and DBP for the '*Finap* x *Test*' interaction;
- Figures 4.5(a-d): plots of agreement for SBP, MAP and DBP in Tests #1 to #4. The analysis results for each test were treated separately (i.e. $n_1 = n_2 = n_3 = n_4 = 11$

subjects) because the null hypothesis was rejected. The respective regression lines show no significant correlations;

- Table 4.5: bias (SD) for Tests #1 to #4. As shown by the ANOVA, Test #1 presented the largest bias, associated with recordings from *Finap2*;
- Table 4.6: mean (SD) of RMSE for Tests #1 to #4.

Table 4.2 ANOVA p-values for SBP (two Finapreses with four tests).
(a) ANOVA results for 'Finap' and 'Test' main effects, and their interaction; (b) post-hoc Scheffe test for 'Test' main effect; (c) post-hoc Scheffe test for 'Finap x Test' interaction. Significant values are printed in bold.

(a)	ANOVA (2 ways 4 levels)
'*Finap*'	**0.010**
'*Test*'	**0.030**
'*Finap*' x '*Test*'	0.162

(b)	Test #1	Test #2	Test #3	Test #4
Test #1	--	0.346	0.062	0.091
Test #2		--	0.800	0.883
Test #3			--	0.998
Test #4				--

(c)			{1}	{2}	{3}	{4}	{5}	{6}	{7}	{8}
Finap1	Test #1	{1}	--	0.984	0.082	0.412	0.272	0.992	0.974	0.859
Finap1	Test #2	{2}		--	0.469	0.926	**0.035**	1.000	1.000	1.000
Finap1	Test #3	{3}			--	0.991	**0.000**	0.408	0.524	0.776
Finap1	Test #4	{4}				--	**0.001**	0.893	0.949	0.996
Finap2	Test #1	{5}		**0.035**	**0.000**	**0.001**	--	**0.045**	**0.028**	**0.010**
Finap2	Test #2	{6}					**0.045**	--	1.000	0.999
Finap2	Test #3	{7}					**0.028**		--	1.000
Finap2	Test #4	{8}					**0.010**			--

Table 4.3 ANOVA p-values for MAP (two Finapreses with four tests).
(a) ANOVA results for 'Finap' and 'Test' main effects, and their interaction; (b) post-hoc Scheffe test for 'Test' main effect; (c) post-hoc Scheffe test for 'Finap x Test' interaction. Significant values are printed in bold.

(a)	ANOVA (2 ways 4 levels)
'*Finap*'	**0.008**
'*Test*'	**0.043**
'*Finap*' x '*Test*'	0.438

(b)	Test #1	Test #2	Test #3	Test #4
Test #1	--	0.475	0.167	0.063
Test #2		--	0.911	0.673
Test #3			--	0.965
Test #4				--

(c)			{1}	{2}	{3}	{4}	{5}	{6}	{7}	{8}
Finap1	Test #1	{1}	--	0.995	0.641	0.470	0.292	1.000	1.000	0.917
Finap1	Test #2	{2}		--	0.970	0.970	0.058	0.997	1.000	1.000
Finap1	Test #3	{3}			--	1.000	**0.004**	0.680	0.897	0.999
Finap1	Test #4	{4}				--	**0.002**	0.509	0.774	0.993
Finap2	Test #1	{5}			**0.004**	**0.002**	--	0.262	0.112	**0.016**
Finap2	Test #2	{6}						--	1.000	0.935
Finap2	Test #3	{7}							--	0.994
Finap2	Test #4	{8}					**0.016**			--

Table 4.4 ANOVA p-values for DBP (two Finapreses with four tests).
(a) ANOVA results for 'Finap' and 'Test' main effects, and their interaction; (b) post-hoc Scheffe test for 'Test' main effect; (c) post-hoc Scheffe test for 'Finap x Test' interaction. Significant values are printed in bold.

(a)	ANOVA (2 ways 4 levels)
'*Finap*'	**0.021**
'*Test*'	0.892
'*Finap*' x '*Test*'	0.510

(b)	Test #1	Test #2	Test #3	Test #4
Test #1	--	0.659	0.287	0.119
Test #2		--	0.915	0.672
Test #3			--	0.962
Test #4				--

(c)		{1}	{2}	{3}	{4}	{5}	{6}	{7}	{8}
Finap1	Test #1	{1}	--	1.000	0.962	0.812	0.486	1.000	1.000	0.989
Finap1	Test #2	{2}		--	0.997	0.952	0.270	0.999	1.000	1.000
Finap1	Test #3	{3}			--	1.000	0.060	0.914	0.997	1.000
Finap1	Test #4	{4}				--	**0.020**	0.707	0.949	0.998
Finap2	Test #1	{5}				**0.020**	--	0.606	0.276	0.098
Finap2	Test #2	{6}						--	0.999	0.966
Finap2	Test #3	{7}							--	1.000
Finap2	Test #4	{8}								--

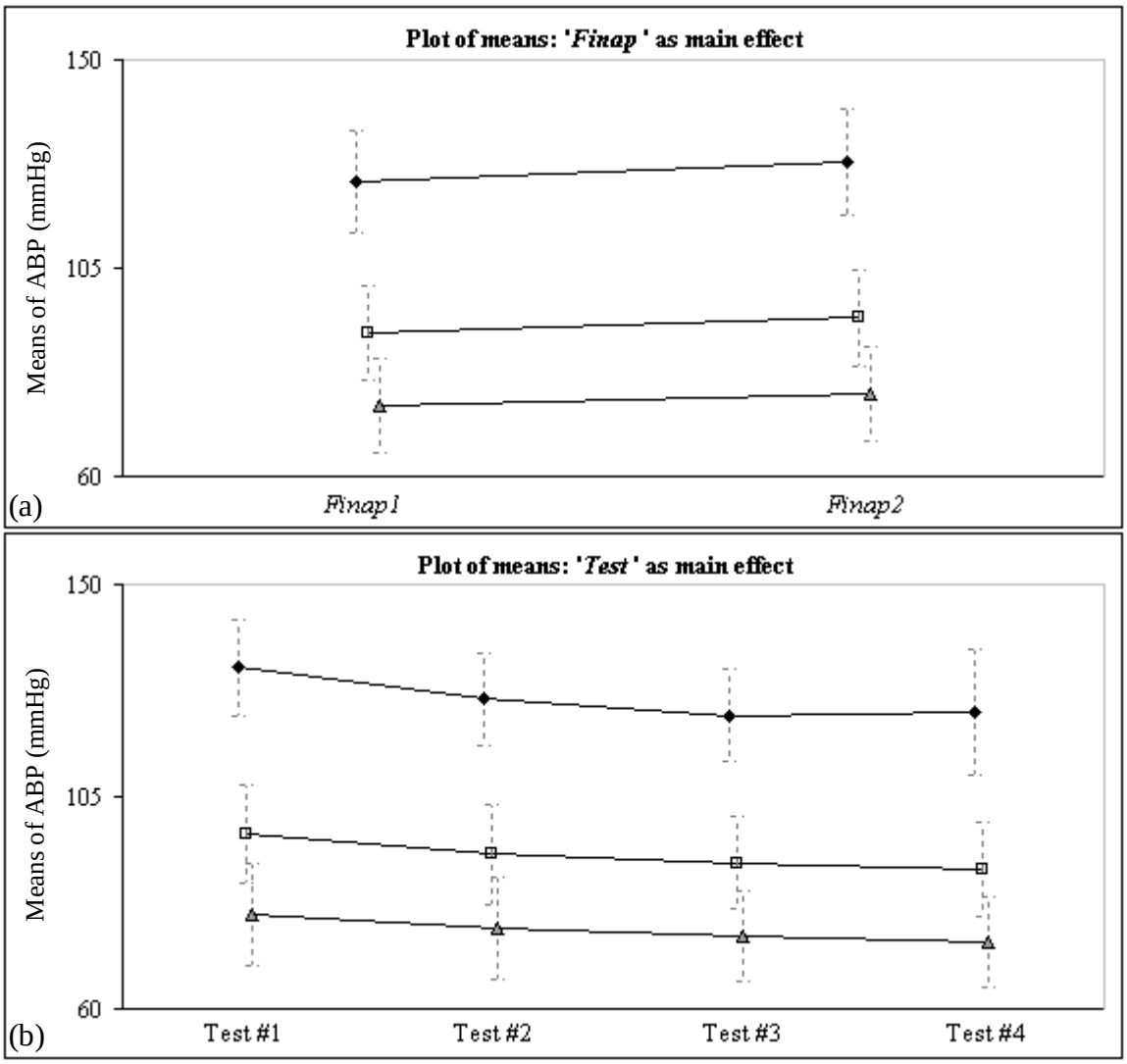

Figure 4.3 Plots of means of ABP for 'Finap' and 'Test' main effects.
(a) 'Finap' main effect (2 levels); (b) 'Test' main effect (4 levels). The plots of means refer to SBP (diamond), MAP (square) and DBP (triangle). The plots are slightly shifted from each other to avoid superposition of the error bars. The error bars are ±1SD of the respective means.

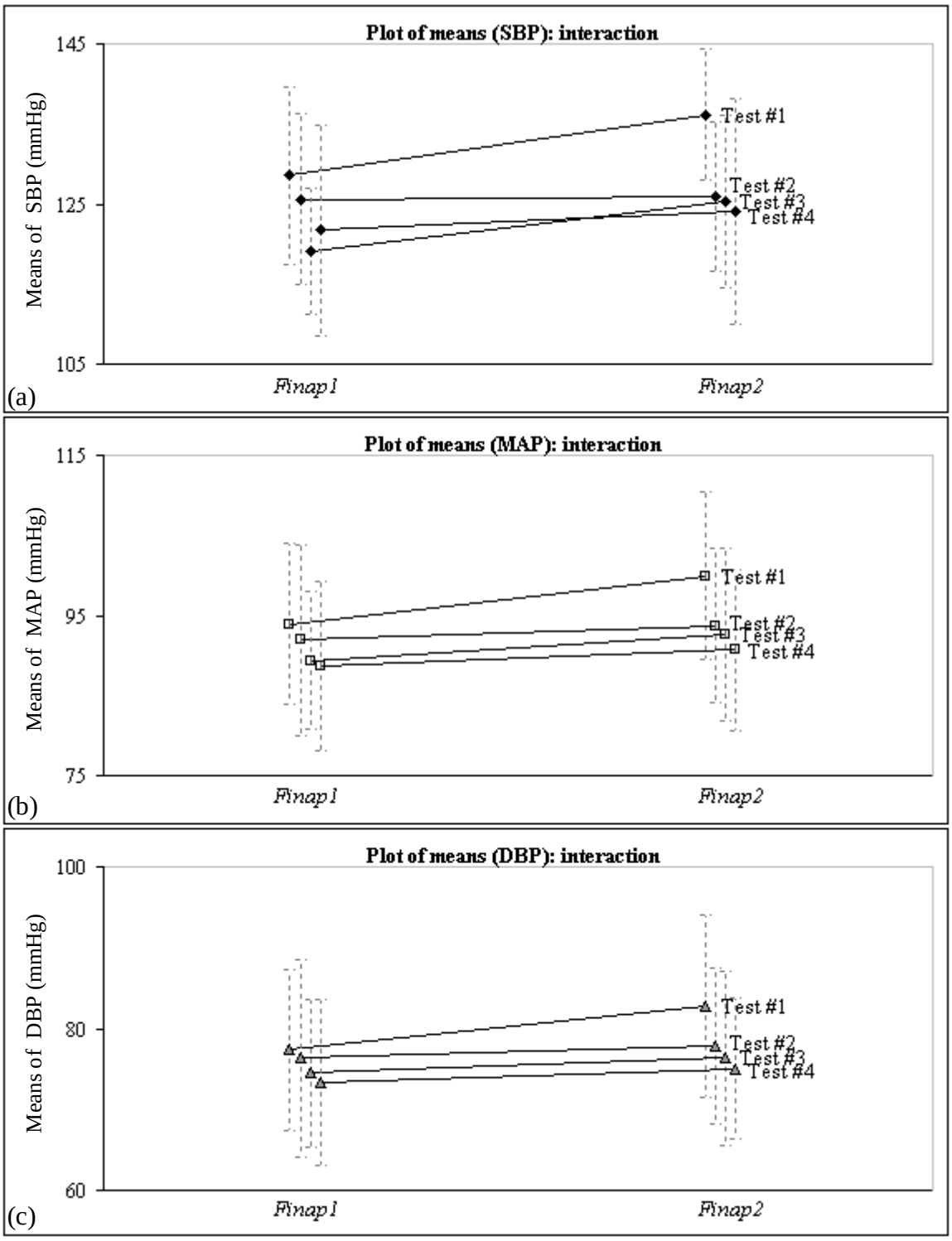

Figure 4.4 Plots of means of ABP for the 'Finap x Test' interaction.
The plots of means refer to (a) SBP, (b) MAP and (c) DBP. The plots are slightly shifted from each other to avoid superposition of the error bars. The error bars are ±1SD of the respective means.

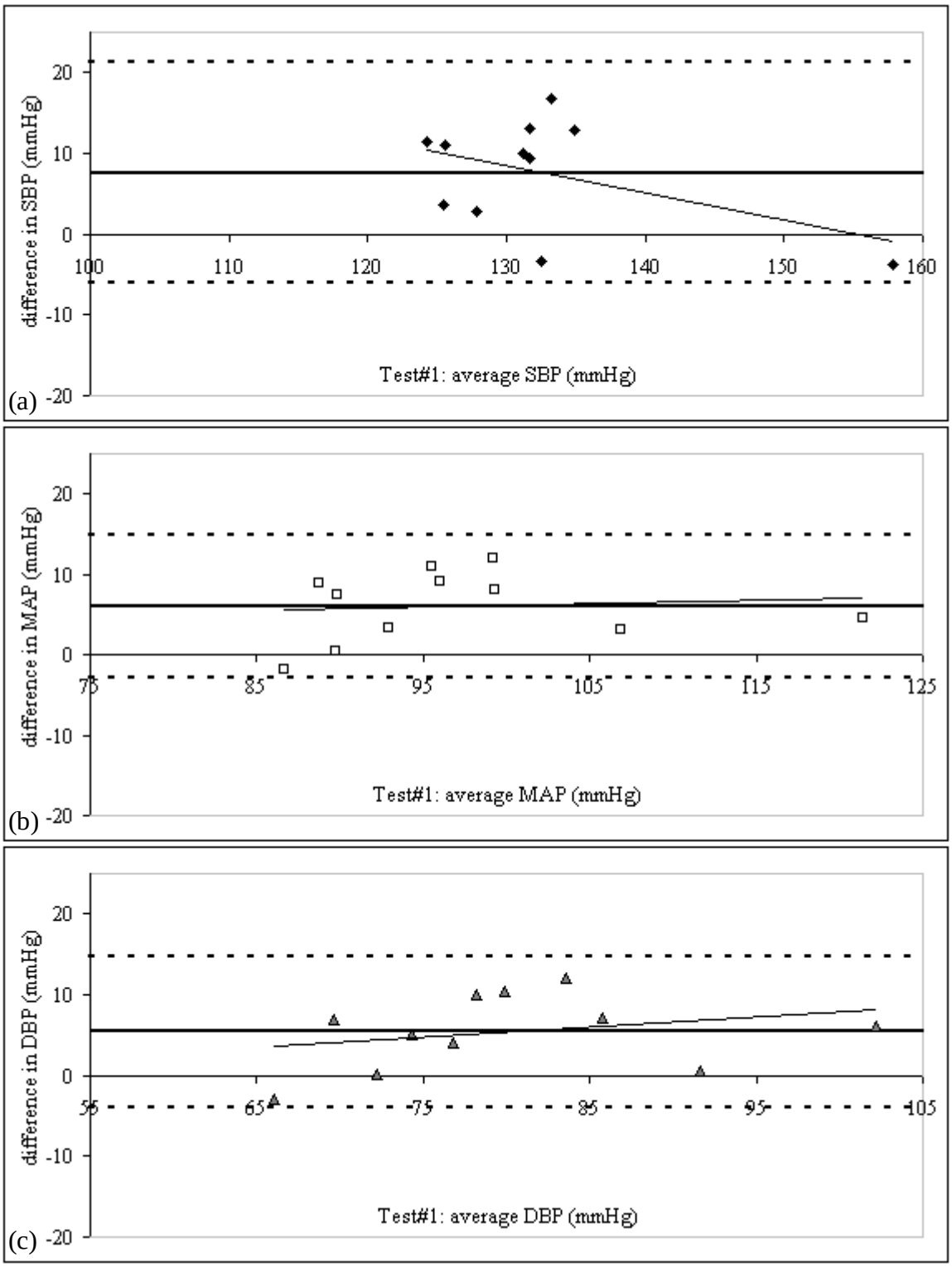

Figure 4.5a Test #1 plots of agreement in resting ABP (Finap2 vs. Finap1).
(a) SBP, (b) MAP and (c) DBP. The thick continuous line in each graph is the bias (n_1=11 subjects) and the dashed lines are the corresponding limits of agreement. The biases (SD) are also presented in Table 4.5. Respective regression lines show no significant correlations.

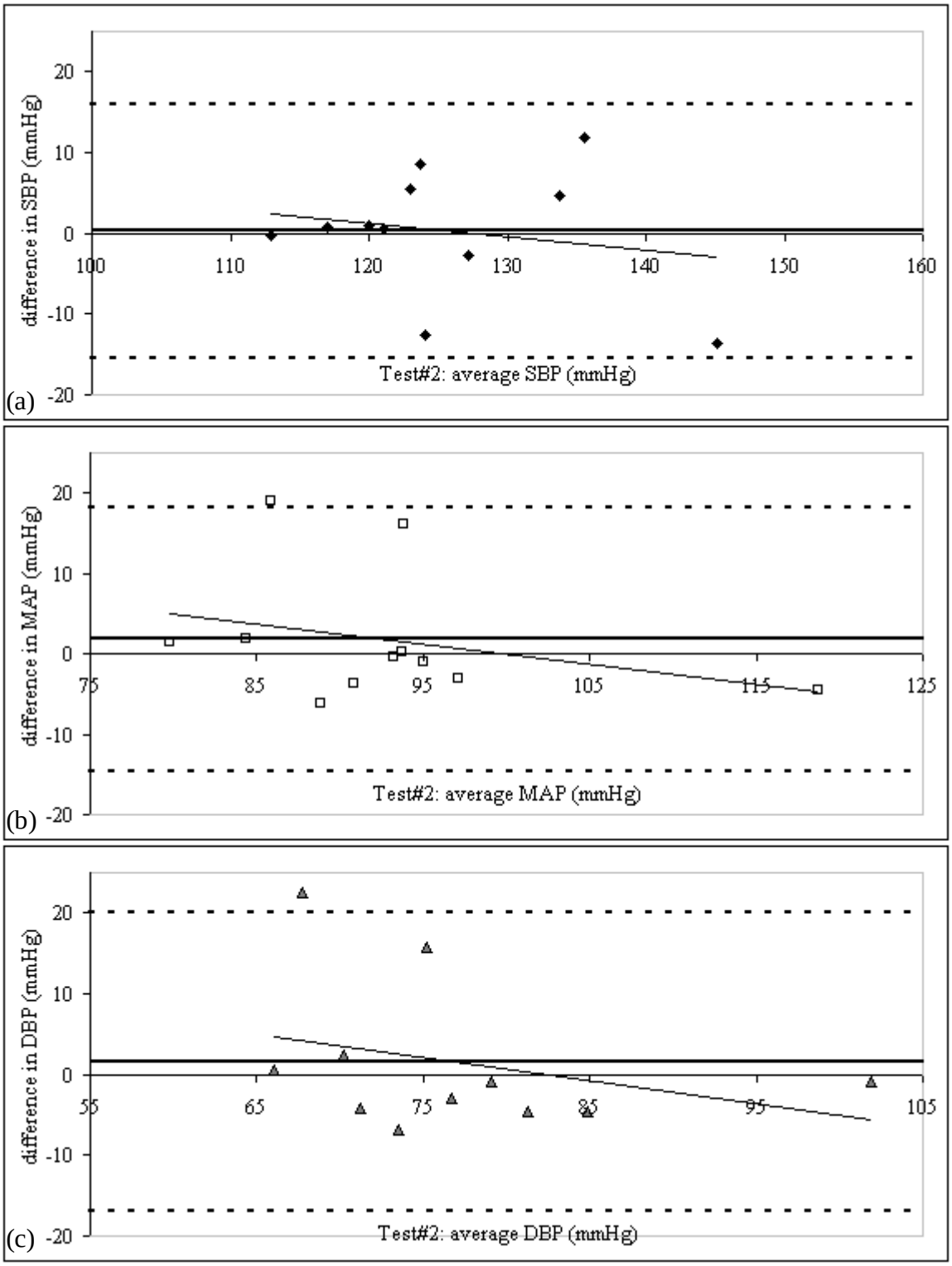

Figure 4.5b Test #2 plots of agreement in resting ABP (Finap2 vs. Finap1).
(a) SBP, (b) MAP and (c) DBP. The thick continuous line in each graph is the bias (n_2=11 subjects) and the dashed lines are the corresponding limits of agreement. The biases (SD) are also presented in Table 4.5. Respective regression lines show no significant correlations.

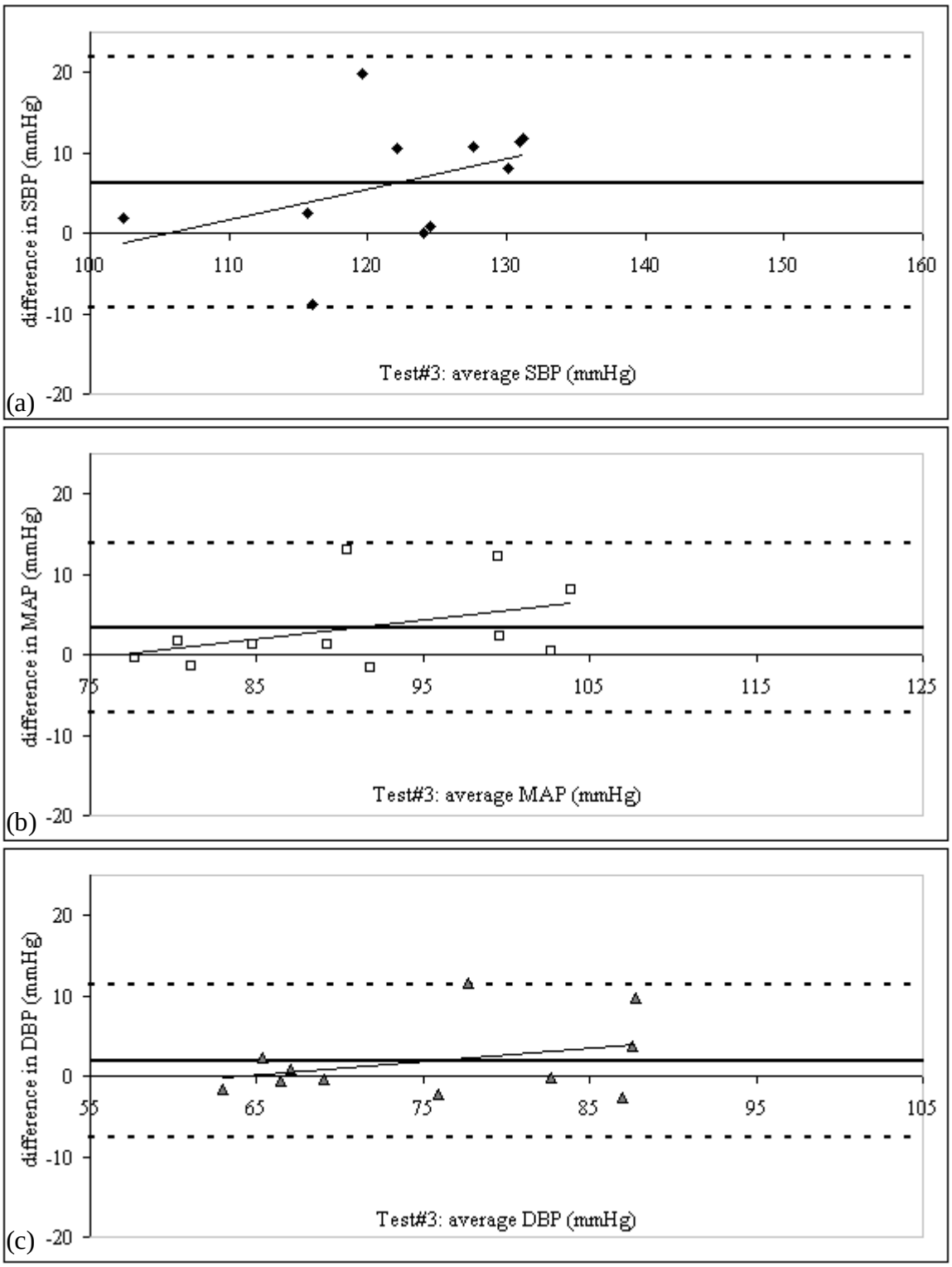

Figure 4.5c Test #3 plots of agreement in resting ABP (Finap2 vs. Finap1).
(a) SBP, (b) MAP and (c) DBP. The thick continuous line in each graph is the bias (n_3=11 subjects) and the dashed lines are the corresponding limits of agreement. The biases (SD) are also presented in Table 4.5. Respective regression lines show no significant correlations.

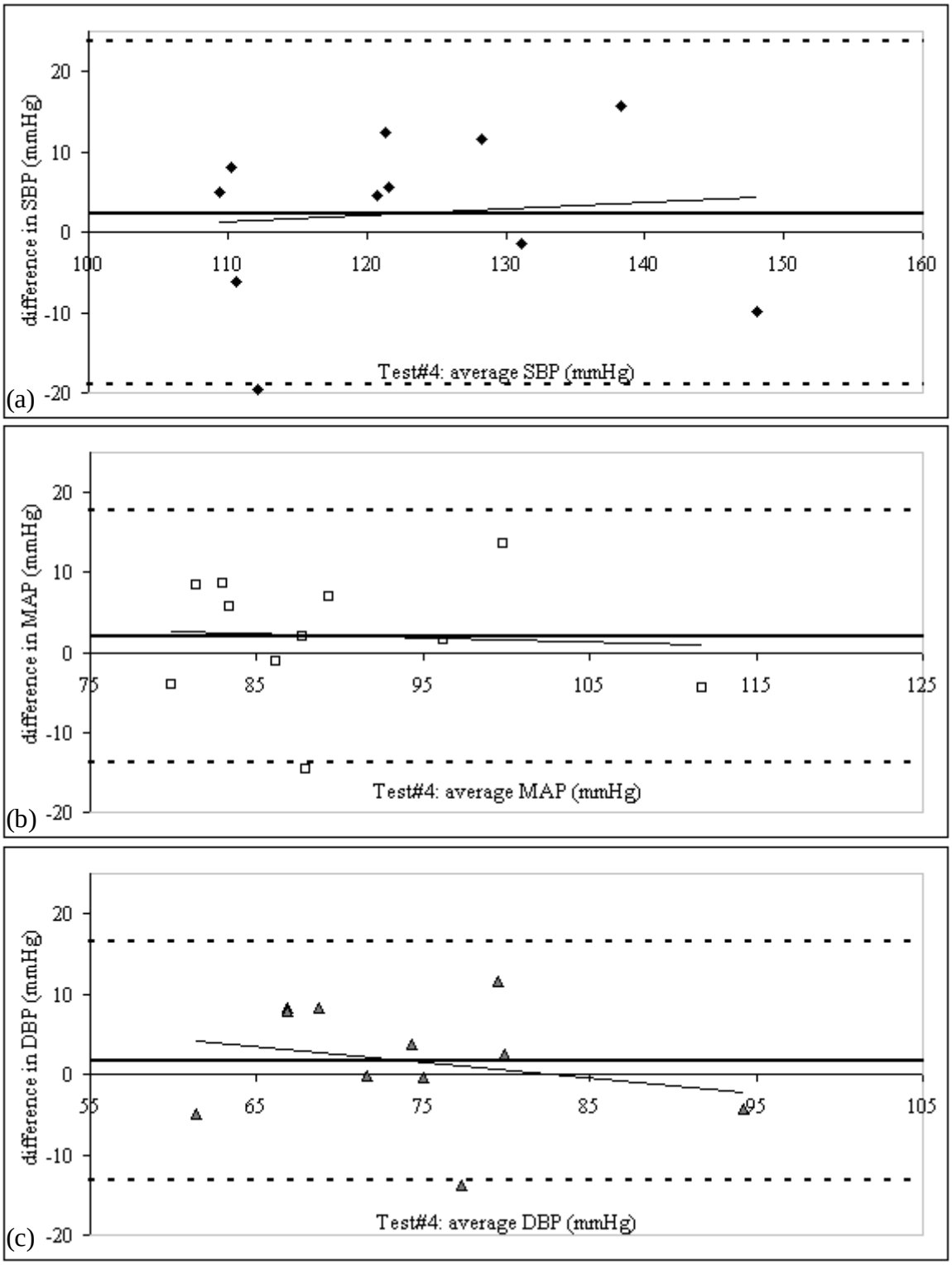

Figure 4.5d Test #4 plots of agreement in resting ABP (Finap2 vs. Finap1).
(a) SBP, (b) MAP and (c) DBP. The thick continuous line in each graph is the bias (n_4=11 subjects) and the dashed lines are the corresponding limits of agreement. The biases (SD) are also presented in Table 4.5. Respective regression lines show no significant correlations.

Table 4.5 Bias (SD) in resting ABP (Finap2 vs. Finap1).
Bias (SD) computed for SBP, MAP and DBP. They are also plotted in Figures 4.5(a-d). Tests #1 to #4 were assessed separately (i.e. $n_1=n_2=n_3=n_4=11$ subjects) because the null hypothesis was rejected.

Test #	SBP		MAP		DBP	
	mean	**SD**	**mean**	**SD**	**mean**	**SD**
1	7.6	6.82	6.0	4.43	5.4	4.67
2	0.3	7.87	1.8	8.25	1.5	9.25
3	6.3	7.80	3.4	5.25	1.9	4.78
4	2.4	10.67	2.0	7.87	1.7	7.43

Table 4.6 Mean (SD) of RMSE in resting ABP (Finap2 vs. Finap1).
Mean (SD) computed for SBP, MAP and DBP. Tests #1 to #4 were assessed separately (i.e. $n_1=n_2=n_3=n_4=11$ subjects) because the null hypothesis was rejected.

Test #	SBP		MAP		DBP	
	mean	**SD**	**mean**	**SD**	**mean**	**SD**
1	9.0	4.71	6.4	3.87	6.0	3.86
2	6.0	5.02	5.4	6.36	6.2	6.83
3	8.2	6.05	4.2	4.80	3.4	3.87
4	9.3	5.28	6.6	4.42	6.2	4.21

4.3.2.2 Resting ABP: Bandwidth

ANOVA results with p-values (2 ways 4 levels design) for ΔK_{95} and ΔK_{99} are shown in Table 4.7. Figure 4.6 shows the plots of means of bandwidth limits for the '*Finap*' and '*Test*' main effects. No significant difference was detected for each bandwidth limit. Hence, the respective results were pooled (n=44). For 95% bandwidth, the mean (SD) of $\overline{K}_{Finap1,95}$ and $\overline{K}_{Finap2,95}$ were obtained as 4.6 (0.76) Hz and 4.5 (0.87) Hz respectively. Similarly, for 99% bandwidth, the mean (SD) of $\overline{K}_{Finap1,99}$ and $\overline{K}_{Finap2,99}$ were obtained as 6.5 (0.66) Hz and 6.4 (0.85) Hz respectively.

4.3.2.3 Resting ABP: Frequency Response and Magnitude Squared Coherence

The analysis in section 4.3.2.2 above showed that there were no significant differences between the measurement devices for the 95% and 99% bandwidths, and the computation results were pooled. This means that $\hat{H}(f)$ and $\hat{\gamma}^2(f)$ generated from individual subjects' spectral curves can also be pooled. Using Equations 4.5 and 4.6, the respective average spectral curves are shown in Figure 4.7.

The average gain spectrum shows that the cut-off frequency to -3 dB value is approximately 13.3 Hz. The average phase spectrum is barely shifted within ±10°. The average magnitude squared coherence of one is achieved up to approximately 7.0 Hz. It is maintained to at least 0.5 up to approximately 12.5 Hz, although the error bars are widening.

Table 4.7 ANOVA p-values for the 95% and 99% bandwidth limits.
The ANOVA results (2 ways 4 levels design) for 'Finap' and 'Test' main effects, and their interaction. No significant difference was detected for each bandwidth limit.

	95%	**99%**
'*Finap*' effect	0.079	0.387
'*Test*' effect	0.864	0.882
'*Finap*' x '*Test*' interaction	0.351	0.397

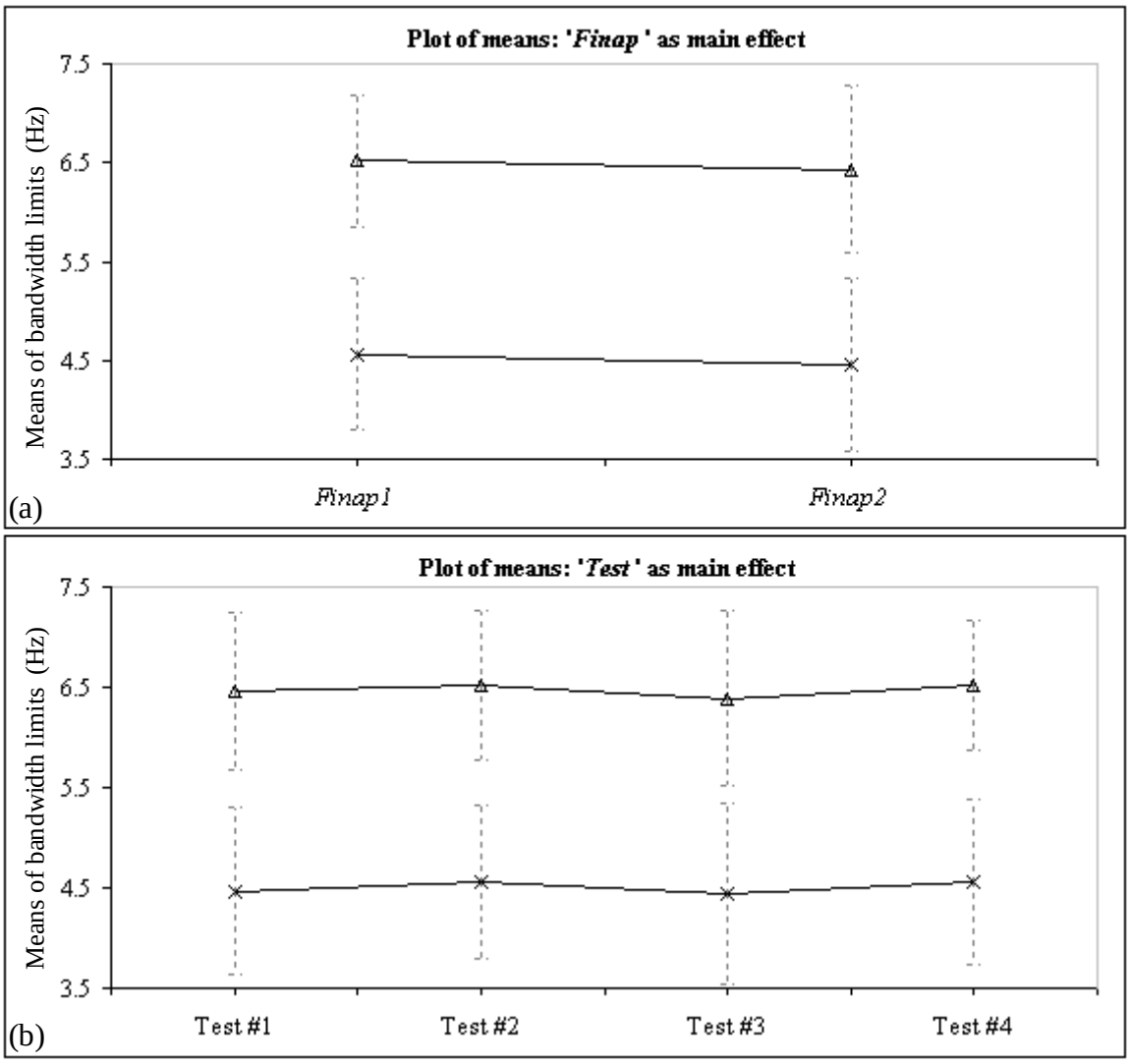

Figure 4.6 Plots of means of bandwidth limits for ABP pulses.
(a) 'Finap' main effect; (b) 'Test' main effect. The effects were plotted for 95% (cross) and 99% (triangle) bandwidth limits. The error bars are ±1SD of the respective means.

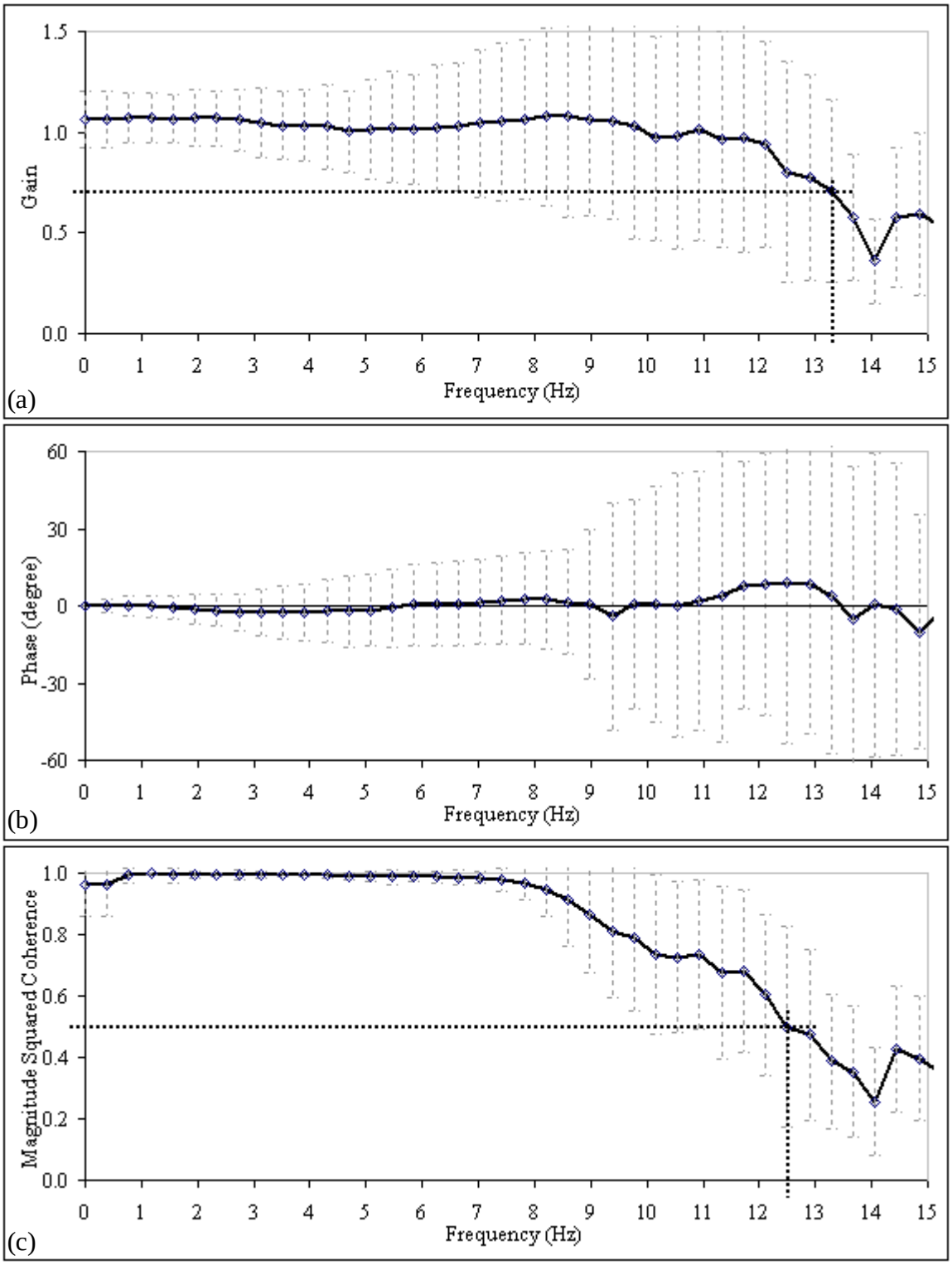

Figure 4.7 Spectral curves between ABP measurements with two Finapreses.
(a) Average gain spectrum: the -3 dB point occurs at approximately 13.3 Hz (dotted lines); (b) average phase spectrum remains stable even beyond 15 Hz; (c) average magnitude squared coherence remains above 0.5 up to about 12.5 Hz (dotted lines). The computation was from pooled results (n=44 measurements). The error bars are ±1SD for respective frequencies.

4.3.2.4 Resting ABP: Assessment of Drift

ANOVA results with p-values (2 ways 4 levels design) for the $\Delta\Psi$ are shown in Table 4.8. Figure 4.8 shows the plots of means of percentage change for the '*Finap*' and '*Test*' main effects. No significant differences were obtained for SBP, MAP and DBP. Hence, the respective results were pooled (n=44). The mean (SD) of Ψ_{Finap1}, Ψ_{Finap2} and $\Delta\Psi$ were computed for SBP, MAP and DBP. The results are:

Ψ_{Finap1} : -0.3 (6.55), -0.7 (4.31) and -1.0 (4.99) %

Ψ_{Finap2} : 1.1 (5.86), -0.1 (4.80) and -0.3 (5.75) %

$\Delta\Psi$: 1.4 (7.66), 0.6 (5.62) and 0.7 (7.01) %

The plots of $\Delta\Psi$ agreement for SBP, MAP and DBP are shown in Figure 4.9. The regression lines produced no significant correlations.

4.3.2.5 ABP Dynamic Change: Valsalva Manoeuvre

ANOVA results with p-values (2 ways 4 levels design) for the $\Delta\Phi_{VM}$ are shown in Table 4.9. Figure 4.10 shows the plots of means of percentage change for the '*Finap*' and '*Test*' main effects. No significant differences were obtained for SBP, MAP and DBP. Hence, the respective results were pooled (n=44). The mean (SD) of $\Phi_{Finap1,VM}$, $\Phi_{Finap2,VM}$ and $\Delta\Phi_{VM}$ were computed for SBP, MAP and DBP. The results are:

$\Phi_{Finap1,VM}$: 11.56 (9.75), 10.15 (7.28) and 9.97 (6.72) %

$\Phi_{Finap2,VM}$: 12.02 (9.51), 10.60 (7.34) and 10.04 (6.73) %

$\Delta\Phi_{VM}$: 0.46 (2.35), 0.45 (2.37) and 0.08 (2.21) %

The plots of $\Delta\Phi_{VM}$ agreement for SBP, MAP and DBP are shown in Figure 4.11. The regression lines produced no significant correlations.

Table 4.8 ANOVA p-values for the assessment of drift.
The ANOVA results (2 ways 4 levels design) for the 'Finap' and 'Test' main effects, and their interaction for SBP, MAP and DBP. No significant differences were detected.

	SBP	**MAP**	**DBP**
'*Finap*' effect	0.429	0.594	0.603
'*Test*' effect	0.670	0.905	0.916
'*Finap*' x '*Test*' interaction	0.056	0.075	0.108

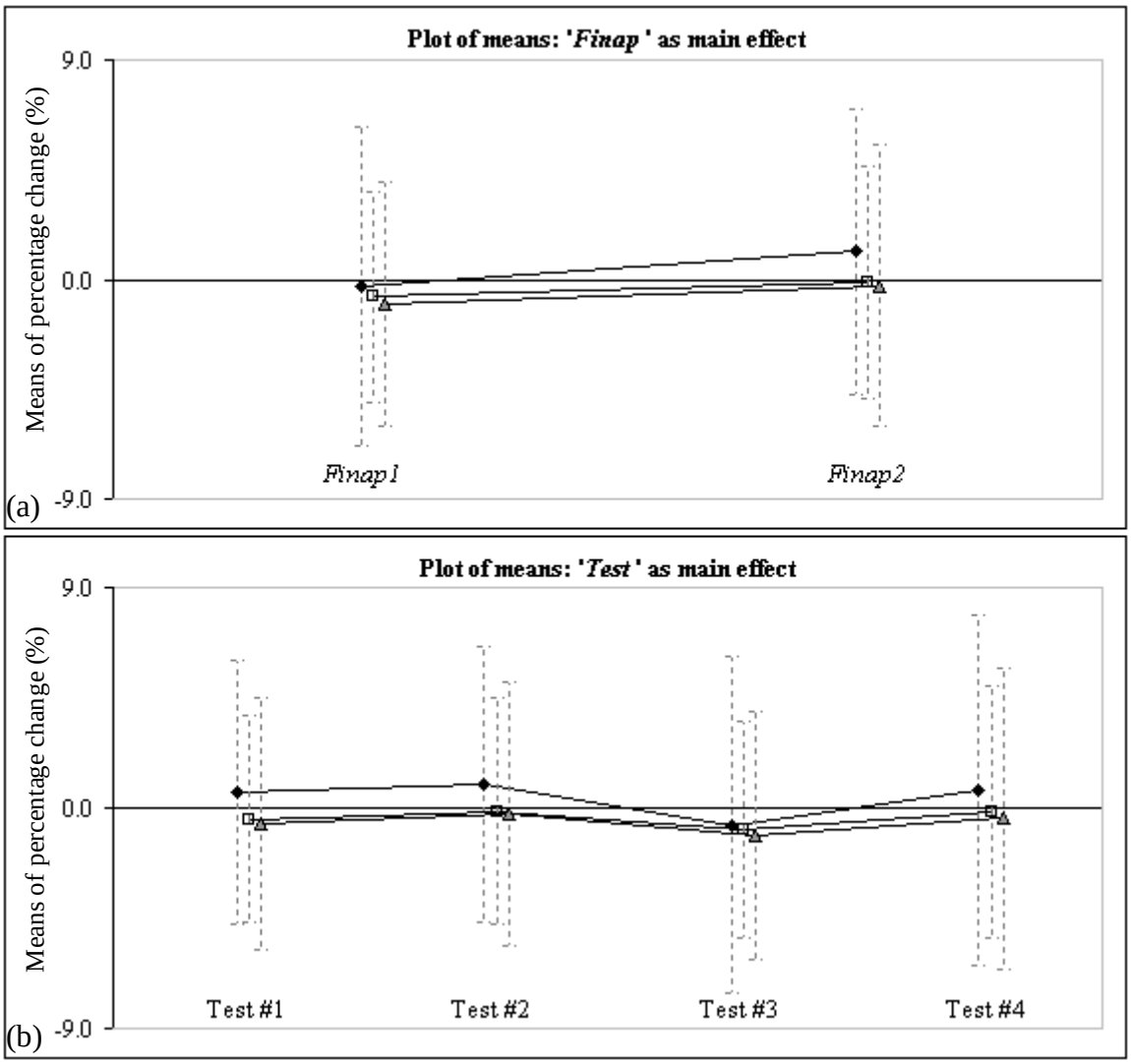

Figure 4.8 Plots of means of percentage change in the assessment of ABP drift.
(a) 'Finap' main effect; (b) 'Test' main effect. The effects were plotted for SBP (diamond), MAP (square) and DBP (triangle). The graphs are slightly shifted from each other to avoid superposition of the error bars. The error bars are ±1SD of the respective means.

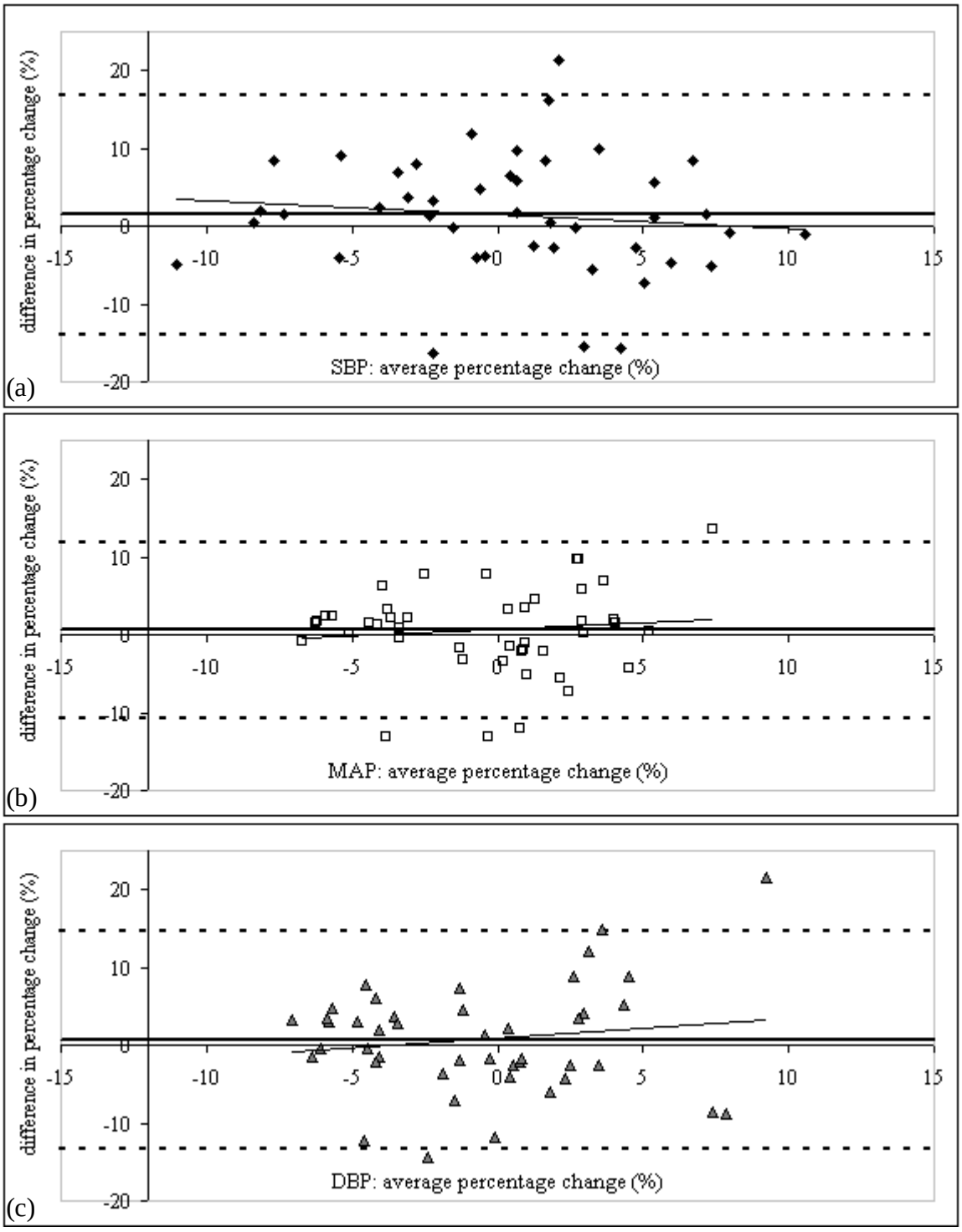

Figure 4.9 Assessment of drift in resting ABP (Finap2 vs. Finap1).
The plots of $\Delta\Psi$ for (a) SBP, (b) MAP and (c) DBP. Respective results were pooled (n=44). The thick continuous lines are the respective means of $\Delta\Psi$ and the thick dashed lines are the corresponding limits of agreement. The regression lines show no significant correlations.

Table 4.9 ANOVA p-values for $\Delta\Phi_{VM}$ during Valsalva manoeuvre.
The ANOVA results (2 ways 4 levels design) 'Finap' and 'Test' main effects, and their interaction for SBP, MAP and DBP. No significant differences were detected.

	SBP	**MAP**	**DBP**
'*Finap*' effect	0.233	0.142	0.794
'*Test*' effect	0.586	0.843	0.976
'*Finap*' x '*Test*' interaction	0.337	0.094	0.160

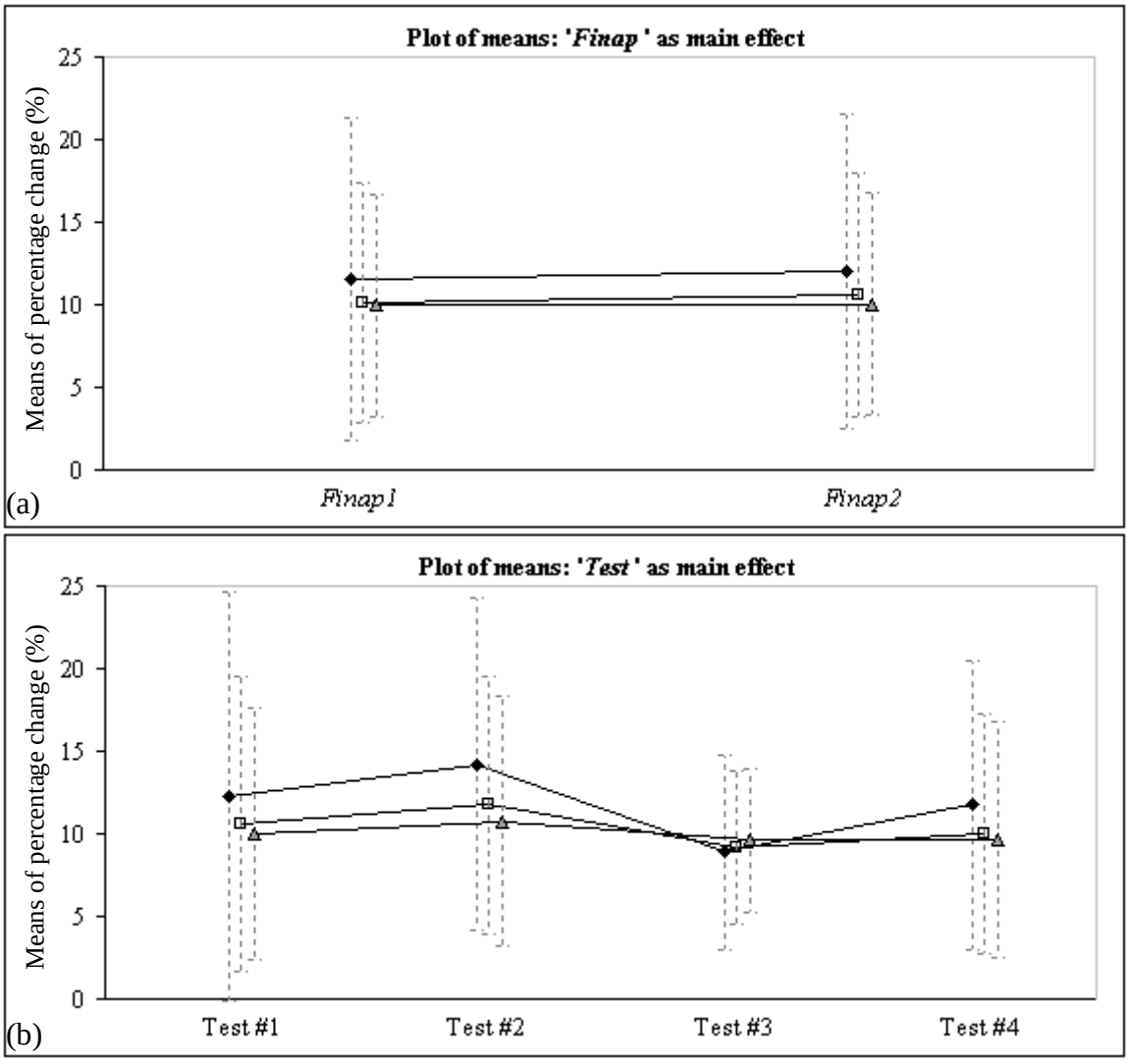

Figure 4.10 Plots of means of ABP percentage change during Valsalva manoeuvre.
(a) 'Finap' main effect; (b) 'Test' main effect. The effects were plotted for SBP (diamond), MAP (square) and DBP (triangle). The graphs are slightly shifted from each other to avoid superposition of the error bars. The error bars are ±1SD of the respective means.

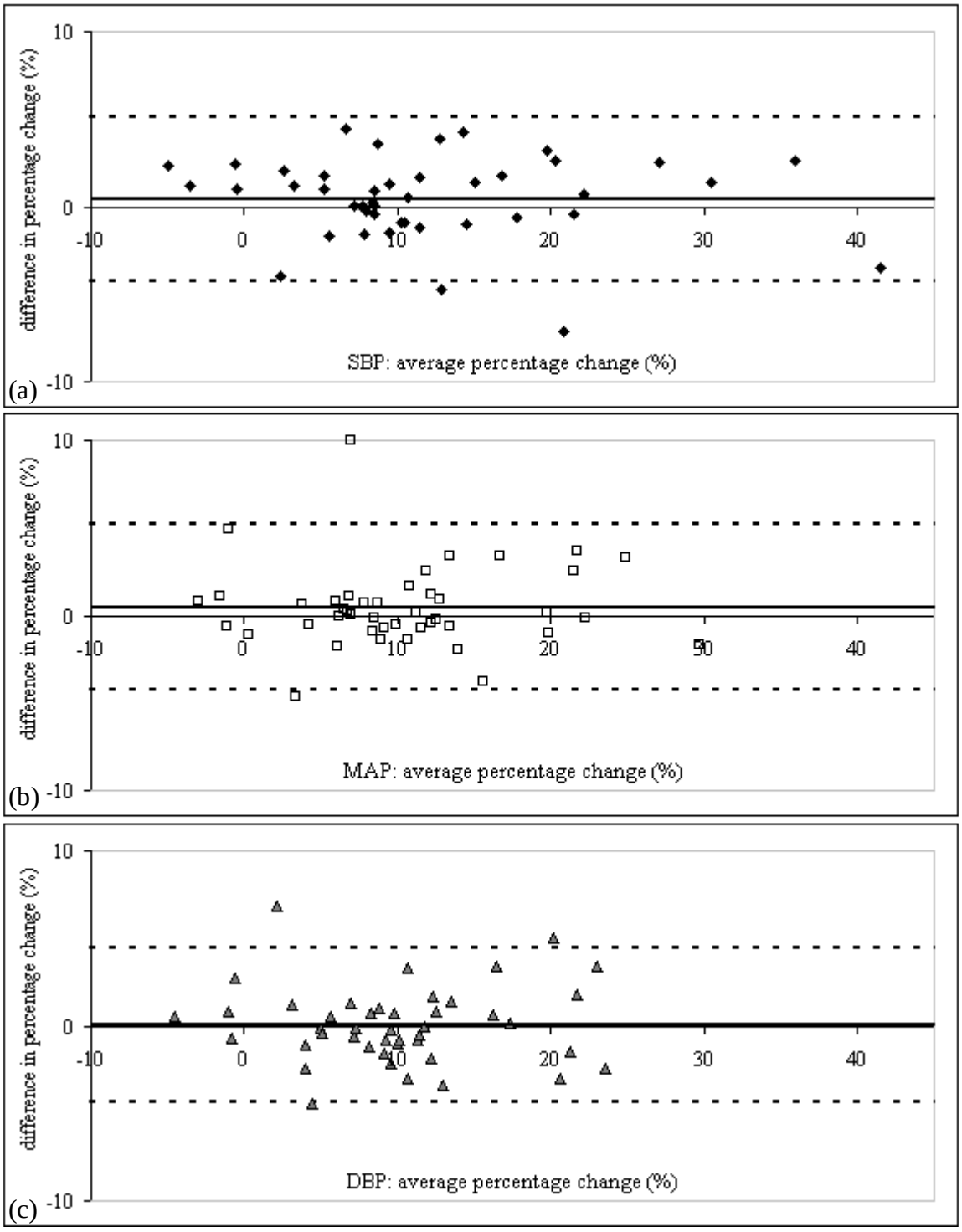

Figure 4.11 ABP dynamic change during Valsalva manoeuvre (Finap2 vs. Finap1). The plots of $\Delta\Phi_{VM}$ for (a) SBP, (b) MAP and (c) DBP. Respective results were pooled (n=44). The thick continuous lines are the respective means of $\Delta\Phi_{VM}$ and the thick dashed lines are the corresponding limits of agreement. The differences are well scattered with no significant correlations.

4.4 Comparative Study of *STAbp* and *Finapres*

The comparative study between two *Finapreses* in the previous section demonstrated that there are differences between simultaneous ABP measurements even though they were monitored with devices of the same specifications and model number. The differences will be compared further in section 4.5. Before that, the *STAbp* prototype (device B) was evaluated against the *Finapres* (device A). *Finap1* was again used as reference. Measurement protocols were very similar to the previous study. As mentioned in section 4.2, this is to enable direct comparisons of results between both studies and to interpret the differences accordingly.

4.4.1 Method

19 subjects were recruited for this study (10 males, 9 females, age (mean ± SD) 34 ± 12 years). The participants were all staff from the Medical Physics department. Written consent was given by each participant prior to the arrangement for the ABP measurements. The study was approved by the Leicestershire ethics committee (reference number: 4680).

To prepare the subject for the experiment, each subject was asked to sit comfortably upright on a chair with back support. The room temperature was maintained at approximately 22 ºC. The right STA was first located by palpation. After that, the head frame of the *STAbp* was fixed with four padded brackets fastened against the scalp. The padded brackets were equally spaced around the head. This was followed by placing the front end of the probe on the skin with the underlying STA. The probe placement was

then fixed by its fastening bracket against the head frame. The probe and head frame were described in sections 3.3.1 and 3.3.2 respectively.

For the finger ABP measurement, an appropriate *Finapres* cuff was selected and fitted onto the right middle finger of the subject. The hand rested on the right lap of the subject. The height difference between the STA and the finger artery was measured. This is to offset the hydrostatic pressure difference between the ABP in the finger artery and the STA. The hydrostatic pressure difference for each centimeter difference in height was taken as $P = h.\rho.g$ = (0.01 x 1060 x 9.81) x 750 / (1 x 10^5) = 0.77 mmHg/cm where h is the height difference (in m), ρ is the blood density (in kg/m^3) and g is the acceleration due to gravity (in ms^{-2}). This equation does not take into account individual values of blood density across the sample population.

When the setup of the experiment was complete, both recorders were switched on to monitor the ABP for several minutes. The subject was asked to relax and breathe normally during measurements. When the waveforms were stable, the self-calibration facilities in both devices were then temporarily switched off. The self-calibration algorithm in the *STAbp* was described in section 3.3.7. The paired resting ABP waveforms were recorded for 3 min.

After the 3 min recording, the respective self-calibration facilities in both measurement devices were re-enabled for several minutes. Both self-calibration facilities were then again temporarily switched off to carry out the IHG exercise.

During the IHG exercise, each subject was asked to squeeze a rolled-up slightly inflated sphygmomanometer cuff at 30% maximal voluntary compression for 2 min (Panerai et al., 2001). The compression on the cuff was monitored with an aneroid pressure gauge. After 2 min, the subject would release the grip suddenly. A dynamic mean ABP drop was expected. The recording of the ABP waveforms continued for another 1 min before the measurements were terminated in both devices.

From the resting ABP recording, 16 cardiac pulses at the beginning and 16 cardiac pulses towards the end of the 3 min recording were retrieved. The analysis techniques for these ranges of waveforms were described in sections 4.2.1 to 4.2.4. The recorded waveforms during the IHG exercise was analysed with the technique described in section 4.2.5. For each parameter considered, the null hypothesis states that there is no statistical significance between mean values. Paired t-tests were carried out to test this hypothesis.

4.4.2 Results

In paired ABP recordings from 19 subjects, both ABP waveforms from the *STAbp* and *Finap1* were visually checked to determine if their quality was satisfactory. Using this exclusion criterion, all recordings with *Finap1* were satisfactory. For resting ABP recordings, one subject was excluded as the ABP waveshape measured with the *STAbp* was very poor. Another two subjects were also excluded. This was because the *Setpt* determined by the self-calibration facility in the *STAbp* did not lead to physiologically meaningful ABP waveforms. These will be further discussed in section 4.6. Hence, the remaining 16 subjects' recordings were analysed by the techniques described in sections

4.2.1 to 4.2.4. The self-calibration algorithm to determine the *Setpt* was described in section 3.3.7.

For the assessment of ABP dynamic change during IHG exercise, the same three subjects above were excluded. Another two subjects' recordings by *STAbp* were also excluded due to poor ABP waveforms. These will be further discussed in section 4.6. Hence, the remaining 14 subjects' recordings were analysed based on the technique described in section 4.2.5.

The presentation of analysis results follows the sequence described in section 4.2 and adopts the same headings. Figure 4.12 shows an example of the paired resting ABP recordings for 16 cardiac pulses at the beginning and 16 cardiac pulses towards the end of the 3 min recording respectively. The former waveform segment was analysed according to the first three data analysis techniques described in sections 4.2.1 to 4.2.3. Both waveform segments were then analysed for the assessment of drift according to the technique described in section 4.2.4. Lastly, the analysis technique described in section 4.2.5 was used for the assessment of the ABP dynamic change during IHG exercise. An example recording is shown with its beat-to-beat SBP, MAP and DBP in Figure 4.13.

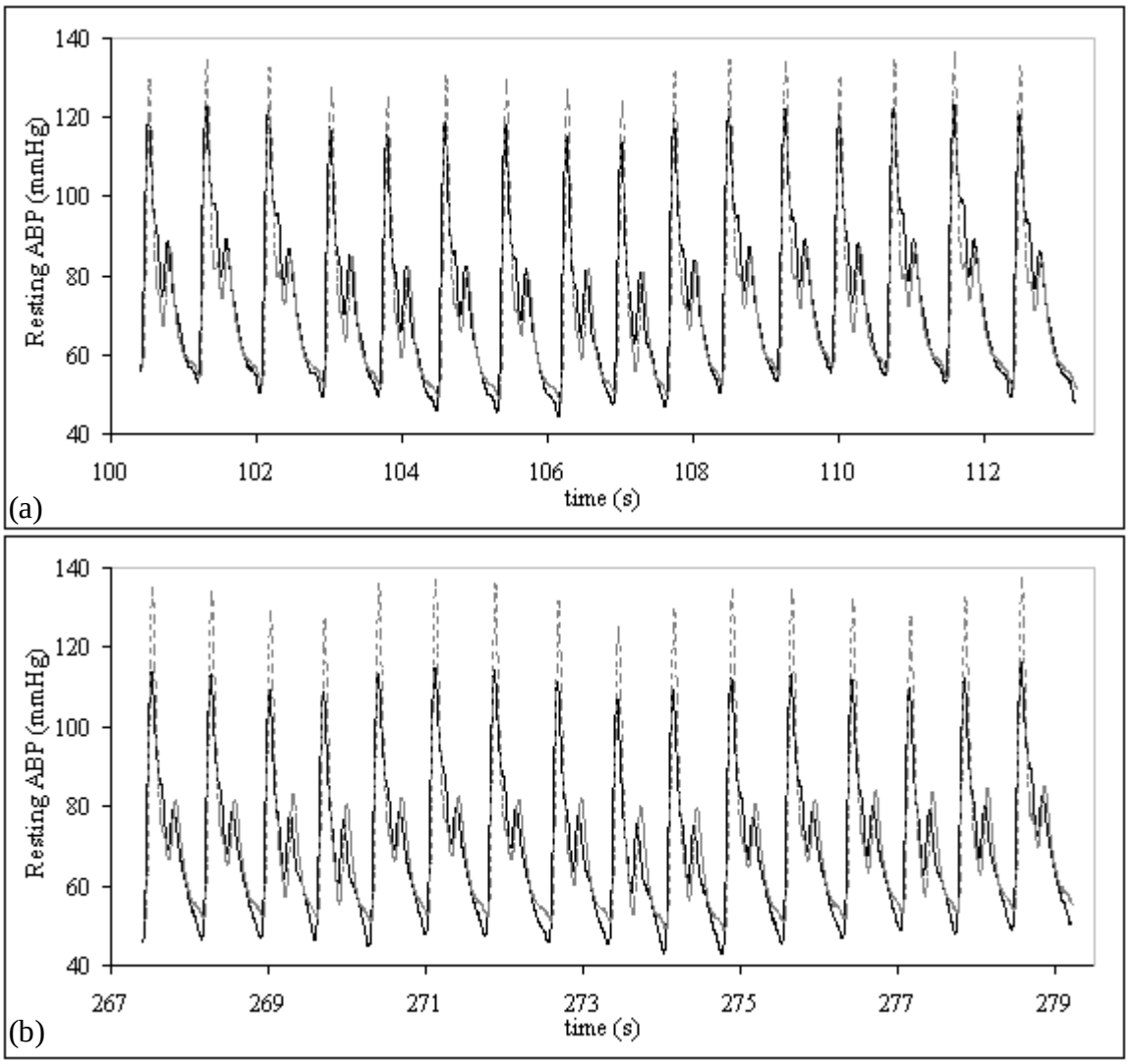

Figure 4.12 Resting ABP waveforms (STAbp vs. Finap1).
Example of 16 cardiac pulses at the beginning (a) and 16 cardiac pulses towards the end (b) of a 3 min recording with STAbp (black continuous line) and Finap1 (grey dashed line). Finap1 was used as reference.

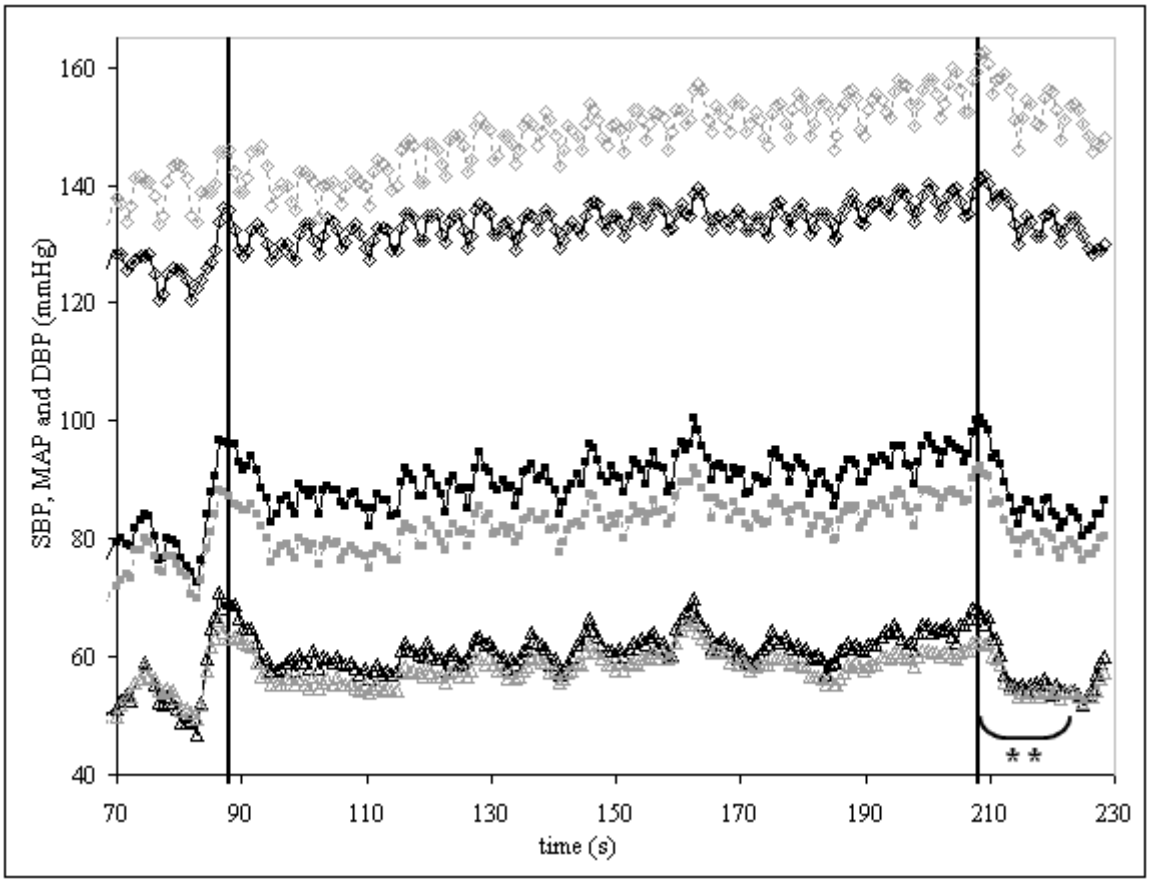

Figure 4.13 SBP, MAP and DBP during IHG exercise.
The beat-to-beat ABP with STAbp (black continuous lines) and Finap1 (grey dashed lines) are shown for SBP (diamond), MAP (square) and DBP (triangle). The vertical lines indicate the beginning and end of the 2 min IHG exercise. When the hand grip was released at the end of the 2 min, a clear dynamic drop in ABP can be observed (as indicated by asterisks).

4.4.2.1 Resting ABP: Agreement

The plots of agreement are shown in Figure 4.14 for SBP, MAP and DBP respectively. The bias (SD) for SBP, MAP and DBP were computed as -23.1 (15.05), -10.8 (13.83) and -12.4 (12.93) mmHg. Similarly, the corresponding mean (SD) of RMSE were obtained as 23.5 (14.56), 13.6 (10.90) and 13.6 (11.65) mmHg respectively. Paired t-tests showed significant differences for SBP, MAP and DBP ($p<0.001$, $p<0.01$ and $p<0.01$ respectively). Hence, the null hypothesis was rejected.

Figure 4.14 also included regression lines. Significant correlations were obtained. The correlation coefficients were 0.61 ($p<0.02$), 0.75 ($p<0.01$) and 0.69 ($p<0.01$) for SBP, MAP and DBP respectively. No significant correlation was detected between subjects' ABP differences with age.

4.4.2.2 Resting ABP: Bandwidth

For the 95% bandwidth limit, the mean (SD) of $\overline{K}_{STAbp95}$ and $\overline{K}_{Finap,95}$ were computed as 3.2 (1.10) Hz and 4.8 (0.88) Hz respectively. Paired t-test showed statistical significance for ΔK_{95} ($p<0.001$). Similarly, for the 99% bandwidth limit, the mean (SD) of $\overline{K}_{STAbp99}$ and $\overline{K}_{Finap,99}$ were computed as 5.3 (1.46) Hz and 6.8 (0.73) Hz respectively. Paired t-test showed statistical significance for ΔK_{99} ($p<0.01$).

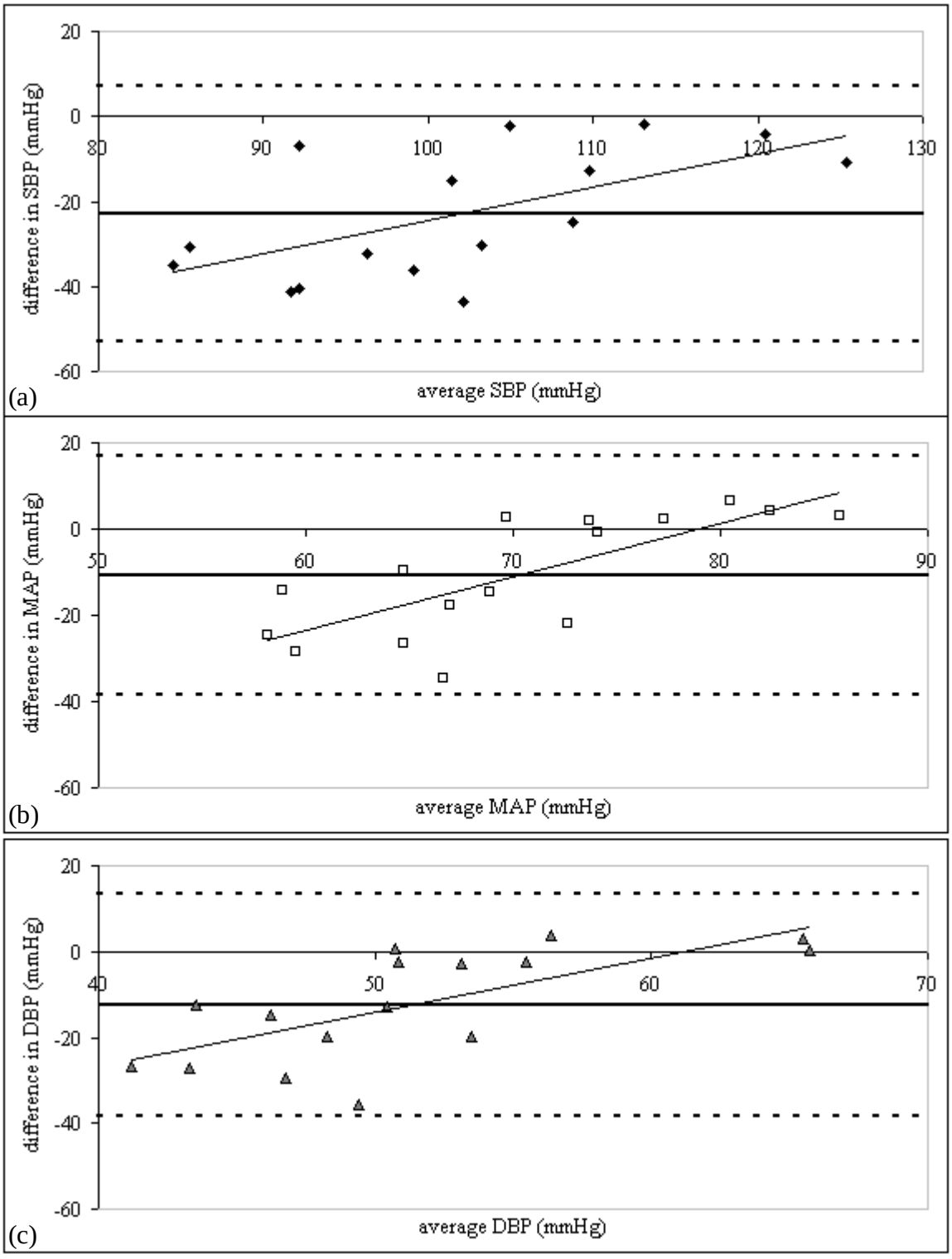

Figure 4.14 Plots of agreement in resting ABP (STAbp vs. Finap1).
(a) SBP, (b) MAP and (c) DBP. The thick continuous lines are the respective biases (n=16 subjects) and the dashed lines are the corresponding limits of agreement. The regression lines show significant correlations. See text in section 4.4.2.1 for detailed results.

4.4.2.3 Resting ABP: Frequency Response and Magnitude Squared Coherence

Figure 4.15 shows the $\hat{H}(f)$ and $\hat{\gamma}^2(f)$ spectral curves (Equations 4.5 and 4.6). The cut-off frequency (-3 dB point) of the average gain spectrum is approximately 3 Hz. There is very little phase shift in the average phase spectrum until about 3.2 Hz when it gradually increases before stabilizing from approximately 9.5 Hz. The average coherence spectrum shows that the coherence is high, remaining above 0.5 even beyond 12 Hz.

4.4.2.4 Resting ABP: Assessment of Drift

The mean (SD) of Ψ_{Finap1}, Ψ_{STAbp} and $\Delta\Psi$ were computed for SBP, MAP and DBP. The results are:

Ψ_{Finap1} : -0.8 (6.43), -1.5 (6.00) and -2.2 (6.60) %

Ψ_{STAbp} : 1.0 (7.16), 0.9 (7.79) and -0.1 (9.00) %

$\Delta\Psi$: 1.8 (5.64), 2.3 (5.23) and 2.2 (6.52) %

The plots of $\Delta\Psi$ for SBP, MAP and DBP are shown in Figure 4.16. $\Delta\Psi$ are well scattered with no significant correlations. Paired t-tests also showed no significant differences.

4.4.2.5 ABP Dynamic Change: IHG Exercise

An example of the paired ABP during IHG exercise is shown in Figure 4.13 with the beat-to-beat SBP, MAP and DBP. The dynamic drop of the ABP after the release of the handgrip is indicated by asterisks. The mean (SD) of $\Psi_{Finap1,IHG}$, $\Psi_{STAbp,IHG}$ and $\Delta\Psi_{IHG}$ were computed for SBP, MAP and DBP. The results are:

$\Phi_{Finap1,IHG}$: 10.5 (11.81), 14.1 (12.34) and 15.8 (14.20) %

$\Phi_{STAbp,IHG}$: 10.3 (9.69), 11.8 (10.45) and 11.3 (11.21) %

$\Delta\Phi_{IHG}$: -0.2 (10.04), -2.3 (9.49) and -4.5 (11.66) %

The plots of $\Delta\Phi_{IHG}$ for SBP, MAP and DBP between *STAbp* and *Finap1* are shown in Figure 4.17. $\Delta\Phi_{IHG}$ are well scattered with no significant correlations. Paired t-tests also showed no significant differences.

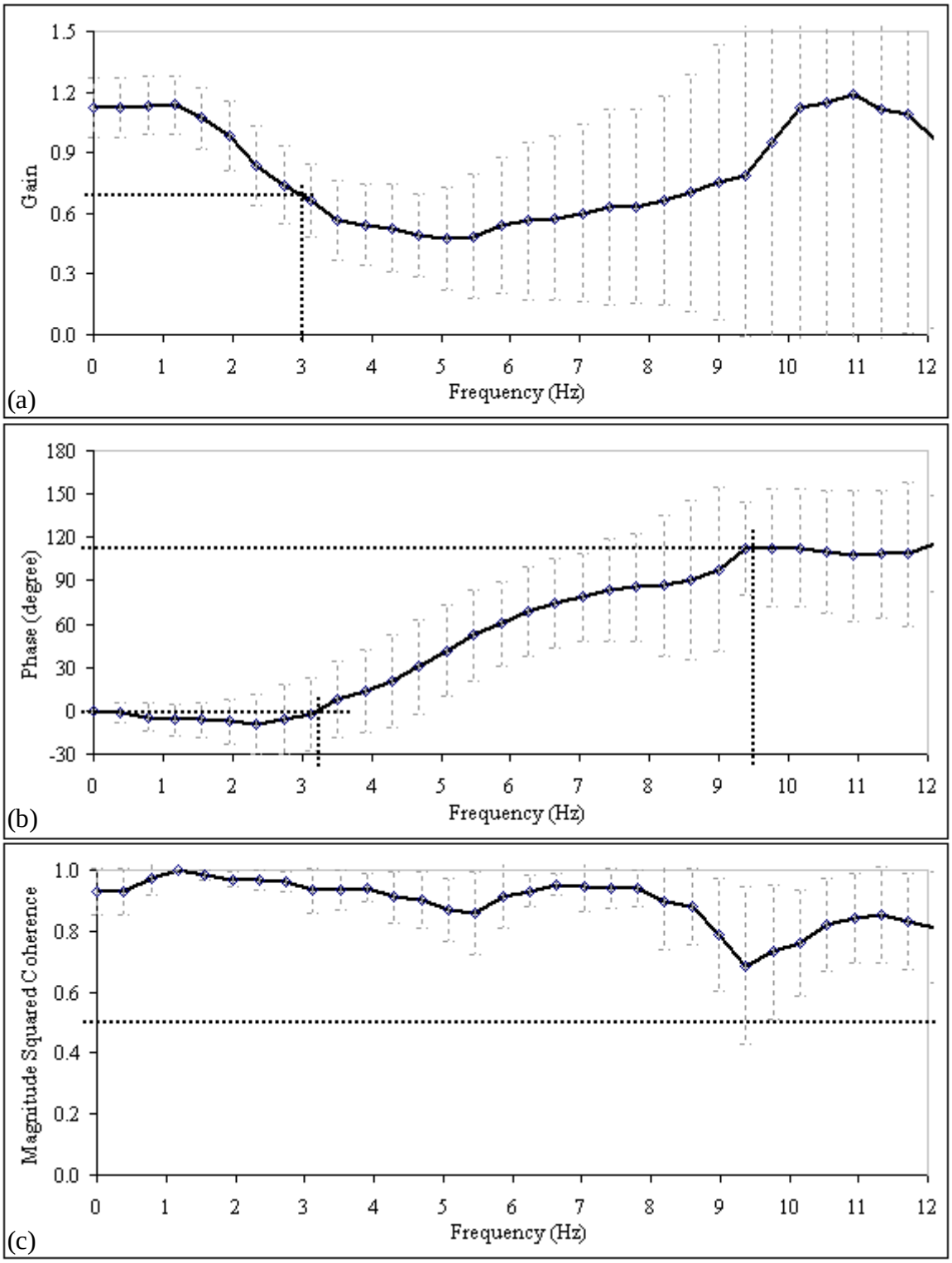

Figure 4.15 Spectral characteristic curves (STAbp vs. Finap1).
(a) Average gain spectrum: the cut-off frequency at -3 dB is approximately 3 Hz (dotted lines); (b) average phase spectrum remains fairly stable up to about 3.2 Hz and gradually increases before stabilising at approximately 9.5 Hz (dotted lines); (c) average magnitude squared coherence remains above 0.5 even beyond 12 Hz (dotted lines). The error bars are ±1SD for respective frequencies (n=16 subjects).

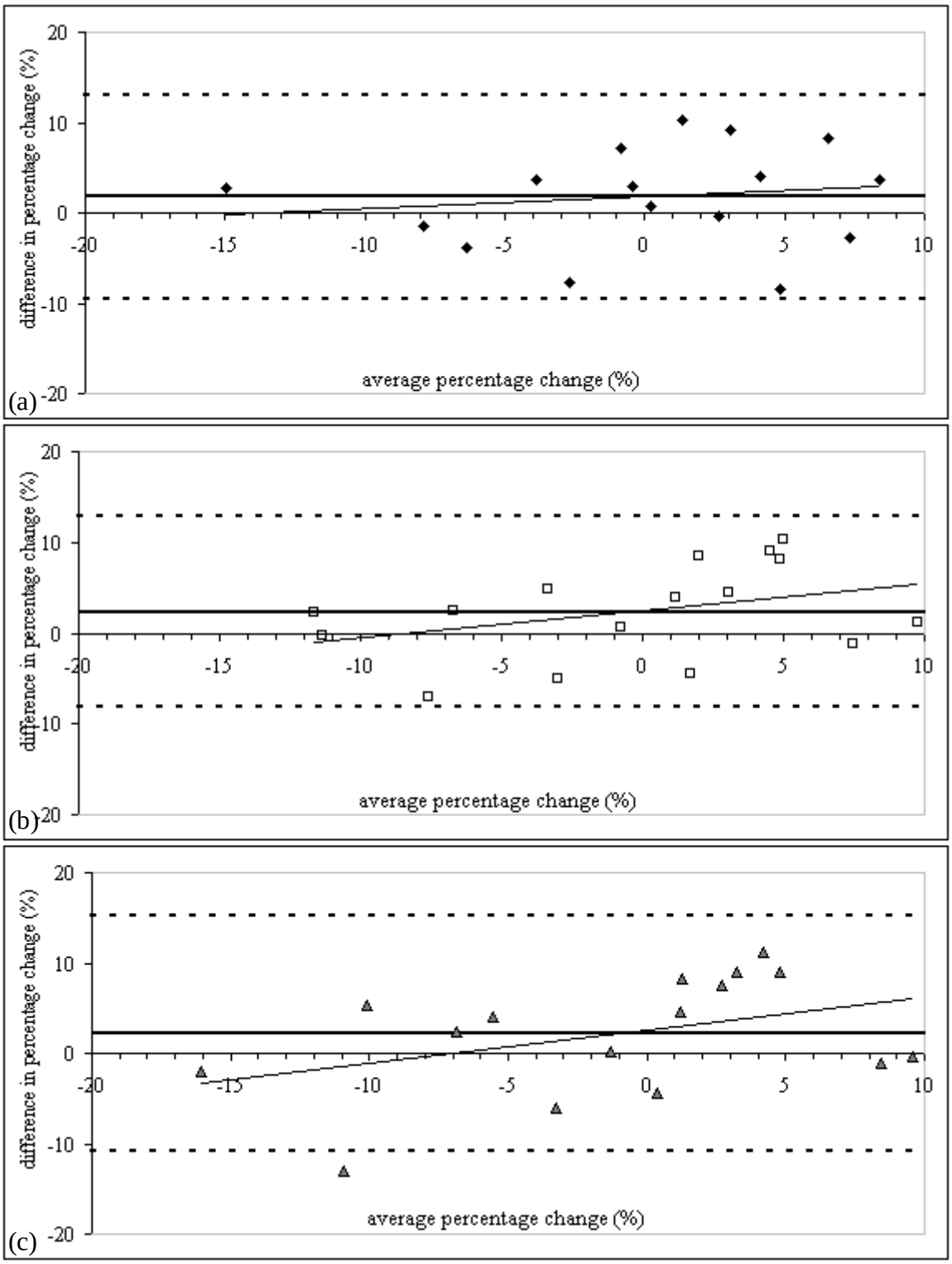

Figure 4.16 Assessment of drift in resting ABP (STAbp vs. Finap1).
The plots of $\Delta\Psi$ for (a) SBP, (b) MAP and (c) DBP (n=16 subjects). The thick continuous lines are the respective means of $\Delta\Psi$ and the thick dashed lines are the corresponding limits of agreement. The regression lines show no significant correlations.

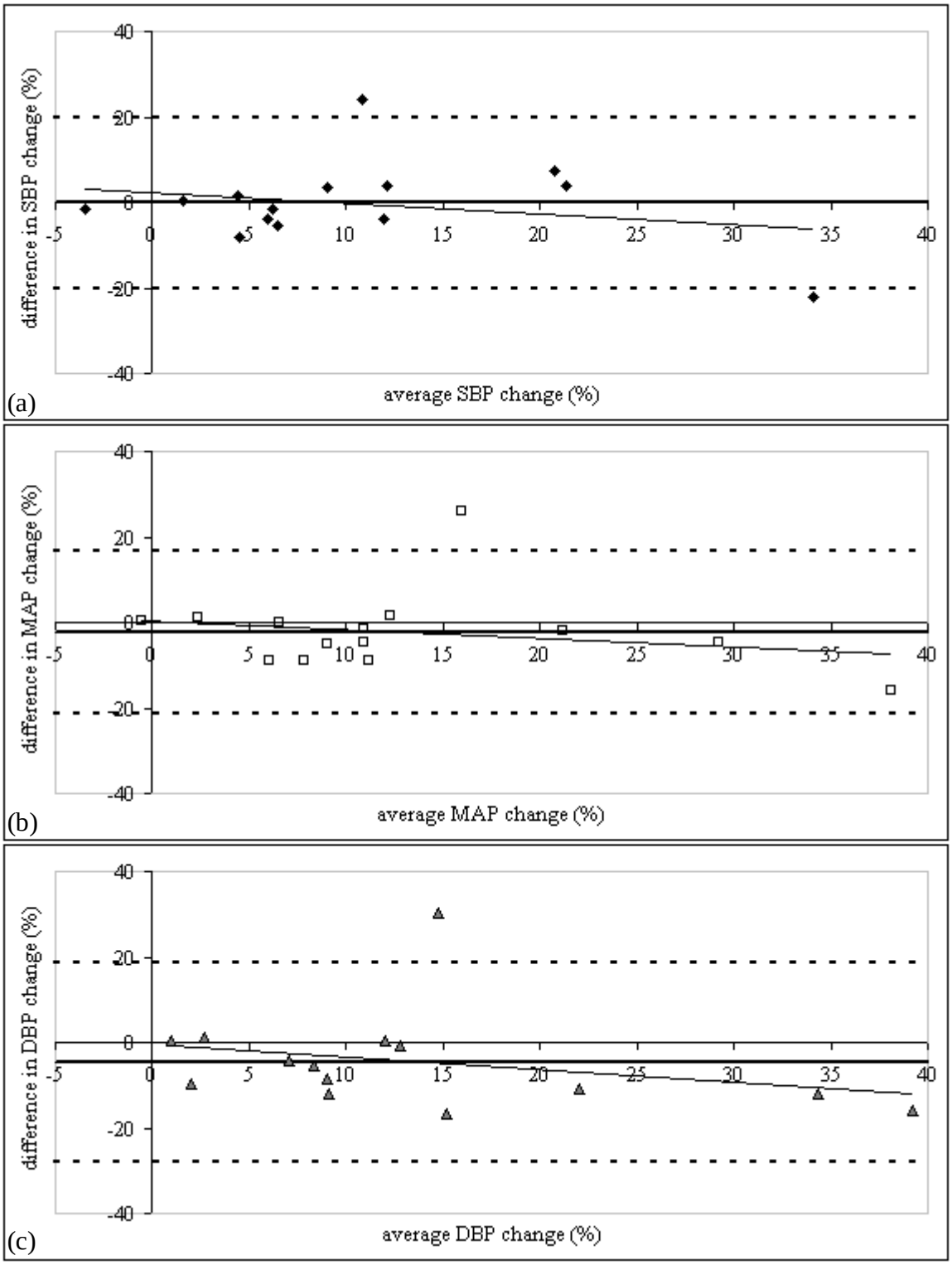

Figure 4.17 ABP dynamic change during IHG exercise (STAbp vs. Finap1).
The plots of $\Delta\Phi_{IHG}$ for (a) SBP, (b) MAP and (c) DBP. The thick continuous lines are the respective means of $\Delta\Phi_{IHG}$ (n=14 subjects) and the dashed lines are the corresponding limits of agreement. The regression lines show no significant correlations.

4.5 Inter-Study Comparisons

Two separate comparative studies (sections 4.3 and 4.4) were performed and the ABP waveforms were analysed according to standard statistical methods (section 4.2). The analysis results from both comparative studies are summarized in Table 4.10, tabulated in two pages. The left column are results for comparative study between two *Finapreses*, whereas, the right column are results for comparative study of *STAbp* and *Finap1*. Results of the four parameters described in section 4.2 are presented in this table, whereas the comparisons of spectral responses (section 4.2.3) are presented in Figure 4.18.

Despite the potential influence of different measurement sites, to be discussed later, further comparison between the two separate studies would be useful to highlight areas of significant differences. Independent t-tests were carried out for the agreement of ABP (SBP, MAP and DBP), 95% and 99% bandwidth limits and the assessment of ABP drift (SBP, MAP and DBP). Statistical results with significant p-values are shown in Table 4.11. The results of ABP dynamic change due to activity were not further compared as different activities were carried out (i.e. Valsalva manoeuvre or IHG exercise).

In the inter-study comparisons of ABP agreement, only Tests #1 and #3 (Table 4.11) were compared with the comparative study of *STAbp* and *Finap1* because the same finger was measured by *Finap1* in all the three experiments, i.e. the right middle finger (Table 4.1). In theory, Bonferroni correction would be needed for these multiple comparisons (Bland, 1995; Campbell and Machin, 1995), but given the very small p-values obtained, it does not make a difference.

Inter-study comparisons of the 95% and 99% bandwidth limits only apply to the *STAbp* and *Finap2* as both studies used *Finap1* as reference. Significant differences were obtained for both bandwidth limits (Table 4.11). Next, the inter-study comparisons of the assessment of ABP drift produced no significant differences for SBP, MAP and DBP.

The spectral curves of Figures 4.7 and 4.15 are replotted in Figure 4.18 to further compare the curves between both studies. In the average gain spectrum, the cut-off frequency at -3 dB apparently dropped from approximately 13.3 Hz to 3 Hz. However, comparisons of the two curves show that *STAbp* gain response seems to recover at higher frequencies suggesting that it should be possible to recover a flat response with further modifications in hardware and/or software.

The average phase spectrum in *STAbp* vs. *Finap1* remained fairly stable until about 3.2 Hz and gradually increased before stabilising at approximately 9.5 Hz (indicated by dotted lines). The phase shift is increasingly leading from 0º to 110º within the frequency range 3.2 Hz and 9.5 Hz. However, between two *Finapreses*, the average phase shift remained stable even beyond 15 Hz. Lastly, the average magnitude squared coherence remained above 0.5 even beyond 12.5 Hz for both studies. Further discussion and interpretation of these curves will be presented in the next section.

Table 4.10 Summary of results from both comparative studies. Only significant p-values are listed.

Section 4.3: *Finap2* vs. *Finap1*			**Section 4.4: *STAbp* vs. *Finap1***		
4.3.2.1 Resting ABP: Agreement			**4.4.2.1 Resting ABP: Agreement**		
	Bias (SD) [mmHg]	**Mean (SD) of RMSE [mmHg]**		**Bias (SD) [mmHg]**	**Mean (SD) of RMSE [mmHg]**
Test #1					
SBP	7.6 (6.82)	9.0 (4.71)	**SBP**	-23.1 (15.05) *see †a*	23.5 (14.56)
MAP	6.0 (4.43)	6.4 (3.87)	**MAP**	-10.8 (13.83) *see †b*	13.6 (10.90)
DBP	5.4 (4.67)	6.0 (3.86)	**DBP**	-12.4 (12.93) *see †c*	13.6 (11.65)
Test #2					
SBP	0.3 (7.87)	6.0 (5.02)		**Paired t-test**	
MAP	1.8 (8.25)	5.4 (6.36)		*†a* p<0.001	
DBP	1.5 (9.25)	6.2 (6.83)		*†b* p<0.01	
Test #3				*†c* p<0.01	
SBP	6.3 (7.80)	8.2 (6.05)			
MAP	3.4 (5.25)	4.2 (4.80)		**Correlation coefficient**	
DBP	1.9 (4.78)	3.4 (3.87)		*†a* 0.61 (p<0.02)	
Test #4				*†b* 0.75 (p<0.01)	
SBP	2.4 (10.67)	9.3 (5.28)		*†c* 0.69 (p<0.01)	
MAP	2.0 (7.87)	6.6 (4.42)			
DBP	1.7 (7.43)	6.2 (4.21)			

4.3.2.2 Resting ABP: Bandwidth			**4.4.2.2 Resting ABP: Bandwidth**		
Mean (SD) [mmHg]	**95%**	**99%**	**Mean (SD) [mmHg]**	**95%**	**99%**
Finap1	4.6 (0.76)	6.5 (0.66)	***Finap1***	4.8 (0.88)	6.8 (0.73)
Finap2	4.5 (0.87)	6.4 (0.85)	***STAbp***	3.2 (1.10)	5.3 (1.46)
			Paired t-test	p<0.001	p<0.01

Table 4.10 Summary of results from both comparative studies (continued).

4.3.2.4 Resting ABP: Drift				**4.4.2.4 Resting ABP: Drift**			
	Mean (SD) [%]				**Mean (SD) [%]**		
	Ψ_{Finap1}	Ψ_{Finap2}	$\Delta\Psi$		Ψ_{Finap1}	Ψ_{STAbp}	$\Delta\Psi$
SBP	-0.3 (6.55)	1.1 (5.86)	1.4 (7.66)	**SBP**	-0.8 (6.43)	1.0 (7.16)	1.8 (5.64)
MAP	-0.7 (4.31)	-0.1 (4.80)	0.6 (5.62)	**MAP**	-1.5 (6.00)	0.9 (7.79)	2.3 (5.23)
DBP	-1.0 (4.99)	-0.3 (5.75)	0.7 (7.01)	**DBP**	-2.2 (6.60)	-0.1 (9.00)	2.2 (6.52)
4.3.2.5 Valsalva Manoeuvre				**4.4.2.5 IHG Exercise**			
	Mean (SD) [%]				**Mean (SD) [%]**		
	$\Phi_{Finap1,VM}$	$\Phi_{Finap2,VM}$	$\Delta\Phi_{VM}$		$\Phi_{Finap1,IHG}$	$\Phi_{STAbp,IHG}$	$\Delta\Phi_{IHG}$
SBP	11.6 (9.75)	12.0 (9.51)	0.5 (2.35)	**SBP**	10.5 (11.81)	10.3 (9.69)	-0.2 (10.04)
MAP	10.1 (7.28)	10.6 (7.34)	0.5 (2.37)	**MAP**	14.1 (12.34)	11.8 (10.45)	-2.3 (9.49)
DBP	10.0 (6.72)	10.0 (6.73)	0.1 (2.21)	**DBP**	15.8 (14.20)	11.3 (11.21)	-4.5 (11.66)

Table 4.11 Further comparison between both comparative studies.
Only Tests #1 and #3 were further compared because both tests and the comparative study of STAbp and Finapres used the same finger for Finap1 (Table 4.1). The inter-study comparisons of the bandwidth limits are between STAbp and Finap2 only as both used Finap1 as reference.

Section 4.5		
Resting ABP: Agreement		
Test #1		
SBP	p<0.001	
MAP	p<0.001	
DBP	p<0.001	
Test #3		
SBP	p<0.001	
MAP	p<0.01	
DBP	p<0.01	
Resting ABP: Bandwidth		
	95%	**99%**
STAbp vs. Finap2	p<0.001	p<0.001
Resting ABP: Drift		
SBP	N. S.	
MAP	N. S.	
DBP	N. S.	

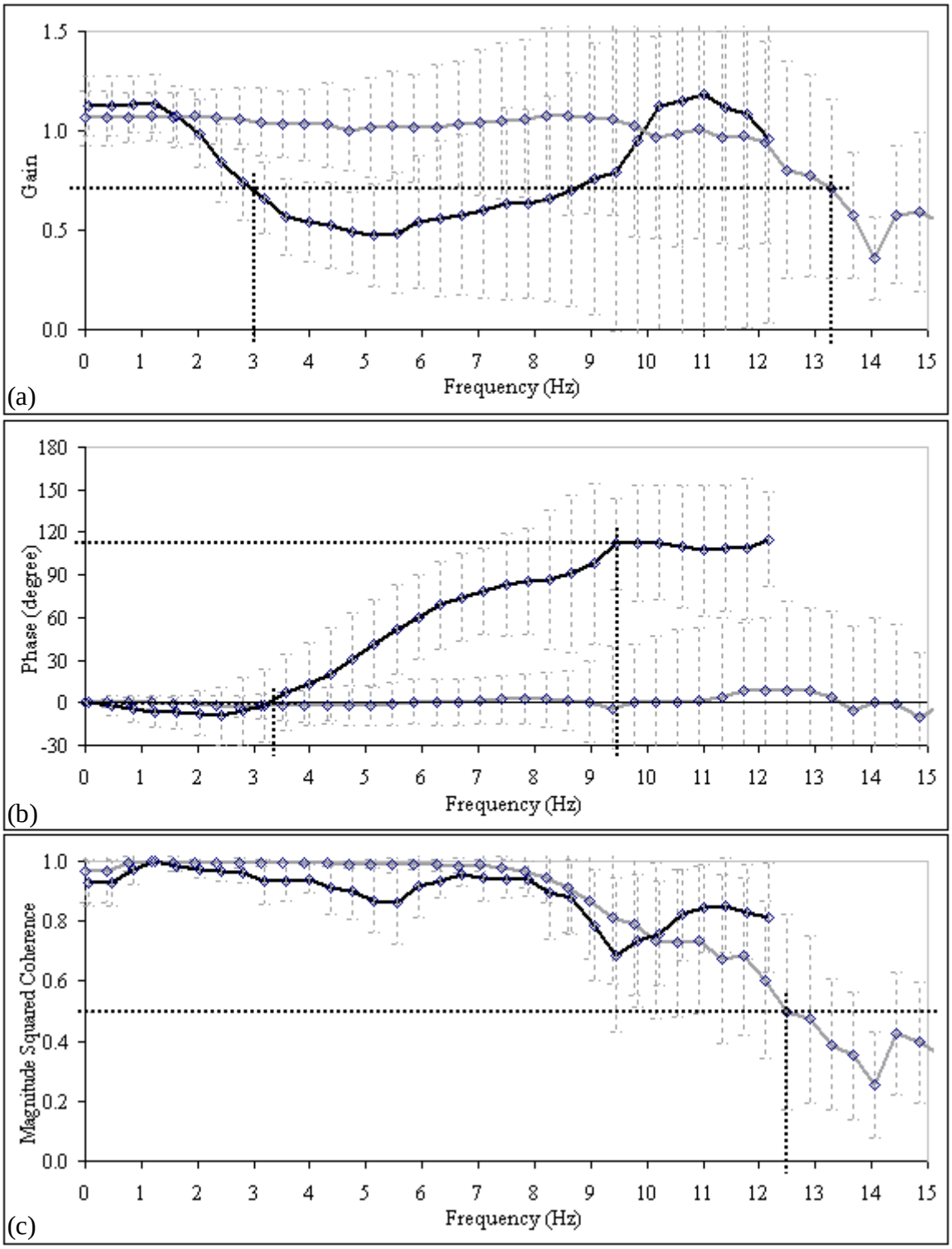

Figure 4.18 Comparison of spectral responses between both studies.
Spectral curves from comparison study between two Finapreses (grey continuous lines) and comparative study of STAbp and Finapres (black continuous lines). They are replotted from Figures 4.7 and 4.15. (a) Average gain spectrum with the cut-off frequency at -3 dB indicated by dotted lines; (b) average phase spectrum, see text in section 4.5 for detailed description; (c) average magnitude squared coherence remains above 0.5 even beyond 12.5 Hz for both curves (indicated by dotted lines). The graphs are slightly shifted from each other to avoid superposition of the error bars. The error bars are the respective ±1SD at each frequency value.

4.6 Discussion

To simplify the following text, *Study1* refers to the comparative study between two *Finapreses*, and *Study2* refers to the comparative study of *STAbp* and *Finapres*.

Both *Study1* and *Study2* are original contributions of this thesis. Evaluations of the *Finapres* against intravascular measurements were reported by a number of authors using different measurement sites, e.g. brachial, radial or ascending aorta (Epstein et al., 1991; Farquhar, 1991; Imholz et al., 1998; Omboni et al., 1993; Pace and East, 1991; van Egmond et al., 1985). For the objectives of this chapter, these reported results are not directly applicable. Instead, *Study1* demonstrated the inherent differences of simultaneous ABP measurements by two *Finapreses* of the same model (Table 4.10). The information generated is useful to gauge the results from *Study2*.

The following subsections begin with further discussion regarding exclusion of several subjects' recordings from analysis. This is followed by discussion of main findings from both comparative studies. Next, potential causes of differences in ABP measurements in both comparative studies are listed, and limitations of the comparative studies are identified. Finally, the follow up of safety evaluation of the *STAbp* device from section 3.4.2 and suggestions for future work are presented.

4.6.1 Recordings Excluded from Analysis

Resting ABP recordings

In *Study2*, three subjects' paired resting ABP recordings were excluded for analysis. In two of them, the *Setpt* determined with the self-calibration algorithm in the *STAbp* did

not lead to meaningful ABP waveform. Figure 4.19 shows an example. With increasing compressing pressure, the PPG baseline remained at a similar level. The span of the compressing pressures in this example is approximately 70 mmHg. This phenomenon may be due to insufficient compression from the inflatable sealed air chamber on the tissue covering the STA. It may also be due to thick and/or stiff skin tissue that attenuates the pressure transmission from the chamber to the STA. In comparison, Figure 3.9 shows a typical PPG waveform with the PPG baseline gradually increasing with compressing pressure.

In another subject, meaningful ABP waveform monitored by the *STAbp* could not be obtained. The morphology of the ABP waveform was very poor. The PPG pulse amplitude was small, which may suggest weak arterial pulse. This was verified by palpation. However, simultaneous recording by *Finap1* in the finger showed good quality ABP waveform. This may also suggest that the STA is embedded deep below the skin surface. The implication of this for clinical practice is that in some subjects with weak arterial pulse or low ABP, the *STAbp* device may struggle to monitor ABP in the STA.

ABP recordings during IHG exercise

Five subjects' recordings during the IHG exercise were excluded. Three of the subjects are the same as the subjects mentioned above. Recordings from another two subjects were excluded due to poor quality ABP waveforms in the *STAbp*. Further attempts with these two subjects did not produce satisfactory ABP waveforms. The precise reasons behind this problem could not be identified at the time. Technical limitations of the *STAbp* device may not be the cause of the poor quality waveform as the resting ABP

recordings from these subjects were satisfactory and accepted for analysis. Thus, other possible causes were considered. For instance, the artery may have been shifted away from its initial position after prolonged compression during resting ABP recording; it may also be possible that the tissue and the artery required time to recover to its initial state after prolonged compression.

Atypical PPG waveform

In one subject (different from those mentioned above), an atypical PPG with inverted waveform was observed during resting ABP recording (Figure 4.20(a)). This is different from the typical PPG shown in Figure 4.20(b). In theory, the PPG decreases as the arterial blood volume increases, and vice versa (section 2.5.2). To overcome this problem, the placement of the probe was repositioned until a satisfactory PPG was obtained. At current development, the repositioning approach is subjective. With this approach, the subsequent ABP recording from this subject was satisfactory and was not excluded from analysis. Inverted PPG waveforms were also observed in the radial (Nijboer and Dorlas, 1982) and carotid (Weinmann et al., 1977) arteries. This contradiction to the theory of *in-vivo* PPG indicates that other factors are affecting the generated PPG. Apart from the arterial blood volume, factors that may affect the light scattering and reflection back to the photodetector include movement of blood vessel walls, orientation of red blood cells (Allen, 2007), bone (Näslund et al., 2006) and venous engorgement (Nijboer and Dorlas, 1982). However, these studies were not based on the *in-vivo* STA and its surrounding tissue. The occurrence of atypical PPG waveforms does pose a technical concern for accurate and reliable ABP measurements based on volume clamping technique with photoplethysmography. Further investigation is needed to clarify the origin of these atypical inverted PPG waveforms.

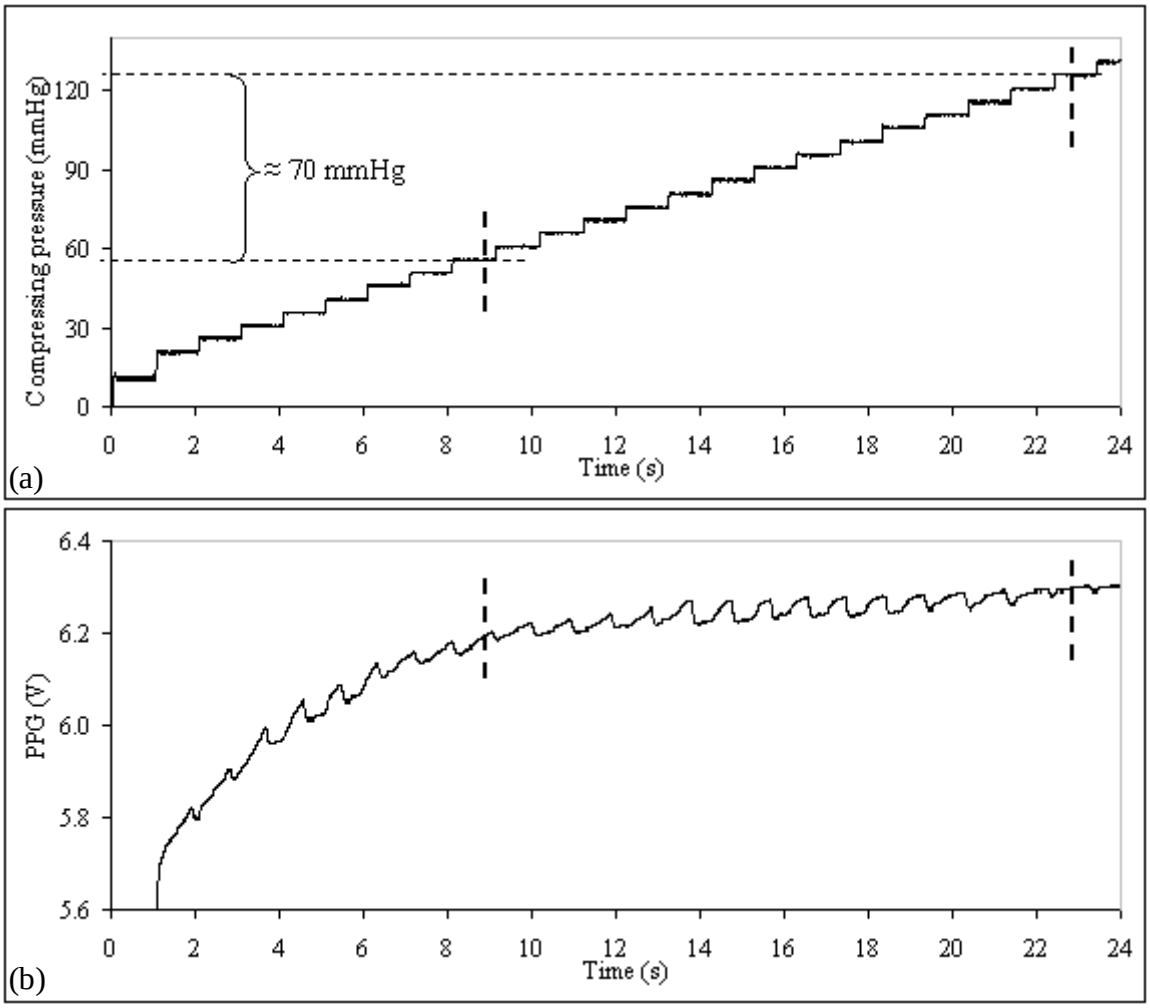

Figure 4.19 PPG with fairly constant baseline.
The waveforms were recorded by the STAbp. (a) The external compressing pressure is increased in steps of 5 mmHg/s; (b) the corresponding PPG baseline barely changes in a span of approximately 70mmHg (indicated within two vertical dashed lines).

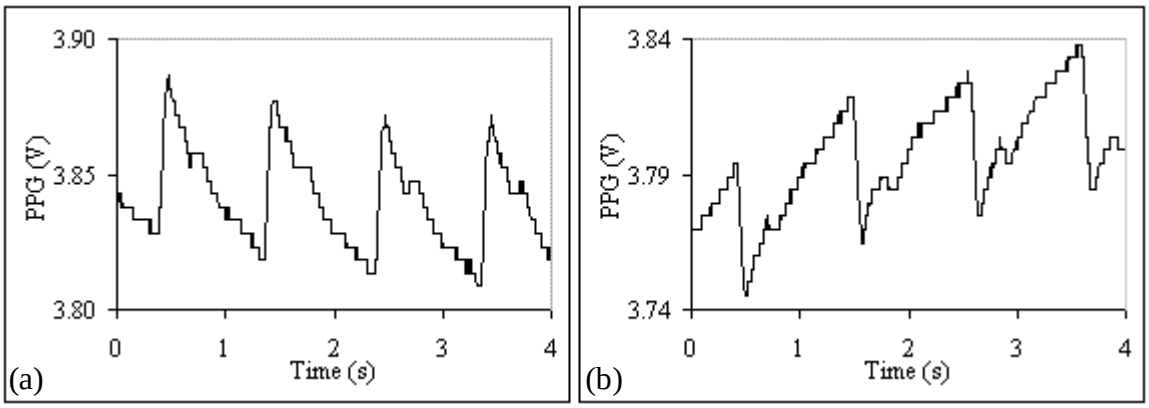

Figure 4.20 Atypical vs. typical PPG waveforms.
(a) An example of an atypical PPG with inverted waveshape; (b) An example of a typical PPG waveform.

4.6.2 Main Findings

Analysis result for the ABP agreement in *Study1* shows that the paired measurements from four combinations of fingers did not allow the measurement results to be pooled, due to significant differences between tests (Tables 4.2 to 4.4). Furthermore, Figure 4.18 demonstrated that the frequency gain response was only achieved up to 13.3 Hz and the coherence ($\geq$0.5) was only achieved up to 12.5 Hz. These findings give some indication of what could be expected from *Study2*.

Resting ABP: agreement

In *Study1*, Tables 4.2 to 4.4 show that all the significant p-values are related to '*Finap2* Test #1' (labelled as $\{5\}$). Definite causes are unclear. There was no significant correlation between the ABP differences and age of the subjects. Thus, it may be due to inappropriate cuff fitting (i.e. too loose or too tight), poorer blood circulation in one finger during ABP measurements, or possibly compression of the fingers as the subject may be leaning forward or backward during ABP measurements.

In *Study2*, the significant p-values for the ABP agreement (Table 4.10) could be due to several key factors. First, the ABP were recorded from two different measurement sites. Referring to Figure 1.2, the SBP tends to be raised in the periphery in younger subjects which may also explain the reason a larger bias in SBP was obtained than the MAP and DBP. The differences in physiological condition in different measurement sites may also have contributed to the differences in ABP measurements. The clinical interpretation regarding the significance of the ABP differences between measurement devices could depend on an individual's baseline ABP. For instance, a person who is already diagnosed with hypertension may require further treatment if the measured ABP

is close to the ABP threshold for hypertension, i.e. approximately 140/90 mmHg (O'Brien et al., 2003). For individuals within the healthy ABP range, i.e. generally considered as 120/80 mmHg, these differences may not cause clinical concerns.

Second, the area of compression by the inflatable sealed air chamber in the probe may not have been optimised in order for the ABP to be measured accurately. Third, the fixing of the head frame against the scalp may not be adequate, which leads to movement as the compressing pressure is continuously adjusted when the ABP is continuously monitored. Fourth, the effectiveness of the pressure transmission at different compressing pressures from the inflatable sealed air chamber in the probe to the STA may not be linear. As the compressing pressure is modulated during ABP monitoring, the STA may not have been compressed sufficiently by the inflatable sealed air chamber which led to a lower ABP measurement values in comparison with *Finap1*.

Resting ABP: bandwidth

The 95% and 99% bandwidth limits of the *STAbp* recording were both significantly lower than those recorded by *Finap1* (Table 4.10). This may be due to a limitation of the *STAbp* hardware to measure the ABP to achieve better agreement with *Finap1*. Having said that, the significant differences may suggest that pulse wave propagation and reflection, differences in local blood flow regulation, vasomotor tone and arterial elasticity play a part in changing the ABP waveshape that increases the frequency content of the peripheral ABP pulses.

Resting ABP: frequency response and magnitude squared coherence

In the comparison of both gain spectrum curves, there is a drop in gain in *Study2* between 1.5 Hz and 10 Hz before it shows gain of approximately the same as the gain in

Study1. Similar to the reason given above, the drop in gain may be due to limitation of the *STAbp* hardware. Another possible explanation is that the averaged gain spectra were computed from measurements in subjects of wide age range. As shown in Figure 1.2 (section 1.1), qualitative comparison between central and peripheral ABP waveshape and amplitude in young subjects show considerable differences; whereas the differences of the ABP waveshape and amplitude are less obvious in older subjects.

Figure 4.18 shows an increase of phase leading between 3.2 Hz and 9.5 Hz in *Study2*. This again, may be related to the limitation of the test equipment in terms of sufficient frequency response to produce ABP waveform with better agreement when compared against the ABP measured by *Finap1*. Having said that, the phase shift in the spectral curve is not surprising due to the influence of pulse wave propagation and reflection in different arteries. As mentioned in section 1.1, in comparison with more central ABP waveform, peripheral ABP waveforms in young individuals with more elastic vessel walls tend to produce delayed systolic peak. However, the frequency range that this phase difference should occur is uncertain.

The magnitude squared coherences in both curves (Figure 4.18) were fairly close to one up to approximately 7.0 Hz. Although the coherences continue to remain above 0.5 beyond 7.0 Hz, the error bars are beginning to widen. This suggests that the evaluation of ABP waveforms in the frequency domain with the *Finapres* as reference could be considered less reliable in frequencies above 7.0 Hz.

Resting ABP: assessment of drift

The results in the assessment of ABP drift need to be interpreted with caution. Non-zero $\Delta\Psi$ values (Table 4.10) can only be considered as a drift in ABP measurements by the

test device if two key assumptions were made. First, there is no measurement drift in the reference device *Finap1*. Second, differences in local physiological conditions are negligible (e.g. local blood flow regulation, vasomotor tone and arterial elasticity).

Nevertheless, the assessment of drift is a useful evaluation parameter to ensure that good quality ABP waveforms are obtained. No significant differences were obtained in the assessment of drift between *Study1* and *Study2* (Table 4.11). This may suggest that *STAbp* is at least as stable as the *Finapres* for recordings lasting 3 to 4 min.

Sample size

Sample size was somewhat tentative due to unknown SD for various parameters, as well as initial objective of obtaining descriptive values for some of the parameters such as frequency response and bandwidth. Due to these reasons, statistical power analysis was not carried out *a priori*. However, retrospective calculation based on the sample SD obtained can be useful for designing future studies. Referring to Table 4.10, a single calculation of sample size is not possible for all the different parameters described. Consequently, they would need to be calculated separately. As an example, to detect a difference of 5 mmHg (O'Brien and Atkins, 1994) for the MAP in *STAbp* using the estimated value of SD = 13.83 mmHg (Table 4.10), with 80% power at 0.05 level of significance for paired data (Campbell and Machin, 1995), the computed sample size would be 60. The same principle can be applied to other parameters. The difference between this estimated sample size and the actual number of subjects involved in *Study2* is not critical because the null hypothesis was rejected for differences that were greater than 5 mmHg.

4.6.3 Potential Causes of Measurement Differences

Although both *STAbp* and *Finapres* operate based on the volume clamping technique with photoplethysmography, the inherent differences in measurement sites and recording devices could affect measurement results. Hence, when interpreting each comparative study, these factors need to be taken into consideration.

Factors that may cause the measurement differences between two *Finapreses* of the same model include:

- anatomical difference between the fingers;
- difference in local blood flow regulation;
- motion artefacts;
- the snugness of each finger cuff fitted on the fingers;
- difference in electronic tolerances between measurement devices.

Factors that may cause differences in the measurements between *STAbp* and *Finapres*:

- anatomical difference of measurement sites;
- differences in design of measurement devices, e.g. area of compression, optoelectronic physical characteristics for tissue illumination and photodetection, electronics circuitry and signal processing algorithm. The detailed algorithm in the *Finapres* is not clear in the literature, most likely due to commercial implications;
- difference in frequency response. The frequency response of the *Finapres* is unknown, no relevant literature could be found. The frequency response of the *Finapres* could not be assessed in-house as appropriate measurement setup is not available. For this reason, the best approach would probably be a comparison with a high-fidelity solid-state catheter-tip intravascular measurement of ABP. The

frequency response of *STAbp* was limited to the block G3 (regulated compressing pressure), as described in sections 3.4.1 and 3.5.2;

- difference in optical pathways, i.e. reflectance configuration in *STAbp* but transmittance configuration in *Finapres*;
- difference in mode of compression, i.e. unidirectional compression in *STAbp*, but concentric compression in *Finapres*. Furthermore, the compression on the STA is supported by the skull at the temporal region.
- pressure transmission through the tissue in the temporal region may be attenuated or amplified differently as compared to the fingers;
- differences in tissue elastic properties, vasomotor tone, local blood flow regulation, and pulse wave propagation and reflection;
- with anastomosis in the extra-cranial circulation (section 2.3.2), there is collateral blood flow in the STA. However, such vascular network may not be available in the finger artery. Hence, a variation of ABP in the STA may not show similar variation in the finger ABP, and vice versa;
- sensitivity to ambient temperature change may be greater in the finger artery if the surrounding temperature is not controlled. Local vasoconstriction may be more significant in the finger artery (Levick, 2003);
- motion artefact. The effect could be larger for the *STAbp* as the device requires a more complex hardware design than the *Finapres* to maintain the placement of the probe on the STA.

4.6.4 Limitations of Comparative Studies

The main limitation of this chapter was the impossibility of comparing the *STAbp* with intravascular recording of ABP. Despite this limitation, comparison with *Finap1* provided very useful information about *STAbp* performance and highlighted important limitations. Reasons for failure to obtain good quality recordings in several subjects were discussed in the previous section 4.6.1. Clearly, this and some of the results of *Study2* point towards broad limitations in the current prototype version of *STAbp*, for example involving its frequency response. Improvements are obviously needed in several different aspects of this prototype.

One aspect that will need particular attention is the non-random distribution of differences observed in *Study2*, as shown by the significant linear regressions in Bland-Altman plots (Figure 4.14). The exact reason for this phenomenon is not known. One possibility would be limitations of the combined frame and probe subsystem to provide uniform compression of the STA across the wider ABP range, for example, due to movement of the frame at higher ABP.

Additional limitations in the comparability of *Study1* and *Study2* followed from differences in protocol and delays to complete the *STAbp* prototype which led to *Study2* only taking place about a year after *Study1*. Due to practical reasons, the two groups of subjects were not exactly the same. Although all participants were staff members of the Medical Physics department, only three subjects participated in both studies. Also, due to an oversight, the analysis of ABP drift in *Study2* used a 3 min duration while the corresponding time interval for *Study1* was 4 min.

4.6.5 Safety Evaluation

As a follow up assessment from section 3.4.2 for the safety evaluation of the *STAbp* prototype device, two safety issues required reassessment after the comparative study of *STAbp* and *Finap1*. They are reported as follows:

- Tissue heating: there was no reported sensation of heating or redness of skin due to the optoelectronic components in the probe placed close to the skin.

- Risk of tissue ischaemia: multiple large and soft paddings fastened around the head with the head frame provide evenly distributed pressure on the scalp tissue (section 3.3.2). The subjects did not report any signs of headache, dizziness or other discomfort.

4.6.6 Suggestions for Future Work

One of the key tasks for future work is the validation of *STAbp* against intravascular measurements. Nevertheless, prior to that, further improvements or modifications of the *STAbp* prototype need to be carried out. One of them is to provide different head frame designs to accommodate different head sizes to improve placement of the probe on the skin covering the STA. It is more difficult to fasten the same head frame design in subjects with smaller head size. Hence, with more choices of head frame sizes, a smaller head frame will also be lighter and more comfortable for participants. In addition to this, subjects were sitting upright during the experiment, the head frame needs to be modified to allow studies with participants in the supine position.

Different arrangements of the optoelectronic components relative to STA will need further review to assess its effect on the quality of the PPG signal, and also the causes for occurrence of atypical PPG waveforms. In addition to that, further review on the area of compression from the front end of the probe on the STA will be useful to optimise the effectiveness of the pressure transmission. The use of mathematical modelling or a suitable experimental test rig to evaluate these factors may be beneficial.

Upon the evaluation of the *STAbp* against intravascular measurement, one future task worth considering is to improve the frequency response of the *STAbp* to provide a flat frequency response over the bandwidth of interest. This could be achieved by using a filter equalisation technique. This would be beneficial to improve the accuracy in the estimation of central ABP waveforms. These developments would be worth pursuing once all other hardware and software possibilities have been explored.

Future studies are recommended to include studies for dedicated applications such as baroreceptor sensitivity, dynamic cerebral autoregulation and autonomic nervous system assessment (e.g. tilt testing, ABP variability and cold pressor test).

4.7 Conclusion

With prior knowledge of the inherent differences in ABP measurements with two *Finapreses*, the interpretation of the results in the comparative study of *STAbp* and *Finap1* was conducted more appropriately.

Limitations of *Finapres* as a measurement tool to validate the *STAbp* were identified. For this reason, validation of the *STAbp* against the gold standard, i.e. intravascular measurement in the ascending aorta is recommended in future work, once further improvements in hardware and software have been implemented.

CHAPTER 5 SENSITIVITY of ABP to PERTURBATION on *Setpt*

5.1 Introduction

Chapter 3 described the system architecture of the *STAbp* prototype device using the volume clamping technique with photoplethysmography. Section 4.4 presented the assessment of the *STAbp* against *Finapres*.

In the *STAbp*, *Setpt* is determined through the self-calibration algorithm incorporated in the prototype device (section 3.3.7). Appropriate *Setpt* determination plays a crucial part to produce an accurate continuous ABP waveform. As the physiology of the ABP measurement site changes, the *Setpt* is re-evaluated from time to time.

The motivation of this chapter is to understand better the influence of *Setpt* on ABP measurements. Articles that discussed this issue particularly for CoNIBP monitoring in the STA could not be found in the literature.

The objective of this chapter is to assess the sensitivity of *STAbp* output to changes in *Setpt* (section 5.2). Measurement and analysis results are presented in section 5.3 followed by discussion (section 5.4) and conclusion (section 5.5).

5.2 Method

5.2.1 Subjects and Measurements

15 subjects were recruited for this study (7 males, 8 females, age (mean ± SD) 34 ± 12 years). The participants were all staff from the Medical Physics department. Consent was given by each participant prior to the arrangement for the ABP measurements. The study was approved by the Leicestershire ethics committee (reference number: 4680).

Each subject was asked to relax while sitting comfortably on a chair with back support in a room at approximately 22 ºC. A suitable *Finapres* finger cuff was fitted snugly on the middle finger of the right hand. The hand rested on the lap of the subject. It was ensured that there was no indication of cold fingers on the subject's hands. The probe of the *STAbp* was placed over the right STA and was fastened by its brackets to the head frame. The hydrostatic pressure difference between the measurement sites was taken into account. Both ABP monitoring devices were allowed to measure the respective ABP simultaneously for several minutes until the waveforms were stable. When this was achieved, the self-calibration facilities in both *STAbp* and *Finapres* were temporarily switched off prior to a series of perturbation values applied on the *Setpt* in *STAbp*. The self-calibration facility in the *Finapres* is better known as *Physiocal* (Imholz et al., 1998; Wesseling et al., 1995; Wesseling, 1996). The perturbation was not applied on the *Finapres* as it was used as reference.

5.2.2 Protocols

A small perturbation value, ΔV, was added to the *Setpt*. Referring back to Figure 3.1, the *Setpt* (=R2) was generated within G9 during the *Open*- or *Closed- Loop Procedure* (section 3.3.7). The algorithms in these procedures were slightly modified to allow the addition of ΔV on the *Setpt* during continuous ABP monitoring. The (*Setpt* + ΔV) was then output as R2 into the closed loop feedback controller circuitry (labelled as G10).

A series of six ΔV perturbations was applied to the *Setpt* during the simultaneous ABP recordings. The ΔV values used were ±0.1V, ±0.2V and ±0.3V. These values were realistic and of the same magnitude as the change of the *Setpt* during real time ABP recordings. Between consecutive perturbations, the self-calibration facilities in both devices were re-enabled briefly. The self-calibration facilities in both devices were then again temporarily switched off before another ΔV perturbation value was applied.

5.2.3 Data Analysis

The effect of the ΔV perturbation on the ABP waveform was quantified as a sensitivity measure. It is presented in two forms. One is the electronic sensitivity (S_E in mmHg/V), the other is the physiological sensitivity (S_P in mmHg/V). S_E only considers the change of ABP in *STAbp* but not the *Finapres*. S_P takes into account the changes that may occur in the *Finapres* ABP. They were derived as:

$$S_E \Big|_{SBP,MAP,DBP} = \frac{\overline{P}_{STA1} - \overline{P}_{STA0}}{|\Delta V|} \Big|_{SBP,MAP,DBP} \tag{5.1}$$

$$S_P \Big|_{SBP,MAP,DBP} = \frac{\left(\overline{P}_{STA1} - \overline{P}_{STA0}\right) - \left(\overline{P}_{F1} - \overline{P}_{F0}\right)}{|\Delta V|} \Big|_{SBP,MAP,DBP} \tag{5.2}$$

where $\overline{P}_{STA0}$ and $\overline{P}_{STA1}$ are the respective average ABP before and after the ΔV perturbation in *STAbp*. $\overline{P}_{F0}$ and $\overline{P}_{F1}$ are the respective average ABP in the *Finapres* before and after the ΔV perturbation in *STAbp*. Each average was computed from 10 cardiac cycles. It is important to emphasise that the ΔV perturbation was applied only in the *STAbp*, not the *Finapres*.

In addition to this, the percentage changes of ABP in *STAbp* and *Finapres* were computed (φ_{STA} and φ_F respectively in %). They were derived as:

$$\varphi_{STA}\Big|_{SBP,MAP,DBP} = \left(\frac{\overline{P}_{STA1} - \overline{P}_{STA0}}{\overline{P}_{STA0}}\right) \times 100\% \Big|_{SBP,MAP,DBP} \tag{5.3}$$

$$\varphi_{F}\Big|_{SBP,MAP,DBP} = \left(\frac{\overline{P}_{F1} - \overline{P}_{F0}}{\overline{P}_{F0}}\right) \times 100\% \Big|_{SBP,MAP,DBP} \tag{5.4}$$

φ_F is useful to ensure stable ABP recording was obtained in a resting condition.

S_E, S_P, φ_{STA} and φ_F were each computed for SBP, MAP and DBP. The computation process was repeated for all subjects. Sample distribution curves with respective mean (SD) of these four parameters were then plotted for the SBP, MAP and DBP.

5.3 Results

5.3.1 Subjects

In the series of ΔV perturbations, ABP waveforms in four subjects during ±0.3V perturbations were excluded. The quality of the ABP waveforms was either poor or the range of ABP became unrealistic. In addition to this, the computation results of S_E and S_P for SBP in one of these four subjects during ±0.1V and ±0.2V perturbations were also excluded. This is because the S_E and S_P curves produced were very different compared to all other subjects' results. For this reason, they were treated as outliers. This will be further discussed in section 5.4.

5.3.2 Data Analysis

Figure 5.1 shows an example of a change in ABP waveform following a perturbation of ΔV = +0.2V on the *Setpt*. It can be observed that there is a corresponding increase of ABP in the *STAbp* recording. The respective averages of SBP, MAP and DBP were computed from 10 cardiac pulses before the ΔV perturbation and 10 cardiac pulses after perturbation. The ABP during the ΔV perturbation (indicated by asterisks) was excluded from the computation. The computation results for this example are presented in Table 5.1. This same computation process was repeated for all ΔV perturbations in each subject's recordings.

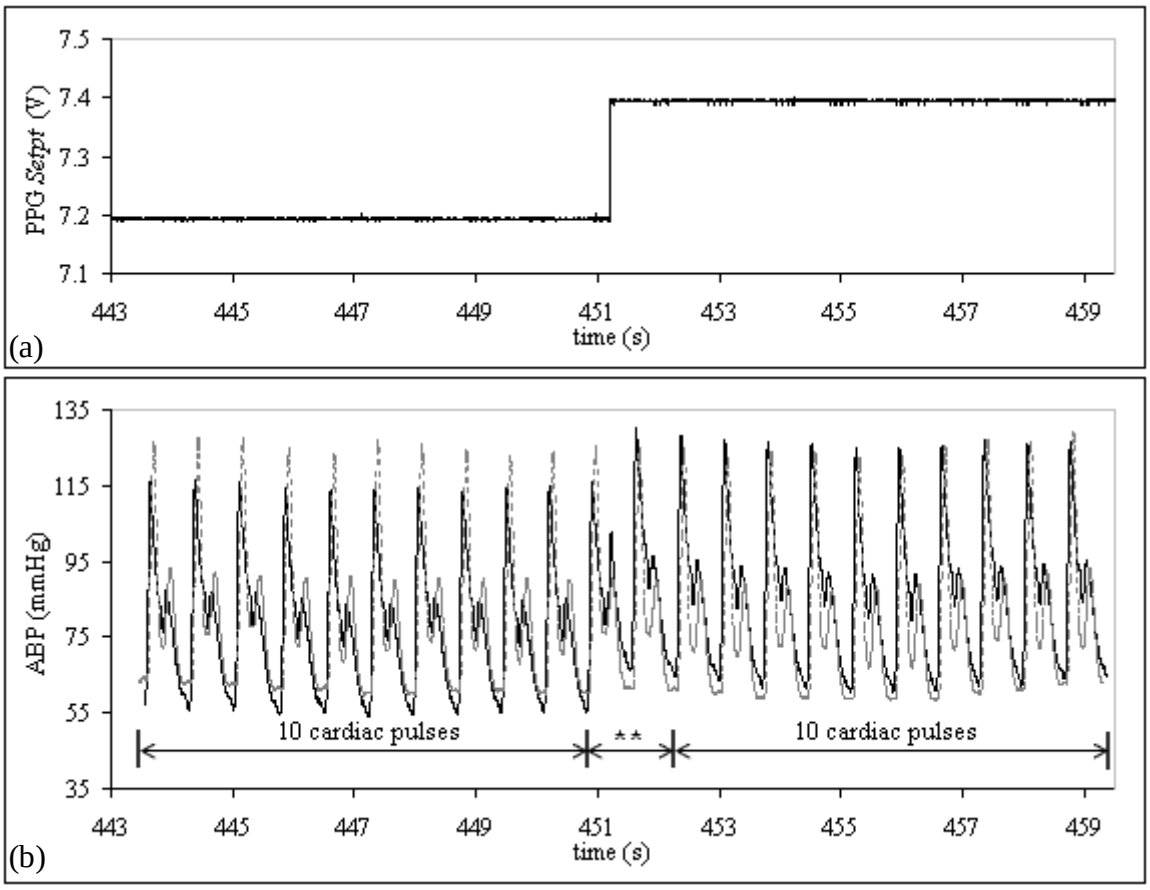

Figure 5.1 ABP waveform after a ΔV perturbation on the Setpt in STAbp.
(a) A perturbation of ΔV=+0.2V was applied on the Setpt; (b) the ABP waveforms in STAbp (black continuous line) as compared to Finapres (grey dashed line) before and after the ΔV perturbation. The respective averages of SBP, MAP and DBP were computed based on 10 cardiac pulses before perturbation and 10 cardiac pulses after perturbation. ABP during the ΔV perturbation (indicated by asterisks) was excluded. The computation results of this example are shown in Table 5.1 below.

Table 5.1 Computation results of S_E, S_P, φ_{STA} and φ_F.
The computation was based on the ABP waveforms before and after ΔV=+0.2V perturbation shown in Figure 5.1 above. Each value is the mean of 10 cardiac cycles.

	Setpt			***Setpt + ΔV***		
	SBP	**MAP**	**DBP**	**SBP**	**MAP**	**DBP**
STAbp (mmHg)	114.9	77.0	54.9	126.3	85.5	62.1
Finapres (mmHg)	125.4	79.2	60.8	124.9	78.5	59.9

	SBP	**MAP**	**DBP**
S_E (mmHg/V)	57.4	42.5	35.9
S_P (mmHg/V)	59.8	45.7	40.3
φ_{STA} (%)	10.0	11.0	13.1
φ_F (%)	-0.4	-0.8	-1.4

The sample distribution curves (mean and SD) for S_E and S_P are shown in Figure 5.2. These are followed by the sample distribution curves (mean and SD) for φ_{STA} and φ_F (Figure 5.3). A zero value point was added at the origin of the axes in each figure to produce a continuous curve. However, it was not included for interpretation of the results. Figures 5.2 and 5.3 were also replotted using only the absolute values, i.e. $|\Delta V|$ on the horizontal axis, with $|S_E|$, $|S_P|$ and $|\varphi_{STA}|$ on the respective vertical axes (Figure 5.4). $|\varphi_F|$ is not shown as it is only needed as reference to ensure that stable ABP waveforms were recorded during the experiment.

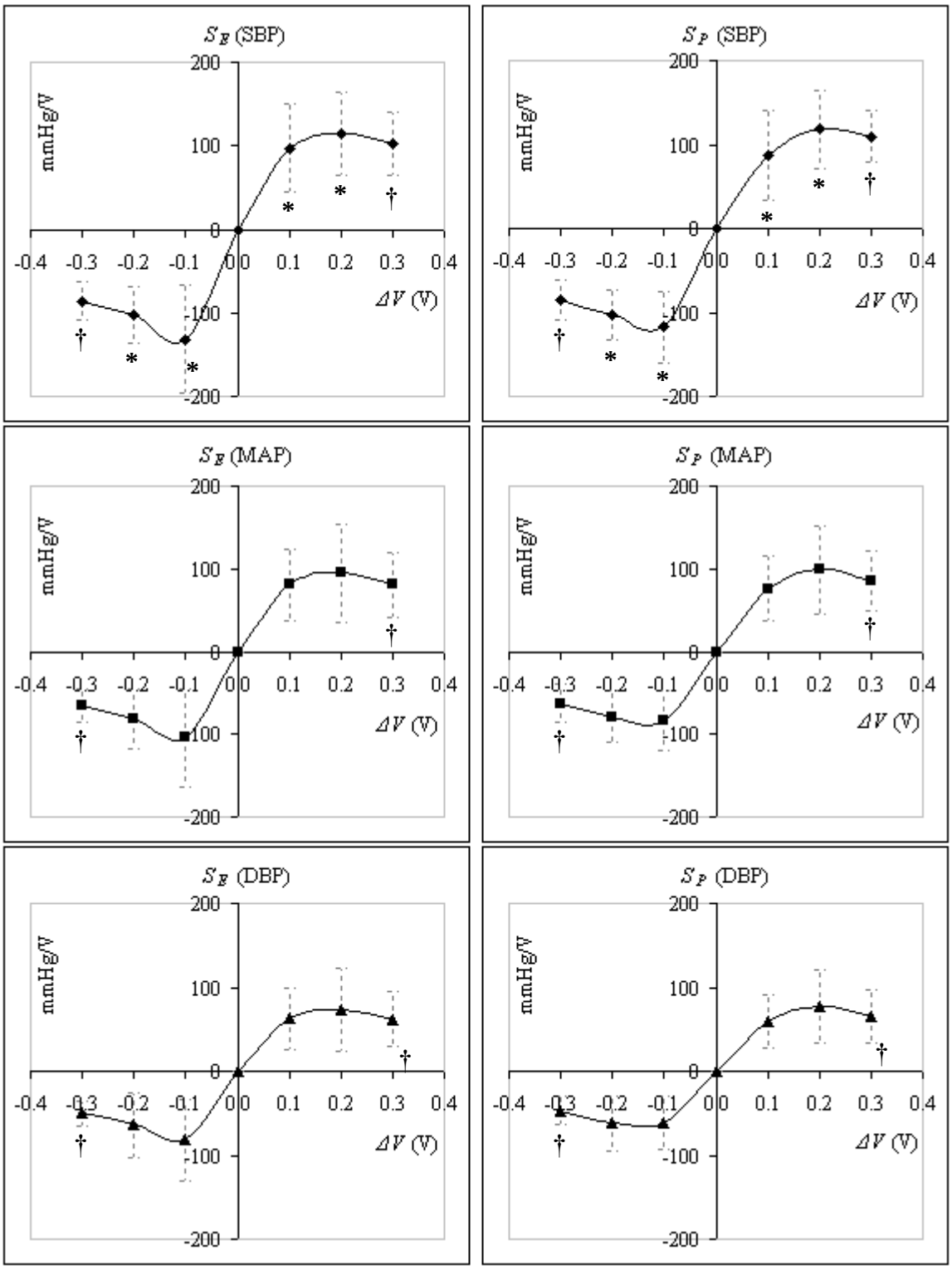

Figure 5.2 Sample distribution curves for S_E and S_P.
*A series of six ΔV perturbations was applied to the Setpt in the STAbp during ABP recording. The ΔV perturbations ranged from -0.3V to +0.3V. S_E (left column) and S_P (right column) were computed for the SBP (top row), MAP (middle row) and DBP (bottom row). The error bars are the respective ±1SD. * indicates n=14 subjects, † indicates n=11 and all others n=15. A zero value point was added at the origin of the axes to produce a continuous curve.*

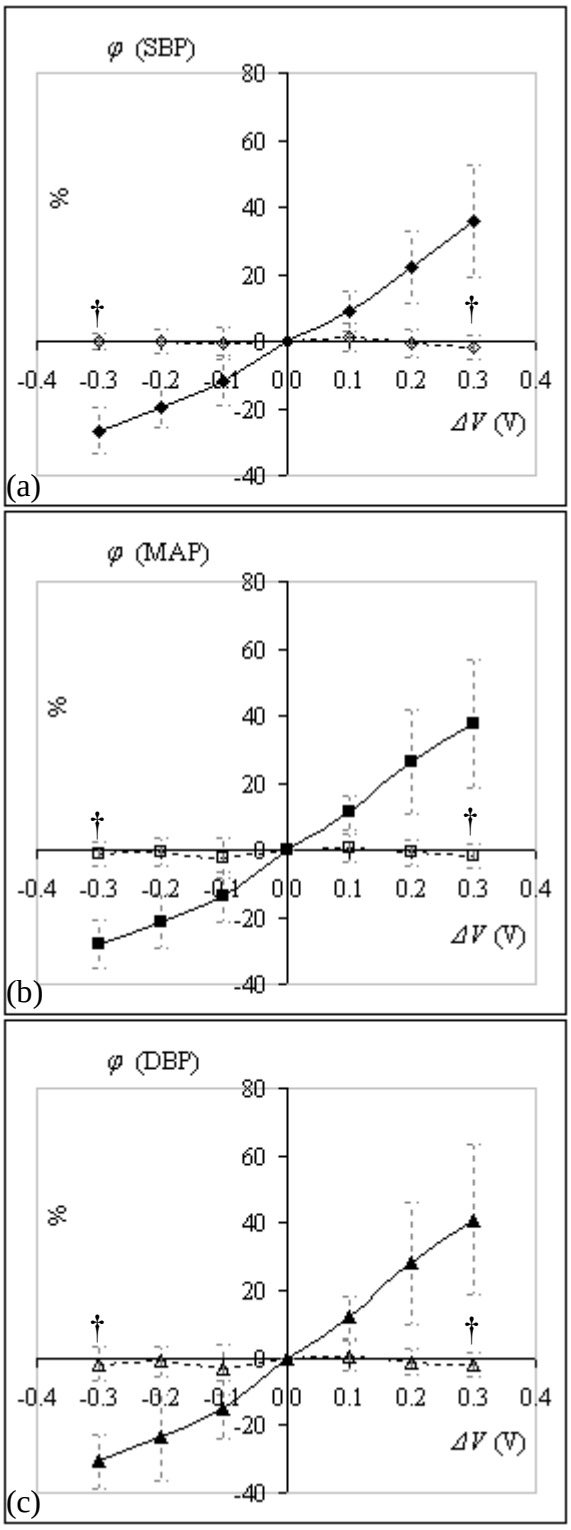

Figure 5.3 Sample distribution curves for φ_{STA} and φ_F.
A series of six ΔV perturbations was applied to the Setpt in the STAbp during ABP recording. The ΔV perturbations ranged from –0.3V to +0.3V. φ_{STA} and φ_F were computed for (a) SBP, (b) MAP and (c) DBP in the STAbp (black continuous line) and Finapres (black dashed line). The error bars are the respective ±1SD. † indicates n=11 subjects for both φ_{STA} and φ_F, while all others n=15. A zero value point was added at the origin of the axes to produce a continuous curve.

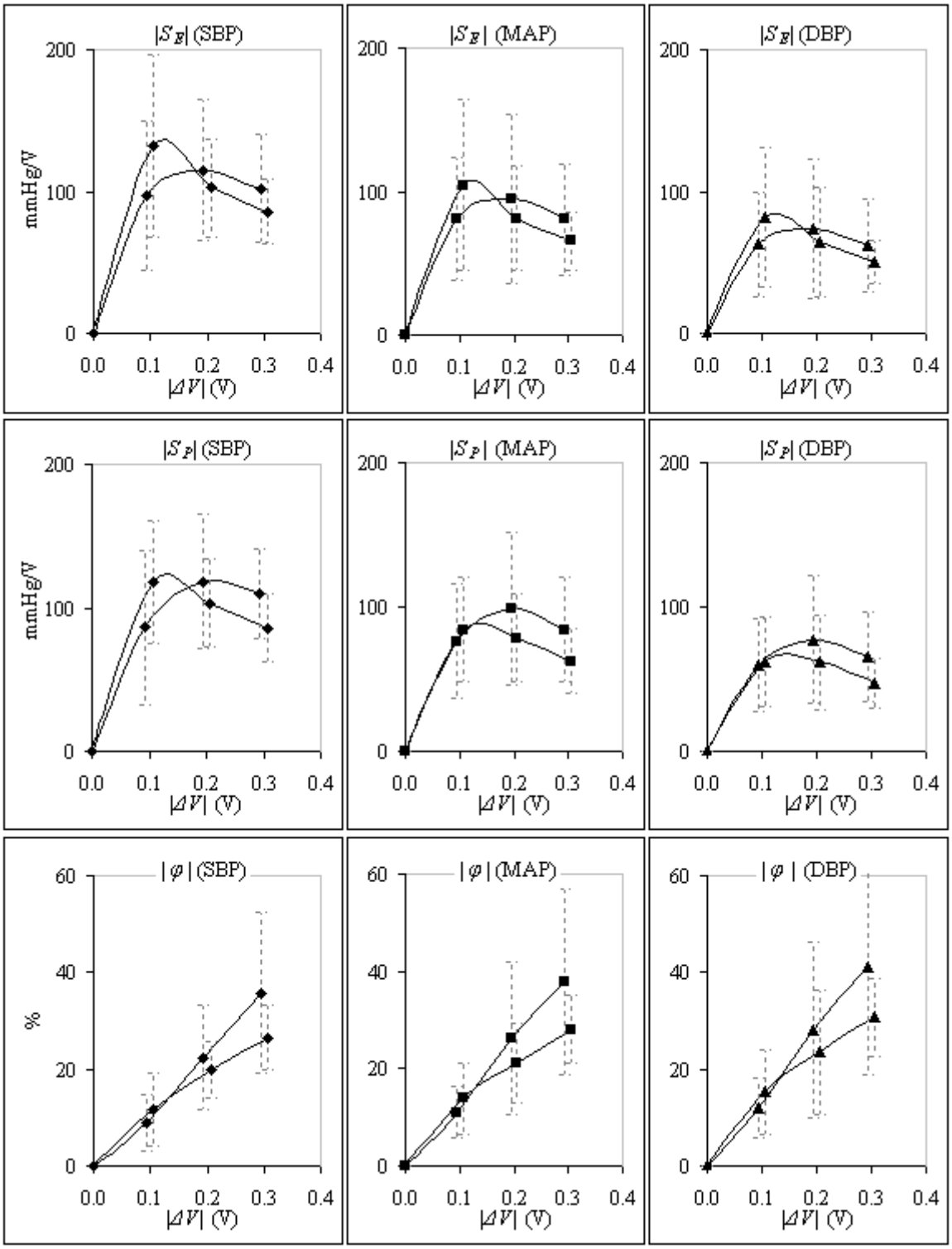

Figure 5.4 Sample distribution curves for absolute values $|S_E|$, $|S_P|$ and $|\varphi_{STA}|$.
Graphs in Figures 5.2 and 5.3 are replotted as absolute values for S_E (top row), S_P (middle row) and φ_{STA} (bottom row). They are for SBP (left column), MAP (middle column) and DBP (right column). The graphs are slightly shifted from each other to avoid superposition of the error bars. The error bars are the respective ±1SD.

5.4 Discussion

The motivation for the work in this chapter is to understand better the influence of *Setpt* on ABP waveforms. The study in this chapter has been an original piece of work as nothing similar had previously been reported in the literature.

5.4.1 Main Findings

Resulting values of SBP, MAP and DBP are highly sensitive to relatively small changes in the *Setpt* voltage, i.e. in the order of hundreds to approximately 1000 mmHg/V (Figures 5.2 and 5.4).

S_E and S_P show nonlinear relationships with ΔV perturbation (Figure 5.2), whereas the relationship of φ_{STA} with ΔV perturbation is approximately linear (Figure 5.3). Very similar values of S_E and S_P were obtained due to relatively minor changes in *Finapres* ABP during the period of observation. This also verifies that the subjects' ABP were relatively stable during recordings in resting condition.

Given the relatively large SD in Figures 5.2, 5.3 and 5.4, the differences due to directional changes in ΔV were not significant and it is reasonable to assume that changes in ABP values were symmetrical for ΔV changes around the *Setpt*.

Although alterations in waveform pattern were not investigated, comparing sensitivity estimates for SBP, MAP and DBP values suggest that their values remained relatively constant. This means that changes in waveform shape were probably minimal and that

changes in *Setpt* involved a parallel shift of the ABP waveform upwards or downwards due to the influence of *Setpt* voltage on the MAP.

Several measurement results were excluded from one subject during ±0.1V and ±0.2V perturbations. These may be due to displacement of the probe for the *STAbp*, motion artefact, or some other unknown causes. Exclusions of measurement results had not been frequent. In this study, it only occurred to one out of 15 subjects.

5.4.2 Implications from Findings

The high sensitivity in *STAbp* ABP values indicates that greater attention must be given to design considerations of the *Open-* and *Closed- Loop Procedures* (section 3.3.7) and its hardware components (Figure 3.1). S_E values around 1000 mmHg/V (Figure 5.4) indicate that to maintain say, MAP values within ±1 mmHg of its correct value would need the *Setpt* voltage to remain within a ±1 mV limit. Due to the complexity of operation in the *STAbp*, it was not possible to predict the amplitude of this design target from the outset. As a result, any future improvements in the system would need to take into account the ±1 mV limit, for example when assessing electronic drift and noise, as well as thermal stability.

5.4.3 Limitations of the Study

Although the *Finapres* waveform remained relatively stable during the period of observation, estimation of S_P would only be entirely reliable if it was based on

intravascular measurements of ABP, ideally in the ascending aorta (Sammons et al., 2007).

To make the *Finapres* measurements comparable to the *STAbp*, the *Physiocal* servo-mechanism was temporarily switched off. However, in retrospect, it would have been useful to perform a similar comparison with the *Finapres Physiocal* servo functioning normally, as this would probably lead to more realistic estimates of S_P. On the other hand, this additional study would be problematic, due to the additional extensive data collection and analysis needed and also due to the need to select segments of data avoiding the time intervals when the *Physiocal* servo was activated.

The population studied was relatively young and comprised only healthy subjects. Different results may be obtained in the elderly or individuals with particular conditions such as obesity, atherosclerosis or hypertension.

5.4.4 Suggestions for Future Work

The high sensitivity of *STAbp* ABP values to the *Setpt* voltage highlights the need for more work on this key component of the system. In addition to the work to be described in chapter 6, it would be extremely useful to compare the *Setpt* voltage as a function of time with intravascular ABP measurements at rest and also during manoeuvres that modulate ABP such as the Valsalva or handgrip. Hence, it is recommended to give the *Setpt* voltage as an additional output in future modifications of the *STAbp*. This would allow monitoring of its variability during different physiological conditions. Analysis of

these data may be useful to learn more about the *Setpt* behaviour and ways to improve its performance.

Future studies should include elderly subjects and patients to clarify whether patho-physiological conditions have a bearing on the *Setpt* sensitivity and stability.

5.5 Conclusion

The study in this chapter demonstrated that the ABP is highly sensitive to a small change in the *Setpt*. Future modifications to the *STAbp* system architecture need to incorporate this to further improve the accuracy and reliability of continuous ABP monitoring.

In the following chapter, the relationship between the external compressing pressure and the PPG waveform will be explored. The study also seeks to understand better additional parameters that can potentially be incorporated into the self-calibration algorithm in the *STAbp* to improve its accuracy of continuous ABP monitoring.

CHAPTER 6 PPG WAVEFORM ANALYSIS

6.1 Introduction

Overview

Section 3.3.7 described the algorithm of *Setpt* determination through the self-calibration facility in the *STAbp* prototype device. The self-calibration feature operates within the *Open*- and *Closed- Loop Procedures*. Section 4.4 then presented a comparative study between the *STAbp* and the *Finapres*. During the operation of *STAbp*, the *Setpt* is reviewed from time to time to obtain accurate continuous ABP monitoring. Next, chapter 5 reported that the ABP is very sensitive to a perturbation value added to the *Setpt*. All these share a common focus, i.e. the *Setpt*.

This chapter aims to analyse the PPG waveform further to identify new information that could contribute towards the design of a more robust algorithm in *Setpt* determination. As was shown in Figure 3.9, the PPG waveform changes in amplitude and shape at different compressing pressures on the STA. With increasing compressing pressure, the pulse amplitude gradually reaches a maximum. It then gradually reduces as the compressing pressure continues to increase. At the peak pulsation amplitude, the compressing pressure is approximately the same as the MAP. Such amplitude characteristic is typically observed in ABP monitoring with the volume clamping technique. This phenomenon agrees with other authors (Penaz, 1992; Tanaka and Yamakoshi, 1996; Wesseling et al., 1995).

Figure 6.1 shows another example of a PPG waveform recorded simultaneously at a narrower range of compressing pressures on a finger artery. The waveforms were recorded by a simpler version of the *STAbp* device, which will be described further in section 6.2.1. With the inverse relationship between the arterial blood volume light absorption and the PPG (section 2.5.2), when the ABP increases during the systolic phase, the PPG decreases. At the peak of the systolic phase, the PPG decreases to the lowest value, indicated as '*s*' in the figure. Conversely, as the ABP decreases to the diastolic pressure, the PPG increases to a maximum, indicated as '*d*' in the figure. Hence, the trough of the PPG waveform occurs approximately at the SBP, while the peak of the PPG occurs approximately at the DBP. The PPG pulse amplitude is between each '*s*' and the preceding '*d*'. In this example, the PPG pulse amplitude is at its largest at 120 mmHg. At lower and higher compressing pressures, the pulse amplitude becomes smaller.

Literature

Table 6.1 lists 12 articles in chronological order. These articles share a common interest, i.e. the relationship between the pulsation amplitude and the intra-arterial MAP. This relationship is commonly integrated into noninvasive measurement devices to determine the ABP, most commonly in non-continuous devices based on oscillometry. The table shows that different approaches were used to study this relationship. The measurement techniques included oscillometry, photo-plethysmography or arterial volume clamping with photoplethysmography. The relationship was evaluated using theoretical models and/or experiments. The experiments carried out were *in vivo* and/or *in vitro*. Subjects included humans, dogs or rats. Finally, the arteries used included the carotid, brachial, finger or radial arteries; others included the rat's tail or arteries in the calf and ankle.

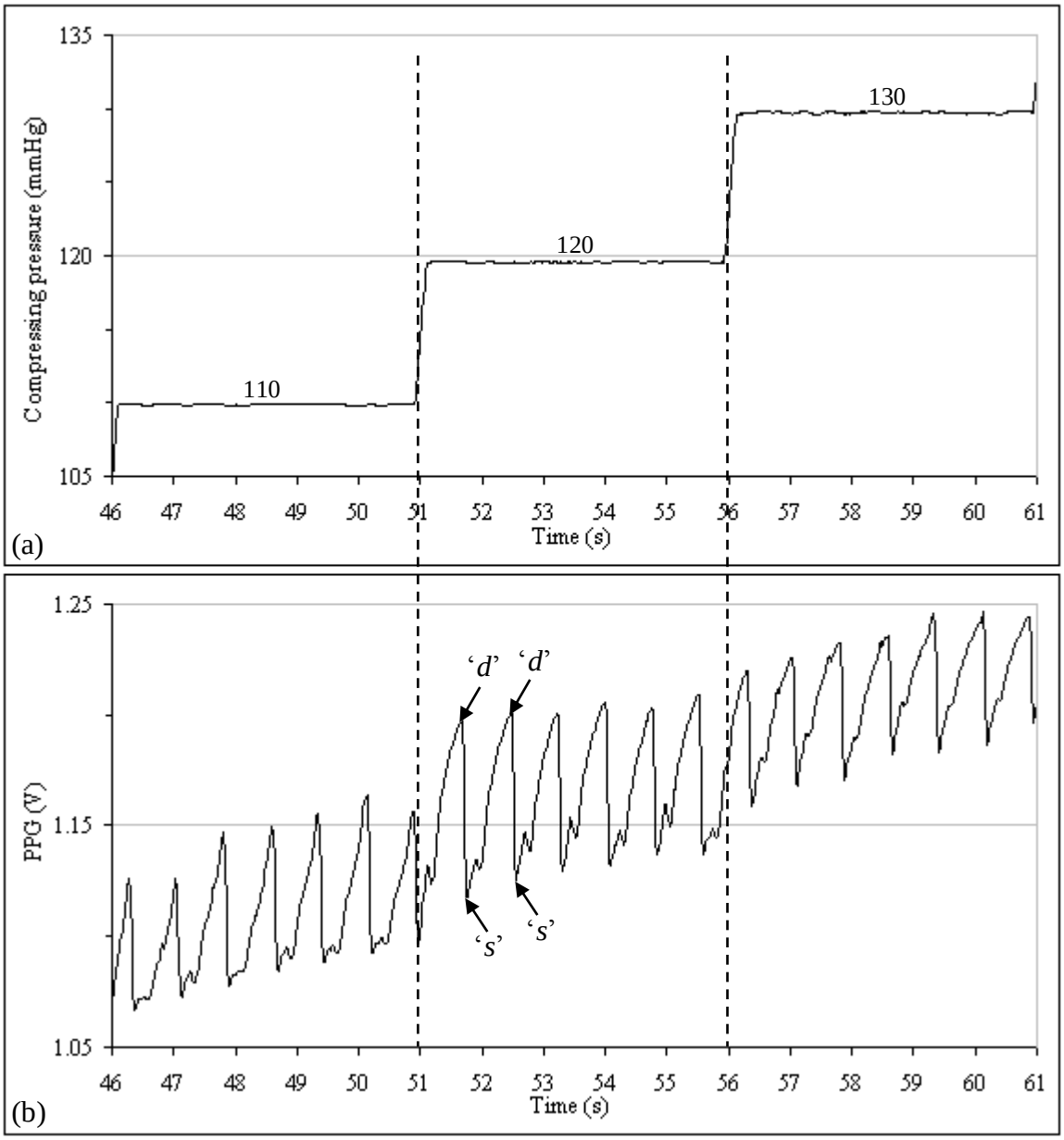

Figure 6.1 Simultaneous recording of the compressing pressure and the PPG.
(a) An example recording of the compressing pressure externally applied on a finger artery. The compressing pressure was increased every 5s in 10 mmHg step from 110 to 130 mmHg; (b) the corresponding PPG waveform was recorded simultaneously. The PPG waveform shows changes in its amplitude and temporal pattern. 's' refers to the lowest PPG value during the systolic phase, whereas 'd' refers to the highest PPG value during the diastolic phase.

Table 6.1 Relationship between pulsation amplitude and intra-arterial MAP.
This relationship was evaluated by authors in the articles listed below. A tick (✓) means that a theoretical model was evaluated in the article. The last row refers to the experimental setup in this chapter.

#	Article	Measurement technique	Theoretical model	Experiment	Subjects	Artery
1.	(Posey et al., 1969)	Oscillometric		*In vitro*	Dog	Carotid
2.	(Ramsey III, 1979)	Oscillometric		***In vivo***	**Human**	Bicep / calf / ankle
3.	(Yelderman and Ream, 1979)	Oscillometric		***In vivo***	**Human**	Brachial
4.	(Mauck et al., 1980)	Oscillometric	✓	*In vitro*	Dog	Carotid
5.	(Yamakoshi et al., 1982)	Photo-plethysmography		*In vitro*	Dog	Carotid
6.	(Forster and Turney, 1986)	Oscillometric	✓			Brachial
7.	(Penaz, 1992)	**Volume clamping**	Not applicable (review article)		**Human**	**Finger**
8.	(Drzewiecki et al., 1994)	Oscillometric	✓			Brachial
9.	(Wesseling et al., 1995)	**Volume clamping**		*In vitro* ***In vivo***	**Human** / rat **Human**	**Finger**/tail **Finger**
10.	(Ursino and Cristalli, 1996)	Oscillometric	✓			Brachial
11.	(Baker et al., 1997)	Oscillometric	✓	***In vivo***	Dog	Radial
12.	(Raamat et al., 1999)	Oscillometric	✓			**Finger**
13.	**This chapter**	**Volume clamping**		***In vivo***	**Human**	**Finger**

The table shows that a large majority of the articles are based on the oscillometric technique. Similar articles based on the volume clamping technique are very limited. Studies that used the oscillometric technique cannot be directly compared with those that used the volume clamping technique. This is due to differences in the working principles of the measurement techniques, the measurement sites and the setup of the studies. Furthermore, the pulse wave in oscillometry is due to the pressure oscillation in the compressing chamber, e.g. the inflatable arm cuff. The pressure oscillation is generated as the ABP is transmitted through the tissue to the cuff. In the volume clamping technique, however, the pulse wave is due to the amount of illuminated light being scattered or reflected by the pulsating blood volume in the artery to the photodetector, which is then measured as the PPG.

The objectives of this chapter are:

i. To assess the relationship between the PPG peak pulsation amplitude and the MAP;
ii. To propose future modifications to the self-calibration algorithm in *STAbp* to improve the *Setpt* determination.

6.2 Method

6.2.1 Subjects and Measurements

In this study, 5 subjects were recruited (3 males, 2 females, age (mean ± SD) 32 ± 15 years). The participants were all staff from the Medical Physics department. Consent was given by each participant prior to the arrangement for the ABP measurements. The study was approved by the Leicestershire ethics committee (reference number: 4680).

Two *Finapres* finger cuffs of appropriate size were fitted on the ipsilateral middle and annulus fingers of the right hand. The fitting and positioning of the finger cuffs adhered to the manufacturer's guidelines. The finger cuff on the annulus finger was used to measure the ABP with the *Finapres*. The finger cuff on the middle finger was operated by an in-house built PPG recording device, which is a simpler version of the *STAbp* system architecture described in Chapter 3. Referring to the block diagram in Figure 3.1, G9 sends out a required sequence of compressing pressures as command output (R1). The mode switch (G11) connects R1 to G3 which supplies regulated compressing pressure. G3 regulates the pressure in the finger cuff to compress the artery. Simultaneously, G1 monitors the arterial blood volume change in the finger. Its output is converted as PPG (G2) and sent (C1) to G9 to be recorded by the desktop computer. A separate channel was used to record the ABP measured by the *Finapres*. Both the *Finapres* and the PPG waveforms were simultaneously sampled at 100Hz (DT302, Data Translation®). The recording was managed with the Agilent *VEEPro*® visual programming software.

Two ipsilateral instead of contralateral fingers were used in order to minimise the potential difference in regional regulation of arterial blood flow between the two hands. The subjects had no known history of cardiovascular or other pathologies that would affect the blood circulation in the fingers.

6.2.2 Protocols

Each subject attended two measurement sessions (Test #1 and Test #2). Throughout the experiment, the right hand rested on a bench at heart level. The subjects were asked to relax their fingers and breathe normally while sitting on a chair with back support. The subjects were also asked not to engage in any conversation, laughter, holding their breath or shifting about in their seated position. This is necessary to minimise artifacts and to obtain stable physiological recordings.

In Test #1, the compressing pressure in the cuff (denoted as P_{com}) was first increased by approximately 10 mmHg every 5s. The range of P_{com} encompassed the physiological range of systolic and diastolic pressures. When P_{com} had increased above systolic pressure, the recording was complete. It was then decreased at the same rate until it was near zero mmHg. This corresponded to a separate recording. The cycle of increasing and decreasing the P_{com} was then repeated, hence giving a total of four sets of recordings.

In Test #2, the same setup and protocol were repeated except that the P_{com} steps were now changed at approximately 2 mmHg every 5s. Again, 4 sets of recordings were obtained in each subject.

The *Finapres* has a built-in physiological self-calibration facility known as the *Physiocal* (Wesseling et al., 1995). It was kept switched on throughout the ABP measurement. This is to prevent any potential drifts in the MAP measured with the *Finapres*.

6.2.3 Data Analysis

As was shown in Figure 6.1, the PPG pulse amplitude is measured between each '*s*' and the preceding '*d*'. It is denoted as *PPGa* (V). Depending on the pulse rate, 3 to 5 pulses were recorded at each P_{com}. The *PPGa* from these pulses during the same P_{com} were then averaged ($\overline{PPGa}$ (SD)). Corresponding ABP pulses were recorded with the *Finapres*, and the average (SD) of systolic, mean and diastolic pressures were also computed (i.e. $\overline{SBP}_F$, $\overline{MAP}_F$ and $\overline{DBP}_F$ respectively). The array of $\overline{PPGa}$ was plotted against the sequence of P_{com}. Figure 6.2(a) shows an example.

Next, the pressure difference (P_{diff}) was defined as

$$P_{diff} = \overline{MAP}_F - P_{com} \tag{6.1}$$

P_{diff} was calculated for each P_{com}. The $\overline{PPGa}$ array was then replotted against the P_{diff} (Figure 6.2(b)). The $\overline{PPGa}$ array was fitted with a polynomial curve ($\hat{PPGa}$) for the pressure range of ±40 mmHg around $P_{diff} = 0$. The first to sixth order polynomials were tested to compare the RMSE of different fitted curves on the $\overline{PPGa}$ array.

Referring to Figure 6.2(b) again, the $\hat{PPG}a$ curve usually shows a peak. The corresponding P_{diff} to this peak was retrieved. This is denoted as P_{diffA} (mmHg). At P_{diff} = 0, Equation 6.1 shows that P_{com} equals to $\overline{MAP}_F$. Hence, P_{diffA} indicates the difference between the P_{com} at the peak of the $\hat{PPG}a$ curve and the P_{com} at P_{diff} = 0. Figure 6.2(b) shows an example where a positive P_{diffA} is obtained, whereas Figure 6.2(c) shows an example where a negative P_{diffA} is obtained.

Statistical Analysis

Provided that all measurements were satisfactory, eight P_{diffA} values would be available per subject. The Kolmogorov-Smirnov normality test was first carried out from all available P_{diffA}. If the distribution was normal, subsequent data analysis would use parametric statistical methods. The collection of P_{diffA} was then tested to assess if it is significantly different from zero mmHg.

Two hypotheses were defined. The first null hypothesis states that P_{diffA} is not different from zero. If this is true, statistical analysis is completed. However, if the hypothesis is rejected, the second null hypothesis states that the setup and protocols in Tests #1 and #2 do not lead to significant differences in P_{diffA}.

According to the setup and protocols in Tests #1 and #2, three factors were identified applicable to each subject. Each factor was tested for non-significant differences in P_{diffA}. For the first factor, it refers to repeated measurements. Second, the direction of the P_{com} sequence was reversed. Third, the step interval of P_{com} was changed. Multiple comparisons were required and for this reason a hierarchical testing approach was adopted. If the parametric methods were appropriate, paired two-tail t-test would be

used for the multiple comparisons. Otherwise, the Wilcoxon non-parametric test would be applied.

The hierarchical test began with the repeated measurements factor. Measurement results with the 2 mmHg step interval were first tested (i.e. higher resolution). This was followed by the direction of the P_{com} sequence. Lastly, the influence of the step interval of P_{com} was tested. If the statistical result in each level showed no significant difference, the corresponding P_{diffA} values were pooled by averaging per subject before the next level of the hierarchy was tested. A value of $p < 0.05$ was taken as the level of statistical significance. Bonferroni correction was applied to account for multiple comparisons (Bland, 1995; Campbell and Machin, 1995), with the α-levels corrected to 0.05, 0.025 and 0.017 for the three factors respectively.

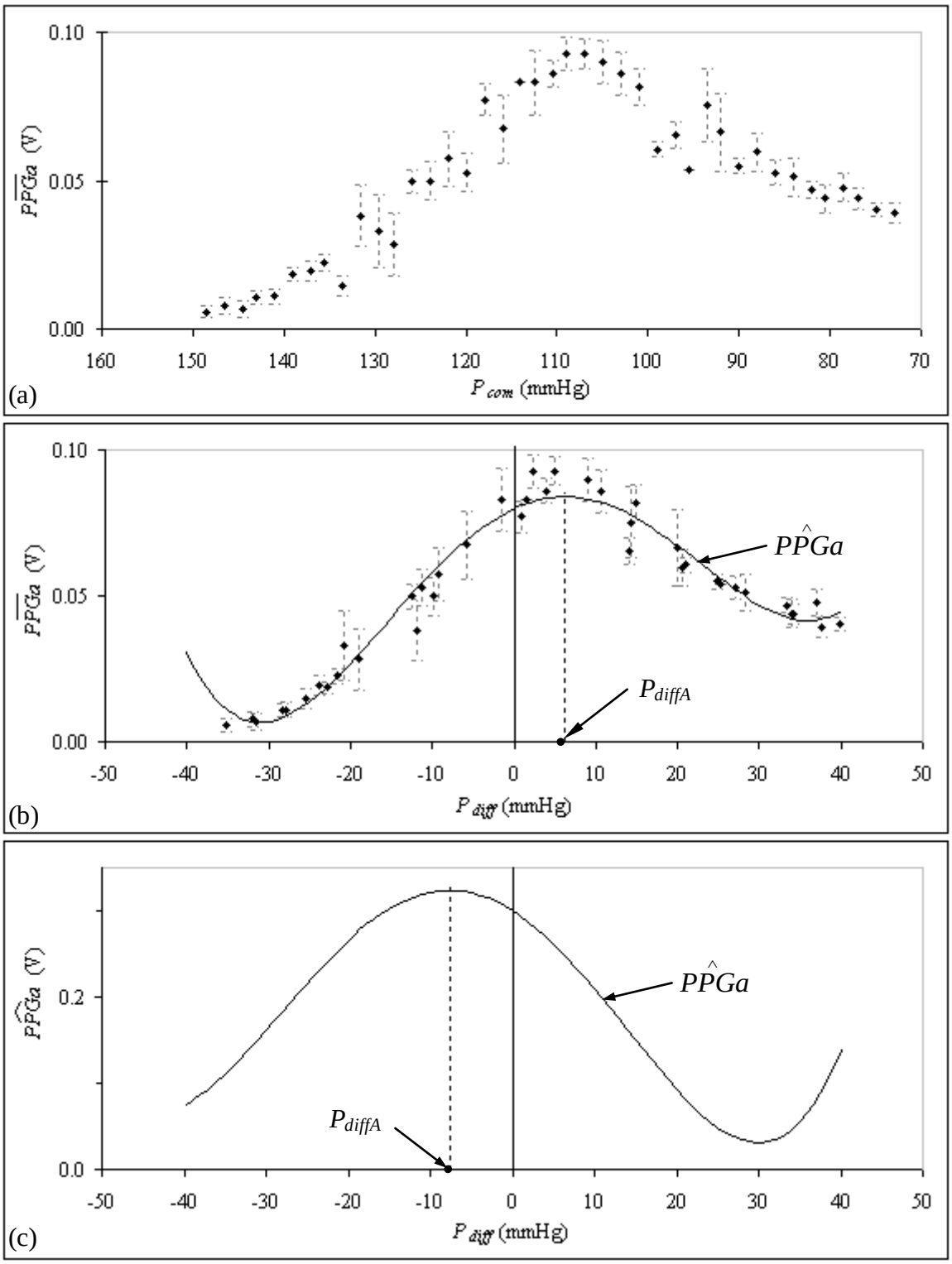

Figure 6.2 Example computation of P_{diffA} from the $\hat{PPGa}$ curve.
(a) Example of $\overline{PPGa}$ array plotted against the sequence of decreasing P_{com}.; (b) the $\overline{PPGa}$ array was replotted against P_{diff}. It is superimposed with a polynomial fitted curve (denoted as $\hat{PPGa}$). The error bars are ±1SD. The P_{diffA} is indicated. In this example, a positive P_{diffA} is obtained; (c) another example where a negative P_{diffA} is obtained.

6.3 Results

Good quality PPG recordings with stable *Finapres* ABP waveforms were obtained in all measurements. In each of the Tests #1 and #2, four sets of recordings were obtained, hence there were eight sets per subject. As there were five subjects, a total of 40 P_{diffA} values would be available.

Figure 6.3 shows the RMSE (mean ± SD) for each of the first to sixth order polynomials fitted to every $\overline{PPGa}$ array. Two graphs were plotted to show the respective mean RMSE for Tests #1 and #2. Each mean RMSE was computed from 20 individual RMSE. Both plots show that above the fourth order, the RMSE does not decrease significantly with higher order polynomials. Therefore, for further data analysis, each of the $\overline{PPGa}$ arrays was fitted with the fourth order polynomial curve. It is to note that the fitted curve was denoted as $\hat{PPGa}$ to differentiate it from the $\overline{PPGa}$ array.

Figure 6.4 shows an example of the data analysis process to obtain P_{diffA}. Figure 6.4(a) shows that the *Finapres* $\overline{SBP}_F$, $\overline{MAP}_F$ and $\overline{DBP}_F$ were stable as P_{com} was decreased at 2 mmHg steps every 5s. Figure 6.4(b) shows the array of $\overline{PPGa}$ with decreasing P_{com}. The P_{diff} was computed (Equation 6.1) for the horizontal axis and the figure was replotted in Figure 6.4(c). The $\overline{PPGa}$ array is shown superimposed by the $\hat{PPGa}$ fitted curve. P_{diffA} was identified from the $\hat{PPGa}$ curve. In this example, P_{diffA} = 6.2 mmHg. The process above was repeated for all other $\overline{PPGa}$ arrays to obtain their respective P_{diffA}.

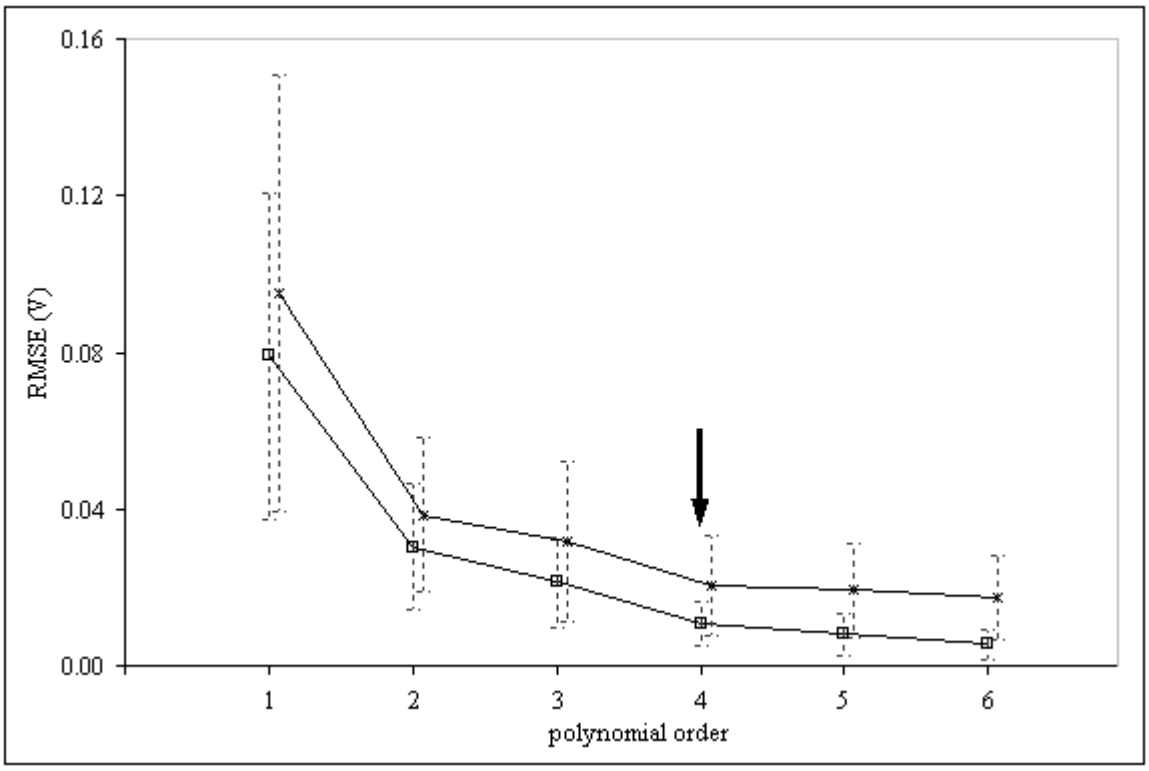

Figure 6.3 RMSE of the polynomial curve fitting of $\overline{PPG_a}$ arrays.
Each mean RMSE was computed from 20 individual RMSE. First to sixth order polynomials were fitted on each of the $\overline{PPG_a}$ arrays for Test #1 (square) and Test #2 (cross). The graphs are slightly shifted from each other to avoid superposition of the error bars. The error bars are the respective ±1SD. The fourth order (indicated by an arrow) has been chosen for the data analysis in this study.

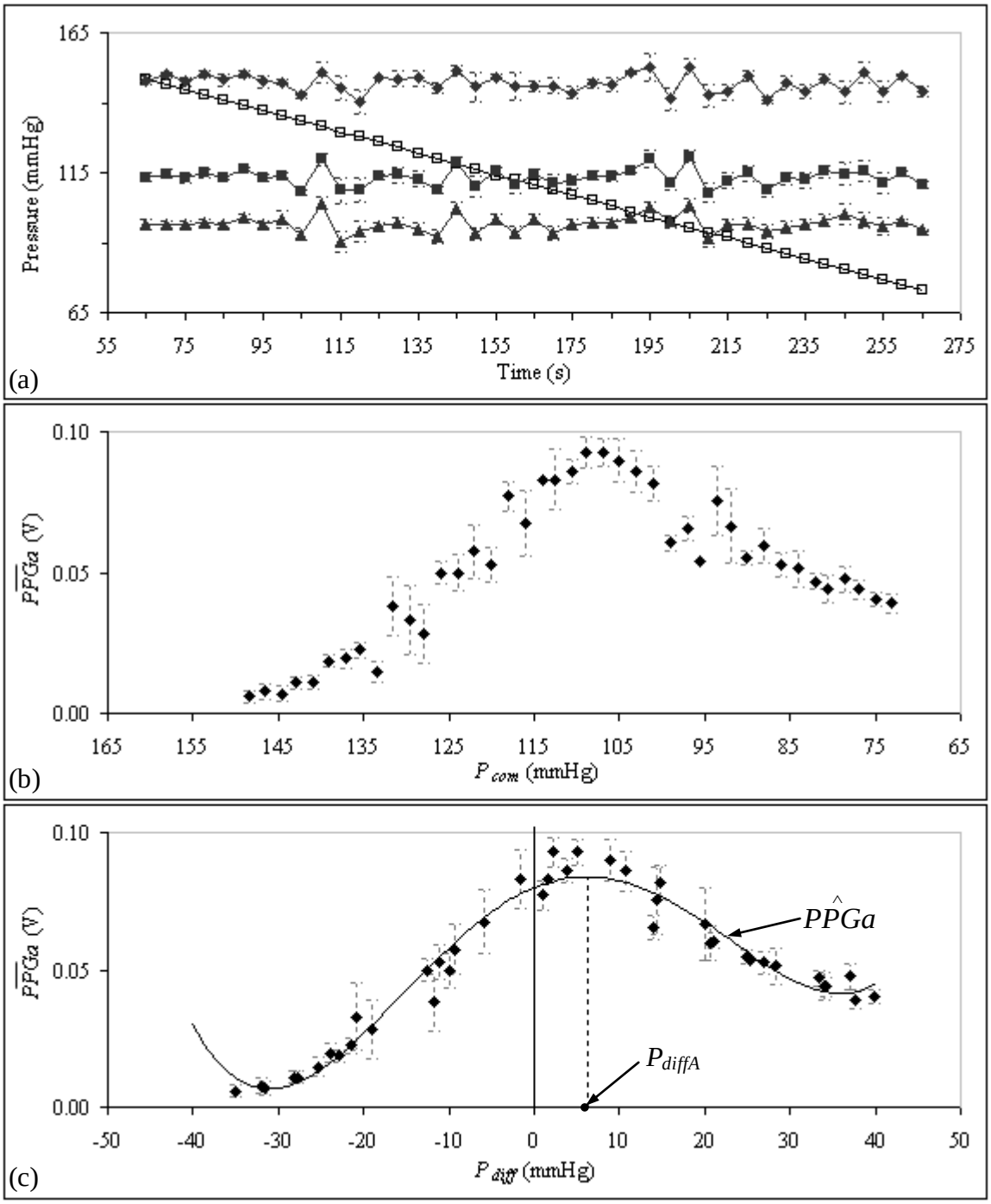

Figure 6.4 Computation of P_{diffA} from the $\hat{PPGa}$ curve.
(a) The P_{com} (light square) was decreased at 2 mmHg steps every 5s. The Finapres ABP is shown as: $\overline{SBP}_F$ (diamond), $\overline{MAP}_F$ (square) and $\overline{DBP}_F$ (triangle); (b) the array of $\overline{PPGa}$ corresponding to decreasing P_{com}; (c) graph in (b) was replotted against P_{diff} (Equation 6.1). The $\overline{PPGa}$ array is superimposed by the fourth order polynomial curve ($\hat{PPGa}$). The P_{diffA} is indicated. In this example, P_{diffA} = 6.2 mmHg. In all the graphs, the error bars are the respective ±1SD.

Table 6.2 presents all the 40 individual results of P_{diffA} from the five subjects. Figure 6.5 shows the histogram of the sample distribution. Seven out of the 40 P_{diffA} (17.5%) are positive values, while the remaining 82.5% are negative values. The positive P_{diffA} are also shown in bold in the table. The Kolmogorov-Smirnov test showed that the distribution was normal ($p>0.20$). P_{diffA} was significantly different from zero mmHg (paired t-test, $p<0.001$). Hence, the first null hypothesis was rejected.

For the second hypothesis, the hierarchical statistical tests for P_{diffA} showed no statistical significance for the three factors. It is to note that when no statistical significance was detected from the paired t-test at each level of the hierarchy, the P_{diffA} values were pooled to obtain an average value. Hence, the mean (SD) of differences between P_{diffA} in the repeated measurements factor ($p>0.20$, n = 5 subjects) were:

- 2.0 (3.91) mmHg for increasing P_{com} sequence at 2 mmHg step interval;
- 0.8 (1.16) mmHg for decreasing P_{com} sequence at 2 mmHg step interval;
- 1.8 (5.70) mmHg for increasing P_{com} sequence at 10 mmHg step interval;
- 2.1 (5.84) mmHg for decreasing P_{com} sequence at 10 mmHg step interval.

Next, the mean (SD) of differences between P_{diffA} for the factor on direction of P_{com} sequence ($p>0.20$, n = 5 subjects) were:

- 0.3 (2.38) mmHg at 2 mmHg step interval in P_{com};
- 2.3 (3.61) mmHg at 10 mmHg step interval in P_{com}.

Finally, the mean (SD) of differences between P_{diffA} for the factor on step interval of P_{com} was computed as -0.4 (4.27) mmHg. With the second null hypothesis accepted, this

means that the setup and protocols in Tests #1 and #2 did not lead to significant differences in P_{diffA}.

The P_{diffA} in Table 6.2 are plotted in Figure 6.6(a) according to subjects. With the exception of subjects 1 and 3, all other subjects only have distributions with $P_{diffA} < 0$. The intra-subject mean (SD) of P_{diffA} are shown in Figure 6.6(b). It is replotted with respect to the subjects' age (Figure 6.6(c)). No significant correlation with age was detected.

In summary, with the P_{diffA} results giving a normal distribution and no statistical significance detected for the three factors considered, the sample average (mean (SD)) for P_{diffA} was computed as -4.7 (5.63) mmHg.

Table 6.2 Individual results of P_{diffA} from five subjects.
A total of 40 values were obtained. The labelling refers to "subject number.step interval.direction.repeated measurement". 'subject number' has a prefix S-. 'step interval' 1 refers to Test #1 (10 mmHg) and 2 refers to Test #2 (2 mmHg). 'direction' [+] *refers to increasing P_{com} and* [-] *refers to decreasing P_{com}.* Lastly, *'repeated measurement' is represented by 1 and 2. Positive P_{diffA} values are shown in bold.*

Label	P_{diffA} (mmHg)		Label	P_{diffA} (mmHg)
S1.1.[+].1	-2.6		S1.2.[+].1	-1.9
S1.1.[+].2	-8.9		S1.2.[+].2	**6.2**
S1.1.[-].1	**1.5**		S1.2.[-].1	**6.2**
S1.1.[-].2	**2.6**		S1.2.[-].2	**6.6**
S2.1.[+].1	-7.9		S2.2.[+].1	-7.6
S2.1.[+].2	-6.5		S2.2.[+].2	-8.9
S2.1.[-].1	-6.8		S2.2.[-].1	-9.9
S2.1.[-].2	-9.3		S2.2.[-].2	-10.8
S3.1.[+].1	-1.2		S3.2.[+].1	-4.1
S3.1.[+].2	**0.8**		S3.2.[+].2	-3.4
S3.1.[-].1	-0.6		S3.2.[-].1	-5.7
S3.1.[-].2	**1.4**		S3.2.[-].2	-3.5
S4.1.[+].1	-3.3		S4.2.[+].1	-3.7
S4.1.[+].2	-1.2		S4.2.[+].2	-4.7
S4.1.[-].1	-1.2		S4.2.[-].1	-4.4
S4.1.[-].2	-3.3		S4.2.[-].2	-3.1
S5.1.[+].1	-19.8		S5.2.[+].1	-10.9
S5.1.[+].2	-10.0		S5.2.[+].2	-7.2
S5.1.[-].1	-16.6		S5.2.[-].1	-9.8
S5.1.[-].2	-4.7		S5.2.[-].2	-8.9

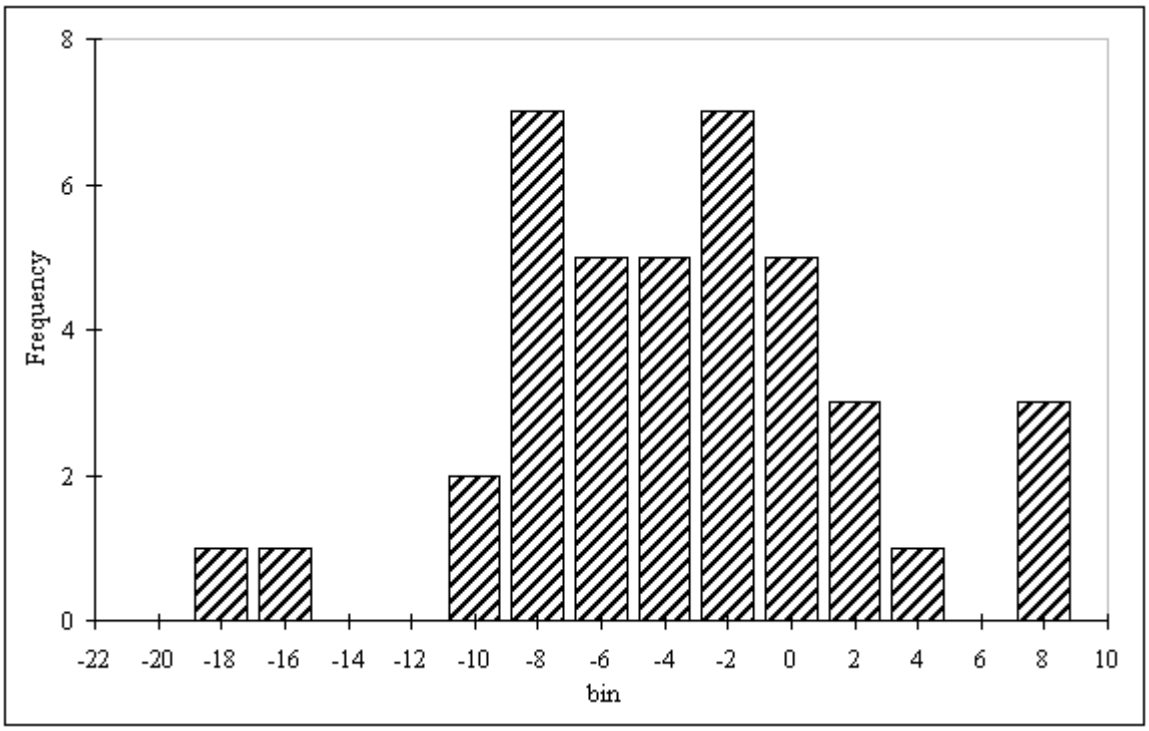

Figure 6.5 Histogram for the sample distribution of P_{diffA}.
Table 6.2 shows the individual results of P_{diffA}. The Kolmogorov-Smirnov test showed that the sample distribution was normal.

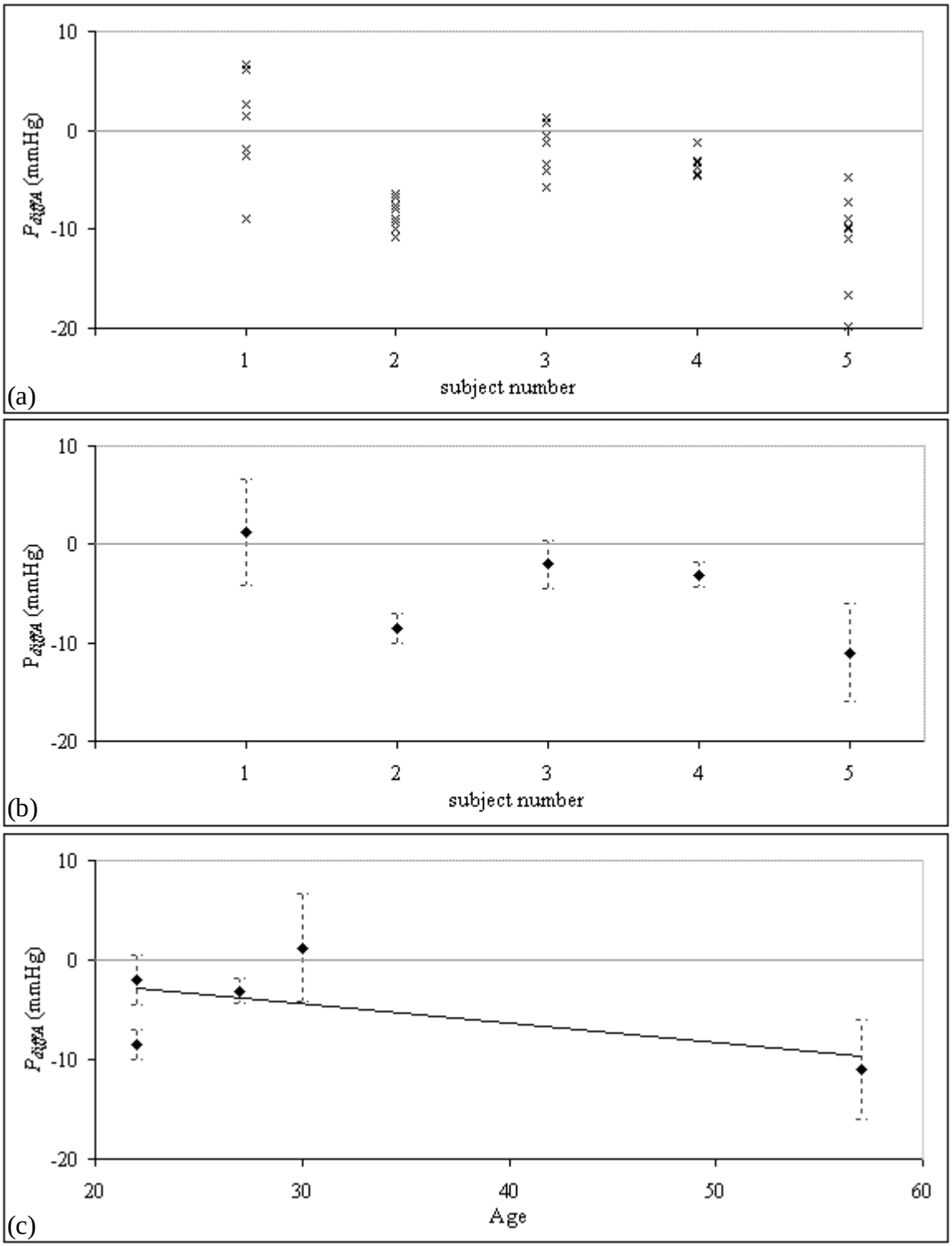

Figure 6.6 Relationship of intra-subject P_{diffA} with age.
(a) Eight P_{diffA} values were obtained per subject; (b) the intra-subject mean of P_{diffA} were computed. The error bars are the respective ±1SD; (c) the intra-subject mean of P_{diffA} are plotted with respect to the subjects' age. The regression line shows no significant correlation.

6.4 Discussion

The level of detail presented in this chapter exceeds those of the published literature. This is particularly the case of the volume clamping technique. The advantage of the study in this chapter is that *in vivo* setup was used on human artery (see Table 6.1). Noteworthy, the study dealt with physiological measurements in humans. This resembles the actual setup of continuous ABP monitoring. Thus, the results are more representative to the *STAbp* prototype device described in chapter 3 and evaluated in chapter 4.

6.4.1 Main Findings

The statistical outcome of the first null hypothesis with the P_{diffA} significantly different from zero mmHg indicates that the peak of $\hat{PPG}a$ curve does not coincide with the MAP estimated with the *Finapres*. Furthermore, the normally distributed P_{diffA} (Figure 6.5) means that a simple correction of addition or subtraction of a constant value may not be suitable. Such phenomenon may affect the accuracy and reliability of ABP measurements in some individuals. On the other hand, it was demonstrated that P_{diffA} was not influenced by the three factors, i.e. repeated measurements, direction of the P_{com} sequence and the step interval of P_{com}.

6.4.2 Previous Work

From the list of articles in Table 6.1, Ramsey III (1979) and Yamakoshi et al. (1982) reported that at the largest pulsation amplitude in oscillometry, the cuff pressure

coincided with the intra-arterial MAP. Penaz (1992) concluded the same except that it was based on the volume clamping technique. Conversely, a much larger number of articles (Table 6.1 numbered 1, 3, 4, 6, and 8-12) reported that the largest pulsation amplitude did not coincide with the MAP. The difference between the cuff pressure at this largest pulsation amplitude and the MAP was found to be small. The reported mean (SD) of differences were -0.2 (4.21) mmHg (Ramsey III, 1979), 1.4 (6.22) mmHg (Yelderman and Ream, 1979), within ±3 mmHg (Yamakoshi et al., 1982), within 2 mmHg (Drzewiecki et al., 1994), and ranged from -8 to 19 mmHg (Raamat et al., 1999). It is to note that the setup and protocols of these results are different from the study presented in this chapter. Most of these articles were based on the oscillometric technique (Table 6.1 numbered 1-4, 6, 8 and 10-12). In addition to the different measurement techniques used, the studies included the use of excised animal arteries (numbered 1, 4, 5, 9 and 11), *in vitro* setup (numbered 1, 4, 5 and 9), theoretical modelling (numbered 4, 6, 8 and 10-12) and subjects with a wide range of existing pathologies (numbered 2, 3 and 9). The diversity of techniques, subjects and preparations do not allow direct comparison with the results of this chapter.

6.4.3 Implications from Findings

A possible solution for implementation into the *STAbp* device is to reduce the P_{com} by 4.7 mmHg in order to improve agreement with the MAP (Equation 6.1). At this compressing pressure (i.e. (P_{com} - 4.7) mmHg), the corresponding PPG pulse is retrieved. The mean of this PPG pulse may then be used as the *Setpt* in the *STAbp*. To implement this in the *STAbp*, it is not a simple numerical calculation but requires a more extensive review of the existing software algorithm.

6.4.4 Limitations of the Study

Several limitations were identified in this experiment:

i. The evaluation of the experiment was based on a small sample size. Statistical power analysis was not carried out *a priori* to determine a suitable sample size as relevant sample SD was not available in existing literature. For the benefits of future studies, the power analysis was calculated retrospectively. To detect a difference of 5 mmHg (O'Brien and Atkins, 1994) for P_{diffA} using the estimated value of SD = 5.63 mmHg, with 80% power at 0.05 level of significance for paired data (Campbell and Machin, 1995), ten subjects would be required;

ii. The MAP in Equation 6.1 was computed from the *Finapres* ABP waveforms. As demonstrated in the comparative study between two *Finapreses* (section 4.3), there are inherent differences even with monitoring devices of the same specification and model number. The accuracy of the *Finapres* ABP measurement may need to be interpreted with caution. Nevertheless, this was the best means for comparisons at the time of the experiment;

iii. The experiment was carried out on the finger arteries instead of the STA. Due to their different locations, it remains to be determined if the results obtained in this study are transferable to the STA;

iv. The experiment was carried out on healthy adults. It is uncertain if the results can be used in teenagers and those younger or the very old, and in subjects with specific conditions (e.g. atherosclerosis, hypertension, diabetes, obesity and others);

v. The recordings were based on resting condition, it is uncertain if the same results would be obtained in situations with varying ABP such as exercise or specific manoeuvres such as Valsalva;

vi. The measurement protocols in Tests #1 and #2 are not practical to search for the appropriate *Setpt* during real time ABP measurement. A large number of PPG pulses is required to construct the $\overline{PPGa}$ array. During the recording of the PPG waveform, the continuous ABP waveform becomes unavailable;

vii. The polynomial curve fitting was applied on the pressure range of ±40 mmHg around $P_{diff} = 0$. A change in this pressure range may affect the result of the P_{diffA};

viii. Only the PPG pulse amplitude has been evaluated in this chapter. Other characteristics of the PPG waveform have not been assessed (Figure 6.1), for instance, the temporal pattern and the frequency content of the PPG waveform.

6.4.5 Suggestions for Future Work

The relationship between the PPG peak pulsation amplitude and the MAP may be more complex than previously anticipated. Additional parameter(s) may be required to develop a more robust algorithm for *Setpt* determination. One possible future work is to further evaluate the temporal pattern and the frequency content of the PPG waveform.

To increase the confidence of the P_{diffA} results, another suggestion is that the experiment described in this chapter may need to be repeated on the STA and evaluated with intravascular measurements. Future studies will also require a larger number of subjects, including different ages and clinical conditions.

6.5 Conclusion

The study presented in this chapter demonstrated that the peak of the PPG pulsation amplitude does not coincide with the MAP estimated with the *Finapres* device. The P_{diffA} is not a constant value which could be applied as a general correction factor since it shows both intra- and inter-subject variability. Instead, the differences are normally distributed. Further evaluation of the PPG waveform is suggested as this may help to provide more answers to improve the determination of *Setpt* in the *STAbp*.

CHAPTER 7 CONCLUSIONS

7.1 Review of Objectives

This thesis focuses on ABP monitoring that generates continuous ABP waveforms. The applications of continuous ABP waveforms encompass a wide range of clinical assessments and physiological research (section 1.3). To encourage wider use of continuous ABP monitoring, the noninvasive approach is preferred. The main benefits of CoNIBP monitoring include better patient safety (i.e. minimise infection and other clinical complications) and minimal running costs.

Currently available ABP measurement devices have several limitations that form the rationale of this thesis (section 1.2). Section 1.2 also explained the reservations of accepting ABP waveforms measured in the periphery to represent the ABP waveform close to the heart (i.e. ascending aorta). These are due to the effects of pulse wave propagation and reflection, differences in local regulations of blood flow, vasomotor tone, arterial elasticity, peripheral resistance, and poor accuracy and reliability to measure peripheral ABP in some patients groups.

The STA is evaluated as the best available alternative measurement site closer to the heart for CoNIBP measurement (section 2.3). The effect of pulse wave propagation and reflection is less prominent than peripheral ABP derived at the finger artery. For this reason, it should be able to predict ABP in the ascending aorta more accurately.

A new CoNIBP measurement device, known as the *STAbp*, was designed and constructed (chapter 3) and then evaluated (chapter 4). Further investigations were carried out (chapters 5 and 6) to seek new knowledge and to consider a more robust algorithm to improve the accuracy of ABP measurement with the *STAbp*. These further investigations focused on the appropriate *Setpt* determination, first by assessing the sensitivity of the ABP to perturbation of the *Setpt*, and then followed by further assessment of PPG waveform to extract information which could be incorporated into the *STAbp* to improve the *Setpt* determination, hence more accurate ABP waveform recordings.

To a large extent these original objectives have been met with the design, construction and testing of the new CoNIBP device. The main conclusions of this work are reviewed in the following sections.

7.2 Original Contributions of Thesis

STAbp system architecture

The design and construction of the *STAbp* prototype device (chapter 3) allowed continuous recording of ABP in the STA. The *STAbp* was developed based on the volume clamping technique with photoplethysmography. It consists of a complex integration of hardware and software components in order to monitor the ABP in the STA with intermittent review of the PPG *Setpt* to ensure an accurate ABP waveform is obtained. The intermittent review of the *Setpt* is carried out by the self-calibration feature in the *STAbp*.

Evaluation of STAbp device

The *STAbp* provided physiologically realistic ABP waveforms with consistent baseline stability (chapter 4). The widespread use of the *STAbp* device in the experiments described in this thesis confirmed its relative reliability and robustness to routine use despite only being a prototype constructed in-house. It was used in the experiments described in chapters 3 to 5 with at least 35 ABP measurement sessions of five to fifteen minutes each. The continuous ABP tracing also responded to manoeuvres such as the Valsalva and the IHG exercise in similar fashion to what has been reported with invasive ABP measurements.

An original assessment of the comparative performance of two *Finapreses* was conducted to provide the background against which to compare the *STAbp* with the *Finapres*. The comparisons between two *Finapreses* produced results which describe their inherent differences even though both devices have the same specifications and

same model number. The differences in measurements could be caused by inappropriate fitting of the finger cuff on the finger, motion artifacts or other physiological conditions that may vary between both fingers. Technical differences in both devices are also potential causes of error.

The spectral analyses between simultaneous ABP measurements by the two *Finapreses* produced a relatively low cut-off frequency in the gain spectral curve (13.3 Hz) with coherence above 0.5 only up to approximately 12.5 Hz (Figure 4.18). Nevertheless, the comparative study between two *Finapreses* formed the necessary boundaries for interpreting the results in the comparative study of the *STAbp* and *Finapres* more appropriately.

In the comparative study of *STAbp* and *Finapres*, significant differences were obtained in the agreement of the SBP, MAP, and DBP, as well as the ABP pulse bandwidth limits. However, the assessment of ABP drift did not show significant differences which suggest that the *STAbp* is at least as stable as the *Finapres* when the ABP in the STA is monitored continuously. Given the fact that the differences of ABP waveshapes and amplitude in different measurement sites, the spectral analyses gave a cut-off frequency in the gain spectral curve lower than 13.3 Hz with a more complex phase response that increases in phase leading between 3.2 Hz and 9.5 Hz up to approximately 110º before stabilising (Figure 4.18). The magnitude squared coherence was retained above 0.5 even beyond 12.5 Hz which is approximately as good as the coherence spectrum between two *Finapreses*.

Further investigations

Following chapter 4, further research studies (chapters 5 and 6) first reported the high sensitivity of the ABP waveform to a small change in *Setpt*, which indicates the need for more stringent selection of hardware components to ensure that the *Setpt* will not be affected by technical issues such as electronic drift, noise and thermal interferences. Greater attention must also be given in future reviews to the software algorithm that determines the *Setpt*. Additionally, the studies also reported that the PPG waveform contains additional information that may contribute to the improvement of the self-calibration algorithm for *Setpt* determination. One aspect of the PPG waveform analysed was the difference between the external compressing pressure at the PPG peak pulsation amplitude and the MAP. The sample average of the differences was considered small (-4.7 mmHg), however, the differences were not constant intra- and inter- subjects, but tended to follow a normal distribution.

The availability of the *STAbp* offers many advantages to the research and clinical communities. The monitoring of the ABP in the STA could be a useful tool to study the pathophysiology of human vascular circulation in the head intra- and extra- cranially. It is also a step forward towards comparing the blood flow and the ABP in the STA simultaneously. These will potentially extend the scope of human physiological research which was not explored previously.

7.3 Limitations of the Thesis

The evaluation of the *STAbp* was compared to the *Finapres*. *Finapres* is currently the best alternative to the gold standard, i.e. intravascular measurement. Inherent differences learnt in the comparative study between two *Finapreses* (section 4.3) indicate the importance of this prior knowledge before the measurement differences between the *STAbp* and *Finapres* (section 4.4) could be evaluated. However, with the influence of pulse wave propagation and reflection, local blood flow regulation, vasomotor tone, arterial elasticity and peripheral resistance, the comparisons of the ABP between these different measurement sites are not definitive.

The subjects recruited for the studies described in the thesis are all relatively young healthy adults with no known pathologies that may affect their blood circulation. The validity of the analysis results obtained may not be applicable to teenagers and those younger or the elderly, and to individuals with specific conditions such as hypertension, cardiac dysfunction, obesity, atherosclerosis or diabetes.

7.4 Suggestions for Future Work

The design of the head frame needs to be modified to improve its stability and fitting during continuous ABP monitoring. It is also necessary to provide enough flexibility for optimal adjustment with varying human head sizes. With current head frame design, the subjects were required to sit in an upright position. A new design is needed to allow subjects to lie in a supine position. Such design will also be more suitable clinically for patients who are not able to sit up for a prolonged duration.

The effect of different surface areas of compression from the front of the probe on the skin with underlying STA needs to be investigated further. This could be carried out in conjunction with exploring the different arrangements of optoelectronic components relative to the STA. The accuracy and reliability of the PPG waveform produced will need further investigation to identify factors that can interfere with the intended PPG output. At the same time, the PPG waveshape can be analysed further to produce new information that may be incorporated into the self-calibration algorithm in the *STAbp* to improve the robustness of *Setpt* determination.

The use of mathematical modelling or a specific experimental test rig could be beneficial to evaluate these variables. It is envisaged that the benefits of mathematical modelling could be multi-fold. These include a better understanding of the mechanical properties of *STAbp* design, for instance, the area of compression of the probe on the tissue with the underlying STA; a better understanding of the optical properties of the artery, the surrounding tissue and the bone at the temporal region; a better understanding of factors that can affect the PPG waveshape; and to predict the accuracy

of ABP waveform measured with the *STAbp* on patient, age and fitness level specific groups.

For validation of the prototype device, an important step forward will be to validate the *STAbp* against intravascular measurement i.e. ABP in the ascending aorta. This is merited by the encouraging results obtained so far, however it must only be considered after further improvements as suggested above.

Successful validation in comparison with an intravascular catheter-tip transducer in the ascending aorta must be followed by wider evaluation to include different age groups and patients with different conditions, particularly those with increased arterial stiffness or other pathologies that might affect the difference between peripheral and central measures of ABP.

7.5 Conclusions

The evaluation of the *STAbp* prototype device demonstrated the ability of the device to produce realistic ABP waveforms and its comparison with *Finapres* showed reasonable agreement. Nevertheless, further hardware developments and software improvements are still necessary before its validation against central intravascular measurement. Further validation in different age groups and patients is also a future target.

The availability of the *STAbp* will provide easier access to a CoNIBP measurement device beneficial for clinical assessments and physiological research. Wider utilisation of CoNIBP measurements is likely to lead to considerable additional knowledge that will further improve the prognosis, diagnosis and management of patients with cardiovascular disease and other conditions.

APPENDIX ELECTRONIC CIRCUITS DIAGRAMS

Figure A.1 IRED Driver and Transimpedance Amplifiers

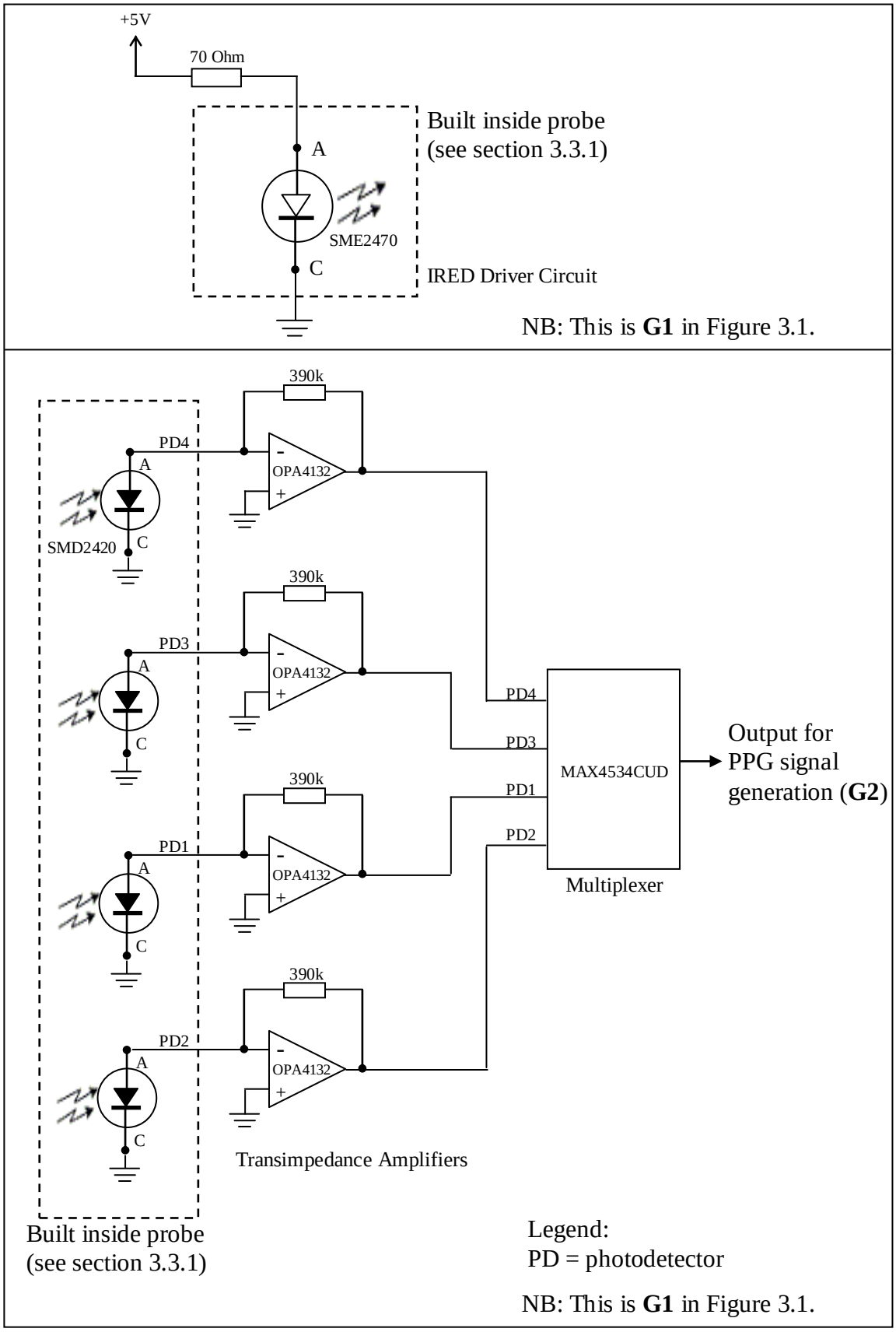

Figure A.2 Piezo Valve with Regulated Compressed Air Supply

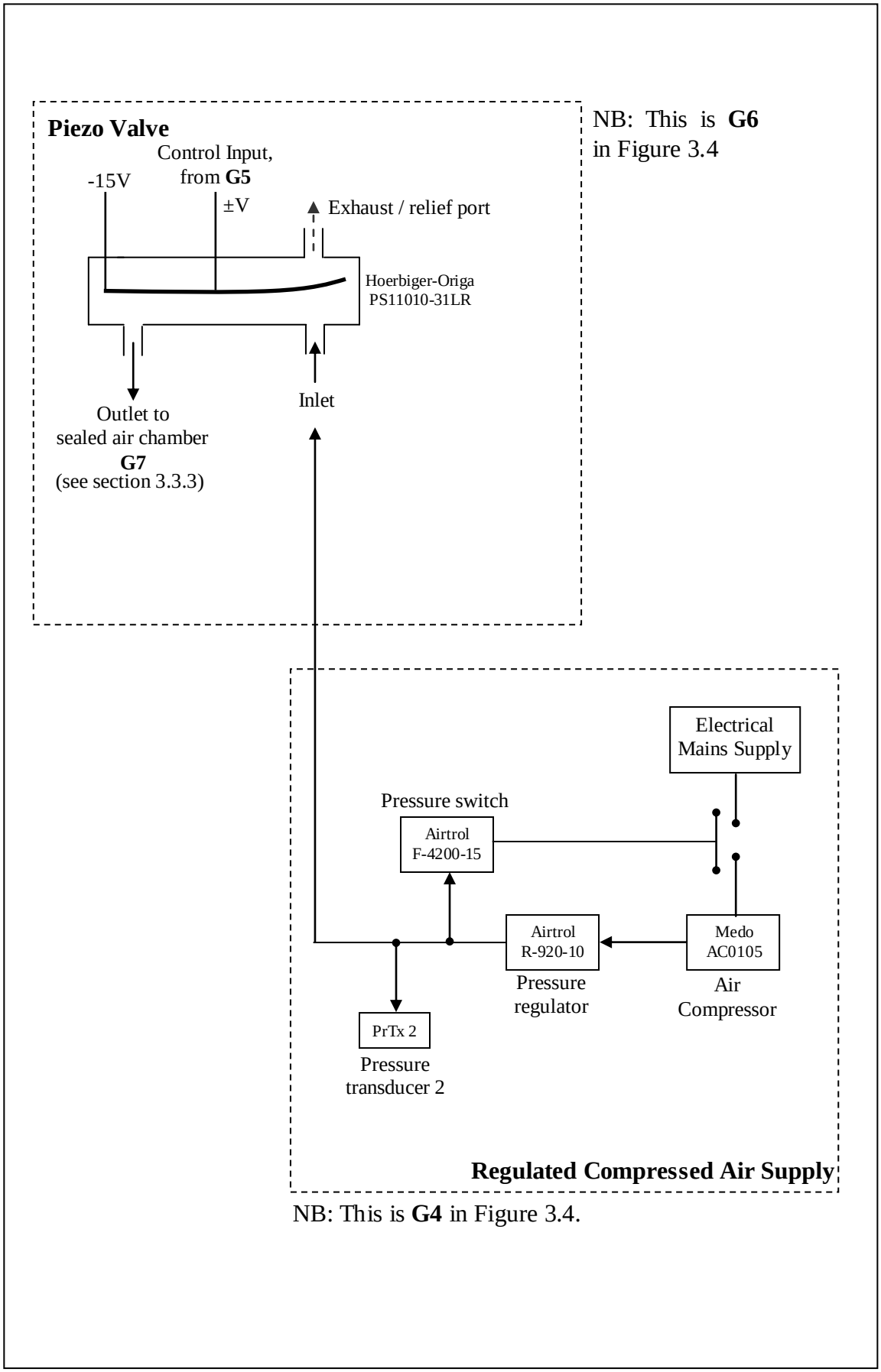

Figure A.3 Controller (for Regulated Compressing Pressure)

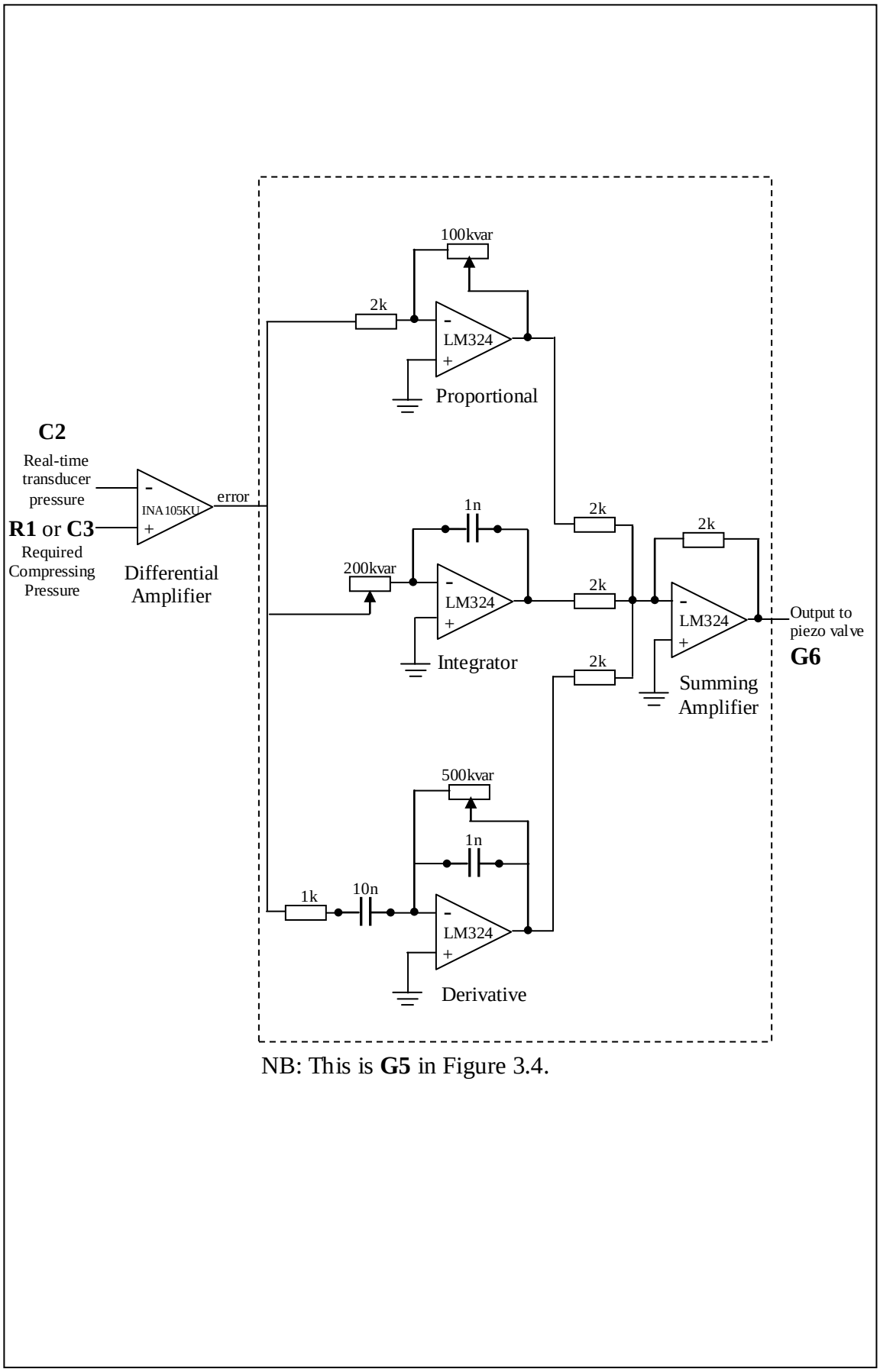

NB: This is **G5** in Figure 3.4.

Figure A.4 Pressure Transducer

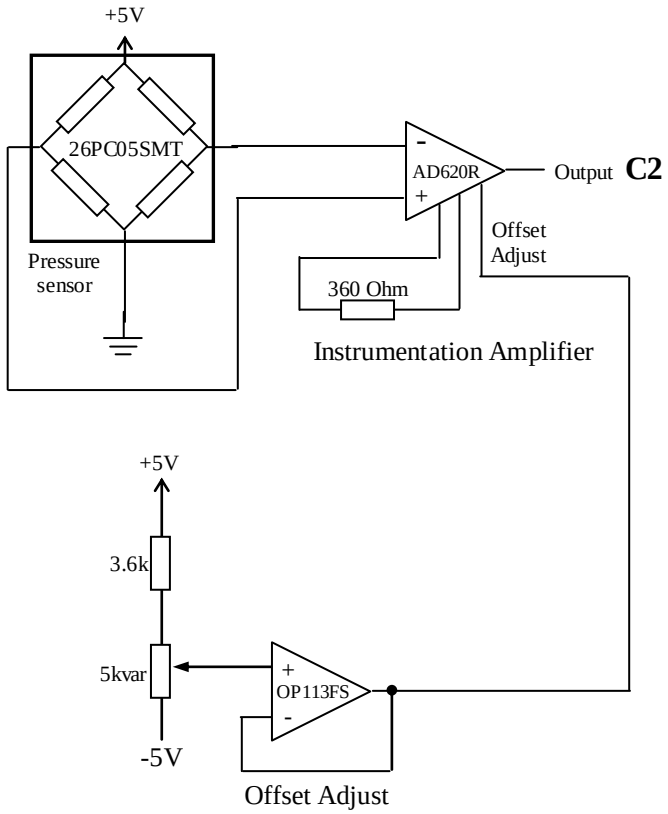

NB: This is **G8** in Figure 3.4.

Figure A.5 PPG Signal Generation

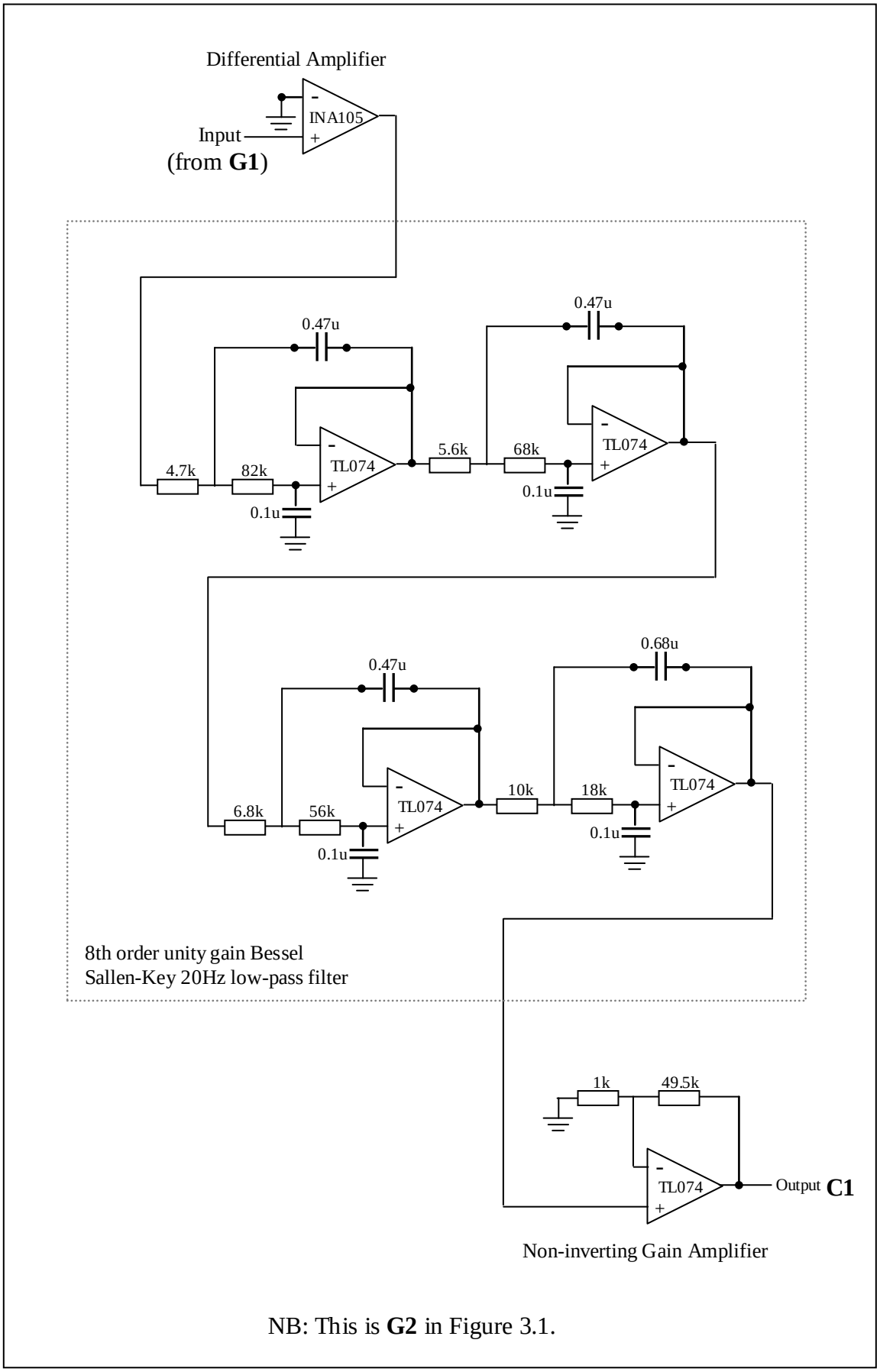

NB: This is **G2** in Figure 3.1.

Figure A.6 Closed Loop Feedback Controller

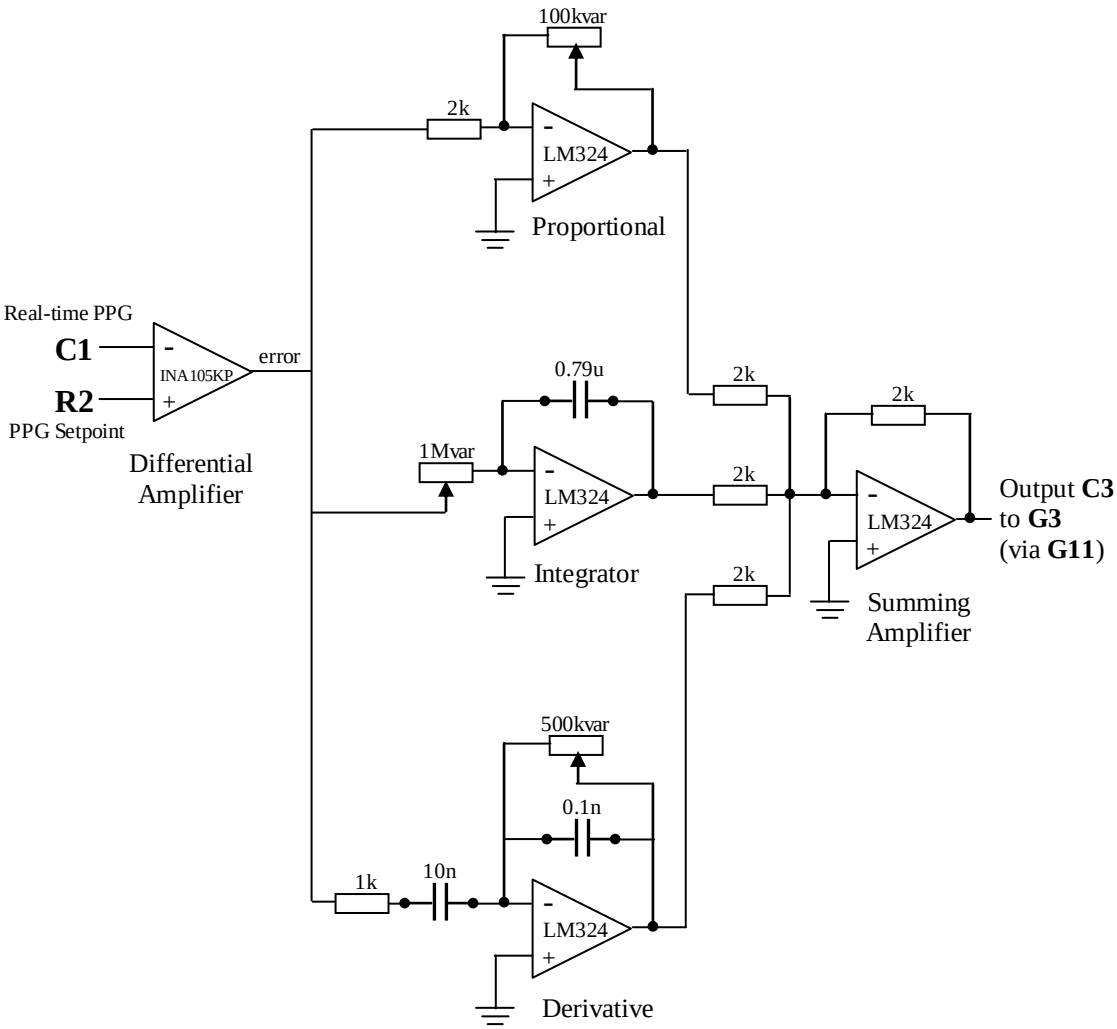

NB: This is **G10** in Figure 3.1.

Figure A.7 Mode Switch

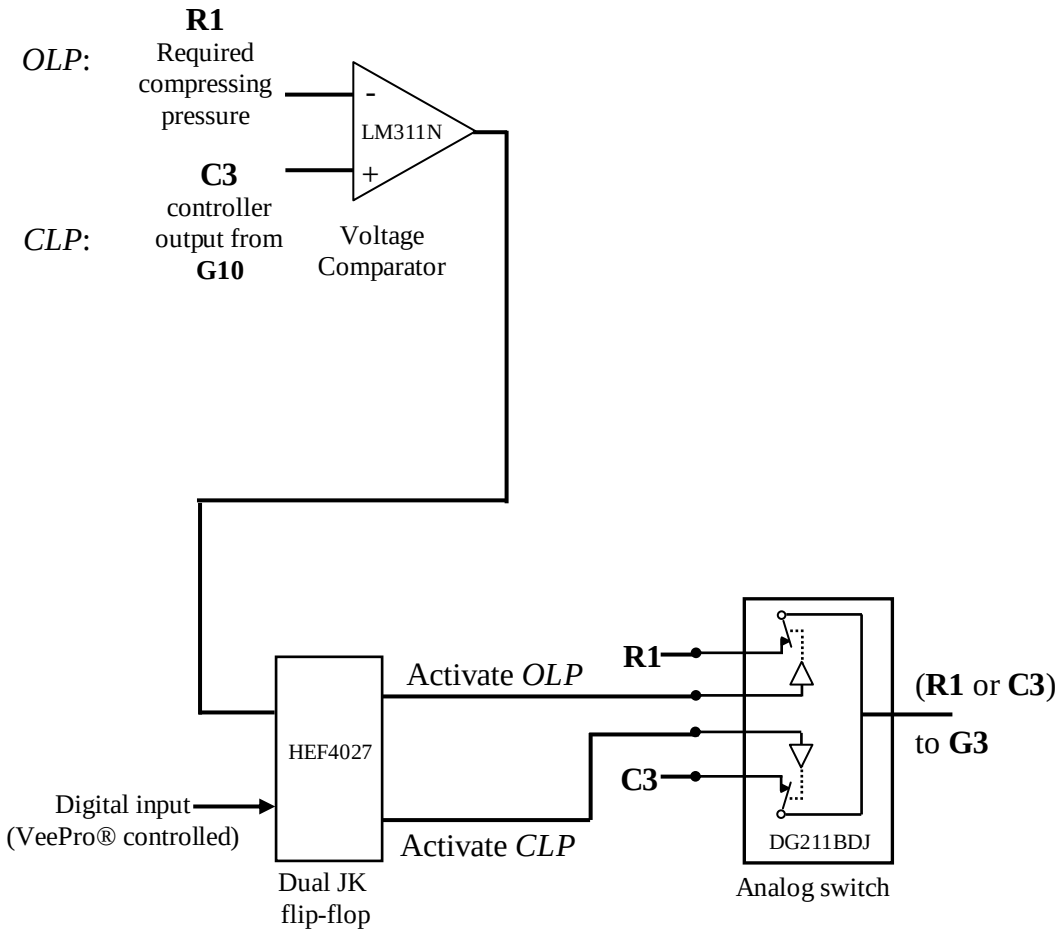

Legend:
OLP = Open Loop Procedure (see description in section 3.3.7.1)
CLP = Closed Loop Procedure (see description in section 3.3.7.2)

NB: This is **G11** in Figure 3.1.

BIBLIOGRAPHY

Aaslid, R., Lindegaard, K.F., Sorteberg, W. and Nornes, H., 1989. Cerebral autoregulation dynamics in humans. *Stroke*, **20**(1), 45-52.

Allen, J., 2007. Photoplethysmography and its application in clinical physiological measurement. *Physiol Meas*, **28**(3), R1-R39.

Amoore, J.N., Guehenec, M., Scordecchia, R. and Scott, D.H., 2010. Auditing the technology used to measure blood pressure. *J Med Eng Technol*, **34**(3), 209-216.

Andriessen, P., Schoffelen, R.L., Berendsen, R.C., de Beer, N.A., Oei, S.G., Wijn, P.F. and Blanco, C.E., 2004. Noninvasive assessment of blood pressure variability in preterm infants. *Pediatr Res*, **55**(2), 220-223.

Astrom, K.J. and Hagglund, T., 1995. PID controllers: theory, design and tuning. 2nd edn, North Carolina: International Society of Automation.

Atkins, E.R., Brodie, F.G., Rafelt, S.E., Panerai, R.B. and Robinson, T.G., 2010. Dynamic cerebral autoregulation is compromised acutely following mild ischaemic stroke but not transient ischaemic attack. *Cerebrovasc Dis*, **29**(3), 228-235.

Aubert, A.E., Vrolix, M., de Geest, H. and van de Werf, F., 1995. In vivo comparison between two tip pressure transducer systems. *Int J Clin Monit Comput*, **12**(2), 77-83.

Avolio, A., 1992. Ageing and wave reflection. *J Hypertens Suppl*, **10**(6), S83-S86.

Avolio, A.P., Deng, F.Q., Li, W.Q., Luo, Y.F., Huang, Z.D., Xing, L.F. and O'Rourke, M.F., 1985. Effects of aging on arterial distensibility in populations with high and low prevalence of hypertension: comparison between urban and rural communities in China. *Circulation*, **71**(2), 202-210.

Baguley, I.J., Heriseanu, R.E., Cameron, I.D., Nott, M.T. and Slewa-Younan, S., 2008. A critical review of the pathophysiology of dysautonomia following traumatic brain injury. *Neurocrit Care*, **8**(2), 293-300.

Baker, P.D., Westenskow, D.R. and Kuck, K., 1997. Theoretical analysis of non-invasive oscillometric maximum amplitude algorithm for estimating mean blood pressure. *Med Biol Eng Comput*, **35**(3), 271-278.

Bedford, R.F., 1978. Long-term radial artery cannulation: effects on subsequent vessel function. *Crit Care Med*, **6**(1), 64-67.

Bedford, R.F. and Wollman, H., 1973. Complications of percutaneous radial-artery cannulation: an objective prospective study in man. *Anesthesiology*, **38**(3), 228-236.

Belardinelli, E. and Cavalcanti, S., 1992. Theoretical analysis of pressure pulse propagation in arterial vessels. *J Biomech.*, **25**(11), 1337-1349.

Bendat, J.S. and Piersol, A.G., 1986, Digital Data Analysis. *Random Data: Analysis and Measurement Procedures*, 2nd edn, New York: John Wiley & Sons, Chapter 11, 361-424.

Bendat, J.S. and Piersol, A.G., 1993. Engineering Applications of Correlation and Spectral Analysis. New York: Wiley.

Bergersen, T.K., 1993. A search for arteriovenous anastomoses in human skin using ultrasound Doppler. *Acta Physiol Scand*, **147**(2), 195-201.

Bienfang, D.C., 1984. Use of the Doppler probe to detect the course of the superficial temporal artery. *Am J Ophthalmol*, **97**(4), 526-527.

Birch, A.A., Dirnhuber, M.J., Hartley-Davies, R., Iannotti, F. and Neil-Dwyer, G., 1995. Assessment of autoregulation by means of periodic changes in blood pressure. *Stroke*, **26**(5), 834-837.

Birch, A.A. and Morris, S.L., 2003. Do the Finapres and Colin radial artery tonometer measure the same blood pressure changes following deflation of thigh cuffs? *Physiol Meas*, **24**(3), 653-660.

Bland, J.M. and Altman, D.G., 1986. Statistical methods for assessing agreement between two methods of clinical measurement. *Lancet*, **1**(8476), 307-310.

Bland, M., 1995, Significance tests. *An introduction to medical statistics*, 2nd edn, New York: Oxford University Press, Chapter 9, 133-151.

Blank, S.G., West, J.E., Muller, F.B., Cody, R.J., Harshfield, G.A., Pecker, M.S., Laragh, J.H. and Pickering, T.G., 1988. Wideband external pulse recording during cuff deflation: a new technique for evaluation of the arterial pressure pulse and measurement of blood pressure. *Circulation*, **77**(6), 1297-1305.

Bloomfield, P., 2000. Fourier analysis of time series : an introduction. 2nd edn, New York: Wiley.

Boehmer, R.D., 1987. Continuous, real-time, noninvasive monitor of blood pressure: Penaz methodology applied to the finger. *J Clin Monit*, **3**(4), 282-287.

Brigham, E.O., 1988. The fast Fourier transform and its applications. Englewood Cliffs, NJ: Prentice-Hall International.

Brinton, T.J., Cotter, B., Kailasam, M.T., Brown, D.L., Chio, S.S., O'Connor, D.T. and DeMaria, A.N., 1997. Development and validation of a noninvasive method to determine arterial pressure and vascular compliance. *Am J Cardiol*, **80**(3), 323-330.

Brown, T.R. and MacGregor, J., 1982. An infra-red reflectance system for ambulatory characterization of left ventricular function. *J Biomed Eng*, **4**(2), 142-148.

Bull, M.J., Schreiner, R.L., Garg, B.P., Hutton, N.M., Lemons, J.A. and Gresham, E.L., 1980. Neurologic complications following temporal artery catheterization. *J Pediatr*, **96**(6), 1071-1073.

Burr-Brown, 1997. ISO 124 Isolation Amplifier. *Burr-Brown*, USA: Texas Instruments Incorporated, 1-12.

Cameron, J.D., McGrath, B.P. and Dart, A.M., 1998. Use of radial artery applanation tonometry and a generalized transfer function to determine aortic pressure augmentation in subjects with treated hypertension. *J Am Coll Cardiol*, **32**(5), 1214-1220.

Campbell, M.J. and Machin, D., 1995. Medical Statistics: a commonsense approach. 2nd edn, Chichester, West Sussex: John Wiley & Sons.

Carroll, G.C., 1988. Blood pressure monitoring. *Crit Care Clin*, **4**(3), 411-434.

Celis, H. and Fagard, R.H., 2004. White-coat hypertension: a clinical review. *Eur J Intern Med*, **15**(6), 348-357.

Chemla, D., Antony, I., Zamani, K. and Nitenberg, A., 2005. Mean aortic pressure is the geometric mean of systolic and diastolic aortic pressure in resting humans. *J Appl Physiol*, **99**(6), 2278-2284.

Chen, C.H., Ting, C.T., Lin, S.J., Hsu, T.L., Yin, F.C., Siu, C.O., Chou, P., Wang, S.P. and Chang, M.S., 1995. Different effects of fosinopril and atenolol on wave reflections in hypertensive patients. *Hypertension*, **25**(5), 1034-1041.

Chen, C.H., Ting, C.T., Nussbacher, A., Nevo, E., Kass, D.A., Pak, P., Wang, S.P., Chang, M.S. and Yin, F.C., 1996. Validation of carotid artery tonometry as a means of estimating augmentation index of ascending aortic pressure. *Hypertension*, **27**(2), 168-175.

Chen, T.H., Chen, C.H., Shyu, J.F., Wu, C.W., Lui, W.Y. and Liu, J.C., 1999. Distribution of the superficial temporal artery in the Chinese adult. *Plast Reconstr Surg*, **104**(5), 1276-1279.

Chia, F., Ang, A.T., Wong, T.W., Tan, K.W., Fung, K.P., Lee, J. and Khin, K., 1990. Reliability of the Dinamap non-invasive monitor in the measurement of blood pressure of ill Asian newborns. *Clin Pediatr (Phila)*, **29**(5), 262-267.

Clearkin, L.G. and Watts, M.T., 1991. How to perform a temporal artery biopsy. *Br J Hosp Med*, **46**(3), 172-174.

Cockcroft, J.R. and Wilkinson, I.B., 2002. Arterial stiffness and pulse contour analysis: an age old concept revisited. *Clin Sci (Lond)*, **103**(4), 379-380.

Colan, S.D., 1984. Combined fluid-filled and micromanometer-tip catheter system for high-fidelity pressure recordings in infants. *Cathet Cardiovasc Diagn*, **10**(6), 619-623.

Cozby, R.C. and Adhami, R.R., 1993. Low-frequency Korotkoff signal analysis and application. *IEEE Trans Biomed Eng*, **40**(10), 1067-1070.

Crombie, I.K., Clark, E.C. and Smith, W.C., 1988. Assessment of the Copal UA-251 automatic blood pressure recorder under field survey conditions. *Med Biol Eng Comput*, **26**(6), 663-664.

Czerwinski, F., 1992. Variability in the course of the superficial temporal artery in man. *Folia Morphol (Warsz)*, **51**(1), 49-54.

Darovic, G.O. and Zbilut, J.P., 2002, Fluid-Filled Monitoring Systems. *Hemodynamic Monitoring - Invasive and Noninvasive Clinical Application*, 3rd edn, Chapter 6, 113-132.

Davies, J.I. and Struthers, A.D., 2003. Pulse wave analysis and pulse wave velocity: a critical review of their strengths and weaknesses. *J Hypertens*, **21**(3), 463-472.

Davis, P.D. and Kenny, G.N.C., 2003. Basic physics and measurement in anaesthesia. 5th edn, Edinburgh: Butterworth-Heinemann.

Dawson, S.L., Panerai, R.B. and Potter, J.F., 2003. Serial changes in static and dynamic cerebral autoregulation after acute ischaemic stroke. *Cerebrovasc Dis*, **16**(1), 69-75.

Dawson, S.L., Panerai, R.B. and Potter, J.F., 1999a. Critical closing pressure explains cerebral hemodynamics during the Valsalva maneuver. *J Appl Physiol*, **86**(2), 675-680.

Dawson, S.L., Robinson, T.G., Youde, J.H., James, M.A., Martin, A., Weston, P., Panerai, R. and Potter, J.F., 1997. The reproducibility of cardiac baroreceptor activity assessed non-invasively by spectral sequence techniques. *Clin Auton Res*, **7**(6), 279-284.

Dawson, S.L., Robinson, T.G., Youde, J.H., Martin, A., James, M.A., Weston, P.J., Panerai, R.B. and Potter, J.F., 1999b. Older subjects show no age-related decrease in cardiac baroreceptor sensitivity. *Age Ageing*, **28**(4), 347-353.

de Boer, R.W., Karemaker, J.M. and Strackee, J., 1985. Relationships between short-term blood-pressure fluctuations and heart-rate variability in resting subjects. I: A spectral analysis approach. *Med Biol Eng Comput*, **23**(4), 352-358.

Dineen, N.E., Brodie, F.G., Robinson, T.G. and Panerai, R.B., 2010. Continuous estimates of dynamic cerebral autoregulation during transient hypocapnia and hypercapnia. *J Appl Physiol*, **108**(3), 604-613.

Dorlas, J.C., Nijboer, J.A., Butijn, W.T., van der Hoeven, G.M., Settels, J.J. and Wesseling, K.H., 1985. Effects of peripheral vasoconstriction on the blood pressure in the finger, measured continuously by a new noninvasive method (the Finapres). *Anesthesiology*, **62**(3), 342-345.

Downs, J.B., Chapman, R.L., Jr. and Hawkins, I.F., Jr., 1974. Prolonged radial-artery catheterization. An evaluation of heparinized catheters and continuous irrigation. *Arch Surg*, **108**(5), 671-673.

Drzewiecki, G., 1995, Noninvasive Assessment of Arterial Blood Pressure and Mechanics. North Carolina: CRC Press Inc., Chapter 73, 1196-1211.

Drzewiecki, G., Field, S., Moubarak, I. and Li, J.K., 1997. Vessel growth and collapsible pressure-area relationship. *Am J Physiol*, **273**(4 Pt 2), H2030-H2043.

Drzewiecki, G., Hood, R. and Apple, H., 1994. Theory of the oscillometric maximum and the systolic and diastolic detection ratios. *Ann Biomed Eng*, **22**(1), 88-96.

Drzewiecki, G.M., Melbin, J. and Noordergraaf, A., 1989. The Korotkoff sound. *Ann Biomed Eng*, **17**(4), 325-359.

Drzewiecki, G.M., Melbin, J. and Noordergraaf, A., 1983. Arterial tonometry: review and analysis. *J Biomech*, **16**(2), 141-152.

Epstein, R.H., Bartkowski, R.R. and Huffnagle, S., 1991. Continuous noninvasive finger blood pressure during controlled hypotension. A comparison with intraarterial pressure. *Anesthesiology*, **75**(5), 796-803.

Erlanger, J., 1916a. Studies in blood pressure estimation by indirect methods II: mechanism of the compression sounds of Korotkoff. *Am J Physiol*, **40**(5), 82-125.

Erlanger, J., 1916b. Studies in blood pressure estimation by indirect methods I: mechanism of the oscillatory criteria. *Am J Physiol*, **39**, 401-446.

Euler, D.E., 1999. Cardiac alternans: mechanisms and pathophysiological significance. *Cardiovasc Res*, **42**(3), 583-590.

Evans, P.J. and Kerr, J.H., 1975. Arterial occlusion after cannulation. *Br Med J*, **3**(5977), 197-199.

Eveson, D.J., Robinson, T.G., Shah, N.S., Panerai, R.B., Paul, S.K. and Potter, J.F., 2005. Abnormalities in cardiac baroreceptor sensitivity in acute ischaemic stroke patients are related to aortic stiffness. *Clin Sci (Lond)*, **108**(5), 441-447.

Ewing, D.J., Martyn, C.N., Young, R.J. and Clarke, B.F., 1985. The value of cardiovascular autonomic function tests: 10 years experience in diabetes. *Diabetes Care*, **8**(5), 491-498.

Farquhar, I.K., 1991. Continuous direct and indirect blood pressure measurement (Finapres) in the critically ill. *Anaesthesia*, **46**(12), 1050-1055.

Ferro, G., Duilio, C., Spinelli, L., Liucci, G.A., Mazza, F. and Indolfi, C., 1995. Relation between diastolic perfusion time and coronary artery stenosis during stress-induced myocardial ischemia. *Circulation*, **92**(3), 342-347.

Forster, F.K. and Turney, D., 1986. Oscillometric determination of diastolic, mean and systolic blood pressure--a numerical model. *J Biomech Eng*, **108**(4), 359-364.

Frattola, A., Parati, G., Gamba, P., Paleari, F., Mauri, G., Di, R.M., Castiglioni, P. and Mancia, G., 1997. Time and frequency domain estimates of spontaneous baroreflex sensitivity provide early detection of autonomic dysfunction in diabetes mellitus. *Diabetologia*, **40**(12), 1470-1475.

Gabe, I.T., 1972, Pressure Measurement in Experimental Physiology. *Cardiovascular Fluid Dynamics*, vol. 1, edited by D. H. Bergel, Burlington: Academic Press Inc, Chapter 2, 11-50.

Gardner, R.M., 1981. Direct blood pressure measurement--dynamic response requirements. *Anesthesiology*, **54**(3), 227-236.

Gardner, R.M. and Hollingsworth, K.W., 1986. Optimizing the electrocardiogram and pressure monitoring. *Crit Care Med*, **14**(7), 651-658.

Geddes, L.A., Voelz, M., Combs, C., Reiner, D. and Babbs, C.F., 1982. Characterization of the oscillometric method for measuring indirect blood pressure. *Ann Biomed Eng*, **10**(6), 271-280.

Geddes, L.A. and Whistler, S.J., 1978. The error in indirect blood pressure measurement with the incorrect size of cuff. *Am Heart J*, **96**(1), 4-8.

Gerhardt, U.M., Scholler, C., Bocker, D. and Hohage, H., 2000. Non-invasive estimation of cardiac output in critical care patients. *J Clin Monit Comput*, **16**(4), 263-268.

Gibbs, N.C. and Gardner, R.M., 1988. Dynamics of invasive pressure monitoring systems: clinical and laboratory evaluation. *Heart Lung*, **17**(1), 43-51.

Golden, D.P., Jr., Wolthuis, R.A., Hoffler, G.W. and Gowen, R.J., 1974. Development of a Korotkov sound processor for automatic identification of auscultatory events. I. Specification of preprocessing bandpass filters. *IEEE Trans Biomed Eng*, **21**(2), 114-118.

Goldstein, D.S., Robertson, D., Esler, M., Straus, S.E. and Eisenhofer, G., 2002. Dysautonomias: clinical disorders of the autonomic nervous system. *Ann Intern Med*, **137**(9), 753-763.

Gravenstein, J.S., Paulus, D.A., Feldman, J. and McLaughlin, G., 1985. Tissue hypoxia distal to a Penaz finger blood pressure cuff. *J Clin Monit*, **1**(2), 120-125.

Gray, H., 1918. Anatomy of the Human Body. Accessed 10-9-2006, www.bartleby.com/107.

Guyton, A.C. and Hall, J.E., 1997. Human physiology and mechanisms of disease. 6th edn, London: W.B. Saunders.

Hackman, C.H., Tan, P.S., Chakrabarti, M.K. and Whitwam, J.G., 1991. A new optical transducer for arterial pressure measurement. *Br J Anaesth*, **67**(3), 346-352.

Hall, R., 2001. The cardiovascular system - blood vessels. Lecture notes, 1 - 13.

Hansen, A.T., 1983. Fibre-optic pressure transducers for medical application. *Sensors and Actuators*, **4**, 545-554.

Harris, F.J., 1978. On the use of windows for harmonic analysis with the discrete Fourier transform. *Proceedings of the IEEE*, **66**(1), 51-83.

Haubrich, C., Kruska, W., Diehl, R.R., Moller-Hartmann, W. and Klotzsch, C., 2003. Dynamic autoregulation testing in patients with middle cerebral artery stenosis. *Stroke*, **34**(8), 1881-1885.

Hessel, P.A., 1986. Terminal digit preference in blood pressure measurements: effects on epidemiological associations. *Int J Epidemiol*, **15**(1), 122-125.

Hirai, M., Nielsen, S.L. and Lassen, N.A., 1976. Blood pressure measurement of all five fingers by strain gauge plethysmography. *Scand J Clin Lab Invest*, **36**(7), 627-632.

Hirai, Y., Fujimoto, S., Toyoda, K., Inoue, T., Uwatoko, T., Makihara, N., Yasumori, K., Ibayashi, S., Iida, M. and Okada, Y., 2005. Superficial temporal artery duplex ultrasonography for improved cerebral hemodynamics after extracranial-intracranial bypass surgery. *Cerebrovasc Dis*, **20**(6), 463-469.

Hoerbiger, 2004. The Art of Interface. *Hoerbiger-Origa Catalogue*, Schongau: Hoerbiger-Origa, 7-9.

Hu, H.H., Kuo, T.B., Wong, W.J., Luk, Y.O., Chern, C.M., Hsu, L.C. and Sheng, W.Y., 1999. Transfer function analysis of cerebral hemodynamics in patients with carotid stenosis. *J Cereb Blood Flow Metab*, **19**(4), 460-465.

Hughes, D.G., Thornton, P.G.N. and Stokes, M.A., 1994, Monitoring in Young Children. *Monitoring in Anaesthesia and Intensive Care*, edited by P. Hutton & C. Prys-Roberts, London: W.B. Saunders Company, Chapter 23, 365-381.

Hughson, R.L., 2009. Recent findings in cardiovascular physiology with space travel. *Respir Physiol Neurobiol*, **169**(Suppl 1), S38-S41.

Hutton, P., 1994, The Direct Measurement of Intravascular Pressures. *Monitoring in Anaesthesia and Intensive Care*, edited by P. Hutton & C. Prys-Roberts, London: W.B. Saunders, Chapter 9, 121-144.

Hutton, P. and Clutton-Brock, T.H., 1994, The Non-invasive Measurement of Blood Pressure. *Monitoring in Anaesthesia and Intensive Care*, edited by P. Hutton & C. Prys-Roberts, W.B. Saunders, Chapter 8, 105-120.

Hutton, P. and Prys-Roberts, C., 1994. Monitoring in anaesthesia and intensive care. edited by Hutton, P. and Prys-Roberts, C., London: W.B. Saunders Company Ltd.

Imholz, B.P., Langewouters, G.J., van Montfrans, G.A., Parati, G., van Goudoever, J., Wesseling, K.H., Wieling, W. and Mancia, G., 1993. Feasibility of ambulatory, continuous 24-hour finger arterial pressure recording. *Hypertension*, **21**(1), 65-73.

Imholz, B.P., Settels, J.J., van der Meiracker, A.H., Wesseling, K.H. and Wieling, W., 1990. Non-invasive continuous finger blood pressure measurement during orthostatic stress compared to intra-arterial pressure. *Cardiovasc Res*, **24**(3), 214-221.

Imholz, B.P., Wieling, W., van Montfrans, G.A. and Wesseling, K.H., 1998. Fifteen years experience with finger arterial pressure monitoring: assessment of the technology. *Cardiovasc Res*, **38**(3), 605-616.

James, M.A., Robinson, T.G., Panerai, R.B. and Potter, J.F., 1996. Arterial baroreceptor-cardiac reflex sensitivity in the elderly. *Hypertension*, **28**(6), 953-960.

Jansen, J.R., Schreuder, J.J., Mulier, J.P., Smith, N.T., Settels, J.J. and Wesseling, K.H., 2001. A comparison of cardiac output derived from the arterial pressure wave against thermodilution in cardiac surgery patients. *Br J Anaesth*, **87**(2), 212-222.

Johnson, P., Shore, A., Potter, J., Panerai, R. and James, M., 2006. Baroreflex sensitivity measured by spectral and sequence analysis in cerebrovascular disease : methodological considerations. *Clin Auton Res*, **16**(4), 270-275.

Jones, R.D., Kornberg, J.P., Roulson, C.J., Visram, A.R. and Irwin, M.G., 1993. The Finapres 2300e finger cuff. The influence of cuff application on the accuracy of blood pressure measurement. *Anaesthesia*, **48**(7), 611-615.

Jones, R.M., Hill, A.B., Nahrwold, M.L. and Bolles, R.E., 1981. The effect of method of radial artery cannulation on postcannulation blood flow and thrombus formation. *Anesthesiology*, **55**(1), 76-78.

Kalaitzakis, K.C., Papamarkos, N.E. and Vachtsevanos, G.J., 1988. Development of a microprocessor-based adaptive technique for blood pressure measurements. *Med Prog Technol*, **14**(2), 63-72.

Karamanoglu, M., O'Rourke, M.F., Avolio, A.P. and Kelly, R.P., 1993. An analysis of the relationship between central aortic and peripheral upper limb pressure waves in man. *Eur Heart J*, **14**(2), 160-167.

Karemaker, J.M., 1995. Blood pressure measurement under extreme circumstances: Finapres in actual and simulated weightlessness. *Homeostasis*, **36**(5-6), 275-280.

Karki, J., 2002a. Active Low-Pass Filter Design (SLOA049B). *Texas Instruments*, Texas: TI Incoporated, 1-24.

Karki, J., 2002b. Analysis of the Sallen-Key Architecture (SLOA024B). *Texas Instruments*, Texas: TI Incoporated, 1-18.

Kawarada, A., Shimazu, H., Ito, H. and Yamakoshi, K., 1991. Ambulatory monitoring of indirect beat-to-beat arterial pressure in human fingers by a volume-compensation method. *Med Biol Eng Comput*, **29**(1), 55-62.

Kelly, R., Hayward, C., Avolio, A. and O'Rourke, M., 1989. Noninvasive determination of age-related changes in the human arterial pulse. *Circulation*, **80**(6), 1652-1659.

Kemmotsu, O., Ueda, M., Otsuka, H., Yamamura, T., Okamura, A., Ishikawa, T., Winter, D.C. and Eckerle, J.S., 1991a. Blood pressure measurement by arterial tonometry in controlled hypotension. *Anesth Analg*, **73**(1), 54-58.

Kemmotsu, O., Ueda, M., Otsuka, H., Yamamura, T., Winter, D.C. and Eckerle, J.S., 1991b. Arterial tonometry for noninvasive, continuous blood pressure monitoring during anesthesia. *Anesthesiology*, **75**(2), 333-340.

Kirkendall, W.M., Feinleib, M., Freis, E.D. and Mark, A.L., 1980. Recommendations for human blood pressure determination by sphygmomanometers. Subcommittee of the AHA Postgraduate Education Committee. *Circulation*, **62**(5), 1146A-1155A.

Kobayashi, H., Shimazu, H., Kawarada, A., Ito, H. and Mizumoto, C., 1990. Indirect Measurement of Eye-Level Arterial Pressure by the Volume Oscillometric Method. *J Clin Eng*, **15**(3), 195-204.

Koizumi, H., Shimada, J., Uenishi, Y. and Tochikubo, O., 2009. A ubiquitous blood pressure sensor worn at the ear. *Jap J Appl Phys*, **48**, 127001.1-6.

Kollensperger, M., Stampfer-Kountchev, M., Seppi, K., Geser, F., Frick, C., Del, S.F., Albanese, A., Gurevich, T., Giladi, N., Djaldetti, R., Schrag, A., Low, P.A., Mathias, C.J., Poewe, W. and Wenning, G.K., 2007. Progression of dysautonomia in multiple system atrophy: a prospective study of self-perceived impairment. *Eur J Neurol*, **14**(1), 66-72.

Korotkoff, N.S., 1905. [On the subject of methods of determining blood pressure (from the clinic of Prof. S.P. Fedorov)]. *Bulletin of the Imperial Military-Medical Academy*, St.Petersburg, Russia, **11**(4), 365-367.

Krediet, C.T., Wilde, A.A., Halliwill, J.R. and Wieling, W., 2005. Syncope during exercise, documented with continuous blood pressure monitoring during ergometer testing. *Clin Auton Res*, **15**(1), 59-62.

Krol, J.R. and Simons, M., 1995. Finapres in aerospace medicine. *Homeostasis*, **36**(5-6), 281-286.

Kurki, T., Smith, N.T., Head, N., Dec-Silver, H. and Quinn, A., 1987. Noninvasive continuous blood pressure measurement from the finger: optimal measurement conditions and factors affecting reliability. *J Clin Monit*, **3**(1), 6-13.

Lal, S.K., Mihailidou, A.S., Cejnar, M., Henderson, R.J., Jones, M. and Hunyor, S.N., 1993. Continuous, non-invasive volume-clamp blood pressure: determinants of performance. *J Hypertens*, **11**(12), 1413-1422.

Langewouters, G.J., Settels, J.J., Roelandt, R. and Wesseling, K.H., 1998. Why use Finapres or Portapres rather than intra-arterial or intermittent non-invasive techniques of blood pressure measurement? *J Med Eng Technol*, **22**(1), 37-43.

Laurent, C., Jonsson, B., Vegfors, M. and Lindberg, L.G., 2005. Non-invasive measurement of systolic blood pressure on the arm utilising photoplethysmography: development of the methodology. *Med Biol Eng Comput*, **43**(1), 131-135.

Lee, J.Y., Kim, J.K. and Yoon, G., 2002. Digital envelope detector for blood pressure measurement using an oscillometric method. *J Med Eng Technol*, **26**(3), 117-122.

Lee, T.K., Silva, F.H., Egbert, T.P. and Westenskow, D.R., 1995. Optimal sites for forehead oscillometric blood pressure monitoring. *J Clin Monit*, **11**(5), 298-304.

Lee, T.K. and Westenkow, D.R., 1998. Comparison of blood pressure measured by oscillometry from the supraorbital artery and invasively from the radial artery. *J Clin Monit Comput*, **14**(2), 113-117.

Lehmann, E.D., Gosling, R.G. and Sönksen, P.H., 1992. Arterial wall compliance in diabetes. *Diabet Med*, **9**(2), 114-119.

Levick, J.R., 2003. An Introduction to Cardiovascular Physiology. 4th edn, London: Arnold.

Levin, A.R., 1972. The science of cardiac catheterization in the diagnosis of congenital heart disease. *Cardiovasc Clin*, **4**(3), 235-273.

Levy, M.N. and Pappano, A.J., 2007. Cardiovascular Physiology. 9th edn, Philadelphia: Mosby Elsevier.

Lind, L., Andren, B. and Sundstrom, J., 2004. The stroke volume/pulse pressure ratio predicts coronary heart disease mortality in a population of elderly men. *J Hypertens*, **22**(5), 899-905.

London, G.M., Blacher, J., Pannier, B., Guerin, A.P., Marchais, S.J. and Safar, M.E., 2001. Arterial wave reflections and survival in end-stage renal failure. *Hypertension*, **38**(3), 434-438.

Looga, R., 2005. The Valsalva manoeuvre--cardiovascular effects and performance technique: a critical review. *Respir Physiol Neurobiol*, **147**(1), 39-49.

Lopez-Beltran, E.A., Blackshear, P.L., Finkelstein, S.M. and Cohn, J.N., 1998. Non-invasive studies of peripheral vascular compliance using a non-occluding photoplethysmographic method. *Med Biol Eng Comput*, **36**(6), 748-753.

Luce, E.A., Futrell, J.W., Wilgis, E.F. and Hoopes, J.E., 1976. Compression neuropathy following brachial arterial puncture in anticoagulated patients. *J Trauma*, **16**(9), 717-721.

Lucini, D., Pagani, M., Mela, G.S. and Malliani, A., 1994. Sympathetic restraint of baroreflex control of heart period in normotensive and hypertensive subjects. *Clin Sci (Lond)*, **86**(5), 547-556.

Maestri, R., Pinna, G.D., Robbi, E., Capomolla, S. and La Rovere, M.T., 2005. Noninvasive measurement of blood pressure variability: accuracy of the Finometer monitor and comparison with the Finapres device. *Physiol Meas*, **26**(6), 1125-1136.

Magee, P. and Tooley, M., 2005. The physics, clinical measurement and equipment of anaesthetic practice. Oxford: Oxford University Press.

Manning, D.M., Kuchirka, C. and Kaminski, J., 1983. Miscuffing: inappropriate blood pressure cuff application. *Circulation*, **68**(4), 763-766.

Marano, S.R., Fischer, D.W., Gaines, C. and Sonntag, V.K., 1985. Anatomical study of the superficial temporal artery. *Neurosurgery*, **16**(6), 786-790.

Marieb, E.N., 2004. Human Anatomy & Physiology. 6th edn, London: Benjamin Cummings.

Markiewitz, H.H., 1960. The so-called Imbert-Fick law. *Arch Ophthalmol*, **64**, 159.

Martin, C.E., Shaver, J.A., Leon, D.F., Thompson, M.E., Reddy, P.S. and Leonard, J.J., 1974. Autonomic mechanisms in hemodynamic responses to isometric exercise. *J Clin Invest*, **54**(1), 104-115.

Matthys, K. and Verdonck, P., 2002. Development and modelling of arterial applanation tonometry: a review. *Technol Health Care*, **10**(1), 65-76.

Mauck, G.W., Smith, C.R., Geddes, L.A. and Bourland, J.D., 1980. The meaning of the point of maximum oscillations in cuff pressure in the indirect measurement of blood pressure--part ii. *J Biomech Eng*, **102**(1), 28-33.

Maurer, A.H. and Noordergraaf, A., 1976. Korotkoff sound filtering for automated three-phase measurement of blood pressure. *Am Heart J*, **91**(5), 584-591.

Maxwell, S.E. and Delaney, H.D., 2004. Designing experiments and analyzing data : a model comparison perspective. 2nd edn, Belmont, California: Brooks-Cole Publishing.

McCutcheon, E.P., Baker, D.W. and Wiederhsielm, C.A., 1969. Frequency spectrum changes of Korotkoff sounds with muffling. *Med Res Eng*, **8**(1), 30-33.

Meaume, S., Benetos, A., Henry, O.F., Rudnichi, A. and Safar, M.E., 2001. Aortic pulse wave velocity predicts cardiovascular mortality in subjects >70 years of age. *Arterioscler Thromb Vasc Biol*, **21**(12), 2046-2050.

Millasseau, S.C., Kelly, R.P., Ritter, J.M. and Chowienczyk, P.J., 2002. Determination of age-related increases in large artery stiffness by digital pulse contour analysis. *Clin Sci (Lond)*, **103**(4), 371-377.

Mobley, J. and Vo-Dinh, T., 2003, Optical Properties of Tissue. *Biomedical Photonics Handbook*, edited by T. Vo-Dinh, North Carolina: CRC Press, Chapter 2, 2.1-2.75.

Murgo, J.P., Westerhof, N., Giolma, J.P. and Altobelli, S.A., 1980. Aortic input impedance in normal man: relationship to pressure wave forms. *Circulation*, **62**(1), 105-116.

Murray, I.P., 1981. Complications of invasive monitoring. *Med Instrum*, **15**(2), 85-89.

Nakagawara, M. and Yamakoshi, K., 2000. A portable instrument for non-invasive monitoring of beat-by-beat cardiovascular haemodynamic parameters based on the volume-compensation and electrical-admittance method. *Med Biol Eng Comput*, **38**(1), 17-25.

Nakajima, H., Imanishi, N. and Minabe, T., 1995. The arterial anatomy of the temporal region and the vascular basis of various temporal flaps. *Br J Plast Surg*, **48**(7), 439-450.

Näslund, J., Pettersson, J., Lundeberg, T., Linnarsson, D. and Lindberg, L.G., 2006. Non-invasive continuous estimation of blood flow changes in human patellar bone. *Med Biol Eng Comput*, **44**(6), 501-509.

Nelesen, R.A. and Dimsdale, J.E., 2002. Use of radial arterial tonometric continuous blood pressure measurement in cardiovascular reactivity studies. *Blood Press Monit*, **7**(5), 259-263.

Netea, R.T., Lenders, J.W., Smits, P. and Thien, T., 1999. Arm position is important for blood pressure measurement. *J Hum Hypertens*, **13**(2), 105-109.

Neufeld, P.D. and Johnson, D.L., 1986. Observer error in blood pressure measurement. *CMAJ*, **135**(6), 633-637.

Neuman, M.R., 1988, Neonatal monitoring. *Encyclopedia of Medical Devices and Instrumentation*, edited by J. G. Webster, New York: Wiley, Chapter 2015-2034.

Ng, K.G. and Small, C.F., 1993. Changes in oscillometric pulse amplitude envelope with cuff size: implications for blood pressure measurement criteria and cuff size selection. *J Biomed Eng*, **15**(4), 279-282.

Ng, K.G. and Small, C.F., 1994. Survey of automated noninvasive blood pressure monitors. *J Clin Eng*, **19**(6), 452-475.

Nichols, W.W. and O'Rourke, M.F., 2005, Pressure pulse waveform analysis. *McDonald's Blood Flow in Arteries : theoretical, experimental and clinical principles*, 5th edn, London: Hodder Arnold, Chapter 26, 463-502.

Nijboer, J.A. and Dorlas, J.C., 1982. The origin of inverted waveforms in the reflection plethysmogram. *Br J Anaesth*, **54**(12), 1289-1293.

Nishimura, R.A. and Tajik, A.J., 1986. The Valsalva maneuver and response revisited. *Mayo Clin Proc*, **61**(3), 211-217.

Nurnberger, J., Keflioglu-Scheiber, A., Opazo Saez, A.M., Wenzel, R.R., Philipp, T. and Schafers, R.F., 2002. Augmentation index is associated with cardiovascular risk. *J Hypertens*, **20**(12), 2407-2414.

O'Brien, E., Asmar, R., Beilin, L., Imai, Y., Mallion, J.M., Mancia, G., Mengden, T., Myers, M., Padfield, P., Palatini, P., Parati, G., Pickering, T., Redon, J., Staessen, J., Stergiou, G. and Verdecchia, P., 2003. European Society of Hypertension recommendations for conventional, ambulatory and home blood pressure measurement. *J Hypertens*, **21**(5), 821-848.

O'Brien, E. and Atkins, N., 1994. A comparison of the British Hypertension Society and Association for the Advancement of Medical Instrumentation protocols for validating blood pressure measuring devices: can the two be reconciled? *J Hypertens*, **12**(9), 1089-1094.

O'Brien, I.A., O'Hare, P. and Corrall, R.J., 1986. Heart rate variability in healthy subjects: effect of age and the derivation of normal ranges for tests of autonomic function. *Br Heart J*, **55**(4), 348-354.

O'Rourke, M.F., 1992. Arterial mechanics and wave reflection with antihypertensive therapy. *J Hypertens Suppl*, **10**(5), S43-S49.

O'Rourke, M.F., Avolio, A. and Qasem, A., 2003. Clinical assessment of wave reflection. *Hypertension*, **42**(5), e15-e16.

O'Rourke, M.F. and Brunner, H.R., 1992. Introduction to arterial compliance and function. *J Hypertens Suppl*, **10**(6), S3-S5.

O'Rourke, M.F. and Gallagher, D.E., 1996. Pulse wave analysis. *J Hypertens Suppl*, **14**(5), S147-S157.

O'Rourke, M.F. and Nichols, W.W., 2005. McDonald's Blood Flow in Arteries: theoretical, experimental and clinical principles. 5th edn, London: Hodder Arnold.

O'Rourke, M.F. and Yaginuma, T., 1984. Wave reflections and the arterial pulse. *Arch Intern Med*, **144**(2), 366-371.

Okada, Y., Shima, T., Nishida, M., Yamane, K., Yamada, T. and Yamanaka, C., 1998. Effectiveness of superficial temporal artery-middle cerebral artery anastomosis in adult moyamoya disease: cerebral hemodynamics and clinical course in ischemic and hemorrhagic varieties. *Stroke*, **29**(3), 625-630.

Omboni, S., Parati, G., Di, R.M., Wieling, W. and Mancia, G., 1996. Blood pressure and heart rate variability in autonomic disorders: a critical review. *Clin Auton Res*, **6**(3), 171-182.

Omboni, S., Parati, G., Frattola, A., Mutti, E., Di, R.M., Castiglioni, P. and Mancia, G., 1993. Spectral and sequence analysis of finger blood pressure variability. Comparison with analysis of intra-arterial recordings. *Hypertension*, **22**(1), 26-33.

Oppenheim, A.V. and Schafer, R.W., 1975. Digital signal processing. London: Prentice Hall.

Pace, N.L. and East, T.D., 1991. Simultaneous comparison of intraarterial, oscillometric, and finapres monitoring during anesthesia. *Anesth Analg*, **73**(2), 213-220.

Panerai, R.B., 1998. Assessment of cerebral pressure autoregulation in humans--a review of measurement methods. *Physiol Meas*, **19**(3), 305-338.

Panerai, R.B., 2008. Cerebral autoregulation: from models to clinical applications. *Cardiovasc Eng*, **8**(1), 42-59.

Panerai, R.B., Dawson, S.L., Eames, P.J. and Potter, J.F., 2001. Cerebral blood flow velocity response to induced and spontaneous sudden changes in arterial blood pressure. *Am J Physiol Heart Circ Physiol*, **280**(5), H2162-H2174.

Panerai, R.B., Dawson, S.L. and Potter, J.F., 1999. Linear and nonlinear analysis of human dynamic cerebral autoregulation. *Am J Physiol*, **277**(3 Pt 2), H1089-H1099.

Panerai, R.B., Rennie, J.M., Kelsall, A.W. and Evans, D.H., 1998. Frequency-domain analysis of cerebral autoregulation from spontaneous fluctuations in arterial blood pressure. *Med Biol Eng Comput*, **36**(3), 315-322.

Panerai, R.B., Sammons, E.L., Smith, S.M., Rathbone, W.E., Bentley, S., Potter, J.F., Evans, D.H. and Samani, N.J., 2006. Cerebral critical closing pressure estimation from Finapres and arterial blood pressure measurements in the aorta. *Physiol Meas*, **27**(12), 1387-1402.

Parati, G., Saul, J.P., Di, R.M. and Mancia, G., 1995. Spectral analysis of blood pressure and heart rate variability in evaluating cardiovascular regulation. A critical appraisal. *Hypertension*, **25**(6), 1276-1286.

Paskalev, D., Kircheva, A. and Krivoshiev, S., 2005. A centenary of auscultatory blood pressure measurement: a tribute to Nikolai Korotkoff. *Kidney Blood Press Res*, **28**(4), 259-263.

Penaz, J., 1973. Photoelectric Measurement of Blood Pressure, Volume and Flow in the Finger. *Digest of the 10th International Conference on Medical and Biological Engineering (Dresden)*, 104.

Penaz, J., 1995. Dynamic vascular compliance and its use in noninvasive measurement of blood pressure. *Homeostasis*, **36**(2-3), 83-89.

Penaz, J., 1992. Criteria for set point estimation in the volume clamp method of blood pressure measurement. *Physiol Res*, **41**(1), 5-10.

Pereira, E., Prys-Roberts, C., Dagnino, J., Anger, C., Cooper, G.M. and Hutton, P., 1985. Auscultatory measurement of arterial pressure during anaesthesia: a reassessment of Korotkoff sounds. *Eur J Anaesthesiol*, **2**(1), 11-20.

Perloff, D., Grim, C., Flack, J., Frohlich, E.D., Hill, M., McDonald, M. and Morgenstern, B.Z., 1993. Human blood pressure determination by sphygmomanometry. *Circulation*, **88**(5 Pt 1), 2460-2470.

Persson, P.B., DiRienzo, M., Castiglioni, P., Cerutti, C., Pagani, M., Honzikova, N., Akselrod, S. and Parati, G., 2001. Time versus frequency domain techniques for assessing baroreflex sensitivity. *J Hypertens*, **19**(10), 1699-1705.

Petrie, J.C., O'Brien, E.T., Littler, W.A. and de, S.M., 1986. Recommendations on blood pressure measurement. *Br Med J (Clin Res Ed)*, **293**(6547), 611-615.

Peura, R.A., 2009, Blood pressure and sound. *Medical instrumentation: application and design*, 4th edn, edited by J. G. Webster, Chichester: John Wiley, Chapter 7, 293-337.

Philips Semiconductors, 2001. Voltage Comparator LM311. *Philips Semiconductors*, USA: Philips Electronics, 1-23.

Philips Semiconductors, 1995. HEF4027B Dual JK flip-flop. *Philips Semiconductors*, USA: Philips Electronics, 1-8.

Pickering, T.G., James, G.D., Boddie, C., Harshfield, G.A., Blank, S. and Laragh, J.H., 1988. How common is white coat hypertension? *JAMA*, **259**(2), 225-228.

Pierson, D.J. and Hudson, L.D., 1983. Monitoring hemodynamics in the critically ill. *Med Clin North Am*, **67**(6), 1343-1360.

Pinna, G.D., La Rovere, M.T., Maestri, R., Mortara, A., Bigger, J.T. and Schwartz, P.J., 2000. Comparison between invasive and non-invasive measurements of baroreflex sensitivity: implications for studies on risk stratification after a myocardial infarction. *Eur Heart J*, **21**(18), 1522-1529.

Posey, J.A., Geddes, L.A., Williams, H. and Moore, A.G., 1969. The meaning of the point of maximum oscillations in cuff pressure in the indirect measurement of blood pressure: Part 1. *Cardiovasc Res Cent Bull*, **8**(1), 15-25.

Prian, G.W., 1977. Complications and sequelae of temporal artery catheterization in the high-risk newborn. *J Pediatr Surg*, **12**(6), 829-835.

Prian, G.W., Wright, G.B., Rumack, C.M. and O'Meara, O.P., 1978. Apparent cerebral embolization after temporal artery catheterization. *J Pediatr*, **93**(1), 115-118.

Proakis, J.G. and Manolakis, D.G., 1996. Digital signal processing : principles, algorithms, and applications. 3rd edn, Upper Saddle River, N.J.: Prentice Hall.

Puri, V.K., Carlson, R.W., Bander, J.J. and Weil, M.H., 1980. Complications of vascular catheterization in the critically ill. A prospective study. *Crit Care Med*, **8**(9), 495-499.

Raamat, R., Talts, J., Jagomagi, K. and Lansimies, E., 1999. Mathematical modelling of non-invasive oscillometric finger mean blood pressure measurement by maximum oscillation criterion. *Med Biol Eng Comput*, **37**(6), 784-788.

Ramsey III, M., 1979. Noninvasive automatic determination of mean arterial pressure. *Med Biol Eng Comput*, **17**(1), 11-18.

Rang, S., Wolf, H., Montfrans, G.A. and Karemaker, J.M., 2002. Non-invasive assessment of autonomic cardiovascular control in normal human pregnancy and pregnancy- associated hypertensive disorders: a review. *J Hypertens*, **20**(11), 2111-2119.

Regueiro-Gomez, A. and Pallas-Areny, R., 1998. A new method for automated blood pressure measurement. *Physiol Meas*, **19**(2), 205-212.

Reinhard, M., Roth, M., Muller, T., Guschlbauer, B., Timmer, J., Czosnyka, M. and Hetzel, A., 2004. Effect of carotid endarterectomy or stenting on impairment of dynamic cerebral autoregulation. *Stroke*, **35**(6), 1381-1387.

Rithalia, S., Sun, M. and Jones, R., 1999, Blood pressure measurement. *The Measurement, Instrumentation, and Sensors Handbook*, edited by J. G. Webster, North Carolina: CRC Press & IEEE Press, Chapter 75, 75-1-75-22.

Riva-Rocci, S., 1896. Un nuovo sfigmomanometro. *Gazetta Medica di Torino*, **47**, 981-986.

Roberts, M.J. and Russo, R., 1999. A student's guide to analysis of variance. New York: Routledge.

Rogers, G. and Oosthuyse, T., 2000. A comparison of the indirect estimate of mean arterial pressure calculated by the conventional equation and calculated to compensate for a change in heart rate. *Int J Sports Med*, **21**(2), 90-95.

Rolfe, P., Kanjilal, P.P., Murphy, C. and Burton, P.J., 1987. Continuous non-invasive beat-by-beat blood pressure (B.P.) measurement in the newborn. *Adv Exp Med Biol*, **220**, 311-314.

Roman, M.J., Pickering, T.G., Schwartz, J.E., Pini, R. and Devereux, R.B., 1995. Association of carotid atherosclerosis and left ventricular hypertrophy. *J Am Coll Cardiol*, **25**(1), 83-90.

Roos, C.F. and Carroll Jr., F.E., 1985. Fiber-optic pressure transducer for use near MR magnetic fields. *Radiology*, **156**(2), 548.

Rüddel, H. and Curio, I., 1991. Non-Invasive Continuous Blood Pressure Measurement - Methods, Evaluations and Applications of the Vascular Unloading Technique (Peñaz-Method). edited by Rüddel, Heinz and Curio, Immo, Peter Lang Publishing Group.

Runciman, W.B., Rutten, A.J. and Ilsley, A.H., 1981. An evaluation of blood pressure measurement. *Anaesth Intensive Care*, **9**(4), 314-325.

Saba, P.S., Roman, M.J., Pini, R., Spitzer, M., Ganau, A. and Devereux, R.B., 1993. Relation of arterial pressure waveform to left ventricular and carotid anatomy in normotensive subjects. *J Am Coll Cardiol*, **22**(7), 1873-1880.

Sammons, E.L., Samani, N.J., Smith, S.M., Rathbone, W.E., Bentley, S., Potter, J.F. and Panerai, R.B., 2007. Influence of noninvasive peripheral arterial blood pressure measurements on assessment of dynamic cerebral autoregulation. *J Appl Physiol*, **103**(1), 369-375.

Sapinski, A., 1992. Standard algorithm of blood-pressure measurement by the oscillometric method. *Med Biol Eng Comput*, **30**(6), 671.

Schmidt, T.F., Wittenhaus, J., Steinmetz, T.F., Piccolo, P. and Lupsen, H., 1992. Twenty-four-hour ambulatory noninvasive continuous finger blood pressure measurement with PORTAPRES: a new tool in cardiovascular research. *J Cardiovasc Pharmacol*, **19 Suppl 6**, S117-S145.

Segall, H.N., 1975. How Korotkoff, the surgeon, discovered the auscultatory method of measuring arterial pressure. *Ann Intern Med*, **83**(4), 561-562.

Sheldon, J.J., 1982. Blood vessels of the scalp and brain. edited by Trench, A. H., Summit, N.J.: CIBA Pharmaceutical Company.

Shenoy, D., von Maltzahn, W.W. and Buckey, J.C., 1993. Noninvasive blood pressure measurement on the temporal artery using the auscultatory method. *Ann Biomed Eng*, **21**(4), 351-360.

Shimazu, H., Ito, H., Kawarada, A., Kobayashi, H., Hiraiwa, A. and Yamakoshi, K., 1989. Vibration technique for indirect measurement of diastolic arterial pressure in human fingers. *Med Biol Eng Comput*, **27**(2), 130-136.

Shinozaki, T., Deane, R.S. and Mazuzan, J.E., 1980. The dynamic responses of liquid-filled catheter systems for direct measurements of blood pressure. *Anesthesiology*, **53**(6), 498-504.

Shinskey, F.G., 1999, PID control. *The Measurement, Instrumentation, and Sensors Handbook*, edited by J. G. Webster, North Carolina: CRC Press & IEEE Press, Chapter 97, 97-1-97-8.

Short, D., 1976. The diastolic dilemma. *Br Med J*, **2**(6037), 685-686.

Sigaudo-Roussel, D., Custaud, M.A., Maillet, A., Guell, A., Kaspranski, R., Hughson, R.L., Gharib, C. and Fortrat, J.O., 2002. Heart rate variability after prolonged spaceflights. *Eur J Appl Physiol*, **86**(3), 258-265.

Sims, A.J., Reay, C.A., Bousfield, D.R., Menes, J.A. and Murray, A., 2005a. Low-cost oscillometric non-invasive blood pressure monitors: device repeatability and device differences. *Physiol Meas*, **26**(4), 441-445.

Sims, A.J., Reay, C.A., Bousfield, D.R., Menes, J.A. and Murray, A., 2005b. Oscillometric blood pressure devices and simulators: measurements of repeatability and differences between models. *J Med Eng Technol*, **29**(3), 112-118.

Sleight, P., 1991. Role of the baroreceptor reflexes in circulatory control, with particular reference to hypertension. *Hypertension*, **18**(5 Suppl), III31-III34.

Smith, N.T., Wesseling, K.H. and de, W.B., 1985. Evaluation of two prototype devices producing noninvasive, pulsatile, calibrated blood pressure measurement from a finger. *J Clin Monit*, **1**(1), 17-29.

Smith, S.M., Samani, N.J., Sammons, E.L., Rathbone, W.E., Potter, J.F., Bentley, S. and Panerai, R.B., 2008. Influence of non-invasive measurements of arterial blood pressure in frequency and time-domain estimates of cardiac baroreflex sensitivity. *J Hypertens*, **26**(1), 76-82.

Smyth, H.S., Sleight, P. and Pickering, G.W., 1969. Reflex regulation of arterial pressure during sleep in man. A quantitative method of assessing baroreflex sensitivity. *Circ Res*, **24**(1), 109-121.

Sollers, J.J., III, Merritt, M.M., Silver, R.A., Sadle, T.N., Ferrucci, L. and Thayer, J.F., 2006. Comparison of arterial compliance indices derived via beat-to-beat blood pressure waveforms: aging and ethnicity. *Biomed Sci Instrum*, **42**, 518-523.

Soule, D.T. and Powner, D.J., 1984. Air entrapment in pressure monitoring lines. *Crit Care Med*, **12**(6), 520-522.

Staessen, J.A., 2000. Blood pressure-measuring devices: time to open Pandora's box and regulate. *Hypertension*, **35**(5), 1037.

Staessen, J.A., Asmar, R., De, B.M., Imai, Y., Parati, G., Shimada, K., Stergiou, G., Redon, J. and Verdecchia, P., 2001. Task Force II: blood pressure measurement and cardiovascular outcome. *Blood Press Monit*, **6**(6), 355-370.

Stergiopulos, N., Segers, P. and Westerhof, N., 1999. Use of pulse pressure method for estimating total arterial compliance in vivo. *Am J Physiol*, **276**(2 Pt 2), H424-H428.

Stock, A.L., Collins, H.P. and Davidson, T.M., 1980. Anatomy of the superficial temporal artery. *Head Neck Surg*, **2**(6), 466-469.

Sugawara, J., Komine, H., Hayashi, K., Maeda, S. and Matsuda, M., 2007. Relationship between augmentation index obtained from carotid and radial artery pressure waveforms. *J Hypertens*, **25**(2), 375-381.

Swenne, C.A., Bootsma, M. and van Bolhuis, H.H., 1995. Different autonomic responses to orthostatic and to mental stress in young normals. *Homeostasis*, **36**(5-6), 287-292.

Sykes, M.K., Vickers, M.D. and Hull, C.J., 1981, Direct Measurement of Intravascular Pressure. *Principles of Clinical Measurement*,13, 159-172.

Takazawa, K., Tanaka, N., Fujita, M., Matsuoka, O., Saiki, T., Aikawa, M., Tamura, S. and Ibukiyama, C., 1998. Assessment of vasoactive agents and vascular aging by the second derivative of photoplethysmogram waveform. *Hypertension*, **32**(2), 365-370.

Tanaka, G., Sawada, Y., Matsumura, K., Nagano, Y. and Yamakoshi, K., 2002. Finger arterial compliance as determined by transmission of light during mental stress and reactive hyperaemia. *Eur J Appl Physiol*, **87**(6), 562-567.

Tanaka, S. and Yamakoshi, K., 1996. Ambulatory instrument for monitoring indirect beat-to-beat blood pressure in superficial temporal artery using volume-compensation method. *Med Biol Eng Comput*, **34**(6), 441-447.

Taylor, D., 1996. Valsalva manoeuvre: a critical review. *Journal of the South Pacific Underwater Medicine Society*, Durham: South Pacific Underwater Medicine Society, **26**(1), 8-13.

ten Harkel, A.D., Baisch, F. and Karemaker, J.M., 1992. Increased orthostatic blood pressure variability after prolonged head-down tilt. *Acta Physiol Scand Suppl*: Department of Medicine, Univ. of Amsterdam Academic Medical Centre, Netherlands., **604**, 89-99.

Terent, A. and Breig-Asberg, E., 1994. Epidemiological perspective of body position and arm level in blood pressure measurement. *Blood Press*, **3**(3), 156-163.

Thibodeau, G.A. and Patton, K.T., 2002. Anatomy and Physiology. 5th edn, London: Mosby.

Toll, M.O., 1984. Direct blood-pressure measurements: risks, technological evolution and some current problems. *Med Biol Eng Comput*, **22**(1), 2-5.

Ursino, M. and Cristalli, C., 1996. A mathematical study of some biomechanical factors affecting the oscillometric blood pressure measurement. *IEEE Trans Biomed Eng*, **43**(8), 761-778.

Vaitkevicius, P.V., Fleg, J.L., Engel, J.H., O'Connor, F.C., Wright, J.G., Lakatta, L.E., Yin, F.C. and Lakatta, E.G., 1993. Effects of age and aerobic capacity on arterial stiffness in healthy adults. *Circulation*, **88**(4 Pt 1), 1456-1462.

van Egmond, J., Hasenbos, M. and Crul, J.F., 1985. Invasive v. non-invasive measurement of arterial pressure. Comparison of two automatic methods and simultaneously measured direct intra-arterial pressure. *Br J Anaesth*, **57**(4), 434-444.

van Egmond, J., Lenders, J.W., Weernink, E. and Thien, T., 1993. Accuracy and reproducibility of 30 devices for self-measurement of arterial blood pressure. *Am J Hypertens*, **6**(10), 873-879.

van Lieshout, J.J., Toska, K., van Lieshout, E.J., Eriksen, M., Walloe, L. and Wesseling, K.H., 2003. Beat-to-beat noninvasive stroke volume from arterial pressure and Doppler ultrasound. *Eur J Appl Physiol*, **90**(1-2), 131-137.

von Recklinghausen, H., 1901. Uber Blutdruckmessung beim Menschen. *Arch Exp Pathol Pharmakol*, **46**, 78-132.

Ware, R.W. and Anderson, W.L., 1966. Spectral analysis of Korotkoff sounds. *IEEE Trans Biomed Eng*, **13**(4), 170-174.

Weinmann, J., Hayat, A. and Raviv, G., 1977. Reflection photoplethysmography of arterial-blood-volume pulses. *Med Biol Eng Comput*, **15**(1), 22-31.

Weissler, A.M., Harris, W.S. and Schoenfeld, C.D., 1968. Systolic time intervals in heart failure in man. *Circulation*, **37**(2), 149-159.

Wesseling, K.H., 1995. A Century of Noninvasive Arterial Pressure Measurement: From Marey to Penaz and Finapres. *Homeostasis*, **36**(2-3), 50-66.

Wesseling, K.H., 1996. Finger arterial pressure measurement with Finapres. *Z Kardiol*, **85**(Suppl 3), 38-44.

Wesseling, K.H., de Wit, B., van der Hoeven, G.M.A., van Goudoever, J. and Settels, J.J., 1995. Physiocal, calibrating finger vascular physiology for Finapres. *Homeostasis*, **36**(2-3), 67-82.

Wesseling, K.H., Settels, J.J., van der Hoeven, G.M., Nijboer, J.A., Butijn, M.W. and Dorlas, J.C., 1985. Effects of peripheral vasoconstriction on the measurement of blood pressure in a finger. *Cardiovasc Res*, **19**(3), 139-145.

West, J.N.W., Sheridan, J.J. and Littler, W.A., 1991, Direct measurement of blood pressure. *Blood Pressure Measurement (Handbook of Hypertension S.)*, vol. 14, edited by E. O'Brien & K. O'Malley, Kidlington: Elsevier, Chapter 16, 315-333.

Westerhof, B.E., Guelen, I., Westerhof, N., Karemaker, J.M. and Avolio, A., 2006. Quantification of wave reflection in the human aorta from pressure alone: a proof of principle. *Hypertension*, **48**(4), 595-601.

Weston, P.J., James, M.A., Panerai, R., McNally, P.G., Potter, J.F., Thurston, H. and Swales, J.D., 1996a. Abnormal baroreceptor-cardiac reflex sensitivity is not detected by conventional tests of autonomic function in patients with insulin-dependent diabetes mellitus. *Clin Sci (Lond)*, **91**(1), 59-64.

Weston, P.J., Panerai, R.B., McCullough, A., McNally, P.G., James, M.A., Potter, J.F., Thurston, H. and Swales, J.D., 1996b. Assessment of baroreceptor-cardiac reflex sensitivity using time domain analysis in patients with IDDM and the relation to left ventricular mass index. *Diabetologia*, **39**(11), 1385-1391.

Williams, B., Lacy, P.S., Thom, S.M., Cruickshank, K., Stanton, A., Collier, D., Hughes, A.D., Thurston, H., O'Rourke, M., CAFE Investigators, Anglo-Scandinavian Cardiac Outcomes Trial Investigators and CAFE Steering Commitee and Writing Commitee, 2006. Differential impact of blood pressure-lowering drugs on central aortic pressure and clinical outcomes: principal results of the Conduit Artery Function Evaluation (CAFE) study. *Circulation*, **113**(9), 1213-1225.

Wolthuis, R., Mitchell, G., Hartl, J. and Saaski, E., 1993. Development of a dual function sensor system for measuring pressure and temperature at the tip of a single optical fiber. *IEEE Trans Biomed Eng*, **40**(3), 298-302.

Wolthuis, R.A., Golden, D.P., Jr. and Hoffler, G.W., 1974. Development of a Korotkov sound processor for automatic identification of auscultatory events. II. Decision logic specifications and operational verification. *IEEE Trans Biomed Eng*, **21**(2), 119-124.

Yamakoshi, K., 1995. Volume-compensation method for non-invasive measurement of instantaneous arterial blood pressure: principle, methodology, and some applications. *Homeostasis*, **36**(2-3), 90-119.

Yamakoshi, K., Kamiya, A., Shimazu, H., Ito, H. and Togawa, T., 1983. Noninvasive automatic monitoring of instantaneous arterial blood pressure using the vascular unloading technique. *Med Biol Eng Comput*, **21**(5), 557-565.

Yamakoshi, K., Rolfe, P. and Murphy, C., 1988. Current developments in non-invasive measurement of arterial blood pressure. *J Biomed Eng*, **10**(2), 130-137.

Yamakoshi, K., Shimazu, H., Shibata, M. and Kamiya, A., 1982. New oscillometric method for indirect measurement of systolic and mean arterial pressure in the human finger. Part 1: model experiment. *Med Biol Eng Comput*, **20**(3), 307-313.

Yamakoshi, K.I., Shimazu, H. and Togawa, T., 1980. Indirect measurement of instantaneous arterial blood pressure in the human finger by the vascular unloading technique. *IEEE Trans Biomed Eng*, **27**(3), 150-155.

Yelderman, M. and Ream, A.K., 1979. Indirect measurement of mean blood pressure in the anesthetized patient. *Anesthesiology*, **50**(3), 253-256.

Zion, A.S., Bartels, M.N., Wecht, J.M., Sloan, R.P., Downey, J.A. and De Meersman, R.E., 2003. Evaluation of blood pressure and baroreflex sensitivity by radial artery tonometry versus finger arteriolar photoplethysmography. *Am J Hypertens*, **16**(5 Pt 1), 371-374.